In vitro and in vivo characterizations of bioactive calcium phosphate ceramic, glass ceramic, and their composite with fibrin glue in osteogenesis and osseointegration for orthopaedic application

A Thesis Presented

By

S. Abiraman

In partial fulfillment of the requirements for
The Degree of
Doctorate of Philosophy of

SREE CHITRA TIRUNAL INSTITUTE FOR
MEDICAL SCIENCES AND TECHNOLOGY
THIRUVANANTHAPURAM
KERALA
INDIA
April - 2002

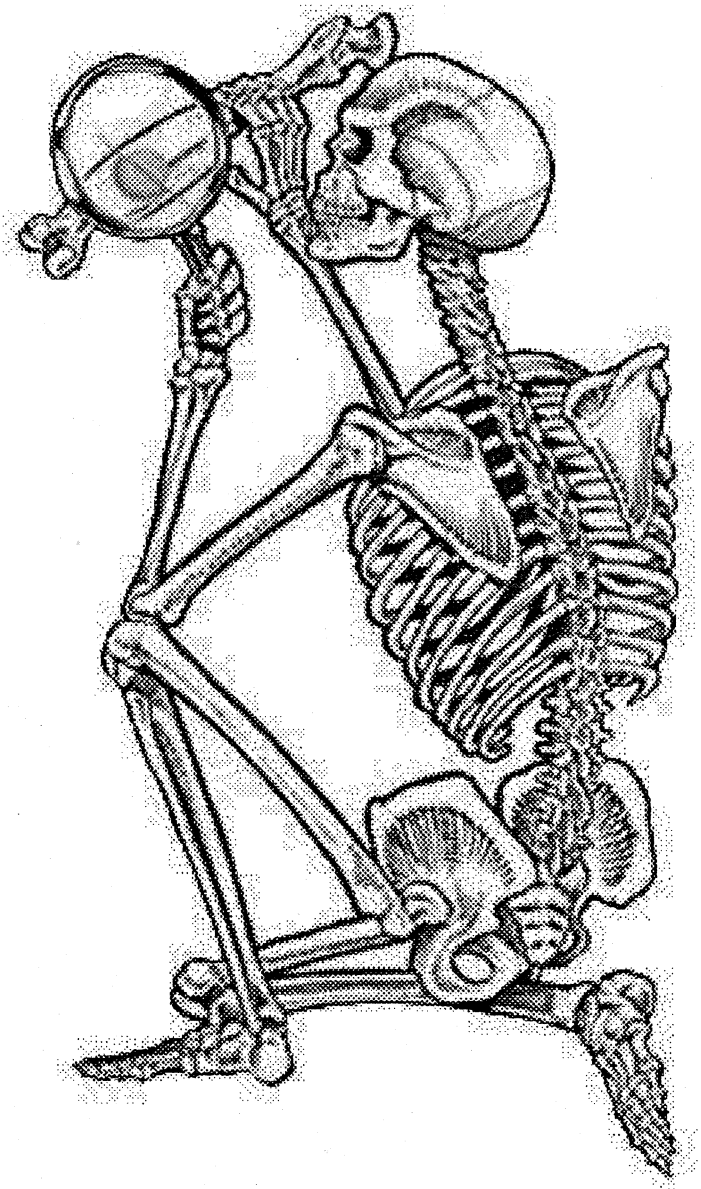

DECLARATION

I, S. Abiraman, hereby declare that I had personally carried out the work depicted in the thesis entitled "In vitro and In vivo characterizations of bioactive calcium phosphate ceramic, glass ceramic, and their composite with fibrin glue in osteogenesis and osseointegration for orthopaedic application" except where internal help sought are acknowledged.

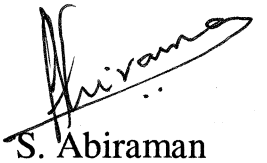

Date: April 15, 2002

S. Abiraman

Tele: 0471-340801
Fax : 0471-341814

Grams: CHITRAMET
Telex : 0435 - 6290

श्री चित्रा तिरुनाल आयुर्विज्ञान तथा प्रौद्योगिकी संस्थान
बायो मेडिकल टैक्नोलॉजी विंग
पूजापुरा, तिरुवनन्तपुरम-695 012, इन्डिया

SREE CHITRA TIRUNAL INSTITUTE FOR MEDICAL SCIENCES AND TECHNOLOGY
BIO MEDICAL TECHNOLOGY WING
POOJAPPURA, THIRUVANANTHAPURAM-695 012, INDIA
(An Institute of National Importance under Govt. of India)

Dr. Annie John,
Scientist C
TEM In-Charge
Division of Implant Biology

CERTIFICATE

This is to certify that Mr. S. Abiraman, in the division of Implant Biology of this Institute, has fulfilled the requirements of the regulations relating to the nature and prescribed period of research for the Ph.D. Degree of Sree Chitra Tirunal Institute For Medical Sciences & Technology, Thiruvananthapuram. The work entitled **"*In vitro* and *in vivo* characterizations of bioactive calcium phosphate ceramic, glass ceramic, and their composite with fibrin glue in osteogenesis and osseointegration for orthopaedic application"** was carried out under my direct supervision.

Annie John

Dr. Annie John

(Guide)

The Thesis

Entitled

In vitro and *in vivo* characterizations of bioactive calcium phosphate ceramic, glass ceramic, and their composite with fibrin glue in osteogenesis and osseointegration for orthopaedic application

Submitted

By

S. Abiraman

For

Doctor of Philosophy

of

SREE CHITRA TIRUNAL INSTITUTE FOR MEDICAL SCIENCES AND TECHNOLOGY
THIRUVANANTHAPURAM
KERALA
INDIA

Evaluated and approved by

Annie John

Dr. Annie John

(Guide)

Dr. K. P. Aravindan

(Name of Thesis Examiner)

ACKNOWLEDGEMENT

I take this opportunity to express my heart felt thanks and gratitude to Dr. Annie John, Scientist, Division of Implant Biology, Biomedical Technology Wing (BMT), Sree Chitra Tirunal Institute for Medical Sciences and Technology (SCTIMST) for suggesting the problem, her valuable guidance and educative criticism throughout the study.

My sincere thanks to the members of my Doctoral Advisory Committee, Dr. R. Sivakumar, Former Head, BMT Wing, SCTIMST; Dr. Mira Mohanty, Head, Division of Implant Biology; and Dr. H. K. Varma, Head, Division of Bioceramics, BMT, SCTIMST; and Dr. K. V. Menon, Chairman and Consultant, Department of Orthopaedics, Amritha Institute of Medical Sciences, Cochin.

I am grateful to the Director, SCTIMST and the Head, BMT Wing, for providing the necessary facilities throughout the doctoral programme..

I am thankful to Dr. T. V. Kumary, Scientist, BMT, SCTIMST for carrying out the *in vitro* studies.

I am greatly indebted to Dr. Arthur Vijayan Lal, Head, Vivarium and Dr. P. R. Umashankar, Scientist, Virarium and BMT, SCTIMST for all the facilities and help provided in the surgical procedures.

I am also thankful to Dr. Lissy K Krishnan, Head, Thrombosis Research Unit, BMT, SCTIMST for providing the fibrin glue for the experiments.

I use this opportunity to thank the scientists: Dr. A C Fernandez Dr. K. Sreenivasan Dr. T. V. Anilkumar, and Dr. Manoj Komath, for their valuable advice and encouragement during the entire course of my study.

I am also thankful to Mrs. Sulekha Baby, Mrs. Usha Vasudev, Mr. Suresh Babu and Mrs. Radha Kumari for their technical assistance during my work.

I am thankful to Dr. Pradeep Kumar, Regional Cancer Centre, Thiruvananthapuram for providing the facility to carry out the Radio Immuno Assay.

I also want to express my sincere gratitude to the late Dr. K Rathinam, Former Head, Division of Toxicology, BMT Wing SCTIMST for his encouraging support in my work.

I have no words to express my personal gratitude to all my colleagues: Mr. Anil Kumar PR, Dr. Santhosh Kumar TR, Mr. Jacob Biboy Varghese, Mr. Ramaswamy Dr. Bindu K. Menon, Miss. Asha. S. Mathew, Miss. Bernadette K Madathil, Dr. Resmi KR and Mr. Manoj Kumar for their unfailing help and moral support. I also take this opportunity to sincerely thank one and all at SCTIMST.

I gratefully and wholeheartedly acknowledge the support from my beloved parents and beloved brother, who have been a pillar of strength and source of inspiration without them this work would not have been possible.

INDEX

LIST OF FIGURES

LIST OF TABLES

Orthopedics is currently one of the largest medical industries and deals with deformities, injuries, and pathology of the bones, joints, ligaments, tendons, and muscles. The arena of orthopedic medicine is widely researched and has led to improved surgical procedures in areas such as bone grafting, joint replacement, and limb supports. Finding suitable biomaterials for a variety of applications is the key aspect of orthopedic research.

Synthetic bone graft materials, whether polymer, ceramic, or metal based, provide only an inherent osteoconductive capacity. More simply put, they provide only a physical platform by which they support cell attachment, shape, constrain and control tissue development. Hence, the focus was on understanding the tissue architecture and the physiology of the intended tissue to be replaced. Based on that biomaterials that are less toxic and biocompatible were developed. To further augment the healing process mitogenic factors are coated on the material or the intended tissue cells autologous or heterologous are seeded on the material and implanted. By incorporating biological growth factor components within synthetic bone scaffolds a closer approximation of native bone graft material is achieved. In addition, control of the specific addition of scaffold and biological components minimizes immunological rejection potential. Thus a synthetic bone graft can be achieved with the inherent osteogenic properties of allograft, without the immunological rejection or disease threat potential, and with the inherent osteogenic properties of autograft, without the complications often associated with the graft donor site morbidity. Furthermore, by controlling growth factor concentrations, these synthetic bone grafts have the capacity to be more osteogenic then either autograft or the receiving host bone bed. Such tissues are often depleted of endogenous growth

factor stores because of various disease and physiological states, including diabetes, osteoporosis, anti-inflammatory drug therapy, and old age.

Ceramics that are specifically designed, synthesized, and fabricated for the repair and reconstruction of the diseased, damaged or worn out parts of the body are known as bioceramics. Most clinical applications of bioceramics relate to the repair of the skeletal system, composed of bones, joints and teeth, and to augment both hard and soft tissue responses. Ceramics are also used to replace parts of the cardiovascular system, especially heart valves, artificial blood vessel, artificial trachea, drug delivery systems, catheters, percutaneous devices, dental applications and special formulations of glasses are also used therapeutically for the treatment of tumors. The bioactive ceramics used in orthopaedic surgery are dense hydroxyapatite, bioglass® and apatite wollastonite-glass ceramic (AW-GC), tricalcium phosphates (bioresorbable ceramics) are most frequently used as bone defect fillers.

The chemistry of the bone mineral is not exactly identical to the chemistry of hydroxyapatite and bone mineral can, at best be regarded as poorly crystalline, contaminated hydroxyapatite. The bone mineral, however, is a complex substance and is not stoichiometric with respect to hydroxyapatite. The Ca/P molar ratio of bone is significantly less than the 10/6 so that the apatite would require, in addition to the Ca^{2+}, PO_4^{3-} and OH^- ions of the apatite, substantial amounts of carbonate ions, lesser amounts of pyrophosphate, Mg^{2+}, Na^+ and K^+ and trace amounts of other ions.

Bioceramics to be used as bone defect filler should satisfy the following:

1. Restore function of surrounding tissues (Non-toxic, and does not cause any Inflammatory reaction)
2. Fill the space (acts as a scaffold)
3. Physiologically interact with the body fluids (Bioactive property)

4. Stimulate osteogenesis (By osteoconduction or osteoinduction pathway) &
5. Enhance osseointegration (Chemical bonding)

The biocompatibility of biomaterials is very closely related to cell behaviour in contact with them, particularly cell adhesion on to their surface. Surface characteristics of the materials such as their topography, chemistry or surface energy, play an essential part in cell adhesion on biomaterials. Thus attachment, adhesion and spreading belong to the first phase of cell/material interactions and the quality of this first phase will influence the cell's capacity to proliferate and to differentiate itself on contact with the implant. Thus, a complete understanding of cell adhesion and particularly osteoblast adhesion on materials is now essential to optimise the bone/biomaterial interface.

Ceramic materials are prepared in various forms such as blocks, granules (porous and non-porous) and as coating on bioinert materials (titanium) to enhance the osseointegration. Ideally the material must have better mechanical strength and bone-bonding ability in unison with its inductive ability.

The objective of the present study was to address the following:

It is well known that bioactive ceramics are ideal bone graft materials. But, the tissue response to these bioactive ceramics is not known fully understood till date. Three different types of bioactive ceramics were taken for the study a) Hydroxyapatite (HA), b) Bioactive Glass System-AW type (BGS) and c) Triphasic Bioactive Composite System (HABGS all synthesized in house.

1) Characterization of the synthesized bioactive ceramic granules for their crystallinity, phase compositions (purity) and the functional groups.
2) To study the dissolution, precipitation and apatite formation of the bioactive ceramic granules by simulated *in vitro* studies.

3) Cytotoxicity and cytocompatibility property of the ceramics by *in vitro* cell culture techniques.

4) To find the histotoxicity, histocompatibility of the bioactive ceramic granules in heterotopic and orthotopic sites without fibrin glue and with fibrin glue (as growth factors).

5) Characterization of the ceramic granules after implantation in rabbit tibia bone for its crystallinity and phase composition by XRD, functional changes by FT-IR and the distribution of the elements by SEM-EDAX techniques.

6) Specific bone labeling techniques as well as staining techniques employed to understand the healing pattern of the bone with respect to different bioactive ceramic granules.

7) Biochemical estimation of the plasma and urine markers of bone for understanding the physiology of the bone before and after implantation.

8) Quantitative histomorphometric analysis of the implanted specimens to understand the bone growth rate at different periods.

9) Suggest a possible mechanism by which the bioactive ceramics would favor osteogenesis and osseointegration in bone and

10) Compare the difference between the commercially available bioactive ceramic bone substitutes with that of the bioactive ceramics synthesized in house.

The dissertation is divided into VII chapters followed by the bibliography section

Chapter I – Introduction

This chapter begins with the importance of bone grafts and the related therapies. In order to develop an ideal bone graft substitute one has to understand the basics of bone structure at the micro and macro level hence, some basic aspects of the embryology, anatomy and physiology are discussed. Special emphasis is given to bone mineral and fracture repair and some pathological conditions where bone fracture are common. Different types of orthopaedic implants (metallic & non-metallic) are used for fracture fixation, of them why bioceramics are given special importance are discussed in detail. This chapter also discusses on the importance of implant evaluation by *in vitro* and *in vivo* techniques, which would be useful to understand the implant property in depth prior to clinical application.

Chapter II- Materials and methods of

a) Synthesis route of bioactive calcium phosphate ceramics, glass ceramics and composite and their chemical composition.

b) Characterization of ceramics by SEM, TEM, XRD, FT-IR, SEM-EDAX for its surface property and pore size, crystal size, phase composition and crystallinity, functional groups, and the distribution of the ions.

c) *In vitro* evaluation of the implant granules using simulated studies in different buffers and medium to monitor the changes that take place with time, with respect to pH, surface of the material, changes in their functional groups, degradation of the granules and ion release were studied by SEM, FT-IR of the granules and biochemical analysis of the medium.

d) Cytotoxicity and cytocompatibility studies by direct and indirect contact with fibroblast cells (L929) and osteoblast cells (MG-63/HOS) for 48 hours on

bioactive ceramic discs and granules were evaluated by SEM and Light microscopy.

e) *In vivo* evaluation of bioactive ceramic granules with and without fibrin glue was evaluated in a heterotopic site for its histocompatibility, histotoxicity, osteoconductive and osteoinductive property in mice quadriceps muscle for 28 days and evaluated by radiography, light microscopy and fluorescence microscopic techniques and image analysis.

f) Orthotopic implantation of the bioactive ceramic granules in rabbit tibia bone with and without fibrin glue fibrin glue was implanted for 3 and 6 months duration, followed by radiographic and biochemical analysis before and after implantation. Retrieved tissues were examined under SEM, TEM and LM for the osseointegration, crystal structure, and histocompatibility and healing pattern. XRD, FT-IR, SEM-EDAX studies were done on the retrieved samples to understand the phase changes, functional groups and the ion distribution.

Results and discussion are given in Chapter –III to VI

Chapter-III deals with the results of the Material characteristics: Surface, Phase composition, functional groups, porosity etc.

XRD of Hydroxyapatite (HA), Bioactive Glass System –AW type (BGS) and Triphasic Bioactive Composite System (HABGS) granules confirmed the crystallinity of the materials. HA has mainly the apatite phase, BGS showed apatite phase and wollastonite ($CaO\ SiO_2$/$CaO\ SiO_3$) as major phase and whitlockite [$(Ca_3\ (PO_4)_2)$-Tricalcium phosphate] as minor phase. HABGS, showed apatite and whitlockite as major phase and wollastonite as minor phase. FT-IR of the ceramic granules confirmed the crystallinity of the ceramic granules as well as the presence of the hydroxyl (3570 cm^{-1} and 630 cm^{-1}) and the phosphate groups (1089 cm^{-1}, 1046 cm^{-1},

960 cm^{-1}, 600 cm^{-1} and 568 cm^{-1}) in the HA. In BGS and HABGS the hydroxyl groups were absent or not detected and the presence of the silicate (1022 cm^{-1}, 715 cm^{-1}) and the phosphate groups were identified. The porosity of the HA material was 100 μm to 120 μm whereas that of BGS and HABGS the pore size was ~30μm.

Chapter-IV deals with the results of the *in vitro* evaluation of the materials in simulated conditions and with fibroblast and osteoblast cells.

Dissolution studies performed on the granules with different buffers and medium in different pH revealed the following:

a) HA: Irrespective of the pH the material showed a slow degradation and calcium phosphate release in acidic and alkaline pH. Apatite formation on HA granules was confirmed with all the buffers and medium after 24 hours by FT-IR.

b) BGS: The material showed rapid degradation and calcium phosphate release in acidic environment and slow degradation in alkaline conditions. Apatite formation was confirmed after 24 hours on the BGS granules with all the buffers and medium.

c) HABGS: The material showed property similar to BGS granules.

Chapter-V deals with the results of the *in vivo* evaluation of the ceramic granules without fibrin glue and with fibrin glue in mice quadriceps muscle and rabbit tibia bone.

Bone induction was observed in FG coated BGS and HABGS granules but not in FG coated HA granules. Bone induction in the extraskeletal site was more pronounced with 5 mg of fibrin glue (FG) coated HABGS and BGS granules rather than 2.5 mg FG coated HABGS and BGS granules. The induction was HA<BGS<HABGS. Uncoated HA, BGS and HABGS granules did not showed any bone induction until 28 days.

HA, BGS and HABGS granules implanted in rabbit tibia bone showed good osseointegration with the host bone by 3 months. HA granules did not show any signs of degradation even after 6 months. BGS granules showed intense degradation at 3 months and by 6 months the material was completely replaced by the host bone. HABGS granules showed bone ingrowth on the surface of the granules at 3 months and by 6 months the material was almost replaced by the host bone, only the HA phase of the granule was seen even after 6 months. The osteogenesis pattern for HA, BGS and HABGS granules were by osteoconduction. HA, BGS and HABGS granules showed variations in the maturation of the bone from woven bone to mature woven bone and to lamellar bone in the cortical-periosteal zone, mid cortical zone and cortical-endosteal zones.

Good osseointegration was observed with 5 mg FG coated HA, BGS and HABGS granules at 3 months. Material degradation was observed only in FG coated BGS and HABGS granules. FG coated HA, BGS and HABGS granules showed osteoinduction, confirmed by bone labeling studies.

Quantitative image of the implanted specimens for the bone growth rate to that of the implant showed clearly the following sequence:

a) 3 months: HA<BGS<HABGS and

b) 6 months: HA<HABGS<BGS

Biochemical analysis of parathyroid hormone (PTH), calcitonin (CT) calcium, phosphorous, alkaline phosphatase, acid phosphatase, protein, and creatinine in serum showed normal levels at 3 and 6 months after implantation.

Physicochemical analysis of the retrieved samples by XRD of uncoated and FG coated HA, BGS and HABGS granules showed amorphous peaks after 3 and 6 months. Phase changes were observed in all the three materials with time. FT-IR

analysis of the functional groups typical of the bone hydroxyl, carbonate and phosphate groups were observed after implantation. SEM-EDAX of the implant site clearly showed the distribution of the calcium and phosphate evenly around the implant site with HA, BGS and HABGS granules. The silica group is also seen evenly distributed along with the calcium and the phosphorous in BGS and HABGS implanted specimens.

Chapter-VI discusses on the impact of biomaterials in the orthopaedic industry and the comparison of the synthetic in-house prepared ceramic granules property with that of the commercially available ones, with respect to their chemical, physical and biological response in *in vitro* and *in vivo* situations and suggesting a possible mechanism of cell-ceramic-tissue-ceramic response.

Chapter-VII summarizes the results and the conclusions based on the findings, which are correlated with data available in the literature.

1. The physicochemical property of the material definitely played a major role in the stimulation of the osteogenesis and osseointegration.
2. The *in vitro* evaluation of the bioactive ceramic granules showed less toxicity and better cell attachment and spreading. The dissolution studies confirmed the bioactive property of the three materials with respect to the pH influence.
3. Heterotopic studies revealed that the uncoated HA, BGS and HABGS material was non-toxic, and evoked less fibrous encapsulation around the material. FG coated granules showed good tissue response without any fibrous tissue encapsulation or inflammatory reaction. BGS and HABGS showed osteoinduction with FG but HA did not. The main observation was that induction of new bone was observed at 15^{th} day after implantation, which is much ahead of the earlier reported data (21 days).
4. The *in vivo* orthotopic implantation studies proved the material to be well tolerated and showed good osteointegration. The degradation of the material

and the bone formation pattern was different for the three granules without FG and with FG.

5. The physicochemical (Material with tissue) and biochemical (Serum and urine analysis) characterization of the orthotopic implanted animals showed definite correlation to the healing pattern of the bone with respect to the three granules.

CHAPTER – I

INTRODUCTION

I. INTRODUCTION

I.1 The Need for Bone Substitutes

The World Health Authority has decreed that 2000–2010 will be the "***Bone and Joint Decade***", and this is now being supported by the United Nations. The rationale for this is that joint diseases account for half of all chronic conditions in people over 65; back pain is the second leading cause of sick leave; and osteoporotic fractures have doubled in the last decade, so that 40 % of all women over 50 will eventually suffer from one. It is estimated that 25 % of health expenditure in developing countries will be spent on trauma-related care by the end of the decade, and many children are deprived of normal development by crippling diseases and deformities.

Many of these cases require bone graft substitutes to repair the injury or defect. There are currently on the order of 500,000 bone grafts performed annually in the U.S. For example, there was an estimated 220,000 spinal fusion cases performed in 1998 requiring bone grafts to secure areas of the spine affected by deformity, trauma, tumors, or degenerative disc disease. There are approximately 170,000 fractures in the United States that fail to heal each year and are diagnosed as 'non-unions' (i.e., fractures that have failed to heal within nine months) that require some form of bone substitutes to repair the fracture.

I.1.1 Current Therapies

To address the need for bone substitutes, current clinical therapies include:

1. Autografting, which represents about 58% of the current bone substitutes, involves harvesting a bone from one location in the patient's body and transplanting it into another part of the same patient. Using autologous grafts, when available, typically

produces the best clinical results; successful clinical outcomes can exceed 80%. Autografting is thus considered the 'gold standard.' An example of one of the most commonly performed bone autografting procedures is for use in spinal fusion. In a fusion procedure, bone graft from the patient's hip is implanted in disc spaces between spinal vertebrae or along the back of the spine. The grafted bone fuses the vertebrae together over several months. The benefit from transplanting an autogenous tissue is obvious: immunogenicity is not an issue. Autografting, however, has several associated problems including the additional surgical costs for the harvesting procedure, and infection and pain at the harvesting site. For example, harvesting an iliac crest graft (i.e., the protruding bony section of the patient's hip) can cost between $1000 to $9,000 per procedure for the harvesting surgery and the additional hospital stay. The morbidity at the harvest site can be tremendous with problems such as pain, infection, and blood loss requiring blood transfusion adding to the associated risks of transfusion reaction and blood borne infection.

2. Allografting, which represents about 34% of the current bone substitutes, involves harvesting and processing bone from a cadaver then transplanting it to the patient. Allogenic implants are acellular and are less successful than autografts for reasons attributed to immunogenicity and the absence of viable cells that become osteoblasts. Another disadvantage of allografting is concern with transmitted disease

3. Man-made materials, including metals, plastics, and ceramics represent approximately 8% of bone substitutes. These materials, however, are subject to fatigue, fracture, toxicity, and wear, and were not replaced with time (i.e., a metal bone implant cannot grow with the patient and it cannot change shape in response to the loads placed upon the implant).

For all these reasons, there is a real need for alternative, off-the-shelf, bone substitutes and better wound healing therapies. To address the problems associated with the bone, the anatomy, physiology and the pathology of the bone at the macro and micro level has to be understood first. This would lead to effectively understand the complexities involved in each individual problem and pave ways for developing better bone substitutes.

I.2 Embryology and Anatomy of the Bone

I.2.1 Development of the skeletal system

The skeleton is a derivative of mesoderm (and some parts of neural crest). It passes through the first, blastemal stage of the mesenchymal condensation, and a second, cartilaginous stage before reaching the final ossification stage. Bone is essentially a highly vascular, living, constantly changing mineralized connective tissue. It is remarkable for its hardness, resilience, characteristic growth mechanism and regenerative capacity.

I.2.2 Organization of the skeleton

Bone has been described as a specialized type of connective tissue, characterized by the presence of cells with long branching process (osteocytes) which occupy cavities (lacunae) and fine canals (canaliculi) in a hard dense matrix consisting of bundles of collagenous fibers in an amorphous ground substance (cement) impregnated with calcium phosphate complexes (Figure I.1). Bone is divided into two forms of structure for easier understanding of their anatomical structure

A. Macrostructure and

B. Microstructure

Figure - I-1

ORGANIZATION OF BONE

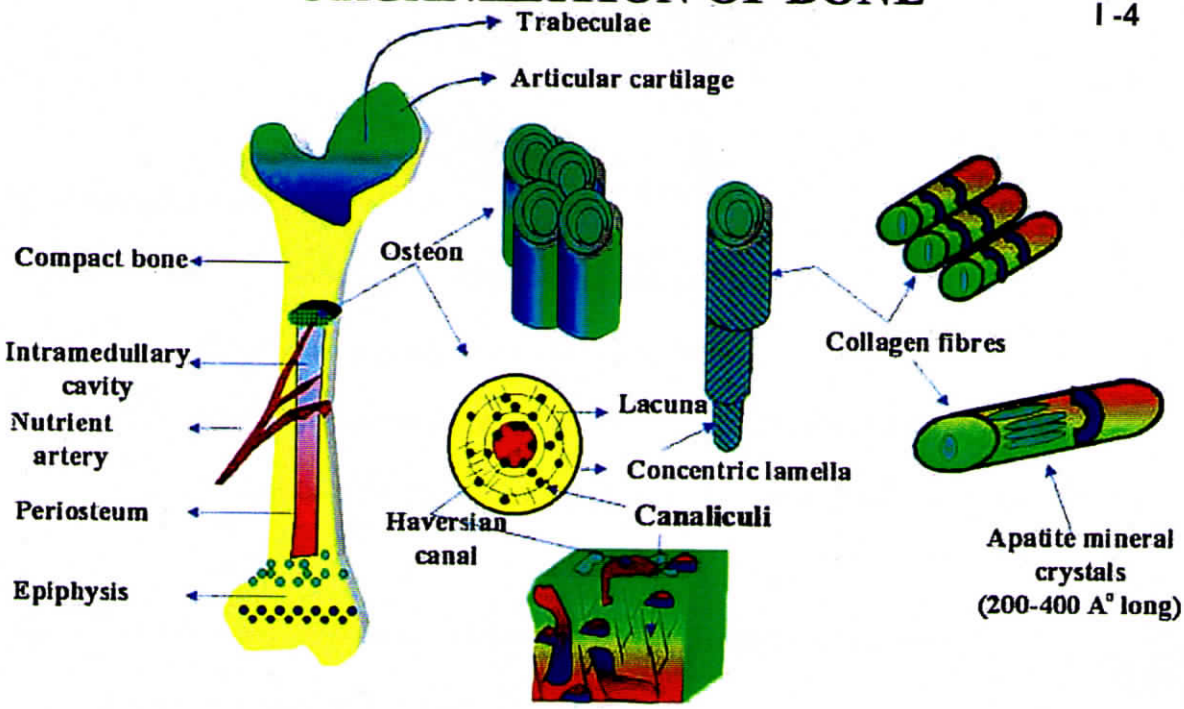

Figure - I-2

FRACTURE REPAIR

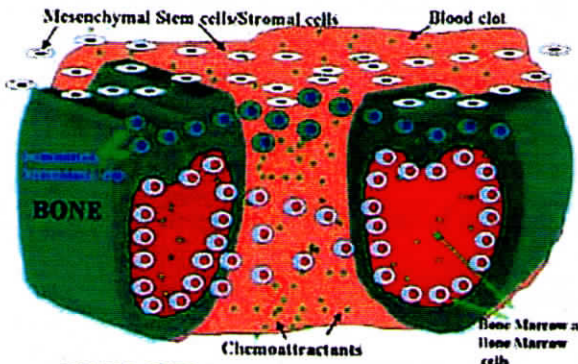

PHASE I : INITIAL SEQUENCE OF BONE REMODELING AFTER A DEFECT/FRACTURE

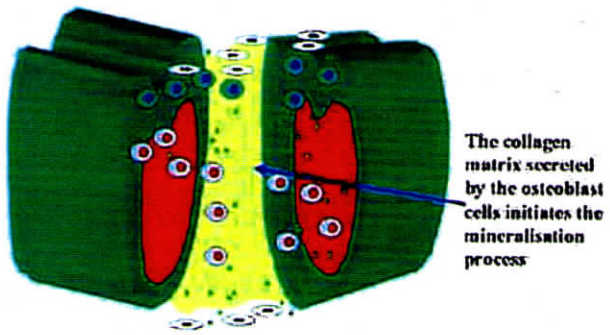

PHASE II : BONE REMODELING AFTER A DEFECT/FRACTURE

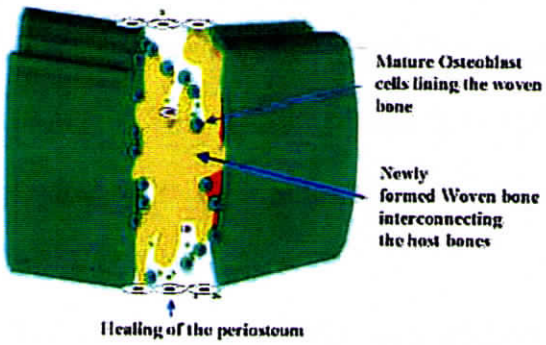

PHASE III : BONE REMODELING AFTER A DEFECT/FRACTURE

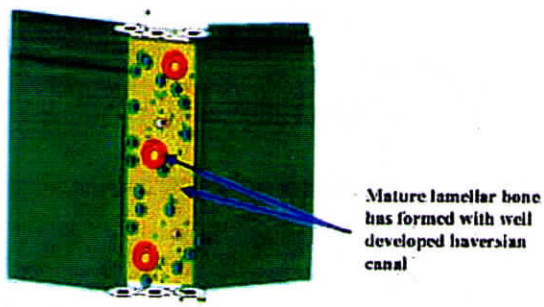

PHASE IV : BONE REMODELING AFTER A DEFECT/FRACTURE

A. Macrostructure

The long bones, e.g. femur are broadly divided into three regions

a. Epiphyses (growing end of the long bones)

b. Metaphysis (transitional region between epiphyses and diaphysis) &

c. Diaphysis (middle compact bone region with a medullary canal or bone marrow

Bone is grouped into three major categories based on its gross appearance

a. Compact bone (*substantia compacta)*

b. Trabecular bone / Cancellous bone / Spongy bone *(substantia spongiosa)* and

c. Chondroid bone (Cartilage bone)

Types of membranes ensheathing the bone

a. Periosteum (outer membrane of the bone, with osteogenic cells, absent in the articular joints)

b. Endosteum (a thin layer of membrane with osteogenic cells lining the inner cavity of the bone in contact with the medullary canal or bone marrow.

Types of bone healing

a. Intramembranous ossification (bone is formed directly)

i) Woven bone (immature bone formed during fracture repair) and

ii) Mature lamellar bone (mature bone with well developed Haversian canal)

b. Endochondral ossification (bone formation takes place in preexisting cartilage)

A. B. Microstructure

The cells associated with bone remodeling - osteoblasts and osteoclasts are phenotypes that are easily recognized and are extensively studied and understood.

I.2.2.1 Osteoblast cells

The cells lining these inactive bone surfaces are best characterized on periosteal surfaces and are most commonly called "bone lining cells", although they have also been described by other names including "inactive osteoblasts", "resting osteoblasts", "surface osteocytes", and "flattened mesenchymal cells" (Miller et al., 1980). While most authors generally accept the name "bone lining cells", it is occasionally used to generically describe all of the bone cells found on a bone surface. Osteoblasts originate from mesenchymal stem cells, which can also give rise to cartilage, muscle, and fat cells, tendon fibroblasts, and possibly other types of fibroblasts (Grigoriadis *et al.*, 1988). Osteoblasts are roughly 20 μm in diameter and actively synthesize many proteins during their developmental and maturation stages. The principal role of these cells is to secrete the matrix framework upon which bone is built. In the active state they appear in histological sections as plump, cuboidal cells lying in a palisade arrangement closely apposed to the bone surface. Active osteoblasts are seen most often in histological sections adjacent to a new osteoid seam. They are rarely seen next to a bare bone surface, since the time interval between cell activation and matrix formation is relatively short. They have eccentric nuclei with prominent Golgi apparatus, and also show abundant rough endoplasmic reticulum and secretory granules. Gap junctions connect the cells with each other and possibly with the more mature osteocytes, which lie within the bone structure. When they are less active, osteoblasts take on a more fusiform appearance and are morphologically similar to fibroblasts lining the bone surface. It is believed that smaller, apparently inactive osteoblasts may still be engaged in bone synthesis, but at a much slower rate. The functional life span of an osteoblast can range between 3 and 18

months with an average of 5-6 months. Osteoblasts are rich in alkaline phosphatase and osteocalcin, both of which may have a role in the mineralisation of the osteoid matrix.

I.2.2.2 Osteocyte cells

As the collagen framework becomes mineralized, some osteoblasts become trapped in the newly formed matrix. These remaining cells, now known as osteocytes, reside in the bone matrix until that portion of bone dies, or is degraded during its normal life cycle. Osteocytes are abundant and easily recognizable being arranged in a relatively ordered fashion, in both cortical and lamellar bone. They provide the bone tissue around them (often deep beneath the surface) with a supply of nutrients from the marrow cavity, by way of cytoplasmic communicating channels known as canaliculi. These channels are never more than a few micrometers apart and represent an effective signaling system. Osteocytes are found in peri-cellular lacunae, small independent regions surrounding each cell. These cells are not capable of division and are lost when the bone in which they reside is degraded - the lifespan of an osteocyte thus being dictated by the lifespan of the bone. The arrangement of these cells with their cytoplasmic communications suggests that they may well be responsible for detecting mechanical strain and organizing bone cell function as necessary.

I.2.2.3 Osteoclast cells

Mineralized bone tissue is degraded by specialized giant cells known as osteoclasts, which originate in the bone marrow. In thin hematoxylin and eosin (H&E) stained sections they appear plump and have abundant foamy eosinophilic cytoplasm. These cells are commonly multinucleate and may reach 100 μm or more in diameter, probably as a consequence of the union of several smaller cells. In addition osteoclasts

contain prominent Golgi apparatus, abundant mitochondria and numerous lysosomes. Osteoclasts are activated in response to low levels of plasma calcium and their reactions to chemical signals such as parathyroid hormone (PTH), di-hydroxy vitamin D and calcitonin, are well characterized. Osteoblasts may also be involved in the activation process. The hallmark of the osteoclast is the high level of lysosomal tartrate-resistant acid phosphatase which when released dissolves the mineralized bone matrix and releases calcium (and other) ions into the circulation (osteoclasts are not active along a non-mineralized bone surface). A characteristic feature of osteoclasts is their close proximity to an eroded bone surface (Howship's lacuna). Electron microscopic studies reveal a distinctive ruffled cell border in the region where these cells are in contact with bone matrix. This may act to increase the surface contact through which they resorb bone. The lifespan of an osteoclast is thought to be in the range of 4 to 6 weeks.

I.2.2.4 Stromal cells

Bone marrow stromal cells are considered to be a heterogeneous population of cells that include cells classified under a number of different names including marrow fibroblasts, reticular cells, dendritic cells, preosteoblasts, vascular pericytes, and in some cases, endothelial cells. One model of the marrow stromal system is that stromal stem cells provide progenitors that are committed to give rise to different cell lines (Owen, 1985), including reticular cells, marrow fibroblasts, and other differentiated cells of the marrow stroma. The precise origin and lineage of hematopoietic stromal cells is, however, controversial and may include some species variability (Perkins and Fleischman, 1988). While endothelial cells are sometimes included as a component of the marrow stromal system, there is little evidence that they arise from stromal stem cells.

The osteogenic precursor cells of the stromal cells are considered as "determined osteogenic precursor cells" if they formed osteogenic tissues without a heterogenic inductive stimulus (Friedenstein 1973). They were considered to be inducible osteogenic progenitors if a heterogenic inductive stimulus was necessary. Inducible osteogenic and chondrogenic precursor cells have been found in other tissues including spleen (Friedenstein, 1973) and embryonic muscle (Nogami and Urist, 1970). More recent studies have demonstrated that marrow stromal cells retain both chondrogenic and osteogenic potential (Ashton *et al.*, 1980) and may conceivably be involved in fracture repair, regeneration of bone and marrow stromal system may also be "determined osteogenic progenitors" and be involved in normal bone remodeling.

I.3 Architecture of Bone

I.3.1 Haversian system

Bones of the mature human skeleton consists of discrete packets or *basic structural units of lamellar bone* (BSUs). Within the diaphyses of long bones of larger long-lived animals they are represented by the Haversian systems (secondary osteons) forming Haversian bone. In adult mammals, regardless of size, similar units of lamellar bone are seen on the periosteal and endosteal cortical and trabecular surfaces; in the diaphyses they are referred to as the external and internal circumferential lamellae. Haversian system is the product of discrete spatially (circumscribed) and temporally (transient) coupled activity of osteoclast and osteoblast populations, forming the basic multicellular unit or *Haversian BMU*.

The structure and the process of formation continue to be a subject of investigation. One of the reasons for this may be that the evolving Haversian system

constitutes a relatively simple *in vivo* model to study the fundamental problems of bone physiology.

Haversian bone consists of a network of osteons aligned parallel to the diaphysis long axis and running a slightly spiral course. Individual osteons are identifiable over the course of several millimeters. Individual osteons measure only a fraction of the total length of the diaphysis (Cohen and Harris, 1958). Consequently, the diaphysis is made of Haversian type of bone tissue. Osteons measure from 200 to 300μm in diameter; the diameter of their central canal varies from 20 to 50 μm and their wall thickness measures up to 80 μm (Johnson, 1964, 1966). Individual osteons are separated from the adjacent tissue by a thin proteinaceous membrane called *cement* or *reversal line*.

The canals are joined every few millimeters by transversally running *Volkmann's canals* together they form a network containing the innervated blood vessels, which communicate both with the blood vessels on the periosteal surface and the bone marrow. Osteons constitute the skeleton's second order structures, the collagen fibers within the lamellae form the third order structure; both the osteons and the lamellae within are aligned parallel to the long axis of the diaphysis.

I.4 Composition of Bone Tissue

Bone is a composite of organic and inorganic phases. Water accounts for approximately 20% of the wet weight of bone whilst about 75% of the dry weight is organic material.

I.4.1 Collagen

Type-I collagen (consisting of two α1 chains and one α2 chain) represents approximately 90% of the organic composition of all bone tissue. Deposition of collagen

in the form of osteoid is the initial event in the bone formation process. There are small amounts of other collagen types in normal bone, but these are present as only a small fraction of the total content. In the normal adult skeleton, collagen is found in layers approximately 3 μm thick on the surface of pre-existing bone, immediately adjacent to the marrow. This lamellar arrangement is normal only after the first few years of life, before this, all newly-formed bone appears as a woven matrix in which collagen fibers are deposited in an irregular mosaic pattern, without any preferential orientation.

I.4.2 Non-collagenous proteins

There are several non-collagenous proteins found in bone, such as acidic glycoproteins, phosphoproteins, serum proteins, lipids, and small proteoglycans. Most of the non-collagenous proteins found in the bone, were thought to be synthesized by specific bone-forming cells known as osteoblasts. Osteocalcin (bone γ -carboxyglutamic acid, BGP) constitutes up to 2% of vertebrate bone protein. The three γ -carboxyglutamic acid residues has a strong affinity for hydroxyapatite. Much of the BGP produced finds its way into the general circulation and is therefore a reliable indicator of osteoblast activity. Another abundant bone protein also synthesized by osteoblasts is osteonectin, which has a molecular weight of around 32,000. It has a strong affinity for both hydroxyapatite and collagen. Osteonectin is also found in platelets. Other less abundant non-collagenous bone proteins include osteopontin (or sialoprotein), some small proteoglycans, bone morphogenetic protein and bone-derived growth factors.

I.5 Bone Mineral

The mechanical strength of bone results from the incorporation of mineral into the osteoid matrix template. This inorganic component, known as "*calcium hydroxyapatite*"

is a crystalline substance, which comprises calcium, phosphate and hydroxyl ions. Apatite is the name given to a group of crystals of the general formula $M_{10}(RO_4)_6X_2$, where R is most commonly phosphorous, M could be one of several metals, although it is usually calcium, and X is commonly hydroxide or a halogen such as fluorine or chlorine. Bone mineral can contain several types of hydrated calcium phosphates, with the most common form being calcium hydroxyapatite [$Ca_{10}(PO_4)_6(OH)_2$]. Trace amounts of magnesium, fluoride, carbonate, citrate and potassium as well as other ions are also found in mineralized bone.

Table. I.1

Composition of Human Bone (Le Geros, 1981)

Ca^{2+}	PO_4^{3-}	Na^+	K^+	Mg^{2+}	CO_3^{2+}	F^-	Cl^-	$P_2O_7^{4-}$	Ash	H_2O	Organic
24.5	10.5	0.7	0.03	0.55	5.8	0.02	0.10	0.05	65	8.7	25

(Note: All the values are given in percentage of total dry weight)

The skeleton is a conveniently accessible source for total body's calcium and other ions, with approximately 98% of the total calcium, 85% of the phosphorus and around 50% of the sodium and magnesium occurring in bones. The exact mechanism of bone matrix mineralisation is highly complex. The chemical composition of bone consists of 25% by weight of organics and the remaining is inorganic matter (Boskey and Posner 1984; LeGeros 1993).

I.6 Calcium Metabolism

Bone in higher organisms represents a sink for most of the Ca^{2+} immobilized as hydroxyapatite. Only a few grams out of a total of about 1250 g circulate in the

extracellular and intracellular fluids. In the extracellular fluid (plasma) about half of the total Ca^{2+} is ionized (free Ca^{2+}), whereas only 0.1 % or less of the total Ca^{2+} is ionized within cells.

"Understanding the complexities of the bone is not complete if the normal bone fracture repair mechanism is not fully understood".

I.7 Fracture Repair

As a consequence of fracture (Figure.I.2), a hematoma results from bleeding within bone marrow, cortical blood supply, periosteal envelopes, and soft tissues. Concurrent with the fracture hematoma is the inflammatory response. Local cell proliferation begins by day one and continues for about three days. On the third day, mesenchymal cells condense and by day five, cartilage formation takes place. Cells such as polymorphonuclear leukocytes, histiocytes, lymphocytes, and mast cells migrate in time dependent waves to remove necrotic debris while endothelial cells proliferate and develop into capillaries penetrating the fracture hematoma. Within the hematoma, degranulating platelets release platelet derived growth factor (PDGF) and transforming growth factor-β (TGF-β) from their alpha granules. These polypeptides are chemoattractants and mitogens that have their initial effect on prefibroblast cell types. Fibroblast phenotypes elaborate a meshwork of loose connective tissue that contains proliferating capillary buds referred to as granulation tissue. The acidic pH and the low oxygen tension within the hematoma result in the development of chondroblastic cells that elaborate hyaline cartilage which calcifies. As the vascular healing response matures, calcified cartilage is degraded and the healing fracture becomes replaced by pre-osteoblasts that differentiate into osteoblasts. The osteoblast cell lines were thought to be

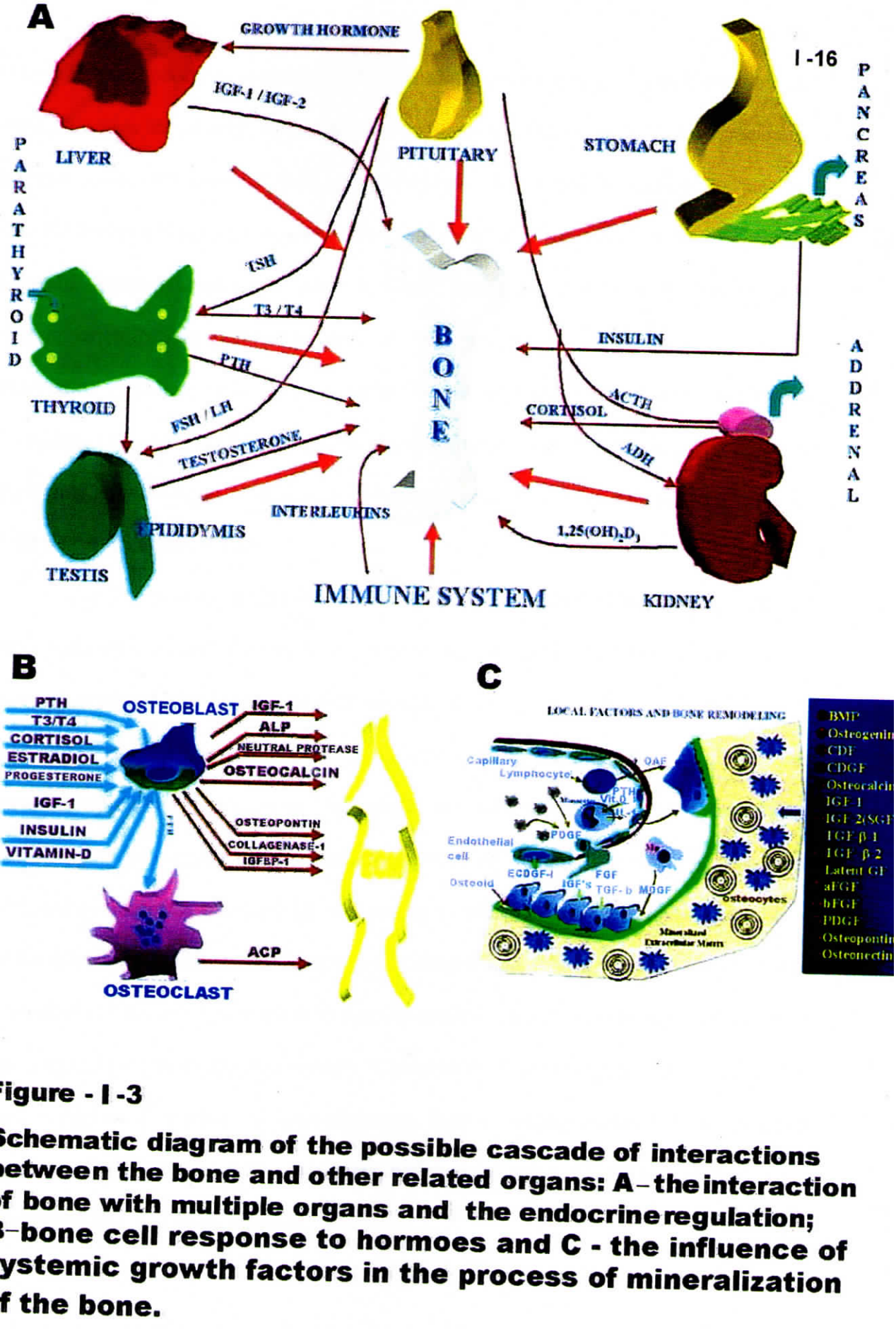

Figure - I -3

Schematic diagram of the possible cascade of interactions between the bone and other related organs: A – the interaction of bone with multiple organs and the endocrine regulation; B – bone cell response to hormoes and C - the influence of systemic growth factors in the process of mineralization of the bone.

originated from pericytes, found in the invading vascular tree (Owen, 1980). Fracture repair, therefore, proceeds in a centripetal direction through the hematoma, developing a bone-like callus that has a contour of greater bone mass and size than the original bone. Despite this added complexity, the cellular events in fracture repair proceed in an orderly and reproducible fashion, leading to the well-defined pattern of repair when viewed in histological sections.

I.8 Vascularity and bone healing

Because of the important role the blood supply plays in the healing process, the vascularity of bone during fracture repair has been extensively investigated. Ham (1930) concluded that interference of the blood supply during fracture repair resulted in cartilage deposits. Others have thought such deposits result from imperfect immobilization (Urist and Mc Clean, 1941).

Rhinelander and Baragry (1962) reported that in the repair of undisplaced closed fractures, periosteal new bone supported by new periosteal capillaries was seen early; a much more abundant proliferative response in endosteal vessels was seen later. Rhinelander (1972) has termed this early increase in periosteal vasculature "extraosseous blood supply", since it is transitory and not conveyed to bone via fascial attachments. The extraosseous periosteal supply is derived from the surrounding soft tissue at the fracture site. During the later phases of repair, even the external parts of the callus were supplied by medullary vessels. In displaced fractures, periosteal vessels appeared to play a larger role, but during the later time periods, medullary vessels once again provided the dominant blood supply. Significantly, the first osseous union following a fracture was always in the medullary callus, never in the periosteal part.

Healing of long bones can be divided into two phases. The initial healing phase leads to the union of the fractured cortical bone and is followed by the second, remodeling phase during which the re-united cortical bone and any callus are extensively remodeled.

I.9 Role of growth factors in fracture repair

Growth factors are operationally defined as agents that increase cell replication, although they may also affect differentiated functions. Most known growth factors are polypeptides synthesized by a variety of cell systems and tissues that act locally or through systemically. Bone is a heterogeneous tissue containing a mixed cell population that includes fibroblasts, osteoprogenitor cells, osteoblasts, bone surface lining cells, osteoclasts and the cells of the marrow tissue. Bone-derived growth factors may originate or affect any of these cells, while bone matrix selectively trap systemic factors, which could then act as putative local regulators of bone growth and remodeling (Figure. I.3).

Growth factors synthesized by macrophages include transforming growth factor–β1 (TGF–β1), the acidic and basic fibroblast growth factors (aFGF and bFGF), as well as interleukins and other cytokines. Platelet degranulation during hematoma formation is also a significant source of growth factors, including TGF–β1 and platelet derived growth factor (PDGF). Other sources of growth factors include osteoblasts (FGF, TGF-b, and PDGF) and the bone matrix itself, which contains high concentrations of FGF and TGF–β. The number of growth factors likely to have a significant role in the regulation of wound repair, osteogenesis, and chondrogenesis is increasing.

Growth factors are synthesized by osteoblasts, macrophages, or chondrocytes and released within the fracture callus. Alternatively, growth factors may be delivered to the fracture callus by the bloodstream, or, more likely, they could be released by platelets into the fracture hematoma. Growth factors may regulate fracture repair by paracrine or autocrine pathways, and can exert a broad spectrum of activities. Consequently, determination of the precise location of different growth factors is important for elucidating its ultimate role. Direct evidence for growth factor regulation can be obtained by adding exogenous factors to specific stages of fracture healing *in vivo* and *in vitro*, or by testing growth factors in models of different aspects of the fracture repair response.

I.10 Bone Mineralization

The factors initiating the deposition of mineral in the calcification of bone are not well understood. Some authors have reported that the first phase that appears in the mineralisation of extracellular matrix vesicles in the growth plates of long bone is amorphous calcium phosphate, while others report HA as the first phase. Many theories have been proposed to explain the initiation of mineralisation, including local elevations of phosphate via hydrolysis of organic phosphates by alkaline phosphatase, enzymatic removal of inhibitors of mineral deposition, and direct nucleation of hydroxyapatite or other calcium phosphate minerals onto bone collagen fibers. However, it should be noted that most of the published work state that the mineral deposited in ossification is formed by epitaxial growth on existing crystals. Clarke et al., (1993) reported on the nucleation and kinetics of growth of phosphate on Type-I collagen and HA at different concentrations, acidities and temperatures, with special emphasis on the crystallographic characteristics of crystals obtained.

Ebrahimpour, Perez and Nancollas (1991) have demonstrated the possibility of calcium oxalate monohydrate (COM) growth on HA and showed that the human serum albumin promoted the growth, while citrate and magnesium acted as inhibitors.

In mature bone, the apatite crystals are observed as irregularly shaped thin plates or rod like structures of carbonate apatite that are rarely stoichiometric or structurally perfect, and are typically 450 A° to 500 A° in length, up to 250 A° in width and with thickness of 20 A° to 30 A° (Weiner, Arad, and Traun 1991). Regardless of which model is correct, the apatite of bone should be accepted as a living mineral since it undergoes continual growth, dissolution, and remodeling involving mineralisation and resorption. The structure and mechanical properties of bone are derived from the organized mineralisation of hydroxyapatite within a matrix of collagen fibrils, proteoglycans, and many other proteins. The combination of the organized structure of the collagen and the hardness of the apatite gives bones its desirable mechanical properties. The mineralisation occurs within holes between adjacent collagen molecules and the plate like crystals are crystallographically oriented in parallel arrays across the fibrils. As early as 1926, bone, tooth, enamel, and dentine were observed to have XRD patterns similar to those of mineral apatites, while urinary or dental calculi and abnormal calcifications in soft tissues have been identified as apatite or apatite-like materials (LeGeros 1991).

From a chemical perspective, it is now quite well established that kinetic factors may be considerably more important in determining the nature of calcium phosphate phases present during a precipitation reaction than considerations based solely upon equilibrium data (Brown and Fulmer, 1991). The initial formation of an amorphous calcium phosphate (ACP) at high pH may be followed by its transformation to HA via

the formation of octacalcium phosphate (OCP), which may serve as template for HA growth. As the acidity of the solution is increased, other precursor phases such as dicalcium phosphate dihydrate (DCPD) may precipitate in accordance with Oswald's rule, which predicts that the least stable phase having the highest solubility is formed preferentially during a sequential precipitation. It has also been shown by Nancollas (1982a) and LeGeros (1981) that different calcium phosphate phases may be stabilized or destabilized by the presence of various cations and anions, which may not be significantly incorporated into the calcium phosphate crystal lattice, but may markedly influence nucleation and subsequent growth processes. Another complicating factor in the mechanism of calcium phosphate crystallization is that mixed solids may form by the growth of one phase upon another in the metastable supersaturated solutions. The formation of these solid phases in supersaturated physiological fluids such as serum and saliva is mediated not only by biological restraints, but also by the nucleation and growth mechanisms. It is also important to consider both the role and the effect of the organic matrix in the nucleation and growth of the apatite crystallites in biological environments.

I.11 Bone mineral disorders

Skeletal formation and resorption are coupled by concerted actions of osteoblasts and osteoclasts. The osteoblast and osteoclast cells are in turn regulated by hormones and a series of systemic as well as local growth factors, any abnormal actions may lead to disorders of bone such as, rickets, osteomalacia, parathyroid bone disease, Pagets disease, osteoporosis, osteogenesis imperfecta and osteopetrosis.

The characteristic skeletal disturbance in Vitamin D deficiency and in some other metabolic disorders is osteomalacia, which means "soft bones". The malacic bone is

subjected to distortion in shape and to fracture, deformity is particularly likely to develop with vitamin D deficiency in infancy and childhood and in adults it causes less severe clinical features.

Osteitis fibrosa cystica is the characteristic bone abnormality of primary or secondary hyperparathyroidism. It is manifested as generalized osteopenia, increased bone resorption and the formation of cysts or cyst-like areas (brown tumors).

Renal osteodystrophy is a major complication of chronic renal failure. The longer life is preserved, as by hemodialysis, the greater the osteodystrophy. Renal osteodystrophy is a complex disturbance of bone comprising varying degrees of osteomalacia, osteitis fibrosa cystica, and osteosclerosis. The etiology is not completely understood, but impaired vitamin D metabolism, secondary hyperparathyroidism, diminished gastrointestinal absorption of calcium and some times aluminium toxicity (dialysis) are involved.

Pagets disease or Osteitis deformans affects 3 % of people older than age 40. This is due to disordered bone remodeling and caused by abnormalities in collagen structure and calcitonin deficiency. A genetic basis is also suggested.

Osteoporosis is a state of reduced bone mass per unit volume with a normal ratio of mineral to matrix. The risk of fracture with minimal trauma is increased in osteoporotic bone, and this risk correlates with the degree of reduced bone mass. Bone mass is lost in almost all persons older than age 50, and a high percentage of the population older than age 70 is at risk for fracture. Bone remodeling is normally regulated by systemic and locally produced agents and metabolic, nutritional, and mechanical factors; it is not surprising that osteoporosis can be due to diverse disease

process. Endocrine abnormalities like glucocorticoid excess, thyrotoxicosis, hypogonadism, hyperprolactinemia, diabetes mellitus, and hyperparathyroidism. Malignant diseases like multiple myeloma, leukemia, lymphoma and mastocytosis. Heparin, ethanol, smoking, dietary habit can also induce osteoporosis.

Substantial knowledge has accumulated in recent years concerning the regulation of bone cells and their functions. The understanding from these findings should lead to the development, maintenance and repair of skeleton and also for treatment and prevention of skeletal disorders

I.12 Bone grafts

Employment of surgical implants is known since the pre-Christian era. Historical records from implantation of natural minerals gemstones goes to the period 600-800 A.D (Epstein, 1989), ivory, inert metals, and bone products (Ludwigson 1964)

I.12.1 Biocompatibility of Implant

Definition

"Biocompatibility is the ability of a material to perform with an appropriate host response in a specific application" (Williams, 1987).

There are three classes of materials: metals, polymers, and ceramics, which are widely used in orthopaedic trauma care.

Metals such as titanium, stainless steel (316-L SS), titanium alloy (Ti 6Al4V), and cobalt-chrome alloys are inert but in wear situations, some solubility and tissue reaction does occur. The organic polymers such as ultra high molecular weight polyethylene (UHMWPE) are chosen for their minimum tissue response. Ceramic components such as

alumina and zirconia are bioinert. As such, all the inert materials are foreign bodies and are walled off by a thin fibrous capsule. The better materials have thinner capsules. However, there is not a direct bond of osseous tissue to the implant. Such implants are successful only if the remaining tissue continues to support it. This will be time dependent because any movement of the prosthesis will increase the thickness of the fibrous capsule, leading to more movement and progressive failure.

The current tendency to employ ceramics that surpasses other materials in orthopaedic surgery is due to their good biocompatibility property to the host tissue after implantation, with negligible foreign body reaction even though they are brittle. Ceramics by nature do not suffer from corrosion, as do metals and plastics.

I.12.2 Ceramics

The transformation of clay by fire into ceramic pottery brought about a revolution in human civilization thousand of years ago. Ceramics and glasses had been used for a long time outside the body for a variety of applications in the health care industry: eyeglasses, diagnostic instruments, chemical ware, thermometers, tissue culture flasks, chromatography columns, lasers and fiber optics for endoscopy.

I.12.3 What are bioceramics?

Ceramics that are specifically designed, synthesized and fabricated for the repair and reconstruction of the diseased, damaged or worn out parts of the body for a short term (bioresorbable) or long term (as a scaffold) within the living tissue with chemical, physical and mechanical properties making them suitable as an ideal implant, are known as bioceramics.

Materials that are not inert but are not walled off by a fibrous capsule and have desirable tissue response are the choice of researchers and clinicians. The only known materials of this nature are calcium phosphates, because of their close chemical similarity towards the bone mineral.

Over the years, bioceramics such as calcium phosphate ceramics, bioglass and glass-ceramics have found extensive use as a hard tissue replacement material all over the world and is an emerging area of research with immense clinical applications.

I.12.4 Are bioceramics confined to hard tissue replacements alone?

Most clinical applications of bioceramics relate to the repair of the skeletal system composed of bones, joints and teeth, and to augment both hard and soft tissue responses. Ceramics are also used to replace different body parts especially: artificial blood vessel, artificial trachea, drug delivery systems, catheters, percutaneous devices, dental materials/implants and special formulations of glasses are also used therapeutically for the treatment of tumors (Aoki, 1994). Ceramics are used widely in dentistry as restorative materials, gold porcelain crowns, glass-filled ionomer cements, endodontic treatments, dentures etc. Ceramics are used in the form of bulk materials of a specific shape called implants, prostheses, or prosthetic devices. Bioceramics are also used to fill bone defects, while the natural repair process restores the defect. In other situations, the ceramic is used as coating on a substrate, or as a second phase in a composite, combining the characteristics of both into a new material with enhanced mechanical and biochemical properties. Bioceramics are also used in neurosurgery for cranioplasty repairing the skull bone defects (Kobayashi *et al.*, 1987), in hand arthroplasty of the metcarpophalangeal joint (Minami *et al.*, 1988), in otolaryngology as implants in the middle ear (Grote *et al.*,

1986), or the use of bioglass or hydroxyapatite materials in the treatment of vocal cord paralysis. In Urology, an injectable form of non-degradable bioglass has been bonded to the soft tissues of the bladder for use as a potential treatment for urinary incontinence (Wilson *et al.*, 1991). Some therapeutic applications involve the use of yttria in a glass-ceramic for localization of radiation at a tumor site. Bioactive glass containing magnetite can be used to kill bone tumors when a magnetic field is applied (Ikenga *et al.*, 1991). Ceramic implants can also be used as drug delivery systems (Snow *et al.*, 1989; Bajpai and Benghuzzi 1988).

I.12.5 Bioceramics: One material several applications?

Bioceramics of one type alone cannot compensate for different types of degenerating bone disorders like, periodontal disease, osteoarthritis, rheumatoid arthritis, bone cancer, avascular necrosis, as well as trauma have increased the need for a suitable bone substitute or a stimulant for osteogenesis. Calcium phosphate ceramic materials has to be produced with varying Ca/P ratios. Since, the Ca/P ratio for bone is 1.77, for dentine the ratio is 1.58, and for tooth enamel it is 1.64 (Drissens, 1980). The most commonly used synthetic calcium phosphate bioceramic material is calcium hydroxyapatite. Hydroxyapatite and other calcium-based ceramic materials can actively encourage bone regeneration at the surface of an implant. Bonfield *et al.*, (1991) have shown the *in vivo* epitaxial growth of natural hydroxyapatite mineral over synthetic hydroxyapatite implant using High Resolution Transmission Electron Microscope (HRTEM) studies. It has been postulated that the use of calcium phosphate ceramic biomaterials might replace the use of autogenous bone grafts in orthopaedic surgery.

Bioceramics are made in many different forms (powder, coating or bulk) and phases of single crystals (Sapphire), Polycrystalline (Alumina or Hydroxyapatite), glass (Bioglass®), glass-ceramics (A-W glass-ceramic) or Composites (Polyethylene-Hydroxyapatite). The phase or phases used depend on the properties and function required

There has been a tremendous increase in the application of bioceramics after 1990's. Concepts of ceramic-polymer, ceramic-metal, ceramic-ceramic composites and ceramics in tissue engineering, gene delivery system and stem cells has opened up new areas of research with bioceramics.

I.13 Synthesis and Microstructure of Bioceramics

The objective of ceramic processing is to make a specific form of the material that will perform a specific function. This requires making a solid object, a coating or particulates (powders). There are two ways of making a specific shape; casting from the liquid state or pre-forming the shape from fine-grained particulates followed by consolidation. When a shape is made from powders, it is called *forming*. The powders are usually mixed with water and an organic binder to achieve a plastic mass that can be cast, injected, extruded or passed into a mold of the desired shape. The formed piece is called *green ware*. Subsequently, the temperature is raised to evaporate the water (drying) and the binder is burned out, resulting in bisque ware. The bisque-fired article is later fired at higher temperature to get dense article. This high temperature heat treatment is called sintering. Properties of this final sintered ceramic depend upon the composition of the material, the phases developed during thermal processing and the microstructure of the material.

Table. I.2

Type of Ceramic Processing	Example
1. Wet chemical method	HA
2. Hydrothermal method	HA (Single crystal)
2. Glass	45S5 Bioglass®
3. Cast or rapidly solidified polycrystalline ceramic	HA Coating
4. Polycrystalline glass-ceramic	Ceravital ®
5. Liquid-phase sintered (vitrified) ceramic	Glass-HA
6. Solid-state sintered ceramic	Alumina, Zirconia
7. Hot pressed ceramic or glass-ceramic	A-W Glass-ceramic
8. Sol-gel glass or ceramic	52S bioactive gel-glass
9. Multi-phase composite	PE-HA

A variety of crystalline calcium phosphate compounds can be produced by precipitation; these include monetite, brushite, whitlockite, hydroxyapatite, and defective forms of hydroxyapatite. Amorphous calcium phosphate is considered to be very finely dispersed form of whitlockite (Meyer and Eanes 1978).

Bioceramic materials are categorized based upon processing method applied and the microstructure produced; i.e., the distribution of phases developed in the material. The difference in the microstructures of the materials are primarily due to the different starting materials and thermal processing steps involved in making the materials.

I.14 Hydroxyapatite Synthesis

Calcium phosphate polycrystalline ceramic materials can be produced by precipitation from aqueous solutions (Jarcho, 1976) and by solid-state reactions (LeGeros, 1967). Materials produced by precipitation from aqueous solution may contain varying amounts of H^+ and OH^- ions in addition to the water; this can be controlled and removed by use of hydrothermal techniques (LeGeros, 1991) at temperatures between 100°C and 1000°C. A chemically pure form of hydroxyapatite $Ca_9 (PO_4)_5(HPO_4) (OH)$ can be produced by subjecting either an unstable precipitate of defective HA or a high temperature product of tetracalcium phosphate $Ca_4 (PO_4)_2O$ to hydrolysis at temperatures up to 90°C (Driessens, 1983). The chemical stability of HA during heat treatment at high temperature at 1300 °C is usually considered as the maximum sintering temperature because, HA dissociates around this temperature into tricalcium phosphate and tetracalcium phosphate (Peelen *et al.*, 1978; and de Groot 1980).

The structure of calcium hydroxyapatite showing the exact atomic positions in the crystal was determined by Beevers and Mc Intyre (1956) and later defined by Kay *et al.*, (1992). Calcium hydroxyapatite crystal belongs to the hexagonal systems, with a space group, $P6_3/m$. This space group is characterized by a six-fold c-axis perpendicular to the three equivalent a-axis (a_1, a_2 and a_3) at angles 120° to each other. The smallest building unit, known as the unit cell, contains a complete representation of the apatite crystal, consisting of Ca/PO_4 and OH groups closely packed together in lattice.

Based on precise and well-defined physicochemical studies, the pure synthetic hydroxyapatite is, therefore, substituted for bone mineral. These controlled studies do not, however, necessarily represent a phenomenon as it may occur on the bone mineral.

Even for pure and well-characterized substances, the crystallographic or geometrical structure and even the chemical nature of the surface may be different from those of the bulk crystal. The evolution of HA is given in Table. I.3.

Table. I.3

EVOLUTION OF HYDROXYAPATITE (HA) IMPLANTS

Year	Event
1971	Suggested use of HA as bone and tooth implant
1974	Suggested use of HA as orthopaedic implant
1975	Suggested use of HA as periodontal treatment
1976	Development of process for preparing dense polycrystalline HA
1976	Use of HA as loaded tooth roots in animals
1977	Bonding of bone to HA
1978	Use of HA powder for periodontal treatment
1979	Clinical application of HA dental root implants in Europe
1980	Role of macro and microporosity in resorption rate and biological response of HA identified
1980	Clinical trials of HA powder in alveolar ridge augmentation
1980	Use of HA powder to stimulate bone growth in porous metal implants
1981	Clinical applications of HA loaded tooth implants in Japan
1981	Clinical use of dense HA in middle ear canal wall prosthesis

From Hulbert, S.F., Bokros, J.C., Hench L.L., Wilson J., and Heimke, G., Ceramics in clinical applications, past, present and future in *Proc. World Congr. On High Tech Ceramics*

I.14.1 Porosity

The most widely used process to fabricate porous hydroxyapatite implants utilizes isostatic compaction and sintering of calcium phosphate powders that contain naphthalene particles (Hubbard, 1974). Sublimation of the naphthalene particles leaves a porosity (100 μm), which consists of spherical voids communicating by a narrow-necked aperture where the particles were in contact. Macropores are created by sintering the material with hydrogen peroxide (Klein *et al.*, 1989).

I.15 BIOACTIVE GLASS SYNTHESIS

Sol-gel processing is a chemical crystallization method for producing ceramics, glass, glass-ceramics and composites at much lower temperatures than the conventional ceramic processing. It was Iler (1979), Brinker and Scherer (1990), and Hench and West (1990) described the history, theory, processing details and applications of sol-gel processing. The sol-gel method was first employed by Jarcho (1981) to synthesize hydroxyapatite. Subsequently, this technique was adopted by others to synthesize glass and glass ceramics.

Methods involve in synthesizing sol-gel materials:

1. Gelation of colloid powders
2. Hypercritical drying
3. Controlled hydrolysis and condensation of metal alkoxide precursors followed by drying at ambient temperature.

All the three methods involve creation of a three-dimensional, interconnected network, termed a gel, from a suspension of very small colloidal particles, called a sol. Colloids are solid particles with diameters < 100 nm. A sol is a dispersion of colloidal particles in a liquid. A gel can be formed from an array of discrete colloidal particles by changing the pH of the sol. The gel network can also be formed from the hydrolysis and condensation of liquid metal alkoxide precursors. The history of bioactive glass evolved is given in Table.I.4.

Table. I.4

EVOLUTION O F BIOACTIVE GLASS AND GLASS-CERAMIC IMPLANTS

Year	Event
1969	Evidence of bone bonding to bioactive glass and glass ceramic (45S5 Bioglass [R])
1973	Mechanism of bone-bioactive glass bond identified
1973	Bone bonding of bioactive glass ceramic in Europe (Ceravital R)
1975	Successful load-bearing orthopaedic prosthesis in monkey using 45S5 Bioglass
1976	Compositional profiles of bioactive glass (45S5 and 45S5F) dental implants in baboon
1980	Comparative histology of implants of variable bioactivity
1981	Ultrastructure analysis of bioactive glass-ceramic and bone
1981	Successful completion of toxicology and biocompatibility tests of bioactive glasses (45S5 Bioglass R) and first evidence of soft tissue bonding
1981	Clinical use of bioactive glass-ceramic (Ceravital R) in middle ear prosthesis
1982	Successful comparison of bioactive glass middle ear ossicular replacement with other inert implant materials
1982	FDA approval of bioactive glass-ceramic (Ceravital R) middle ear devices
1982	High-strength bioactive implant material (A/W-glass ceramic) and vertebral prosthesis
1983	Machinable bioactive glass-ceramic
1984	FDA approval of bioactive glass (45S5) as middle ear prosthesis
1986	Successful clinical trial of bioactive glass implants (45S5 Bioglass R) for alveolar ridge maintenance.

From Hulbert, S.F., Bokros, J.C., Hench L.L., Wilson J., and Heimke, G., Ceramics in clinical applications, past, present and future in *Proc.World Congr. On High Tech Ceramics*

I.16 Material Characterization

Once the material is synthesized, it is essential to characterize the material for its properties before the intended *in vivo* application. "*Characterization*" has been defined by the Materials Advisory Board of the National Research Council in United States as:

"***Characterization describes those features of the composition and structure (including defects) of a material that are significant for a particular preparation, study of properties, or use, and suffice for the reproduction of the material***"

I.16.1 Characterization for the materials are classified into five major aspects:

a. Chemical composition: (Gravimetric Analysis/ Atomic Emission Spectroscopy, Atomic Absorption Spectroscopy, Energy Dispersive X ray Analysis (EDAX))

b. Phase state and structure: (X-Ray Diffraction)

c. Size, shape, and surface of particulates

d. Microstructure: (Optical/Scanning Electron Microscopy)

e. Surface processes: (Fourier Transform Infrared Spectroscopy, Scanning Electron Microscopy with Energy Dispersive X-ray Spectroscopy, Electron Microprobe Analysis, Auger Electron Spectroscopy, Secondary Ion Mass Spectroscopy, Atomic Force Microscopy).

I.17 How to choose a ceramic implant for an appropriate *in vivo* response

When used as substitutes for natural tissues like bone, ceramics may be required to

1. Restore function of surrounding tissues,
2. Fill a space,
3. Physiologically interact with the body fluids and should not elicit toxic reactions upon degradation.
4. Stimulate osteogenesis, provide strong bonding with the implant and the newly formed bone and host bone, without intervening fibrous tissue formation.
5. Provide permanent stress-bearing skeletal repair and
6. Should degrade over a period of time and completely replaced by the host bone.

I.18 Apatite formation and bone mineralization - is there any relationship?

Calcium phosphate and glass ceramics (bioceramics) that are extensively explored as synthetic bone-graft materials in dental and orthopaedic applications are hydroxyapatite (Passuti *et al.,* 1990), bioglass (Schepers *et al.,* 1993), apatite wollastonite (Kitsugi *et al.,* 1989), β-tricalcium phosphate (β-TCP) and biphasic calcium phosphate (BCP), (Denissen and de Groot, 1979; Jarcho, 1981; Holmes and Hagler, 1988; Daculsi *et al.,* 1989; Daculsi *et al.,* 1990). Chemical reactions occurring on the ceramic surfaces play a significant role in the bone- bonding mechanism (van Blitterswijk *et al.,* 1985), because the crystal chemistry of the ceramic surface and the chemical constituents of the surrounding extracellular fluid in unison determines the nature of the solids to be formed on the surface of the material. Over the past decade of ceramic research, it is apparent that different bioactive ceramics undergo different mechanisms of apatite formation by interacting with the surrounding physiological medium and likewise it is possible to improvise surface apatite layers on a range of bioceramics through chemical interactions with simulated body fluid.

There are many controversies regarding the bioresorbability of HA, while that of TCP is unambiguously demonstrated both *in vitro* and *in vivo* (Jarcho, 1981). When HA and TCP were exposed to Ca^{2+} and PO_4^{3-} free environment, dissolution of both ions occurred, but to a lesser degree with HA. Among the various calcium phosphate ceramics studied, dense and stoichiometric hydroxyapatite dissolved the slowest (Ducheyne *et al.,* 1993). This could be attributed to the material preparation methods and their chemical composition. After implantation of the calcium phosphate ceramics in osseous or non-osseous sites [Heughebaert (1988); Neo (1993)] or after incubation in various solutions

(Hyakuna *et al.*, (1990), dissolution of the material causes supersaturation of Ca^{2+} and PO_4^{-3} ions in the local environment, resulting in the precipitation of carbonated apatite microcrystals in the microporosity of the ceramic surface and subsequent intimate association with an organic matrix leading to new bone formation. Calcium phosphate is observed to decrease in solubility in the order - brushite > monetite > octacalcium phosphate > β-TCP > hydroxyapatite

I.19 Glass ceramics

For materials, such as bioglasses, it has been concluded [Hench (1991); Kokubo (1993)] that immersion in simulated body fluids (SBF) can cause exchanges of cations such as Na^+ and K^+ with H^+ and H_3O^+ ions from solution, at the glass surface leading to loss of soluble silica and the formation of Si-OH (Silanols) at the glass-solution interface. This stage is followed by migration of calcium and phosphate ions through the silica rich layer to the surface and the formation of an amorphous calcium phosphate layer, which can then crystallize by the incorporation of hydroxyl, carbonate or fluoride ions to create the respective apatite layer.

I.20 Hydroxycarbonate Apatite (HCA)

The formation of the "*biological apatite*" (Hydroxycarbonate-apatite) on the surface of implanted synthetic calcium phosphate ceramics and bioactive glasses through a sequence of chemical reactions may be one of the events leading to bonding with bone (Jarcho, 1981); Hench *et al.*, (1988); Fuji *et al.*, (1983); Gross *et al.*, 1988; Kokubo, 1990). CHA can form directly by precipitation or indirectly by hydrolysis or from precursor phases. Thus, suspension of amorphous calcium phosphate (ACP); monobasic calcium phosphate (MCP), dicalcium phosphate dihydrate [(DCPD)-$CaHPO_4.2H_2O$],

anhydrous [(DCPA)-$CaHPO_4$], octacalcium phosphate [(OCP- C_8H_2 $(PO_4)_6.5$ H_2O], in CO_3^{2-} containing solutions; or suspension of calcium carbonate $CaCO_3$, or calcium fluoride (CaF_2) in solutions containing HPO_4^{2-}/PO_4^{3-} and CO_3^{2-} ions resulted in CHA formation (Le Geros 1965; Okazaki *et al.,* 1981; Le Geros *et al.,* 1989; and Meyer *et al.,* 1994). It has been suggested that the bond strength between bone and bioactive material is determined by the rate of formation of apatite (Fujiu *et al.,* 1983). Although conclusive evidence is not currently available, it is hypothesized that one of the mechanisms underlying the phenomena of bioactivity with respect to bone mineralization and bone tissue bonding could be due to the dissolution of ions from the ceramics. The dissolution and precipitation of the ions might initiate the early organic matrix deposition, mineral precipitation and subsequent bone formation. Although the morphology and chemical components of the precipitate microcrystals are close to that of bone apatite crystals, their formation is due to the secondary nucleation (by proteins) following dissolution-precipitation process and not to an osteogenic property of BCP ceramic (Daculsi *et al.,* 1990). The dissolution-precipitation process could thus be a factor in improving the mechanical properties of implanted ceramics due to their chemical bonding to the host bone (Trecant *et al.,* 1994).

I.21 Role of hydrogen ion concentration (pH) in apatite formation

The hydrogen ion concentration (pH) 9 – 10.5 influences the ceramic-SBF interfaces on HA formation and it is well known that HA is formed at pH values greater than 8. A buffered solution is the one, which resists changes by minimizing the effects in pH, when the solution is exposed to acids or alkalis. Each buffer is only effective over a rather narrow pH range, and so different buffers are used at different pH values.

and so different buffers are used at different pH values. The intracellular environment in most systems has a pH that is near to 7.0 i.e. neutrality. Both the hydrogen and hydroxide ions are very reactive and have many damaging effects on biological structures and processes. Quite small changes in pH can bring about profound disturbances in biological systems. The pH of blood is usually about 7.4 and a relatively small shift in pH to 7.1 or 7.6 can elicit the clinical conditions of acidosis or alkalosis. Very few biological process, whether *in vivo* or *in vitro* are unaffected by pH changes. Because of the logarithmic nature of the pH scale, a change in pH of one unit is equivalent to a 10-fold increase or decrease in hydrogen ion concentration. The structure of the water molecule makes it efficient to interact with charged ions. The stronger the ion, the more is its ability to interact with water. Therefore, pH forms an integral part of the design of all experiments.

I.22 Proteins

In vivo the dissolution -precipitation process is not simply the end result of the precipitation of inorganic crystals from a supersaturated solution in the microenvironment containing the organic molecules. In fact, biological factors such as protein and enzymes in the vicinity of the implant *in vivo* are important in establishing the density, size, shape, and orientation of precipitated microcrystals (Orly *et al.*, 1989; Martin *et al.*, 1994). Proteins play a dual role in mineralisation, depending on their concentration and whether they are immobilized or free in solution, they could promote crystal nucleation by serving as nucleating agents or inhibit crystal growth through binding to certain crystal planes [Fisher *et al.*, (1985); Boskey (1996)]. Proteins contain many groups that can gain or lose hydrogen ions; when they do so, can acquire new structures that have quantitative or qualitative differences in biological activity. As a function of their concentration and

mobility, these proteins could nucleate, inhibit, or promote apatite formation and growth (Boskey, 1996). Proteins could also bind to the crystal surface of the ceramic and control secondary nucleation, thereby affecting the dissolution, re-precipitation process in the ceramic. They could also act as nucleator of mineral crystals and the protein matrix provides a protected, stable environment in which the crystal nucleus forms. Nucleation occurred when the proteins were adsorbed into a rigid substrate whereas, inhibition of crystal growth occurred when the proteins interacted with a previously formed crystal (Addadi and Weiner 1985). Many specific and non-specific proteins have been considered as possible candidates for the control of bone mineralisation.

I.23 *In vitro* Evaluation of Biomaterials

The cell/material compatibility has to be assessed for any material before the intended *in vivo* application. The preliminary study is designed to rule out the acute toxicity or cytotoxicity (level - 1) of materials, regardless of their final use. Then, the materials that were non-toxic are further inspected by cytocompatibility tests (level - 2). At this stage, the responses more specific to the materials are examined; the changes in cell functions following contact with the material are investigated.

I.24 Cell culture

The use of mammalian cell cultures for assessing *in vitro* biocompatibility offers many advantages; cells are extremely sensitive to toxic agents and the biological responses is well understood at the cell level, and thereby the material can be avoided if toxic, which may elicit chronic inflammatory reaction when implanted *in vivo*.

I.24.1 Cell type

The established cell lines, either commercially available or following subculture of primary cells, are recommended by most cytotoxicity evaluation protocols.

I.25 Cytotoxicity Evaluation

The cytotoxicity tests essentially consist of the assessment of cell morphology and viability; cells killed or injured by materials are examined and, if possible, quantified using relatively uncomplicated testing methods. Both primary and established cells are used.

Examination by light microscopy, electron microscopy, and recently by means of quantitative imaging allows the cell morphological changes and cell death to be observed. The uptake or exclusion of a vital stain (neutral red, Trypan blue, erythrosin B, etc.), by checking the membrane permeability, provides an index of cell viability. A cell's ability to adhere onto material surfaces is generally considered as a sign of compatibility, even though the failed adhesion of a cell type does not necessarily indicate toxicity of the material.

Methods yielding qualitative results are preferred. The neutral red uptake can be measured spectrophotometrically to express cell viability, while tetrazolium salt reduction (MTT test) was shown to be able to measure cell activation. Membrane integrity can be monitored using a variety of methods, including those involving intracellular lactate dehydrogenase, lysosomal enzymes, chromium 51 and fluorescein diacetate (FDA) release, and ethidium bromide uptake.

Cell growth in the presence of biomaterials can be measured by direct cell enumeration, protein content measurement and crystal violet or methylene blue staining

or tritiated thymidine uptake. The DNA of cells can be quantified through the intercalation of diaminobenzoic acid or bis-benzimide. The validity of these types of assay should be always established by comparison with the more direct visual methods.

I.26 Cytocompatibility

Cells isolated from bone are used to study the interactions with the materials to be implanted in bone. Osteoblasts come from both animals and humans (Chicken, rat-embryo calvaria; periosteum; cancellous bone). Some established lines of osteoblasts come from either humans, like MG-63, HOS, SaOS2, or animals, like rat ROS 17/2 and mouse MC3T3/E1.

The biocompatibility of biomaterials is very closely related to cell behaviour on contact with them and particularly to cell adhesion to their surface. Surface characteristics of materials, whether their topography, chemistry or surface energy, play an essential part in cell adhesion on biomaterials. Thus attachment, adhesion and spreading belong to the first phase of cell/material interactions and the quality of this first phase will influence the cell's capacity to proliferate and to differentiate itself on contact with the implant.

The term adhesion in the biomaterial domain covers different phenomena: the attachment phase, which occurs rapidly and involves short-term events like physicochemical linkages between cells and materials involving ionic forces, van der walls forces, etc. and the adhesion phase occurring in the longer term and involving various biological molecules: extracellular matrix proteins, cell membrane proteins, and cytoskeleton proteins which interact together to induce signal transduction, promoting the action of transcription factors and consequently regulating gene expression.

Bone cell cultures have been intensely used for evaluating the biocompatibility of implant materials and are of great interest in studying the step-by-step interactions occurring at the cell-material interface (Gregoire *et al.*, 1990). However, to validate an *in vitro* model system, the mineralization process must occur by the same mechanisms that have been demonstrated *in vivo*.

I.27 Why implantation studies are essential?

Due to the inherited limitations of the cell culture systems, animal implantation studies are needed in order to assess the histotoxicity and histocompatibility of the materials. Implantation permits assessment of local pathologic effects on living tissue, at both the gross level and microscopic level, of sample material that is surgically implanted or placed into an appropriate site (ISO Document 10993-1). Histotoxicity and histocompatibility are usually assessed by heterotopic or orthotopic implantation.

I.28 Heterotopic Implantation Studies

"Heterotopic implantation refers to the inserting of an implant not intended for the host bed but for different tissue".

Materials to be tested are usually implanted subcutaneously (mainly rats) or by creating a pouch in the muscle (rabbits).

The interpretation of results from soft tissue implants is based on the knowledge of the healing process in surgical wounds in the experimental animal and following implantation. The events occurring during a wound reaction has been extensively described (Schilling, 1976; Boucek, 1984; Movat, 1985).

I.28.1 Animal model

Calcium phosphate ceramics has been evaluated *in vivo* extraskeletally in rats, rabbits, dogs, sheeps, goats, pigs, monkeys, and baboons. But the response of implant varied from animal to animal and also from species to species. Anderson, (1971) reported that the extent and duration of the inflammatory response are similar in rodent, dog or rabbit to those found in primates, allowing accurate inferences to be obtained from responses in test animals as to the anticipated responses in man. Yang (1996) reported that bone induction with HA was observed in dogs and pigs after 45 days in muscle and in subcutaneous tissue after 60 and 90 days. But, no bone induction was observed in goats, rabbits and rats until 120 days. Hence, the right kind of animal model has to be chosen for the desired response.

I.28.2 Material-Tissue Response

When implanting devices or products made of biomaterials into the body, our first concern was the tissue destruction caused by surgical intervention, i.e. implantation, irrespective of its purpose and site.

I.28.3 Toxicity

In the biological responses of soft tissues to the implant, the physiological wound healing process is more or less modified depending on the toxicity of the implanted material . Different tissue responses are triggered depending on the shape and toxicity of the implanted material. Upon implantation of a solid material that is neither toxic nor degradable, the inflammatory response is not sharply altered by the presence of the material.

I.28.4 Systemic influence

The implant site is filled with blood, plasma proteins are adsorbed onto the material surface and modified, and a fibrin mesh is formed to guide the collagen regeneration.

I.28.5 Necrosis

Necrosis, the death of cells and tissues, sets in motion a series of events aimed at leading to healing and restitution of function. Necrosis sets the inflammatory response in motion, permitting the removal by digestion of dead cells (Golden, 1982).

I.28.6 Inflammatory response

Unlike the simple surgical wound, the persistence of local inflammation has been shown two to three days postimplantation. In general, the implant cannot be regarded as a foreign substance that will be eliminated, but it acts as a persistent stimulus (Krizek, 1983). This is responsible for the delay or inhibition of the healing process. The sequence of events as described rarely occurs because of the inability of materials to be totally inert. Actually, titanium, alumina, and some polymers may induce a minimal fibrous reaction but, in these cases, changes in the exudate composition as well as in the macrophage chemotaxis or phagocytosis also are likely to occur. If the balance between the release of particles into perimplant tissues and the clearing of them is reached, then a steady state is achieved; a fibrous tissue layer with few inflammatory cells will encapsulate the implant. When foreign substances are released too quickly to be scavenged efficiently, inflammatory cells are recruited at the implant site. The severity of cell reaction is related to the toxicity of the foreign substance. Such a cell response might develop into chronic inflammation, which impairs complete healing. The reaction is not

necessarily proportional to the implant duration, but it depends on other variables; the surface passivation of some metals or protein adsorption can reduce the host's reaction, whereas corrosion phenomena can amplify it. After phagocytosis of the small particles, they are not always degraded intracellularly. During the process, the macrophage is activated and a lot of mediators and lysosomal enzymes are released. Outside the cell, the chemotactic mediators and the destructive enzymes operate local cell recruitment and the tissue damage, respectively; the resulting picture is referred to as a foreign body reaction. The more severe the tissue reaction is, the greater the degradation of the material will be; the process is now self-maintaining.

I.28.7 Soft tissue response to implants

Soft connective tissue, by its very nature, is invariably in contact at some time with implants and the biomaterial from which they are made. The type, quantity, and stability of the tissues and its interaction with the implant govern the success or failure of that implant in the long term. Given that the biomaterial is nontoxic and contains no leachables, if it is harder than the connective tissue, there will be mechanical damage to the interfacial tissue, fragments of which will promote a cellular, phagocytic response which will continue for as long as the movement does; if it is softer than the interfacial tissue, fragments of the implant will be generated and disposed off in the same way. The consequence of movement is invariably a connective tissue capsule in which the collagen fibers are wrapped around the implant parallel with the surface, with variable numbers of cells at the interface and in the capsule, which produce numerous agents, which maintain the fibrous response. There is always a space between implant and capsule, and it is with events in that space and with the long-term status of the capsule that the explanation of

the phenomenon of solid-state carcinogenesis is thought to reside. The consequences of such a series of events after mammoplasty and breast augmentation surgery are well known. Elimination of problems associated with such connective tissue encapsulation can be simply achieved by elimination of microscopic movement at the interface.

Suitability of a biomaterial for any application is determined at the interface between implant and host (Hench and Ethridge, 1982). The presence of soft-tissue components should not disturb the bonding of biomaterial to hard tissue. Bioactive materials now are available in range of compositions and forms with variable bioactivity indices, which depend on the rate at which the bonding to tissues takes place (Hench, 1988).

Crystalline multiphase materials provide greater mechanical strength than those, which are produced as glass and glass ceramics (Holand *et al.,* 1985; Nakamura *et al.,* 1985). The interaction of crystalline materials with soft tissues has not been positive and in some situations the implant material must be protected from soft tissues to function well, as by the interposition of bone plate, this effect appears to be due to preferential attack by cellular enzymes of one of the phases of the material, releasing the other as granules (Gross *et al.,* 1981). Failure to soft tissue bonding could be due to the inappropriate preparation of material and selection of an inappropriate site (muscle) and when the implant is successfully immobilized in the soft tissue during the experimental period soft tissue adhesion to 45 S5 was observed (Hench and Paschall, 1981). Crystalline glass ceramic Ceravital does not bond to soft tissues. Previous experiments have shown soft tissue-Bioglass® adhesion in sheep (Wilson and Nolletti), dogs (Wilson and Merwin, 1988), monkeys (Wilson *et al.*, 1987) and rats (Wilson *et al.,* 1981).

Bioglass® compositions containing from 42 to 52 mol % of SiO_2 can bond to soft tissues, in a sheep model, between 1 and 3 months (Wilson and Merwin, 1988). Substitution of CaF_2 for some of the CaO in 45S5 Bioglass® did not affect this ability.

The bioactive surface of Bioglass® implant serves as a template for amorphous apatite precipitation from surrounding fluids, with the collagen connecting the implant and bone supplying the micronucleation sites for apatite crystallization. Eventually when the apatite crystallization is complete, the resultant interface is stronger than bone (Pietrowski *et al.*, 1971).

I.28.8 Heterotopic Osteoinduction

The term "tissue induction" means cell differentiation by contact with other cells or their products. A number of embryonic systems of induction, including cartilage and bone differentiation, have been described (Holtzer, 1968; Lash *et al.*, 1957; 1960). The inducing system is composed of at least two components, inducing tissue or its products and undifferentiated, responding tissue, which under the influence of the former are stimulated to differentiate. It is generally accepted that inductors activate or inactivate the genes of the responding cells by initiating a chain of events known as differentiation processes. The extracellular components containing a substrate for enzymes anchored to the cell surface can work as morphogenetic substance.

I.28.9 Do ceramics possess osteoinductive property?

An ideal bone graft substitute would be a material with osteoinductive properties. H.G. Wells (1911) proposed a theory that calcium salts exert a stimulatory effect on osteogenic activity. Based on this hypothesis several investigators confirmed that synthetic calcium phosphates and solutions containing these salts lead to a stimulatory

effect on osteogenesis (Albee and Morrison, 1920; Stewart, 1934; Shands, 1937). Two theories run parallel till today that, calcium phosphate ceramics does not have and have osteoinductive property.

I.28.10 Calcium Phosphate Ceramics are not Osteoinductive

Based on these observations synthetic calcium phosphate ceramics were tested for their biological response in nonosseous sites without the addition of an inducing stimulus such as marrow or growth factors and found that the ceramics by themselves did not induce bone in those animal models at different time periods. Piecuch, (1982) investigated the biological response to coralline replamineform hydroxyapatite implants placed in canine axillary subcutaneous sites till 8 weeks. Misiek *et al.,* (1984) reported that non-porous smooth and rough HA surface in buccal soft tissue pouches of dogs did not produce any bone even after 6 months. Pettis *et al.,* (1990) evaluated HA and HA with demineralised bone in rat subcutaneous tissue. HA alone did not produced any bone till 3 weeks, but endochondral bone formation was observed in the composite implants in the same time period. Bucholz *et al.,* (1987) summarized that there is no conclusive evidence that any of the porous calcium phosphate biomaterials are osteoinductive. Most are considered osteoconductive, that is, allowing for bone ingrowth from an osseous bed. No bone ingrowth will occur if the implant is inserted into muscle or subcutaneous tissue. Ripamonti, (1996) observed that porous HA did not promote any bone intramuscularly till 90 days in rabbit.

I.28.11 Calcium Phosphate Ceramics have Osteoinductive Property

Ripamonti, (1990 and 1991) implanted porous HA without marrow or growth factors in baboons and observed woven and lamellar bone formed by intramembranous

osteogenesis at 3, 6 and 9 months. Vagervik, (1992) reported *de novo* bone formation in porous HA blocks without marrow or growth factors. The HA blocks were implanted in subcutaneous tissue, in muscle tissue, and attached to a muscle flap in rhesus monkeys. None of the HA blocks initiated bone formation in any of the sites till 4 weeks. But after 4 weeks consistent bone formation was observed in subcutaneous tissue. Shors *et al.,* (1993) found bone formation in porous HA disks implanted intramuscularly and subcutaneously in dogs at 3, 6 and 12 months. Yang *et al.,* (1996) reported that bone formation could be detected in HA/TCP implanted intramuscularly and subcutaneously in dogs and pigs, but no bone differentiation was found in any specimen implanted in rabbits, goats or rats.

I.28.12 Tissue induced osteogenesis

This concept was formulated by Baschkirzew and Petrow (1912), who observed that periosteal aspect of autografts of fresh cortical bone when implanted intramuscularly into rabbits showed metaplasia of the connective tissues around the grafts. Later several other investigators proved osteoinduction by fibroblast cells in subcutaneous tissue in rabbit's ear (Nageotte, 1920), urinary bladder induced osteogenesis in dogs, rabbits, sheep (Phemister, 1923), amniotic fluid (Morrison *et al.,* 1937) in mice (Anderson *et al.,* 1964), osteogenic induction by bone was demonstrated by (Orell, 1934) in dogs, rabbits, mice and other animal models.

I.29 ORTHOTOPIC IMPLANTATION

I.29.1 Animal Model

Fracture healing under different mechanical conditions has been investigated in dogs, rabbits, rats and sheep. The rat has the advantage of greater economy, but also has disadvantages. Rat cortical bone is not Haversian and remodeling occurs primarily along the endosteal and periosteal surfaces (Kelley *et al.*, 1990). Its reaction to injury will, therefore, differ from that of human, or other Haversian bones. Second, the small size of rat bones mitigates against their use as models for different methods of internal fixation. Fracture models using rat bones, such as femur, tibia, and metatarsals, frequently relies on manual fracture and no splintage.

The rabbit as an experimental animal for studying fracture healing has several advantages over the rat. First, the cortical bone is Haversian and so the stimulation of remodeling after injury is more similar to that of other larger mammals. Second, the larger size of rabbit bone enables the use of several methods for the stabilization of fractures. Thus, plates of various designs, medullary nails or external fixators have been used to stabilize osteotomies of the femur and tibia.

Defect size plays a critical role in the healing of bone. The events in bony union between the cortical fragments of mechanically unstable fractures depend on the width of the gap. If it is narrow, cells do not enter until the external callus can stabilize the fracture completely. In rabbits 2 mm defect is the critical width (Grieff, 1978) to evaluate the bone healing.

I.29.2 Tissue response to implants

The material response and the tissue response should complement each other in healing of the defect. The attachment of the tissue onto the material surface is based on the physicochemical property of the material. Based on the tissue response to the material, the materials are classified into four types

a) Nearly inert implants (Alumina, zirconia), which does not favor bone bonding
b) Porous implants, favors the mechanical fastening with the host bone by encouraging bone infiltration into the pores (HA and HA coated metals)
c) Bioactive implants, forms an ionic bonding at the interface with the host bone (Bioactive glass, Bioactive glass -ceramics and HA) and
d) Resorbable implants (TCP and Bioglass), the material will degrade with time and replaced by new bone.

I.29.3 Bioinert Ceramics

Polycrystalline sintered alumina is very strong compared to most of the ceramics, although it is brittle. Its strength, abrasion resistance, and chemical inertness have made it attractive for dental and bone implants as artificial hip joint. Smith (1963) developed an interconnected, porous alumina ceramic and tested the material for its inert property in rabbit femur bone, and the later works of Benum *et al.*, (1977) with porous ceramic material (Al_2O_3) in the sheep tibia confirmed the bone ingrowth into the ceramic material even though the material was inert. The disadvantage of alumina ceramics is that they are inert material and bonding of the non-porous material to the bone is poor.

I.29.4 Bioactive Calcium Phosphate Ceramics

The main purpose of using calcium phosphate ceramics as an implant material is to enable it to be gradually substituted by newly formed bone or at least to become integrated with the host bone. Hydroxyapatite Ca_{10} $(PO_4)_6$ $(OH)_2$ is the structural prototype of the bone mineral and the inorganic constituent of tooth and bone. Dense, pore-free tricalcium phosphate Ca_3 $(PO_4)_2$ or the mineral whitlockite can be made by sintering precipitated fine crystals, very similar to the method of making hydroxyapatite (Jarcho *et al.*, 1979). The material is less fatigue resistant than hydroxyapatite. Bonds (chemical) with the bone well and reabsorbed over a period and replaced by bone.

Biphasic calcium phosphate (BCP) macroporous ceramic consisting of an intimate association of β-TCP and HAP, with β-TCP/HA weight ratios of 15/85, 35/65 and 85/15 has been developed (Daculsi *et al.*, 1989). *In vivo* studies in dogs revealed a decrease in average size of crystals in BCP ceramics had taken place, together with an increase in the size of microporosities in the surface and at the core of the ceramic, indicating that *in vivo* dissolution had taken place. The *in vivo* resorption of the BCP ceramics was said to depend on their β-TCP/HA ratios. Formation of crystals with crystallographic properties and a Ca/P ratio similar to those of bone crystals were also observed. The abundance of these crystals was said to be directly related to the β-TCP/HA ratio of the BCP ceramic prior to implantation. It was postulated by Daculsi et al., (1989) that the formation of the bone apatite like crystals may be due to the precipitation of calcium and phosphate ions released from the dissolving ceramic crystals (the β-TCP component dissolving preferentially to the HA component). It was suggested

that one of the means of controlling the *in vivo* resorption of BCP ceramic is by varying its β-TCP/HA ratio.

Table.I.5

Calcium Phosphate Ceramics	Commercially available source
Calcium hydroxyapatite ($Ca_{10}(PO_4)_6(OH)_2$	Calcite™, Durapatite™, Alveograf™, Osteograf™, Himed™ -HA, Bioapatite™, Periobone (Sree Chitra)
β-Tricalcium phosphate ($Ca_3(PO_4)_2$	Synthograf™, Augmen™, Himed™-TCP
Biphasic calcium phosphates (BCP) (mixture of HA & β-TCP)	Triosit™, Himed™-TCP
Resorbable calcium phosphate materials	Osteogen™, Himed™-AP

I.29.5 Bioactive Glass and Glass-Ceramics

Materials of controlled surface activity (or biodegradability) showing direct bonding to bone have been termed "bioactive". Such glass compositions may allow release of ions conducive to osteogenesis. Bioactive glasses capable of forming chemical bonds may offer potential for long-term stabilization of implants. Strength of bioactive ceramic coatings on the metal is important due to the action of stress transfer from the implant prosthesis to surrounding tissues, which could decide the success or failure of the implant in *in vivo* situation.

Glass and ceramic materials can be customized using wet chemical methods to produce materials with a wide range of mechanical properties (Mazdiyansi, 1984). Such materials can be made to have varying degrees of degradation and ionic release (Rizkalla *et al.*, 1992). Bioactive glasses having an interfacial response that can result in tissue bonding can be produced from mixtures of silica, phosphate, calcium and sodium (Hench, 1988; Matsuda and Davies, 1987; Schepers, *et al.*, 1988; Pazzaglia *et al.*, 1989). These materials have the potential to elicit the formation of natural tissues at their surface

(Hench *et al.*, 1972; Gross *et al.*, 1988; Kokubo *et al.*, 1990). Unique class of materials - glass-ceramics are also important (Kasuga *et al.*, 1992). Such materials start as an amorphous glass and by application of an appropriate heat treatment may precipitate a much stronger and stiffer crystalline ceramic phase within the glassy matrix (Kokubo *et al.*, 1986). Synthetic hydroxyapatite and bioactive glass have been coated onto the surface of titanium implants (Ducheyne *et al.*, 1986). A glass-ceramic containing crystalline oxyapatite and fluroapatite [$(Ca_{10}(PO_4)_6$- (O, $F_2)$] and β-wollastonite (SiO_2-CaO) in an MgO-CaO-SiO_2 glassy matrix (A-W type) was developed by Nakamura *et al.*, (1985). A-W glass-ceramic bonds to living bone, through a thin calcium and phosphorous rich layer that is formed at the surface of the glass ceramic (Nakamura *et al.*, 1985). This glass ceramic not only bonds to living bone in a short period, but also holds a fairly high mechanical strength for a long time, even under load-bearing conditions in a body environment (Kokubo *et al.*, 1985).

Table.I.6

Glass/Glass Ceramic	Commercial Names
Bioactive glass	Perioglass®
Bioactive Glass-ceramic	Ceravital

I.29.6 Calcium Phosphate Cement

More recently water setting HA cements have been employed to create hydroxyapatite materials with various porosities (Brown and Chow, 1986). Most commonly HA cement is produced by reacting tetracalcium phosphate and calcium hydrogen phosphate in an aqueous environment. Under *in vitro* conditions at 37 °C the

HA cement sets approximately within 15 min and the isothermal chemical reaction is completed by 4 h. Porosity is obtained by mixing the cement prior to set with sucrose granules and then dissolving the granules in water. The main disadvantage of calcium phosphate cements is its lack of macropores. As a result, biodegradation takes place layer-by layer, from the outside to the inside (Bohner, 2000).

Table.I.7

Calcium phosphate cements	**Commercial names**
Monocalcium phosphate cements (MCPM) with α-TCP	Cementek
Dicalcium phosphate (DCP)	Bonesource and Biocement D, Biopax
β-Tricalcium phosphate α-Tricalcium phosphate	ChronOS Norian SRS, Biopax

I.30 Physico-chemical properties of the ceramic materials

I.30.1 Solubility

The concept of bioactivity is based on the release of the ions into the medium, which will evoke a proper biological response. HA was until recently considered to be non-resorbable. Calcium phosphate biomaterials differ in their solubility or extent of dissolution: ACP> α-TCP>β-TCP>CdA>HA (Daculsi, 1998). Driessens (1983) showed that there are only two calcium phosphate materials that are stable at room temperature when in contact with aqueous solutions, and it is the pH of the solution that determines which one is stable. At a pH lower than 4.2, the component $CaHPO_4.2H_2O$ (dicalcium phosphate) is the most stable, while at higher pH (>4.2), hydroxyapatite is the stable phase.

I.30.2 Biodegradation

Biodegradation on different calcium phosphate ceramics is contradicting. Many authors (Bhaskar *et al.*, 1971; Boyne *et al.*, 1982; Klein *et al.*, 1983) report rather fast degradation of β-whitlockite, while others (Wagner 1981 and Nery *et al.*, 1989) report a minimal or very slow resorption. Many investigators found no degradation of HA (Klein *et al.*, 1983; van Blitterswijk *et al.*, 1986), where as others described resorption (Strub and Gaberthuel 1978). It is thought that the chemical composition of the ceramic determines whether or not calcium phosphate materials with <1 Ca/P ratio or >2 are degradable (Koster *et al.*, 1977; Thomas *et al.*, 1987). A well-defined series of experiments show that the composition, Ca/P ratio, impurities like F^- or Mg^{++} and structural relationships (micro/macrostructure) are important factors associated with biodegradation. Microporosity determines the geometry of "necks" between sintered particles, while macroporosity determines the amount of necks in contact with the environment. The neck formation depends on preparation technique, sintering temperature, pressure applied to compress the powder into a tablet before sintering.

I.30.3 Porosity

A major factor in the use of such materials is the control of the size of porosity. Passuti and Daculsi (1989) evaluated the effect of porosity by an *in vivo* experiment in the cortical bone in dogs. Three kinds of porosity were tested (from 100μm to 600 μm). The results of the study demonstrated that the porosities up to 100 μm are efficient for the bone ingrowth, however, during the first months of implantation, larger macropore sizes are more suitable for bone ingrowth.

I.30.4 Mechanical property

Ceramic material of choice for load-bearing implantation in orthopaedic prosthesis has been alumina (Christel *et al.*, 1988). Ceramic materials of the type have been in use now for over 20 years. Such prostheses are constructed from high-purity (less than 0.05 % SiO_2) fine particulate alumina by hot isostatic pressing to produce sintered alumina, having high-density and very smooth surface. The compressive strength of the alumina implants is between 4000-4500 MPa when compared to that of cortical bone (100-230 MPa). The biocompatibility, low wear and good mechanical strength have been the main criteria for this choice. In the past 10 years, material scientists have looked at constructing the femoral head from ceramic and the stem from the traditional metal, rather than constructing the complete prostheses from ceramic, in order to minimize fracture due to the lack of toughness of the ceramic material (Asada *et al.*, 1987). Mechanical strength tests of such systems have judged that such devices have strength adequate for clinical use. Ceramic materials can exhibit a relatively high modulus of elasticity values 30-35 GPa (cortical bone 7-30 GPa). The strength of some ceramics is also reasonably impressive, being very much greater than that of polymers. Ceramics and glass tend to be quite strong in compression and shear but weak in tension (40- 60 MPa, whereas cortical bone has 100-230 MPa). Ceramic and glass materials fail at a very low critical strain of approximately 0.1-0.2 %. The three dimensional primary nature of the covalent and or ionic atomic and molecular bonds in ceramic material dictates the strength and rigidity as well as limiting the strain and increasing the fracture toughness. The strength of the material may be understood from the surface condition, porosity, second phases and defects; these properties are not intrinsic properties of the materials

that will decide the strength, rather it depends on how the material is processed and treated (Doremus, 1992).

I.31 Growth factors induced osteogenesis

Artificial bone substitutes like metals and ceramics tend to be too stiff and their low osteogenic potential often lead to loosening of the implant and functional failure in months to years. This failure may be avoided if implants have a capacity to induce bone and thereby promote stabilization through osseointegration with the host. In order to develop osteoinductive bone graft substitutes, attempts to incorporate bone growth factors into biomaterials have been initiated.

The interest for biochemical enhancement of bone healing and bone formation has led to a larger number of experimental studies that use growth factors in various clinically related situations. Growth factors have been used to stimulate fracture healing, long bone (Lind *et al.*, 1993) and calvarial defect (Beck *et al.*, 1991) healing and as substitute for bone grafts during spine fusions (Cook *et al.*, 1994). The major phases of the osteoinduction are chemotaxis, mitosis, and differentiation. Various osteoinductive substances were tried to enhance bone growth like cartilage powder (Heimburger *et al.*, 1967), collagenous bone matrix as local mitogen for connective tissue cells (Rath and Reddi, 1979), bone morphogenetic protein (Mahy and Urist, 1988) insulin-like growth factor (IGF-I and II), transforming growth factor-β (Noda and Camilliere, 1989), acidic and basic fibroblast growth factor (Hauschka *et al.*, 1986), platelet derived growth factor, calcitonin (Thompson and Urist, 1973), vitamin-D (Tabuci *et al.*, 1989), parathyroid hormone, growth hormone, marrow derived growth factors, hemopoietic factors, and several cytokines (Yoshikawa *et al.*, 1988) were used for bone induction studies.

that will decide the strength, rather it depends on how the material is processed and treated (Doremus, 1992).

I.31 Growth factors induced osteogenesis

Artificial bone substitutes like metals and ceramics tend to be too stiff and their low osteogenic potential often lead to loosening of the implant and functional failure in months to years. This failure may be avoided if implants have a capacity to induce bone and thereby promote stabilization through osseointegration with the host. In order to develop osteoinductive bone graft substitutes, attempts to incorporate bone growth factors into biomaterials have been initiated.

The interest for biochemical enhancement of bone healing and bone formation has led to a larger number of experimental studies that use growth factors in various clinically related situations. Growth factors have been used to stimulate fracture healing, long bone (Lind *et al.*, 1993) and calvarial defect (Beck *et al.*, 1991) healing and as substitute for bone grafts during spine fusions (Cook *et al.*, 1994). The major phases of the osteoinduction are chemotaxis, mitosis, and differentiation. Various osteoinductive substances were tried to enhance bone growth like cartilage powder (Heimburger *et al.*, 1967), collagenous bone matrix as local mitogen for connective tissue cells (Rath and Reddi, 1979), bone morphogenetic protein (Mahy and Urist, 1988) insulin-like growth factor (IGF-I and II), transforming growth factor-β (Noda and Camilliere, 1989), acidic and basic fibroblast growth factor (Hauschka *et al.*, 1986), platelet derived growth factor, calcitonin (Thompson and Urist, 1973), vitamin-D (Tabuci *et al.*, 1989), parathyroid hormone, growth hormone, marrow derived growth factors, hemopoietic factors, and several cytokines (Yoshikawa *et al.*, 1988) were used for bone induction studies.

I.31.1 Fibringlue as Osteoinductive Protein

Fibrin Sealant or Fibrin Glue (FG) as it is popularly known, has been used in a number of orthopaedic procedures to enhance osteogenesis in human maxillary and mandibular bone (Marrini *et al.*, 1994), on Kiel heterologous bone graft (Bosch *et al.*, 1980) in the fixation of osteochondral fractures (Bosch *et al.*, 1977), in spinal surgery (Ono *et al.*, 1992) on an early enhancement of bone using TCP (Palacios and Monia, 1986), and fixation of osteochondral fragments (Marvin *et al.*, 1984), bone chips (Arbes *et al.*, 1981), and perichondrium grafting (Hominga *et al.*, 1990). Nevertheless, this positive effect of osteogenesis with FG was not observed in a bone growth chamber and significant bone repair was not observed too in bone defects of dogs (Mulliken *et al.*, 1984). Furthermore, this biological adhesive, a derivative of blood is widely used in surgery for their adhesive properties, haemostatic activity and wound healing process (Lerner and Binur, 1990; Sierra, 1993; Wornom and Buchman, 1992). However their role in bone fracture healing or bone tissue response is not fully understood (Schlag and Redl, 1988) and controversies do exist, despite the fact that this biologic "glue" can be an interesting effective osteoinductive substitute.

The nature and the development of the interface between an implanted bioceramic and bone are affected by many factors. It is being recognized that key aspects of the interaction between bone cells and the implant depend on modification of the bioceramic surface that occur due to interactions with the local environment with respect to pH, protein adsorption, Ca^{2+} and PO_4^{3-} deposition.

I.32 The objectives of this study:

It is well known that bioactive ceramics are ideal bone graft materials. But, the tissue responses to these bioactive ceramics are not fully understood till date. Three different types of bioactive ceramics were taken for the study a) Hydroxyapatite (HA), b) Bioactive Glass System-AW type (BGS) and c) Triphasic Bioactive Composite System (HABGS) synthesized in house.

1) Characterization of the synthesized bioactive ceramic granules for their crystallinity, phase compositions (purity) and the functional groups.
2) To study the dissolution, precipitation and apatite formation of the bioactive ceramic granules by simulated *in vitro* studies.
3) Cytotoxicity and cytocompatibility property of the ceramics by *in vitro* cell culture techniques.
4) To find the histotoxicity, histocompatibility of the bioactive ceramic granules in heterotopic and orthotopic sites with and without fibrin glue (as growth factors).
5) Characterization of the ceramic granules after implantation in rabbit tibia bone for its crystallinity and phase composition by XRD, functional changes by FT-IR and the distribution of the elements by SEM-EDAX techniques.
6) Specific bone labeling techniques as well as staining techniques employed to understand the healing pattern of the bone with respect to different bioactive ceramic granules.
7) Biochemical estimation of the serum and urine markers of bone for understanding the physiology of the bone before and after implantation.

8) Quantitative histomorphometric analysis of the implanted specimens to understand the bone growth rate at different periods.

9) Suggest a possible mechanism by which the bioactive ceramics would favour osteogenesis and osseointegration in bone and

10) Compare the data of the in house synthesized bioactive ceramics with that of commercially available bioactive ceramic bone substitutes.

CHAPTER – II

MATERIALS AND METHODS

II. MATERIALS AND METHODS

II.1 Materials

Hydroxyapatite, [HA-($Ca_{10}(PO_4)_6(OH)_2$] porous, 300 – 350 μm sized granules, Bioactive glass system-AW type [BGS - 45 % CaO, 34 % SiO_2, 16 % P_2O_5, and 5 % MgO] non-porous, 300 – 350 μm sized granules and Triphasic bioactive composite system [HABGS- 55 %CaO, 17 % SiO_2, and 28 % P_2O_5] non-porous, 300 – 350 μm sized granules (synthesized as part of the on going developmental programme of bioceramics in our Institute - SCTIMST, Trivandrum, India), were used for this study to evaluate the efficacy of the materials for orthopaedic application.

II.1.1 Preparation of the freeze-dried hydroxyapatite (HA) powders

Hydroxyapatite was prepared by a precipitation method (Varma and Sivakumar, 1996) starting from calcium nitrate and ammonium dihydrogen phosphate ($NH_4H_2PO_4$) (Ranbaxy) solution. Calcium nitrate was dissolved in the distilled water. Ammonia solution was added to the above solution to maintain the pH of the solution above 11. Ammonium dihydrogen phosphate was dissolved in distilled water and was brought to pH 10 by adding NH_3 solution. The phosphate solution was then added drop by drop to the calcium nitrate solution under continuous stirring on a hot plate. After the completion of the precipitation, the stirring was continued for another one hour and aged for 24 hours at room temperature. The precipitate was filtered and the filter cake was thoroughly washed with distilled water to remove ammonium and nitrate adsorbed over the precipitate surface. After repeated washing with distilled water, the precipitate was then subjected to freeze drying in a laboratory model lyophilyzer. By the above process, sublimation of the frozen water occurred leaving behind a free flowing powder inside the jar. The powder thus obtained was heat

treated at various temperatures in a Muffle furnace (Thermosystems) and later characterized for phase purity, composition and morphology.

II.1.1.1 Preparation of HA Porous Granules

The freeze-dried powder was first calcined and the calcined powder was mixed with an appropriate volume percentage of a pore former (naphthalene) and thoroughly mixed in a ball mill. The milled powder - pore former mix was then compacted and heat-treated at high temperature to get sintered porous blocks. These pellets were manually crushed in an agate mortar and, 300 - 350 μm sized fractions were separated using standard test sieves. The HA powder was compressed to form dense discs (10 x 3 mm).

II.1.1.2 Chemical Analysis

The powder as well as the granules were analysed for calcium and phosphate content. Estimation of calcium was carried out by a substitution titration method using EDTA solution as described in Vogel (1980). The phosphorous content was analysed by a gravimetric method (Vogel 1980). Here the phosphate was precipitated as ammonium phosphomolybdate by adding excess ammonium molybdate to the hot and acidic solution of phosphate ions.

II.1.2 Preparation of Bioactive Glass-Ceramic -A-W Type (BGS)

The synthesized calcium phosphate based glass ceramic is non-porous and 300 – 350μm in size. The material was synthesized by a sol-gel method involving silicon ethoxide, calcium nitrate and phosphorous pentoxide (Ranbaxy). A uniform sol was made by dissolving calcium and phosphorous pentoxide in distilled water and mixed and refluxed with silicon ethoxide solution. The clear solution thus obtained was allowed to gel and the dried gel was then sintered at 1200°C - 1300°C. BGS granules

were obtained by sieving the crushed dried gel through a 300 – 350 μm mesh. The disc forms were obtained by compressing the powder in a specially designed die under pressure.

II.1.3 Preparation of Triphasic bioactive composite system (HABGS)

The synthesised hydroxyapatite glass ceramic composite is non-porous and 300 – 350 μm in size. HABGS was prepared by mixing calcium silicate powder synthesised by a sol gel method and hydroxyapatite powder was synthesized by the precipitation method as described above (II.1.1 and II.1.2). The two powders were mixed thoroughly in a ball mill, compacted and sintered at 1250 °C for getting dense HABGS pellets. The sintered discs were crushed in an agate mortar and the powder thus obtained was sieved through a 350 - 300 μm pore sized mesh.

Both HABGS and BGS contain pores in the range of 10 - 30 μm. The bulk density of both HABGS and BGS was around 80 – 85 % having intergranular porosities in the range of 10 - 30 μm.

II.1.4 Material Sterilization

The separated granules and discs were first washed with distilled water and later subjected to ultrasonic cleaning (Cole parmer) for the complete removal of the fine powders adhered over the surface. The materials were then sterilized by autoclaving prior to *in vitro* and *in vivo* experiments.

II.1.5 CHARACTERIZATION OF MATERIAL

II.1.5.1 X- Ray Diffraction (XRD)

Characterization of the phase purity and crystallinity of the freeze-dried HA BGS and HABGS powder were analysed by XRD (Siemens D-5005). The samples were analysed at tube voltage of 40 kV and current 30 mA at a scan rate of 2 degrees

per minute in the range between 20 ° - 35 ° with copper K-Alpha 1 radiation. Phase purity and crystallinity identification was done comparing the data with the Joint Committee on Powder Diffraction Standards (JCPDS) files.

II.1.5.2 Fourier Transform Infrared Spectroscopy (FT-IR)

The IR spectra of the synthetic HA, BGS and HABGS granules were recorded in a Nicolet impact 410 FT-IR spectrophotometer using the potassium bromide (KBr) pellet technique. The granules were pulverized in a mortar and 1 mg of the sample was mixed with 100 mg of KBr (AR-grade-Merck) and was pelletized at 10,000 psi. in a hydraulic press. The pelleted sample was then analysed in FT-IR spectrophotometer. The spectra were recorded in absorbance mode averaging 100 scans in the range of 400 cm^{-1} - 4000 cm^{-1} with a resolution of 4 cm^{-1}.

II.1.5.3 Scanning Electron Microscopy (SEM)

SEM of the granules will help in understanding the surface topography, porosity, and size of the materials. The granules were washed with acetone and deionized distilled water, air dried, and critically point dried (HCP2-Hitachi) to remove moisture, and then coated with gold in sputter coating unit (E101-Hitachi). Subsequently the topography of the samples was viewed using SEM (S2400 - Hitachi).

II.2 *IN VITRO* SIMULATED STUDIES

HA, BGS and HABGS granules were immersed separately in different media with varying pH at a constant temperature (37 °C) in a shaker incubator (Shandon) for 12 and 24 hours, to validate the rate of dissolution and subsequent apatite formation on the materials, in response to hydrogen ion concentration (pH), protein adsorption, calcium and phosphorous release / deposition. The incubation of the granules were

conducted in a 24 -well tissue culture plate (NUNC-Polystyrene) with a sample to medium ratio of 20 mg / 2 mL.

II.2.1 Incubation Media

The ion concentration of the Simulated Body Fluids (K-9) was based on the method of Kokubo *et al.*, 1991. 4.2 mM-$NaHCO_3$, 137.8 mM- NaCl, 3 mM- KCl, 1 mM- K_2HPO_4, 2.5 mM- $CaCl_2$, 1.5 mM - $MgCl_2$ were added to prepare the SBF. The ionic content of the SBF thus prepared is similar to that of the human serum plasma concentration (Table.II.1).

Table.II.1

Concentration (mM)						
Na^+	K^+	Mg^{2+}	Ca^{2+}	Cl^-	$(HCO_3)^-$	$(HPO_4)^-$
142.0	5.0	1.5	2.5	148.8	4.2	1.0

HA, BGS and HABGS were incubated in the following media:

a. Acetate Buffer (0.45M) + SBF - pH 5.2

b. Tris (50 mM) and HCl (45 mM) + (SBF) - pH 7.3

c. Simulated Body Fluid (SBF) - pH 7.1

d. Minimum Essential Medium (MEM) - pH 8.12

e. Foetal Calf Serum (FCS)- pH 8.6

f. Rabbit serum - pH 7.2

II.2.2 Evaluation

The media was analyzed for pH, calcium, phosphorous and protein before and after immersion of HA, BGS and HABGS granules. The granules were removed and air-dried at room temperature for SEM, image analysis and FT-IR evaluation.

II.2.2.1 pH Measurements

The pH of the solutions was measured using a pH/ion conductivity meter (Accumet ® Model-50) before and after the dissolution experiments.

II.2.2.2 Calcium

O-cresolpthalein complexone method (Anderegg *et al.,* 1954; Gitelam, 1967; Baginski, 1973) was used to estimate calcium (Qualigens - India). Calcium in alkaline medium reacts with O-cresolpthalein complexone to form a purple coloured complex whose absorbance is proportional to the calcium concentration. The interference due to magnesium and iron is eliminated by using 8-hydroxy quinoline.

The sample was mixed well with the working reagent and allowed to stand at room temperature for 5 min. The absorbance of the standard (S) and test (T) against a blank (B) was measured in the spectrophotometer (Hitachi, 220) at a wavelength of 570 nm.

Calculation

$$\text{Calcium in mg \%} = \frac{\text{Absorbance of (T)}}{\text{Absorbance of (S)}} \times 10$$

II.2.2.3 Phosphorous

Phosphorous was detected using the Monozyme Phosphorous modified Metol method (Monozyme - India)

Inorganic phosphorous is present in a small but significant amount, mainly as phosphate ions. The molybdate ion react with inorganic phosphorous in an acidic medium to form phosphomolybdate, which is reduced by metol to give a blue coloured complex. The absorbance of the blue coloured complex at wavelength of 680 nm is directly proportional to the phosphorous concentration. The test sample and blank was mixed thoroughly with the working reagent and allowed to stand at room

temperature for 5 min and the absorbance of test (T) and standard (S) was measured against the reagent blank (B) in a spectrophotometer (Hitachi, 220) at a wavelength of 680 nm.

Calculation

$$\text{Phosphorous in mg \%} = \frac{\text{Absorbance of (T)}}{\text{Absrobance of (S)}} \times 5$$

II.2.2.4 Protein

Protein concentration in foetal calf serum, rabbit serum and minimum essential medium were assayed using the Biuret method (Qualigens - India).

Proteins bind with copper ions in an alkaline medium of the Biuret reagent and produce a purple coloured complex, whose absorbance is proportional to the protein concentration. The test was mixed well with the working reagent and incubated at 37 °C for 10 min in an incubator (Shandon) and the absorbance of standard (S) and test (T) was read against the blank (B) in a spectrophotometer at a wavelength of 555 nm (Hitachi, 220).

Calculation

$$\text{Total protein in gm \%} = \frac{\text{Absorbance of (T)}}{\text{Absorbance of (S)}} \times 6$$

II.2.2.5 Surface Analysis: Scanning Electron Microscopy (SEM)

The granules were critical point dried (HCP2-Hitachi) to remove moisture, and coated with gold in an ion sputter (E101-Hitachi) and observed by SEM (S2400-Hitachi) to envisage any gross change on the material topography before and after dissolution. The size of the granules, the pores and apatite-like deposits were measured by the standard scale available on the SEM micrographs.

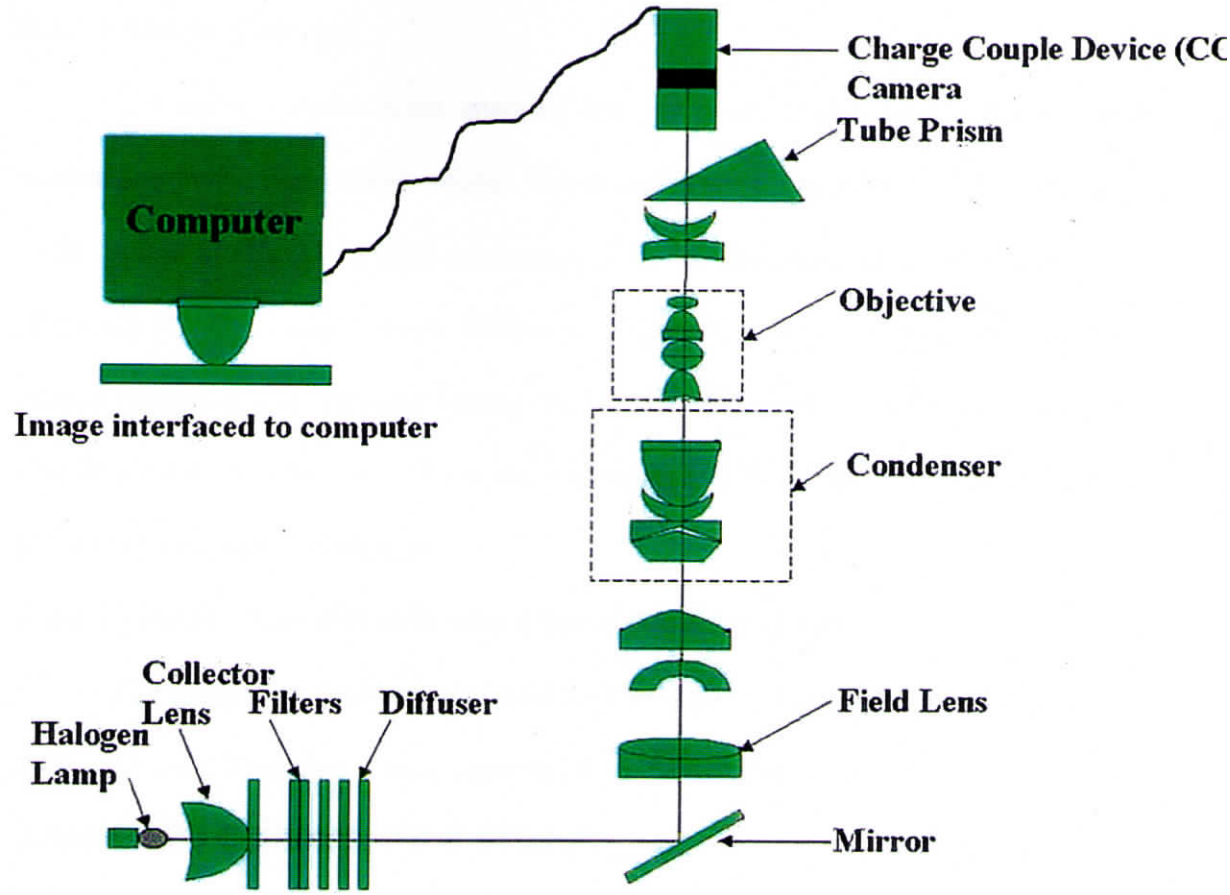

Figure - II-1

Schematic diagram of the quantitative image analysis technique: The image of the histological sections were captured by the charged couple device (CCD) attached to the microscope which is interfaced to a computer with an image analysis software (Optimas 6.1 version).

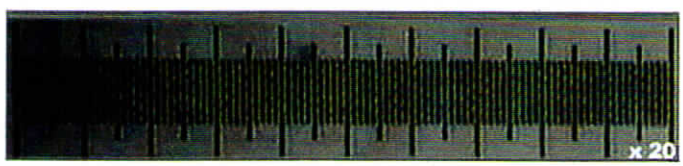

1 mm is divided into
0.01 mm divisions

Figure - II-2

Image of stage micrometer captured under CCD camera for calibration: The stage micrometer is captured under respective magnification and by using the image analysis software the scale is taken as a reference, for measuring the size of the histological images captured under the same magnification.

II.2.2.6 Image Analysis

The dried granules were analysed for any gross change in size under light microscope in the transmission mode. The granules were captured with the help of a CCD camera attached to a light microscope (Nikon, Optiphot), linked to a computer (Figure.II.1). The images were calibrated (Figure.II.2) after suitable thresholding (image enhancing) and measured using the OPTIMAS 6.1 version software. The data obtained were compared with the control granules and Students-t test was performed to find any statistical significance.

II.2.2.7 Fourier Transform Infrared Spectroscopy (FT-IR)

The dried granules were analysed for the functional groups after immersion in different media. The spectra were recorded as explained above (II.1.5.2).

II.3 *IN VITRO* CELL CULTURE STUDIES

To test HA, BGS and HABGS granules for toxicity and cytocompatibility, an *in vitro* model comprising L929 mouse fibroblast cells and MG 63 human osteoblast-like cells from National Centre for Cell Sciences (NCCS), Pune, India were used.

II.3.1 Direct Contact with materials.

Cells (1 x 10^3 cells per well) were seeded in wells of 24 -well tissue culture polystyrene plate enriched in Dulbecco's minimum essential medium (DMEM) with Earl's salt (High media, Pune, India), supplemented with 10 % foetal calf serum (FCS), 100 units and 100 mg/mL respectively of penicillin and streptomycin and incubated at 37 °C for 24 h and 5 % CO_2 air. When the cells attained confluency, the cleaned and sterilized HA, BGS and HABGS granules were placed separately in direct contact with the cells in the wells and left for 24 h under the same condition. Thereafter the cells were observed under Phase Contrast Microscope for any change

in morphology or any other cytopathic effect when compared with negative and positive controls.

II.3.2 Cell Viability (MTT Assay)

Known weight of the HA, BGS and HABGS granules were placed separately in DMEM with Earl's salt for 24 h, after which the material extract was taken. Known volume of the extract was then placed in contact with the confluent layer of fibroblast cells in 96-well Tissue Culture Plate (Nunc) enriched with 1 mL of DMEM with Earl's salt supplemented with 10 % FCS and containing 100 units and 100 mg/mL respectively of penicillin and streptomycin. Cultures were maintained in a humidified atmosphere of 95 % relative humidity (RH) 5% CO_2, at 37 °C. To the control groups of cells no material extract was added. After contact with the material extract for 24 h, cells were washed with phosphate buffer and allowed to react with MTT dye solution (3-4,5-dimethylthiazol-2yl)-2,5-diphenyl-tetrazolium bromide). MTT assay is a common assay for testing cellular viability based on the reductive cleavage of yellow tetrazolium salt to a purple formazon compound by the dehydrogenase activity of intact mitochondria.

Consequently, this conversion only occurs in living cells. Plates were incubated at 37 °C for 4 h for the cells to react with the dye. MTT solutions were removed and *n*-propanol was added to all the wells. The plates were slightly shaken for 10 min to ensure crystal dissolution and absorbance was measured in a multiplate reader (Biotek) at the wavelength of 570 nm. The percentage of live cells with the materials extract were determined by comparing their respective absorbance with that of the control cells.

II.3.3 Cytocompatibility of ceramics with L929 – Mouse Fibroblast cells

To visualize cell adhesion on the surface of the material, cells (1 x 10^3 cells) were seeded on the surface of the conditioned (disc soaked in DMEM with Earl's salt for 24 h) bioactive ceramic discs (HA, BGS and HABGS) (10 x 3 mm size). They were then maintained in the same culture medium for 48 h.

Thereafter the discs seeded with the cells were fixed in 3 % glutaraldehyde, post-fixed in 1% osmium tetroxide, dehydrated in acetone, critical point dried (HCP2-Hitachi), gold coated in an ion sputter (E101-Hitachi) and viewed in SEM (S2400 Hitachi).

II.3.4 Cytocompatibility of ceramics with MG63 – Osteoblast cells

MG 63 osteoblast-like cells (NCCS, Pune) maintained in Iscoves Modified Dulbecco's Medium (IMDM- Sigma) supplemented with 5 % foetal calf serum (Sigma) and 100 µg /mL streptomycin (sarabhai chemicals) and 100 IU/mL penicillin (benzyl penicillin; Alembic) were used. Cells were subcultured using 0.25 % Trypsin (Sigma) – EDTA solutions and seeded on materials in a concentration of 1,500 cells/well seeded on the surface of HA, BGS and HABGS discs (10 x 3 mm size). The materials were preconditioned in culture medium for 15 min before cell seeding and thereafter the discs with cells were incubated at 37 °C in an atmosphere of 5 % CO_2 and 95 % relative humidity.

After 48 h, the culture medium was collected separately and the cells with material were washed in phosphate buffered solution (PBS) and fixed in 3 % glutaraldehyde, post-fixed in 1 % osmium tetroxide, dehydrated in acetone, critical point dried (HCP2-Hitachi), gold coated in an ion sputter (E101-Hitachi) and viewed in SEM (S2400 Hitachi).

II.4 *In Vivo* Evaluation Of Bioactive Ceramics: Heterotopic Evaluation

II.4.1 Preparation of the materials

HA, BGS and HABGS granules were thoroughly cleaned using acetone and finally in deionized distilled water for 30 min in an ultrasonic cleaner to remove any powder or debris attached on the surface of the granules and vacuum dried to remove any water or moisture from the material. The samples were sterilized by autoclaving prior to implantation.

II.4.2 Preparation of Fibrin Glue

A biologic tissue adhesive, which is two-component system, was prepared in-house. Fibrinogen concentrate was prepared from single donor screened human plasma by cryoprecipitation method (Ratnoff *et al.*, 1951; Silver *et al.*, 1995). The lyophilized cryoprecipitate, which consists of fibrinogen, factor XIII and VIII, was reconstituted in distilled water to get the desired concentration. Bovine thrombin was obtained as a lyophilized powder from a commercial source (E.Merck Germany), and reconstituted in 25 mM calcium chloride.

II.4.2.1 Preparation of Fibrin Glue-Ceramic Composite

Sterilized HA, BGS and HABGS (50 mg) samples were placed in 96 well flat bottom culture plates (Nunc) and mixed with 2.5 mg and 5 mg fibrinogen followed by polymerization with 50 U/mL of thrombin in calcium chloride. All the samples were incubated at 37 °C for half an hour, then frozen at –70 °C for 24 hours and freeze-dried in a lyophilyzer (Edward Modulyo).

II.4.3 Scanning Electron Microscopy (SEM)

Coated granules with lyophilized FG and uncoated granules were critically point dried with a – HCP 2-Hitachi, and then coated with gold in an ion sputter (E

101-Hitachi). Subsequently sample surfaces were viewed using SEM (S 2400 - Hitachi).

II.4.4 Experimental Animal Groups

Twenty-seven Swiss albino, male mice, with an average body weight of 30 to 35 g, and one defect per leg were divided into three groups as shown in Table II.2. Management of animal husbandry and postoperative care of the animals are standardized at SCTIMST, Vivarium, as per the guidelines of the Committee for the Purpose of Control and Supervision of Experiments on Animals (CPCSEA) from the Indian National Science Academy (INSA).

Table.II.2

Material	**I-Uncoated**	**II- FG Coated (2.5 mg)**	**III-FG Coated (5 mg)**
	No. of animals	No. of animals	No. of animals
HA	3	3	3
BGS	3	3	3
HABGS	3	3	3

Note:
I, II and III represents the animal groups implanted with HA, BGS, and HABGS; 2.5 mg FG and 5 mg FG represents the concentration of Fibrin Glue coated with the material and No. represents the number of animals used for the surgery.

II.4.5 Surgical Procedure

Animals were anesthetized with ketamine 50 mg/kg and xylazine 10 mg/kg body weight, intramuscularly. The skin was shaved and disinfected with betadine-povidone iodine. A one centimeter longitudinal skin incision was made exposing the quadriceps muscle in which a small pouch was created. Sterilized materials were implanted deep into the muscle pouch and the wound closed with 4.0 mer silk sutures.

After closure, the sutured wound was swabbed with betadine and dressed with neosporin. Animals were kept in cages (2 per cage) and fed with standard diet and water *ad libitum*. After 28 days, the animals were euthanised intraperitoneally with an over dosage of thiopentone sodium. Tissues were retrieved for histological analysis.

II.4.6 Flurochrome labeling

All the twenty-seven mice were given subcutaneous dose of Tetracycline (30 mg/kg) and Calcein blue (25 mg/kg) 15 days and 24 days respectively after the surgical implantation of the granules.

II.4.7 Radiography

Radiographs (Dental X-ray Unit- N Villa Sistemi Medicali - Model 83603) were taken immediately after implantation and prior to sacrifice at 28 days.

II.4.8 Histological evaluation

The retrieved tissue from one animal of each group was fixed in 10 % phosphate-buffered formalin, dehydrated in graded series of alcohol and embedded in polymethyl methacrylate (PMMA). For fluorescence microscopy, the tissues from the remaining two animals of each group were fixed in 70 % alcohol, dehydrated in ascending grades of ethanol and embedded in polymethyl methacrylate (PMMA). The sections (200 μm) were cut on the Isomet (Isomet-Buehler) with a diamond circular blade and subsequently ground to a thickness of 100-130 μm and polished (Buehler-Polisher). These sections were stained with Stevenel's blue/Acid Picrofuschin stain (Gurr 1973; del Cerro *et al.*, 1980), and viewed with a Light Microscope (Nikon-Optihot) and photographed. Unstained sections were viewed with the fluorescence

microscopy (Nikon- Eclipse E600) and viewed under wavelengths 390 - 560 nm for tetracycline (filter BV2A) and 375 - 435 nm for calcein blue (filter UV2A).

II.4.9 Image Analysis: Histomorphometry

Computer assisted image analysis was performed to quantify the percentage of new bone formed in the soft tissue with uncoated and FG coated HA, BGS and HABGS, granules after 28 days in mice quadriceps muscle.

The resin embedded sections was captured by a CCD camera attached to light microscope (Nikon, Optiphot), linked to the computer having Optimas 6.1 version software (Coreco Oculus-Tci Driver, Version 1.20 Beta 1 Mode, pixel format -8 bit gray scale and 24 - bit Red, Green, Blue (R G B) mode with a frame width of 768/576 pixels) for image analysis. The images are suitably calibrated using the inbuilt image configuration. All the images were captured in respective magnifications x 4 and x 10 and suitable filters were used to improve the resolution of the images.

The images were then evaluated for the percentage of new bone formed around the implant in the soft tissue. The interface of the implant with the soft tissue and the newly formed bone was analysed using the 3D-Luminance method. Three sections were evaluated per animal in all the groups. The implant size was measured by line morphometry method. Student's-t test was performed for statistical significance

II.5 Orthotopic Evaluation

II.5.1 Materials for Implantation

HA, BGS and HABGS granules were implanted in rabbit tibia bone to study the osteoconductive, osteoinductive and osseointegration mechanism at two different periods with FG for 3 months and without FG for 3 and 6 months.

II.5.2 Experimental Animals

Eighteen male young adult New Zealand White rabbits having an average body weight of 2.5 ± 0.25 kg were used for this study, for 3 and 6 months period. Animals were divided into two major groups as shown in Table II.3 and 4. Animals were fed with standard rabbit feed and water was given *ad libitum.*

Table.II.3

Material	Group -I (Without FG) Experiment Duration		
	3 Months (No. of Animals)	6 Months (No. of Animals)	
HA	4	4	
BGS	4	4	
HABG	4	4	
Control (Sham)	2	2	
	14	14	Total = 28

Group I: Rabbit implanted with uncoated HA, BGS, and HABGS granules. The duration of the experiment was 3 and 6 months. Four animals/material/period and two animals/period for defect alone (sham) were used for this study.

Table.II.4

Material	Group - II (FG) -3 Months (No. of Animals)
HA	4
BGS	4
HABG	4
Sham	2
Total	14

Group II: Rabbit implanted with FG coated HA, BGS, and HABGS granules. The duration of the experiment was for 3 months. Four animals/material and two animals for defect alone (sham) were FG alone is filled in the defect without any ceramic implants.

II.5.3 Surgical procedure-Rabbit: Group-I

The animals were monitored as per the norms of **CPCSCEA**. The transcortical bone-pin model for assessment of the *in vivo* bone response is adapted from the ASTM standard F981-91 *Standard Practice for Assessment of Compatibility for Surgical Implants with Respect to Effect of Materials on Muscle and Bone* (American Society for Testing of Materials, West Conshohocken, PA). The animal was given premedication, atropine (0.5 mg/kg body wt) and diazepam (10 mg/kg body wt) *i.m* and anaesthetized with ketamine (40 mg/kg body wt) and xylazine (3 mg/kg body wt) *i.m.* The tibial cortex was exposed along the medial aspect through a single deep incision. Periosteum was retracted to the sides using a periosteum elevator, to prevent damage during drilling. Two defects of 2 mm diameter size were created on the mid diaphysis area using a surgical drilling unit (Satellac, France), reamed to a depth of 3 mm, while continuously irrigated with cold saline to prevent thermal necrosis. The defect was packed with the respective granules. The incision was sutured in layers with 4.0 mer silk and the wound was dressed with neosporin. Postoperative care with medication and management of the animals were taken care as standardized in the Vivarium of the Institute. At post-implantation periods of 3 and 6 months, the rabbits were sacrificed using an excess dose of sodium thiopentone and the tibiae were removed to resect the implant site.

II.5.4 Surgical procedure-Rabbit: Group-II

Ceramic granules coated with 5 mg of lyophilized FG were taken for the bone implantation studies. The bone implantation procedure was same as that of Group-I experimental animals. Care was taken during implantation to prevent the FG coated granules from moving out of the cavity. A drop of sterile saline was added to prevent

air pouches and the defect was filled compactly. The animals were sacrificed after 3 months as mentioned above (II.5.3).

II.5.5 Bone labeling

To study the dynamic analysis of bone activity with the implant fluorochrome labeling was performed. Out of four animals in each group two animals was administered fluorochrome dye.

Group-I animals were injected with oxytetracycline (50 mg/kg body weight), *i.m* (intra muscular) one month post-implantation and 20 days prior to sacrifice.

Group -II animals were injected with oxytetracycline (50 mg/kg body weight), *i.m.* one month post-implantation, and alizarin complexone/calcein blue (30 mg/kg body weight) *i.m.* two months post-implantation and again one week prior to sacrifice tetracycline (50 mg/kg body weight *i.m.*) was administered.

II.5.6 Radiography (Bone)

X rays were taken at zero day (immediately after implantation) and before sacrifice using a dental X-ray unit (Dental X-ray Unit- N Villa Sistemi Medicali - Model 83603).

II.5.7 Microangiography: Barium sulphate method

An attempt was made to study the neo-vascularization after implantation. Briefly, before sacrificing the animal, barium sulphate and Indian ink were infused separately to study the vasculature status of the implanted site.

Femoral artery and femoral vein were cannulated, and flushed the bloodline with ringer lactate (heparinised) 1L. Once the out let flow became clear/ blood less, 30 % barium sulphate ($BaSO_4$) with Indian ink 140 mL + 500 mL ringer lactate was infused via a cardioplegia infusion set at 120 - 150 mm Hg, 15 min later 30 % of

$BaSO_4$ with 140 mL of Indian ink + 10 % buffered formalin was flushed as above for 15 min. The whole leg with the surgical cannula *in situ* was kept in 10 % buffered formalin for 3 days for fixation and then X- ray was taken. Thereafter sections of the implant area was taken, decalcified, dehydrated, embedded in PMMA, sectioned and viewed using light microscopy for any blood capillaries at the implant site.

II.5.8 Gross Evaluation

Soft tissues over the implanted bone specimens were removed manually and care was taken not to disturb the implant site. Gross photographs of the implant-bone interface were taken using a Diaplan Stereomicroscope (LEICA).

II.5.9 Scanning Electron Microscopy (SEM)

The SEM enables to study the surface extent of the mineralized bone with the implant. The bonding of implant to the bone and the surface porosity could be understood from the SEM observations. Thin sections of bone (100 - 150 μm) with the implant was cut and processed in ascending grades of acetone/ethanol and post fixed with isoamyl acetate for 5 min. The samples were dried using the critical point dryer (HCP2-Hitachi), and coated with gold in an ion sputter (E101-Hitachi) and viewed by SEM (S2400 - Hitachi).

II.5.10 SEM-Energy Dispersive X-ray Analysis (EDAX)

The samples were screened for the Ca, P, Si, and Mg distribution around the newly formed bone, implant and in the interface between the implant and the new bone. Samples were processed for Energy Disperse X-ray Analysis (EDAX- Oxford) as described above (II.5.9) but, instead of gold, carbon coating was done using a carbon coater (HINDHIVAC- Shadow Casting Unit, Model 12A4SC) and observed

using SEM attached with the EDAX unit (Oxford), interfaced to the computer for elemental analysis.

II.5.11 X-ray Diffraction (XRD)

The surrounding bone with the implant was dissected out carefully from the tibia bone and the specimen was thoroughly dried in a vacuum oven at 60 ° C for two days and pulverized into powder in a mortar and observed by XRD (Siemens D-5000) for the crystallinity and for any change in the material phase that had formed after implantation.

II.5.12 Fourier Transform Infrared Spectroscopy (FT-IR)

The bone specimen with the implant are cut into thin sections and thoroughly dried in a vacuum oven at 60 ° C for two days to remove water from the sample. The dried bone was pulverized in a mortar and was mixed with KBr in the ratio of 1:100 mg and pelleted and analyzed in FT-IR spectrophotometer as described earlier (II.1.5.2).

II.5.13 Histological evaluation

The tibia bone resected from rabbit was fixed in 10 % phosphate-buffered formalin immediately, and dehydrated in graded series of alcohol and embedded in polymethyl methacrylate (PMMA). For fluorescence microscopy, the tissues from the remaining two animals of each group were fixed in 70 % alcohol, dehydrated in ascending grades of ethanol and embedded in polymethyl methacrylate (PMMA). The sections (200 μm) were cut on the Isomet (Isomet-Buehler) with a diamond circular blade and subsequently ground to a thickness of 100-130 μm and polished (Buehler-Polisher). These sections were stained with Stevenel's blue and counter stained with

Van Gieson acid picrofuschin stain (Gurr 1973; del Cerro *et al.*, 1980), and viewed using light microscope (Nikon-Optiphot).

Unstained fluorochrome sections were viewed with the fluorescence microscopy (Nikon- Eclipse E600), viewed under wavelengths of 390-560 nm for oxytetracycline (filter BV2A) and 375-435 nm for calcein blue (filter UV2A) and alizarin complexone (Filter G2A).

Unstained normal bone and bone with implants were viewed under polarized light to understand the mineralization pattern.

II.5.14 Image Analysis: Histomorphometry

Computer assisted image analysis was performed to quantify the percentage of new bone formed with HA, BGS and HABGS granules implanted in rabbit tibia bone with and without FG after 3 and 6 months. The mode of image capturing is described in section II.4.9.

The images were then evaluated for the percentage of new bone formed in the defect with an implant. The implant - bone interface was analysed using the 3D-Luminance method. Three sections were evaluated per defect in all the groups. The implant size, pore size and the cell size were measured by line morphometric method.

II.5.15 Biochemical Estimation

II.5.15.1 Serum Collection

The blood was collected before implantation and after implantation. Rabbit ear vein was punctured with a 20 gauge sterile needle and the blood was collected in a dry clean test tube. The blood thus collected was kept in an incubator at 37 °C for 1 hour and allowed for the serum to separate. The serum was aliquoted into fresh eppendorf tubes and stored at - 20 °C until further experiments. To minimize the protein

denaturation from the freeze-thaw process, the samples were carefully separated into different eppendorf tubes for different biochemical evaluations. Haemolysed samples were always avoided.

II.5.15.2 Calcium

O-cresolpthalein complexone method was used to estimate calcium, as described in II.2.2.3.

II.5.15.3 Phosphorous

Phosphorous was detected using the Monozyme Phosphorous modified Metol method, as described in II.2.2.3.

II.5.15.4 Protein

Protein concentration in foetal calf serum, rabbit serum and minimum essential medium were assayed using the Biuret method, as described in II.2.2.4.

II.5.15.5 Alkaline phosphatase

Alkaline phosphatase (ALP) was estimated by the "Kind and King's Method" (Kind and King; Mayne, 1994) (Dr. Reddy's Laboratories). Serum ALP hydrolyzes phenyl phosphate into phenol and disodium phenol hydrogen phosphate at pH 10.0. The phenol so formed reacts with 4-Aminoantipyrine in alkaline medium in presence of oxidizing agent potassium ferricyanide to form a red coloured complex whose absorbance is proportional to the enzyme activity (Table.II.5).

$$\text{Disodium Phenyl Phosphate} + H_2O \xrightarrow[\text{pH 10.0}]{\text{ALP}} \text{Phenol} + \text{Disodium Hydrogen Phosphate}$$

$$\text{Phenol} + \text{4 Amino Antipyrine} \xrightarrow[\text{Potassium ferricyanide}]{\text{Alkaline medium}} \text{Red coloured complex}$$

Table.II.5

Reagent	Blank	Standard	Control	Test
Working buffered substrate	1.0 mL	1.0 mL	1.0 mL	1.0 mL
Deionised water	3.1 mL	3.0 mL	3.0 mL	3.0 mL
Mix well and incubate at 37 °C for 3 min				
Serum	---	---	---	0.1 mL
Standard (Phenol)	---	0.1 mL	---	---
Mix well and incubate at 37 °C for 15 min				
Colour Reagent	2.0 mL	2.0 mL	2.0 mL	2.0 mL
Serum	---	---	0.1 mL	---

The working buffer substrate is mixed with deionized distilled water and incubated for 3 min at 37 °C and the serum (Test sample), standard and blank reagent was then added and incubated for 15 min at 37 °C for 15 min and colour reagent was added and the absorbance (A) for blank (B), Standard (S), Control (C) and Test (T) against deionized water on spectrophotometer at 510 nm.

Calculation

$$\text{Serum ALP in KA units/dl} = \frac{A(T) - A(C)}{A(S) - A(B)} \times 10$$

II.5.15.6 Acid phosphatase

Acid phosphatase (ACP) was estimated by modified "King's Method" (King, 1959) (Dr. Reddy's Laboratories). Serum ACP hydrolyzes disodium phenyl phosphate to phenol and disodium phosphate at pH 5.0. The phenol so formed reacts with 4 - aminoantipyrine in alkaline medium, in the presence of oxidizing agent potassium ferricyanide to form a red coloured complex whose absorbance is proportional to the

enzyme activity. Prostatic ACP activity is inhibited by tartrate. The ACP assay in presence of tartrate measures non-prostatic fraction.

$$\text{Disodium Phenyl Phosphate} + H_2O \xrightarrow[\text{pH 5.0}]{\text{ACP}} \text{Phenol} + \text{Disodium Hydrogen Phosphate}$$

$$\text{Phenol} + \text{4 Amino Antipyrine} \xrightarrow[\text{Potassium ferricyanide}]{\text{Alkaline medium}} \text{Red coloured complex}$$

The working buffer substrate is mixed with deionised distilled water and incubated for 3 min at 37 °C and the Tartrate solution (Ts) serum (Test sample), standard and blank reagent was added and incubated for 15 min at 37 °C for 60 min and the colour reagent was added and the absorbance (A) for blank (B), Standard (S), Control (C) and Test (T) and tartrate solution (Ts) against deionized water on spectrophotometer at 510 nm (Table.II.6).

Table.II.6

Reagent	**Blank**	**Standard**	**Control**	**Test**	**Tartrate Solution**
Buffered substrate	1.0 mL	1.0 mL	1.0 mL	1.0 mL	1.0 mL
Deionised water	3.2 mL	3.1 mL	3.0 mL	3.0 mL	3.0 mL
Mix well and incubate at 37 °C for 3 min					
Tartrate Solution	---	---	---	---	One drop (approximately) 100 µL
Serum	---	---	---	0.2 mL	0.2 mL
Standard (Phenol)	---	0.1 mL	---	---	---
Mix well and incubate at 37 °C for 60 min					
Colour Reagent	2.0 mL	2.0 mL	2.0 mL	2.0 mL	2.0 mL
Serum	---	---	0.2 mL	---	---

Calculation

$$\text{Total Serum ACP activity in KA Units} = \frac{\text{A of (T) - A of (C)}}{\text{A of (S) - A of (B)}} \times 5$$

II.5.15.7 Creatinine

The creatinine estimation was done by "alkaline picrate method" (Bonses and Tausskay, 1945) using a kit method (Qualigens-Glaxo). In alkaline medium picric acid reacts with creatinine and produces a red coloured complex, whose absorbance is proportional to the creatinine concentration. Picric acid reagent has a dual role, as deproteinizing agent and as a reactant.

Deproteinization of specimen

Serum was mixed with picric acid reagent and mixed well and centrifuged at 2000 - 3000 rpm for 10 min, to obtain a clear supernatant.

Colour development

Aliquots of the deproteinized serum supernatant were added to the test (T). Picric acid reagent was added to Blank (B) and Standard (S). To the test, blank and standard solutions sodium hydroxide was added and allowed to stand at room temperature for 20 min and read against the distilled water in a spectrophotometer at 520 nm (Table.2.7).

Table.II.7

Reagent	Blank (B)	Standard (S)	Test (T)
Supernatant from deproteinized serum	---	---	3.5 mL
Creatinine Standard	---	0.5 mL	---
Picric acid reagent	3.0 mL	3.0 mL	---
Sodium hydroxide	2.0 mL	2.0 mL	2.0 mL

Calculation

$$\text{Serum creatinine in mg \%} = \frac{\text{A of (T) - A of (B)}}{\text{A of (S) - A of (B)}} \times 2.0$$

II.5.15.8 Parathyroid hormone

Method description

The DiaSorin intact PTH SP immunordatiometric assay (IRMA) utilizes 2 different polyclonal antibodies that have been purified using affinity chromatography. These purified antibodies are specific for 2 different regions of the PTH molecule. The first antibody, specific for PTH 39-84, is bound to a solid phase (polystyrene beads). The second antibody is specific for PTH 1-34 and is labeled with iodine-125. Samples are incubated simultaneously with both antibodies. Intact PTH 1-84 contains both the 1-34 and 39-84 amino acid sequences and is the only form of PTH that will be bound by both the antibody on the bead and the antibody labeled with iodine-125.

Since the antibody coupled to the solid phase is specific for C-terminal and mid-region fragments as well as intact PTH, the capacity of the solid phase has been designed to accommodate very high levels of PTH. This prevents interference by extremely elevated C-terminal and mid-region PTH fragments in unknown samples.

Following the incubation period, each bead is washed to remove any unbound labeled antibody. The radioactivity present in the remaining bound labeled antibody is then measured using a gamma counter.

Reagents

1. N-tact PTH SP 0 Standard

Contains human serum with 0.1 % sodium azide added as a preservative.

2. N-tact PTH SP Standards (A-E)

Set of 5 human PTH 1-84 standards, at nominal concentrations ranging from 15-2000 pg/mL, contains 0.1 % sodium azide and other stabilizers. Reconstitute each vial of lyophilized standard with 2.0 mL of the 0 standard, mixed thoroughly and allowed to settle for 5 min at 2-8 °C or until the contents are completely dissolved.

3. N-tact PTH SP Beads

Polystyrene beads are coated with affinity-purified goat antibody specific for the 39-84 sequence of PTH.

4. ^{125}I N-tact PTH SP Antibody

Each vial contains 5.0 mL of affinity purified goat antibody specific for PTH 1-34, labeled with ^{125}I. The labeled antibody is diluted in buffered serum containing red dye and 0.1 % sodium azide.

5. N-tact PTH SP wash Solution Concentrate

Contains a concentrated buffered surfactant. A working wash solution was prepared by diluting the entire vial contents with 450 mL of distilled or deionized water and stored at room temperature.

6. N-tact PTH SP Control, Level 1 and Level 2

Human serum is spiked with hPTH 1-84 to obtain a concentration within a specified range 0.1 % sodium azide. Lyophilized control were reconstituted with 2.0 mL of distilled or deionized water, mixed and allowed to stand at 2 - 8 °C until the contents are completely dissolved.

Materials

PTH standards, Beads coated with antibody to hPTH 39-84 and ^{125}I antibody hPTH 1-34, PTH control and disposable borosilicate glass tubes.

Assay Procedure

Lyophilized reagents were reconstituted and the frozen specimens were thawed completely. Keep reagents and thawed specimens on ice while setting up assay.

1. Set up labeled 12 x 75 mm borosilicate glass tubes in duplicate
2. Reagents were added as follows:
    a. Total count tubes
       100 µL ^{125}I N-tact PTH SP Antibody (red)
    b. 0 Standard
       200 µL 0 standard
       100 µL ^{125}I N-tact PTH SP antibody (red)
    c. Standards (A-E)
       200 µL standard
       100 µL ^{125}I N-tact PTH SP Antibody (red)
    d. Control and unknown samples
       200 µL sample
       100 µL ^{125}I N-tact PTH SP Antibody (red)
3. The samples were thoroughly mixed in a vortexer
4. Beads were dispensed into each tube with teflon-coated forceps.
5. Tubes were incubated for 22 (±2) hours at 20-25°C
6. The reaction mixtures were aspirated from each tube
7. The beads were thoroughly washed by vigorously with 1 mL of wash solution. The procedure was repeated 3 times.
8. The radioactivity in each tube was measured using a gamma counter.

Calculation

To determine the concentration of intact PTH found in unknown and control samples, a standard curve was prepared using the standard concentrations stated on the vial labels.

1. The average counts per minute (CPM) was calculated for each standard, control, and unknown sample.

2. The average CPM was subtracted from the 0 standard tubes from all other average counts to obtain corrected CPMs

$$\text{Values of unknown} = \frac{\text{Corrected CPM (unknown)}}{\text{Corrected CPM (Std.A)}} \times \text{value of Std. A}$$

II.5.15.9 Calcitonin

Method description

Calcitonin was estimated by Radio Immuno Assay (RIA) method (DiaSorin). The DiaSorin calcitonin II RIA is a disequilibrium procedure using delayed tracer addition to increase sensitivity. The antibody was produced in a goat against pure synthetic human calcitonin. In this RIA, sample and first antibody are combined and incubated for 16 - 24 hours at 2 - 8 °C. Tracer was added, followed by a second incubation for 16 -24 hours at 2 - 8 °C. A pre-precipitated second antibody complex was added to separate the bound from free tracer. The sample was centrifuged and decanted after 15 - 20 min incubation at 20 - 25 °C.

Reagents

1. Calcitonin 0 standard

   BSA-borate buffer with sodium azide (0.25%) added (lyophilized). The standard was reconstituted with 10 mL of deionized distilled water, mixed and allowed to stand for 15 - 20 min until the contents were completely dissolved. The reconstituted sample is stored at -15°C.

2. Calcitonin II standard

   Human synthetic calcitonin, at a nominal concentration of 1,000 pg/mL, was diluted in BSA-borate buffer with sodium azide (0.2 %) and other stabilizers added (lyophilized). Exact concentration values were assigned with each lot. The

lyophilized standard was reconstituted with 1.0 mL of deionized distilled water, mixed and allowed to stand for 15 - 20 min on crushed ice until the contents were completely dissolved. In order to obtain the entire standard curve, serial dilutions were made by adding 500 µL of standard to 500 µL of 0 standard.

3. Calcitonin Antiserum

   Goat anti-calcitonin serum was diluted in BSA-borate buffer with sodium azide (0.1 %) and blue dye added (lyophilized). The blue dye was reconstituted with 14 mL of deionized distilled water, mixed and allowed to stand for 15 - 20 min until the contents were completely dissolved.

4. ^{125}I Calcitonin

   Synthetic human calcitonin was labeled with iodine-125 (1.5 µCi/55.5 kBq) and diluted in BSA-borate-EDTA buffer with sodium azide (0.4%) and red dye added (lyophilized). The lyophilized sample was reconstituted with 7 mL of deionized distilled water, mixed and allowed it to stand for 15 - 20 min until the contents were completely dissolved.

5. Calcitonin precipitating complex

   Normal goat serum, pre-precipitated with donkey anti-goat serum and polyethylene glycol (PEG), was diluted in BSA-borate buffer with sodium azide (0.1%)

6. Calcitonin control (Level 1)

   Human serum was spiked, if necessary, with the appropriate amount of synthetic human calcitonin to obtain a concentration within a specified range. Sodium azide (0.1%) and other stabilizers are added (lyophilized). The lyophilized control was

reconstituted with 1.0 mL of deionized distilled water, mixed and allowed to stand for 15 - 20 min until the contents are completely dissolved

Materials

Calcitonin standard, Calcitonin II standard, Calcitonin antiserum, ^{125}I calcitonin, Calcitonin precipitating complex, Calcitonin control (Level 1), Calcitonin control (Level 2) and disposable borosilicate glass tubes.

Assay Procedure

1. The sample was thawed and kept in an ice tray.
2. The tests were performed in duplicate
3. The rack tubes along with the borosilicate tubes were kept in crushed ice.
4. The tubes were divide into
   a. Total count tubes
   b. Non specific binding (100 µL of 0 standard)
   c. 0 standard (100 µL of 0 standard and 200 µL of calcitonin antiserum)
   d. Calcitonin standards (100 µL of calcitonin standard, 200 µL of calcitonin antiserum)
   e. Quality control and unknown samples (100 µL of serum, 200 µL of calcitonin antiserum)
5. The tubes were gently vortexed without foaming and incubated for 16 - 24 hours at 2 - 8 °C.
6. 100 µL of ^{125}I calcitonin was added to all tubes
7. The tubes were gently vortexed without foaming and again incubated for 16 - 24 hours at 2 - 8 °C

8. The samples were mixed vigorously and 500 µL of the precipitated complex was added to all tubes except the total count tubes.
9. The tubes were vortexed and incubated for 15 - 25 min at 20 - 25 °C.
10. The samples were then centrifuged at 760 x g for 20 min at 20 - 25 °C.
11. Immediately the supernatant was decanted from all the tubes except the total count tubes by inverting them for a maximum of 2 min. The tubes were blotted with an absorbent paper to remove any drops of supernatant that may be remaining on the rims before turning the tubes upright.
12. Using a gamma scintillating counter, the precipitate of each tube and the total count tubes were counted for a sufficient time (30 sec) to achieve statistical accuracy.

Calculation

1. The average CPM for each standard, control and unknown sample was calculated.
2. The average CPM was subtracted for the NSB tubes from all counts.
3. Then divide the corrected CPM of each standard, control or unknown sample by the corrected CPM of the 0 standard.

$$B/B_0\ \% = \frac{\text{CPM of standard or unknown sample - CPM of NSB}}{\text{CPM of standard - CPM of NSBs}} \times 100$$

II.5.16 STATISTICAL ANALYSIS

The data were statistically analyzed and expressed as Mean ± Standard Error of Mean (SEM). The SEM was calculated by the following formula (Ostle, 1966).

$$SEM = \frac{\sqrt{\Sigma x^2 - (\Sigma x)^2}}{n(n-1)}$$

where x = individual observations, and

n = number of observations

Students 't' test was used to compare the mean value of two groups, 't' values were calculated by the following formula:

$$t = \frac{\Sigma x_1 / n - \Sigma x_2 / n}{s\sqrt{1/n_1 + 1/n_2}}$$

Where 's' is the standard deviation, which is calculated as follows:

$$S = \sqrt{\frac{\Sigma x_1^2 - (\Sigma x_1)^2 / n_1 + \Sigma x_2^2 - (\Sigma x_2)^2}{(n_1 + n_2) - 2}}$$

Where n_1 and n_2 stand for the number of observations in the two classes being compared. The value of probability was obtained from the degree of freedom by using the standard table given by Fisher and Yates (1948). If the calculated value was greater than the table value, it is significant at the probability level.

The levels of significance used are as follows: $p < 0.001$, $p < 0.01$ and $p < 0.05$ were considered as significant while values above $p < 0.05$ was considered to be non-significant.

CHAPTERS – III - VI

RESULTS AND DISCUSSIONS

CHAPTER – III

MATERIAL CHARACTERIZATIONS

III. Material Characterizations

III.1 Material Characterizations- Results

III.1.1 Scanning Electron Microscopy (SEM)

SEM of the porous HA granules (Figure III.1 A) showed dense surface with an average pore size of approximately 100 - 150 μm; BGS granules (Figure III.1 B) revealed rough surface with pore size ranging from 30 to 50 μm in size and HABGS granules (Figure 111.1 C) showed dense rough surface with pore size of 10 - 30 μm.

III.1.2 Transmission Electron Microscopy (TEM)

TEM showed submicron crystallites of tibia bone (Figure III.2 A), HA, 200-400 nm in size (Figure III.2 B), BGS (Figure III.2 C) and HABGS approximately 1μm in size (Figure III.2 D).

III.1.3 X-Ray Diffraction (XRD)

XRD spectra of HA, BGS and HABGS powders revealed crystalline peaks (as observed by means of JCPDS file). The major peaks observed in the HA spectrum (Figure III.3) were assigned to apatite and few brushite peaks. In BGS (Figure III.4), apatite and wollastonite were observed as major peaks with a few whitlockite peaks. HABGS (Figure III.5) revealed whitlockite, apatite and wollastonite as major peaks.

III.1.4 Fourier Transform-Infrared Spectroscopy (FT-IR)

FT-IR spectrum of HA powder (Figure III.6 A) revealed the presence of the hydroxyl groups ($^-$OH), a sharp peak at 3569 cm^{-1} with a bend at 3435 cm^{-1}. The ν_3 phosphate (PO_4) peaks (antisymmetric stretching) were observed at 1092 and 960 cm^{-1} and ν_4 PO_4 peaks (antisymmetric bending) at 600 cm^{-1} and 568 cm^{-1}. The peak at 476 cm^{-1} was assigned to ν_2 PO_4 groups. Some carbonate (CO_3) absorption was observed at 1410 cm^{-1}. The stretch observed between 1700-1614 cm^{-1} could be assigned to the C=O/C=C. The peak at 631 cm^{-1} could be due to the $^-$OH liberational

mode of the hydroxyl ion. Two peaks at 2076 cm^{-1} and 1988 cm^{-1} could be assigned to the P-O vibrations.

FT-IR spectrum of BGS (Figure III.6 B) powder revealed the absence of the -OH peak. The peaks at 1117 to 1022 cm^{-1} could be due to the Si-O stretch of the wollastonite. The Si-O-Si stretch were observed between 1117 -716 cm^{-1}. The three peaks observed at 1117, 1051, 1022 and the peak at 938 cm^{-1} could be assigned to ν_3 and ν_4 vibration of the phosphate. The peaks at 587-554 cm^{-1} could be assigned to the ν_4 and the peak at 554-429 cm^{-1} could be due to the Si -O-Si (bend).

FT-IR spectrum of the HABGS (Figure III.6C) powder did not show any -OH. The peaks at 1118 to 1020 cm^{-1} could be due to the Si-O stretch of the wollastonite. The Si-O-Si stretch was observed between 1118 to 716 cm^{-1}. The ν_3 PO_4 peaks were observed at 1118, 1053, 1020 and the ν_1 PO_4 peaks at 938 cm^{-1}. The peaks at 610-551cm^{-1} could be assigned to ν_4 of PO_4. The Si-O-Si (bend) was observed between 551-430 cm^{-1}. The peaks observed at 1700-1579 cm^{-1} could be assigned to the C-H (bend) or N-H (bending).

III.1.5 Energy Dispersive X-ray Analysis (EDAX)

EDAX analysis of the raw sample of HA revealed the presence of calcium (Ca), phosphorous (P) as the major inorganic components (Figure III.7 A). BGS showed Ca, P and silica (Si) as major minerals, Ca and Si was comparatively high than P (Figure III.7 B). HABGS granules showed Ca, P and Si as major inorganic components. In HABGS, Ca and P was comparatively higher than Si (Figure III.7 C).

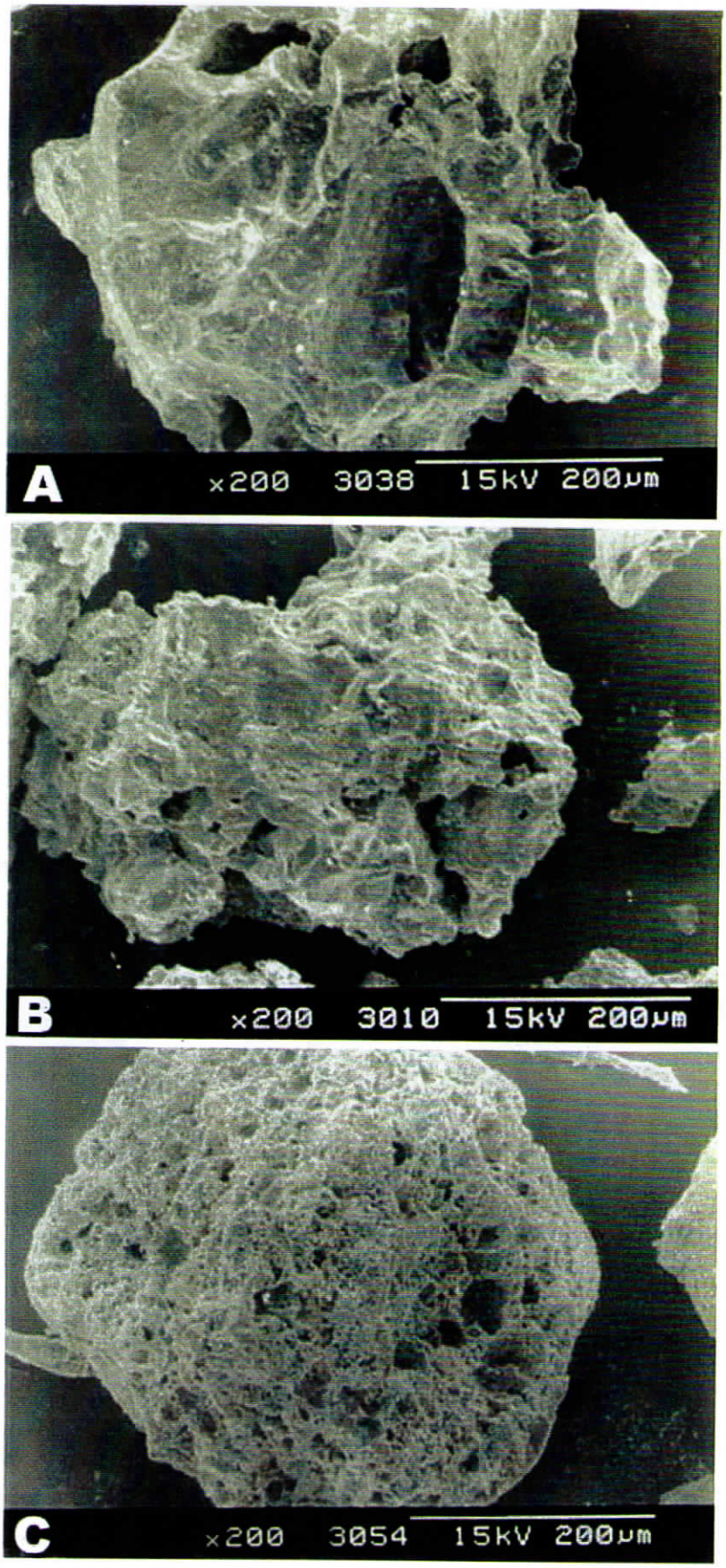

Figure - III-1

Scanning Electron Micrographs of bioactive ceramic granules A- HA; B-BGS and C- HABGS granules (300 - 350 µm)

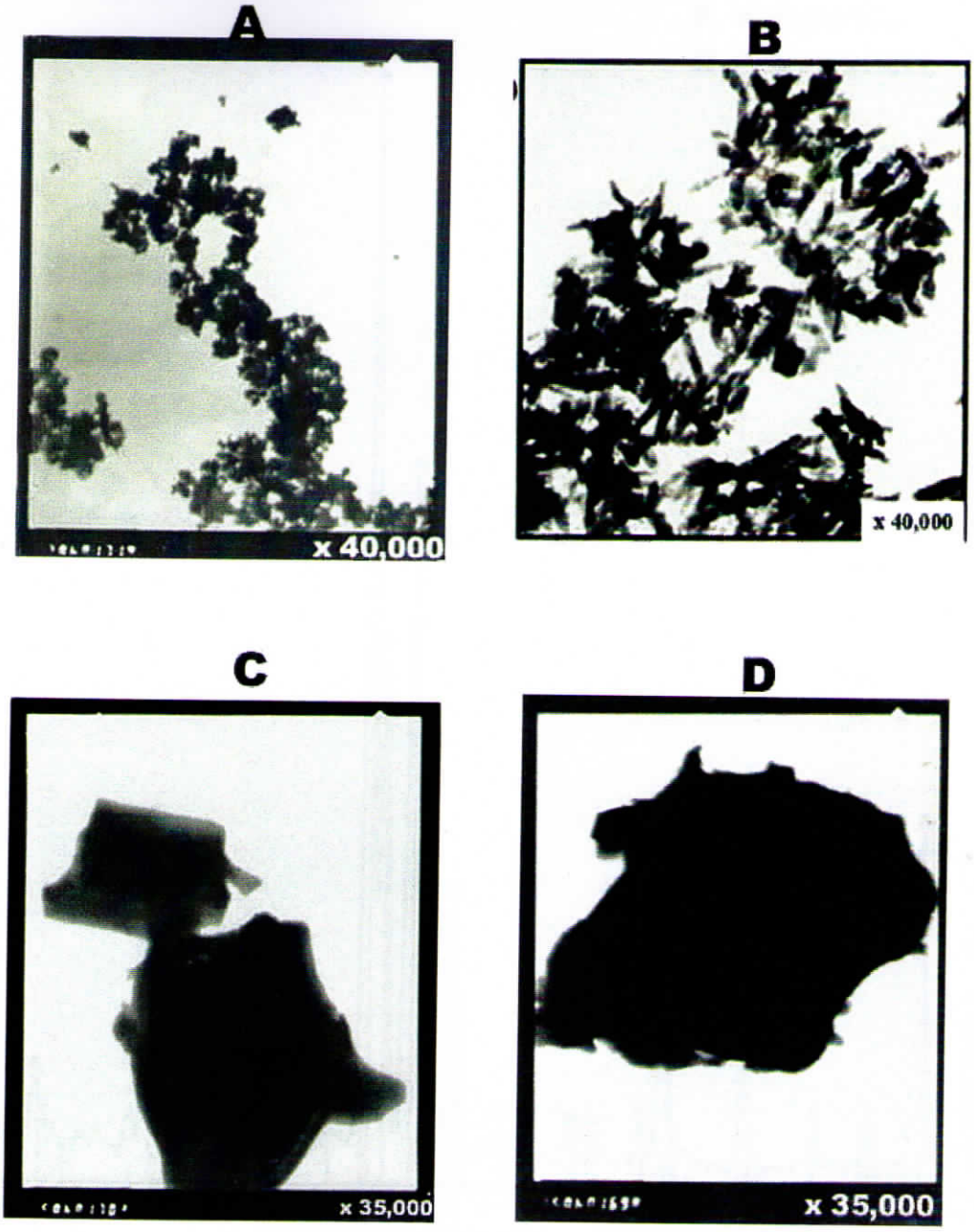

Figure - III-2

Transmission electron micrographs of raw powder samples : A - tibia bone; B - HA; C - BGS and D - HABGS.

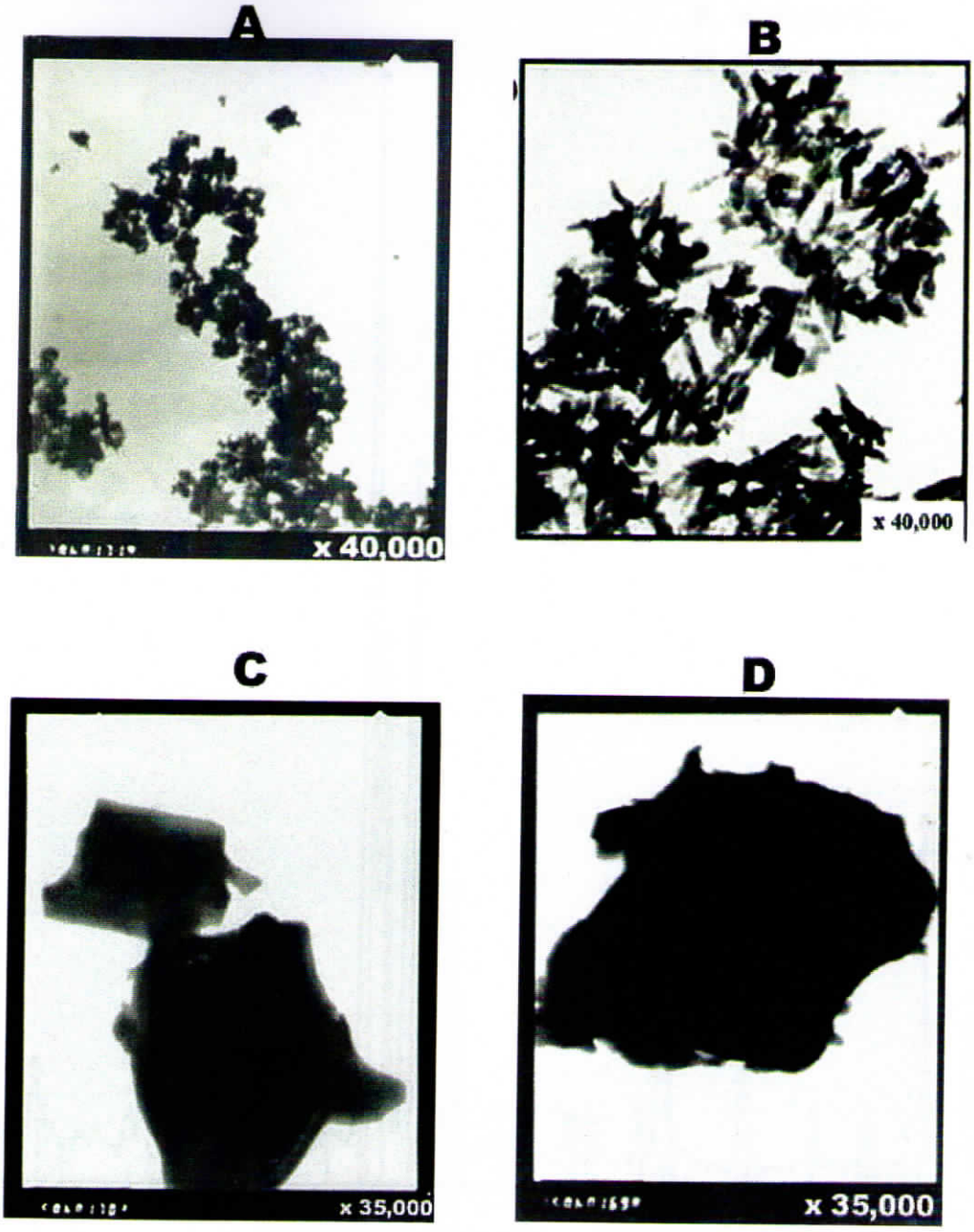

Figure - III-2

Transmission electron micrographs of raw powder samples : A - tibia bone; B - HA; C - BGS and D - HABGS.

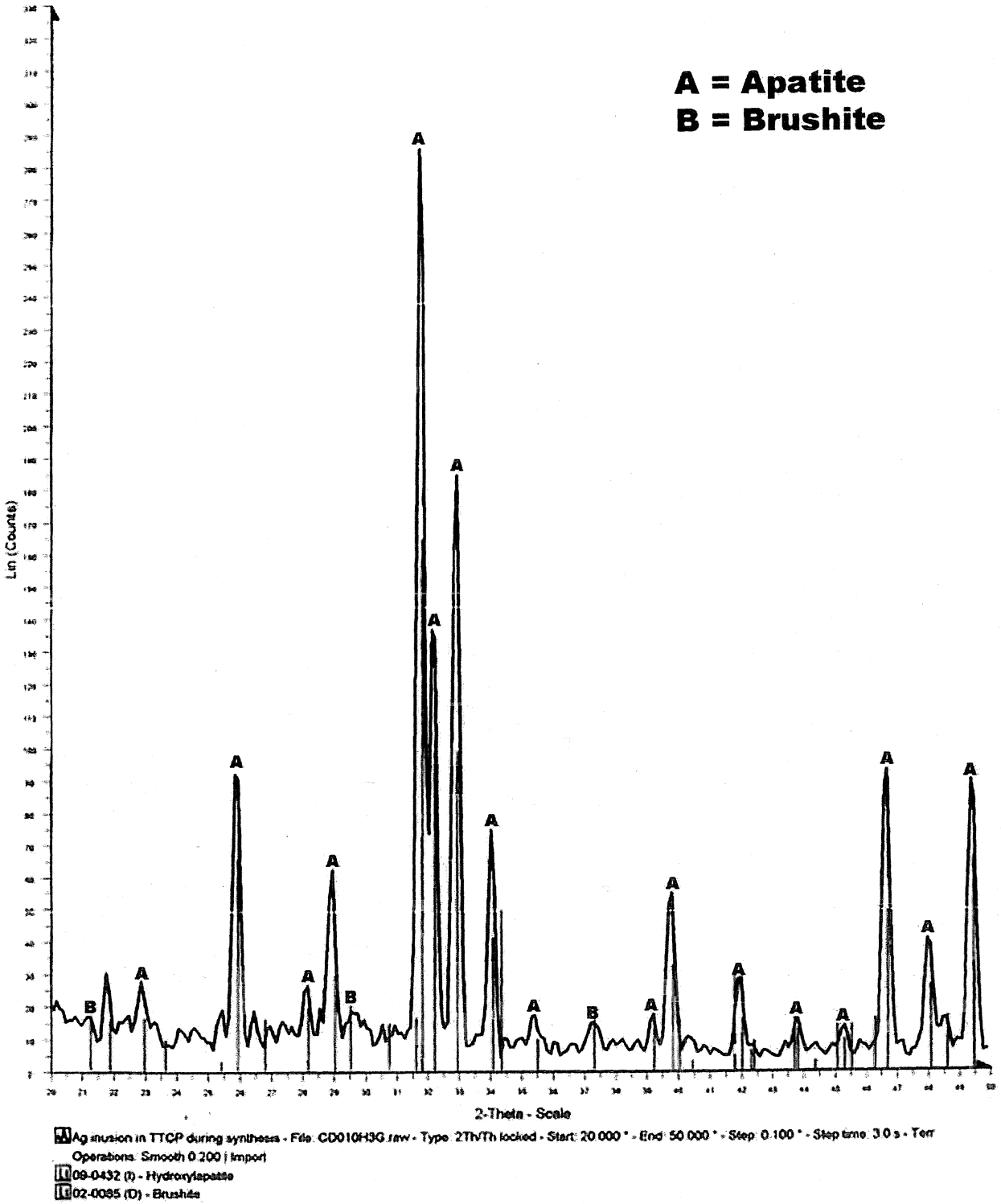

Figure - III-3

X- ray diffraction spectrum of HA sintered granule powder: The major peaks were apatite and few brushite peaks. A - denotes apatite ($Ca_{10}(PO_4)_6 OH_2$) and B - denotes brushite peaks ($CaHPO_4 . 2H_2O$).

Figure -III-4

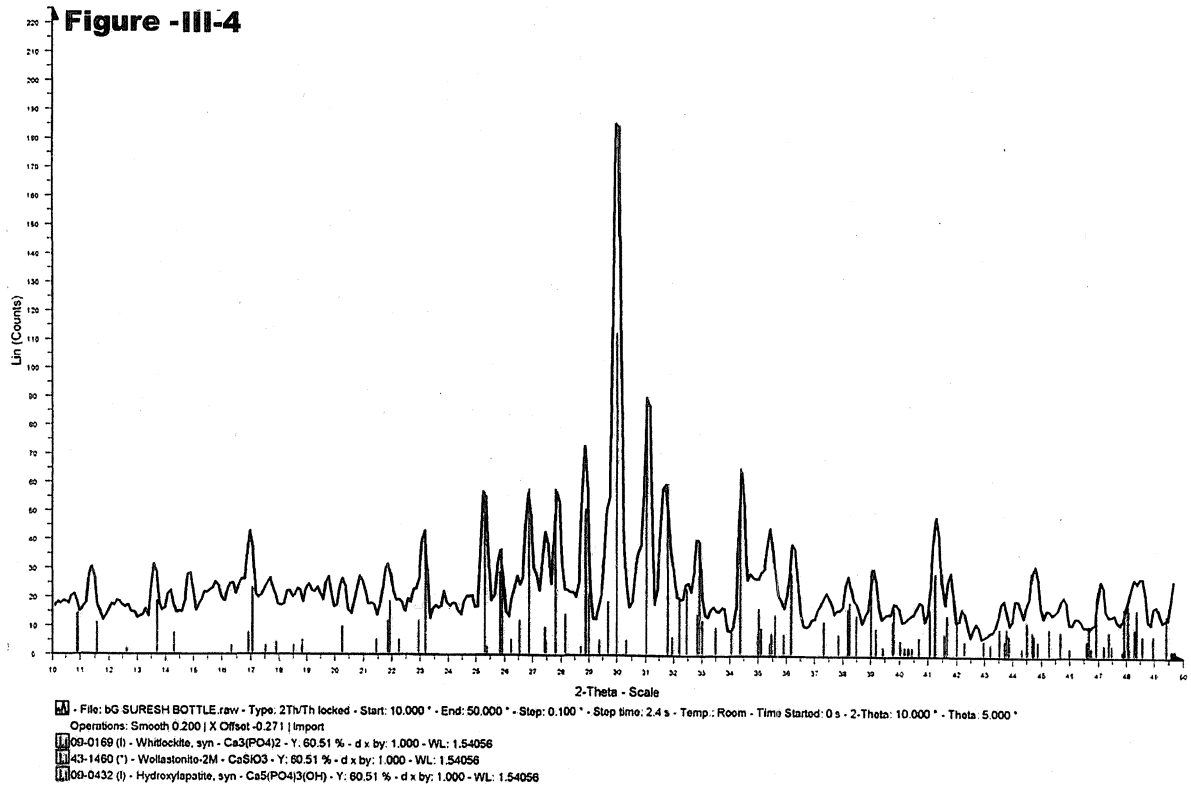

X- ray diffraction spectrum of BGS sintered granule powder: The major peaks were apatite, whitlockite and wollastonite peaks. Blue bar denotes- whitlockite (Ca_3 $(PO_4)_2$); brown bar- wollastonite ($CaSiO_3$); purple bar- apatite on the x-axis of the scale.

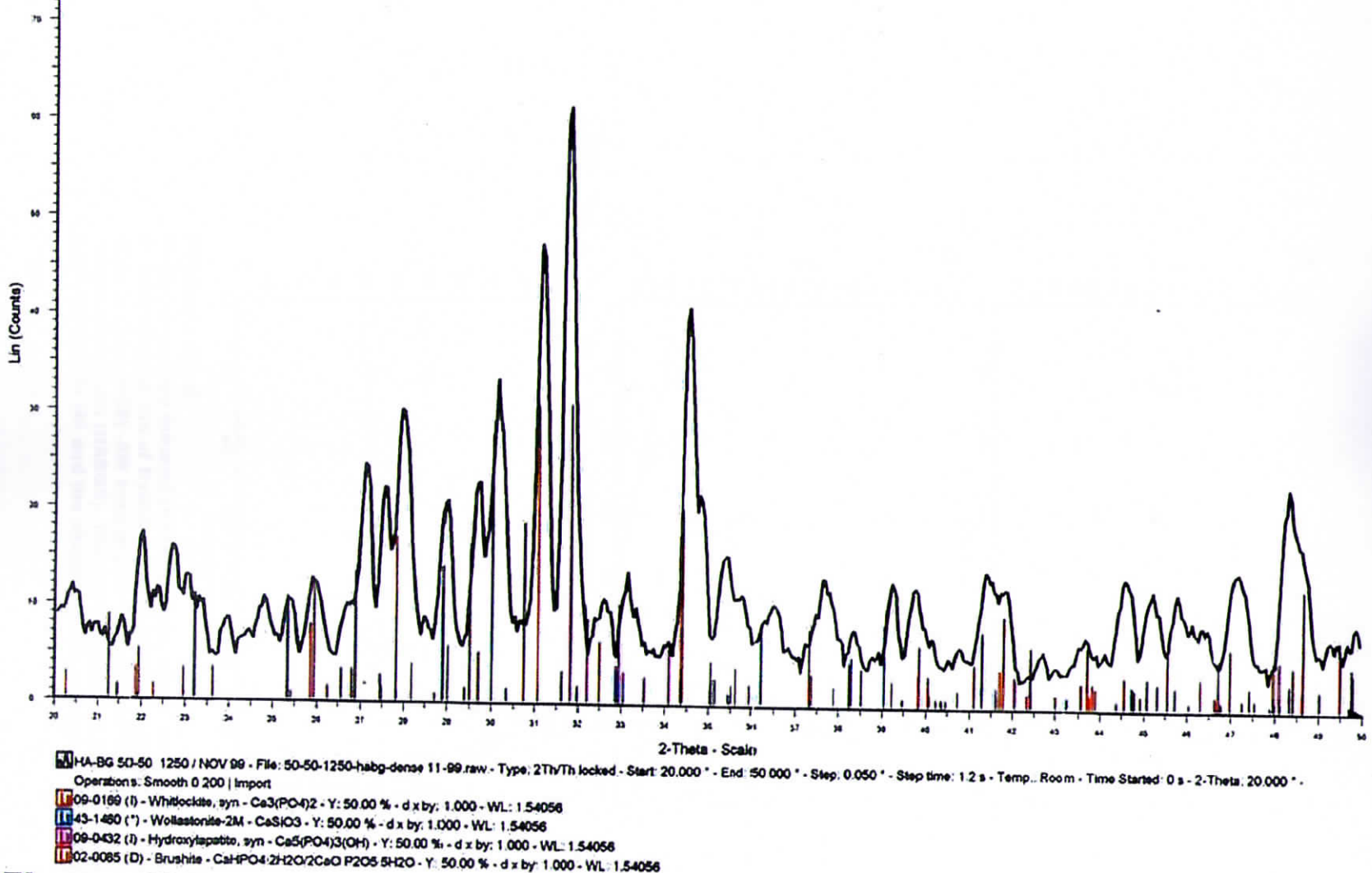

Figure -III-5

X- ray diffraction spectrum of HABGS sintered granule powder: The major peaks were apatite, whitlockite, wollastonite and few brushite peaks. Green bar denotes - whitlockite ($Ca_3(PO_4)_2$); blue bar- wollastonite ($CaSiO_3$); purple bar- apatite and brown bar - brushite ($CaHPO_4 \cdot 2H_2O$) on the x-axis of the scale

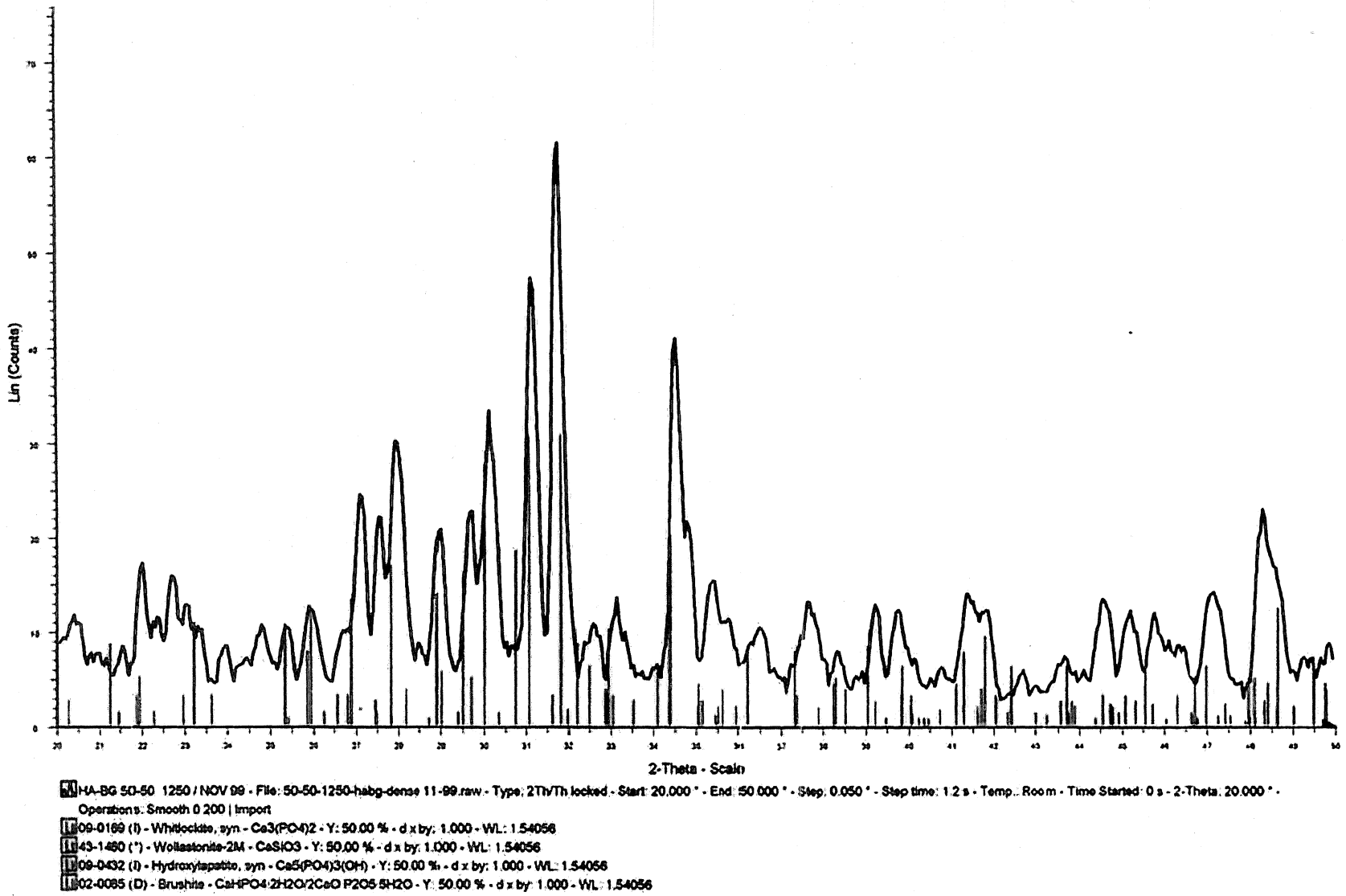

Figure -III-5

X-ray diffraction spectrum of HABGS sintered granule powder: The major peaks were apatite, whitlockite, wollastonite and few brushite peaks. Green bar denotes - whitlockite ($Ca_3(PO_4)_2$); blue bar- wollastonite ($CaSiO_3$); purple bar- apatite and brown bar - brushite ($CaHPO_4 \cdot 2H_2O$) on the x-axis of the scale.

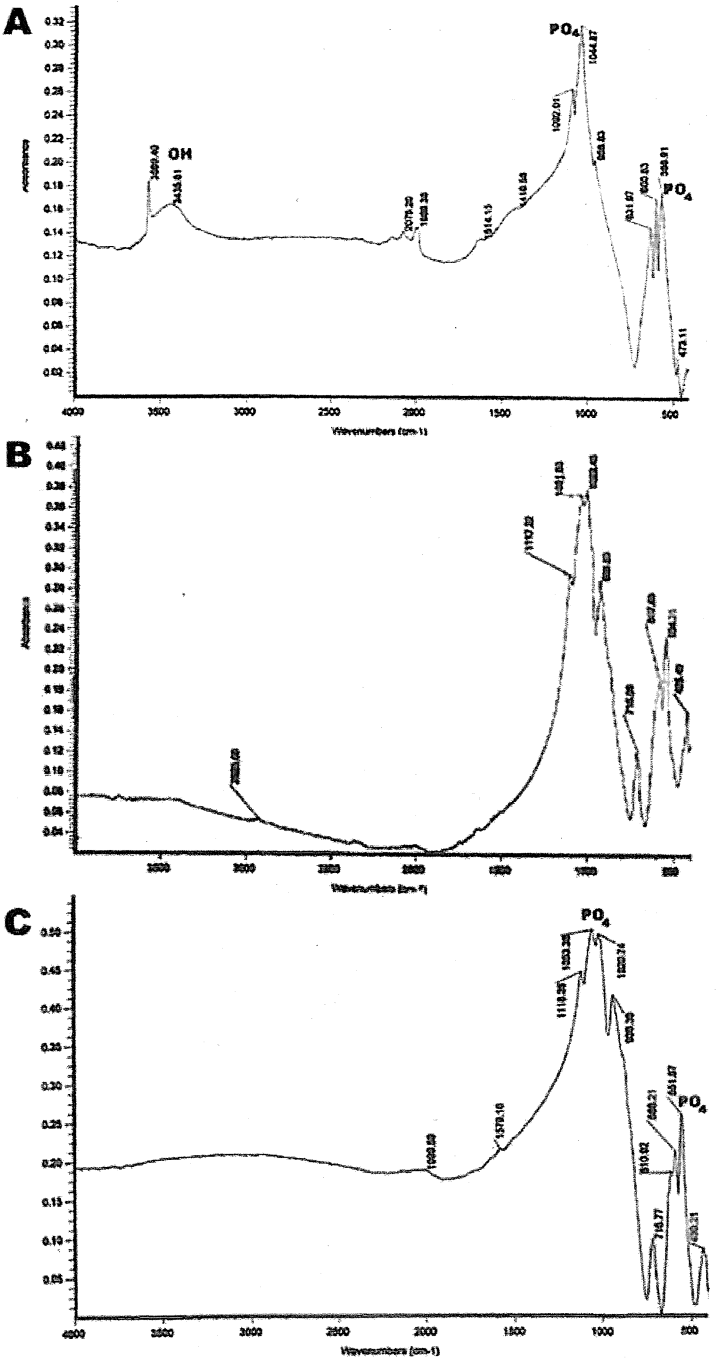

Figure - III-6

Fourier transform infrared (FT-IR) spectra of raw ceramic granules: A- Typical spectrum of Hydroxyapatite (HA); B - spectrum of Bioactive glass system (BGS) -AW type and C - spectrum of Triphasic bioactive composite system (HABGS). The spectra revealed the presence of the hydroxyl (OH) in HA and the phosphate PO_4 groups in HA, BGS &HABGS.

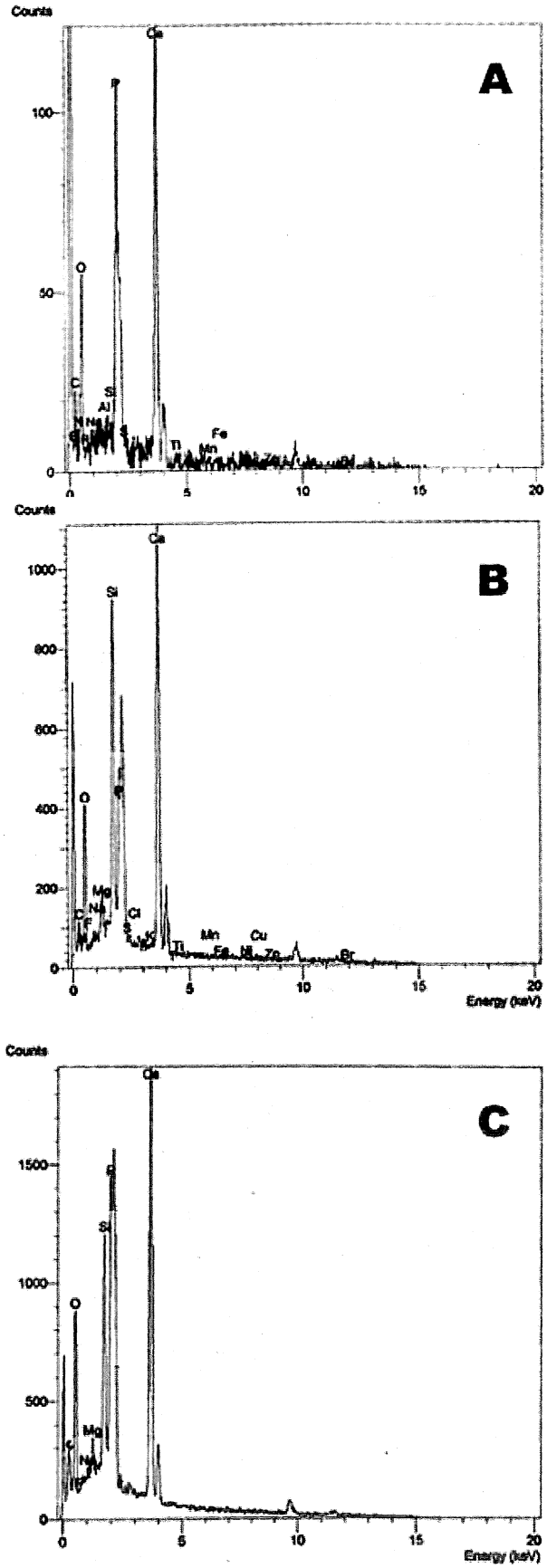

Figure - III-7

Energy Dispersive X-ray Analysis (EDAX) spectra of bioactive ceramics: A - HA ; B - BGS & C - HABGS raw sintered granule powder. The major peaks of HA, BGS & HABGS are Calcium (Ca) & Phosphorous (P) and Silicate (Si) peaks of BGS & HABGS. Other minor elements were also identified.

III.2. Material Characterizations- Discussion

Ceramic materials are the most biologically acceptable of all materials. They are fully oxidized or chemically stable compounds and because of their chemistry, ceramics are less likely to produce any adverse effects compared with metals and polymers, which are not as chemically, stable. Concern has been expressed in literature regarding the use of many alloys due to the production of wear particles and the release of ions by corrosion or, in the case of synthetic polymers, due to leaching of oligomer or plasticizer constituents (Williams 1981 and Smith and Williams 1982). The argument in support of ceramics or glasses as biomaterials is that, chemically ceramics degrade in comparison to metals and organic-carbon-based compounds and are more wear resistant. The chemical inertness of ceramics is greater than that for organic or metallic materials since the overall bond strength of the three-dimensional covalent/ionic structure is greater. Enough literature evidence exists to show that ceramic and glass composition can bond to bone (Hench, 1988).

The major advantage of ceramics as biomaterials is that they can be produced almost completely inert or bioactive with the potential of varying degrees of interaction within the physiological environment. Thereby, the surface and bulk chemistry of ceramic materials can be easily controlled.

XRD of HA, BGS and HABGS revealed that the ceramic granules were crystalline. HA showed apatite (Ca_{10} $(PO_4)_6$ $(OH)_2$) as the major phase with few brushite phases (dicalcium phosphate dihydrate- Ca $HPO_4.2H_2O$). The identification of the brushite peaks at an angle of 21.3°, 36.6°, 35.5°, 37.5° and 40.5° in the hydroxyapatite powder is not clear. It is understood that if the calcium phosphate (Ca/P) ratio is 1.67, only HA phase will be visible in the XRD and IR spectra. HA upon sintering above 900 °C revealed dicalcium phosphate anhydrous (DCP-

$CaHPO_4$). However, DCP is not stable at these temperatures and gets transformed to β-TCP and calcium pyrophosphate ($Ca_2P_2O_7$) (de groot *et al.*1990).

XRD spectrum of BGS and HABGS share apatite and wollastonite ($CaO\ SiO_2$/$CaO\ SiO_3$) as the major phase, but the whitlockite (β-tricalcium phosphate - $Ca_3\ (PO_4)_2$) phase is more conspicuous in HABGS. If the Ca/P is higher than 1.67, calcium oxide (CaO) will be present with the HA phase. If the Ca/P is lower than 1.67, β - TCP and other phases such as tetracalcium phosphate (TTCP) will be present with the HA phase in the sintered material, depending on the temperature and condition of sintering (Le Geros 1993).

FT-IR of HA revealed the material is crystalline and contained trace amounts of CO_3^{2-}, which is evident from the IR peak observed at 1410 cm^{-1}. This could be due to the apatite prepared from highly alkaline solution in the presence of air (LeGeros 1993). Stoichiometric synthetic HA apatite showed peaks due to ^-OH and PO_4^{3-} groups only. The sharp ^-OH peak at 3569 cm^{-1} is due to the ^-OH stretching vibration, confirming the presence of OH ions in the apatite crystal lattice. This peak is due to the characteristic O-H stretching mode of the hydroxyl ion vibration in the crystal. The ^-OH liberational mode at 631 cm^{-1} is present only in the synthetic HA, but absent in the bone. Most of the intense peaks associated with the PO_4^{3-} vibrations in calcium phosphate materials are the antisymmetric stretching mode at 1092 – 1044 cm^{-1} (ν_3 band) (Termine 1973). Synthetic stoichiometric apatites showed three bands for each of the ν_3 (1092, 1044 and 958 cm^{-1}) and ν_4 (631, 600 and 568 cm^{-1}) modes (Ben-Nissan *et al.* 1980,).

BGS material and HABGS material shared the same functional groups. The ^-OH peak was absent in both BGS and HABGS material. No CO_3^{2-} peak was

observed. The peaks between 1117 - 1022 cm^{-1} in BGS and 1118 -1020 in HABGS revealed the Si-O stretch. The Si-O-Si stretch in BGS was observed between 1117 to 716 cm^{-1} and in HABGS the peak was observed between 1118-716 cm^{-1}. The phosphate modes appeared as four peaks assigned to phosphate ν_3 1117, 1051, 1022 and 938 cm^{-1} in BGS and in HABGS the ν_3 mode is observed at 1118, 1053, 1020 and 938 cm^{-1}. Minor peaks of P-O crystalline were observed at 610 - 588 cm^{-1} in HABGS granules whereas, in BGS granules the P-O crystalline peak was absent. The amorphous P-O peaks was observed at 588 - 551 cm^{-1} in HABGS granules while, in BGS it was observed between 587- 554 cm^{-1}. The Si-O-Si bend was observed at 551 - 430 cm^{-1} in HABGS and in BGS it was observed at 554 - 429 cm^{-1}.

One approach to improved interfacial stability is the use of a porous implant. Bone will grow into pores > 100μm diameter and maintain a blood supply necessary for cell maintenance (Hulbert *et al.,* 1974; Hench and Ethridge, 1982 and Holmes *et al.,* 1984). HA granule has a porosity of approximately 100 μm and it is anticipated that this would enhance the process of bone ingrowth. Soft tissues will grow into pores of smaller diameter. This method of tissue attachment is often called biological fixation. The interconnected pores can exist throughout the implant; however, large pores severely degrade strength and toughness (Holmes *et al.,* 1984; and Hench 1991). Porous ceramics cannot be used for load bearing devices but are suitable for space filling applications (Holmes *et al.,* 1984; and Hench 1993). The A-W type glass ceramic is the only ceramic that has higher mechanical strength than cortical bone (Nakamura, 1996). HABGS and BGS granules, the pore size is less than 30 μm in diameter and hence bone infiltration into the material is very unlikely. However, the bioactive nature of these materials release Ca^{2+} and PO_4^{3-} ions necessary for the

mineralization process at the defect site favoring a chemical bonding with the host bone (Hench *et al.,* 1972; Gross *et al.,* 1988; Kokubo *et al.,* 1990).

Conclusion

The indigenously synthesized bioactive ceramics were of 300 - 350 μm size granules were confirmed by sieving and measured using SEM. The porosity of HA was roughly around 100 - 120 μm and BGS and HABGS showed pore size of 30 μm. HA, BGS and HABGS granules were crystalline as observed under XRD. FT-IR analysis of the bioactive ceramic powders confirmed the presence of hydroxyl (OH^-) and phosphate (PO_4^{3-}) groups in HA and a carbonate peak (CO_3) peak at 1410 cm^{-1}. The hydroxyl peaks were absent in BGS and HABGS, prominent Si-O stretching (may be wollastonite) was observed in BGS at 1117 - 1022 cm^{-1} and in HABGS at 1118 - 1020 cm^{-1}. EDAX observations confirmed the presence of silica (Si) in BGS and HABGS apart from calcium and phosphorous, in HA only calcium and phosphorous was observed. The physicochemical evaluation confirmed the bioactive property of HA, BGS and HABGS ceramic granules.

CHAPTERS – IV

IN VITRO STUDIES

IV.1 *In Vitro* – Simulated studies

IV. *IN VITRO* STUDIES

IV.1 *IN VITRO* - SIMULATED STUDIES : Results

IV.1.1 Scanning Electron Microscope (SEM)

IV. 1.1.1 Surface topography of Hydroxyapatite (HA)

The surface of the HA granules (Figure IV.1 A & B) in acetate buffer did not show any change after 12 h, such as cracking, pits etc. But the pores and the periphery of the granules showed the opening of the grain boundaries due to dissolution. After 24 h, the surface of the granules cracked and showed apatite-like deposits (> 1 μm in size to <1 μm) on the material surface. The pores and the periphery of the granules showed ruffled appearance.

After immersion in Tris-HCl, HA surface (Figure IV.1 C & D) showed flake-like in the pore zone and on the periphery, fine deposition of apatite-like (> 1μm in size) substances could be seen on the surface after 12 h. After 24 h the surface showed few cracks and fine deposition of apatite-like substances (> 1μm in size) on the pore zone and on the periphery of the granules.

HA immersed in SBF (Figure IV.1 E & F) showed dense, intact surface and no cracks were observed. Fine deposition of apatite-like substances could be seen (> 5 μm to < 1 μm in size). After 24 h the granules surface was intact and did not show any cracks in the pore and on the periphery of the material. Apatite-like substances of < 2 μm could be seen.

HA immersed in MEM (Figure IV.1 G & H) after 12 h did not show any significant change in the surface morphology. But, fine deposition of apatite-like substances of less than 2 μm were seen on the material surface. The material was intact even after 24 h and did not show any change in the surface morphology.

HA immersed in foetal calf serum (Figure IV.1 I & J) after 12 and 24 h

showed thick deposition of serum proteins, and large flakes of the HA (> 20 μm in size) were seen with cracks of less that 2 μm width. Apatite-like depositions could be seen on the material surface covered by the protein matrix.

HA immersed in rabbit serum (Figure IV. 1 K) showed large > 2 μm cracks in the pore zone and on the periphery. A thick coating of protein matrix on the material could be seen. Apatite-like depositions (< 2 μm) were seen on the protein-adsorbed surfaces after 12 h. The surface showed cracks (> 2 μm) in the pore and on the periphery. Very few deposits of apatite-like substances were observed after 24 h (image not included).

IV.1.1.2 Surface topography of bioactive glass system composite-AW type (BGS)

BGS granules immersed in acetate buffer (Figure IV.2 A & B) after 12 h showed opening up of the surface pores and aggregates of apatite-like on the material surface could be seen. Few cracks were seen on the periphery and the center of the material (> 15 μm). Even after 24 h the material surface showed the same surface topographical features as that of 12 h.

BGS granules immersed in Tris-HCl buffer (Figure IV.2 C & D) after 12 h showed intense opening up of the intergranular interface/ boundaries. Pores of > 2 μm could be seen. After 24 h, the material surface showed intense opening up of the intergranular interface and showed ruffled like surface with pores of > 5 μm in size.

BGS granules immersed in SBF (Figure IV.2 E & F) after 12 h showed surface with large number of pores > 5 μm with apatite-like deposition. The intergranular interface has completely opened up. After 24 h, the intergranular interface is reduced and fine deposits of apatite-like substances could be seen. Very few cracks could be seen on the periphery of the material.

Acetate Buffer

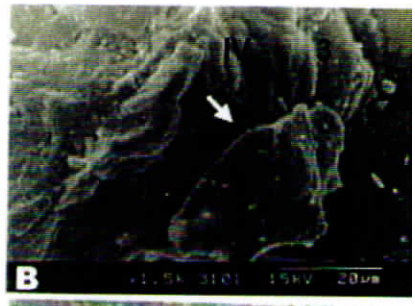

Tris-HCl

Simulated Body Fluid

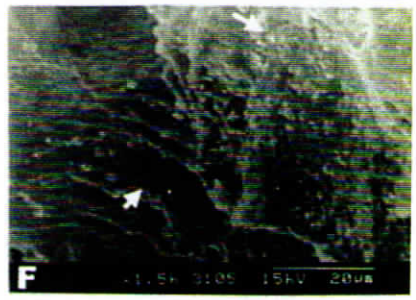

Minimum Essential Medium (MEM)

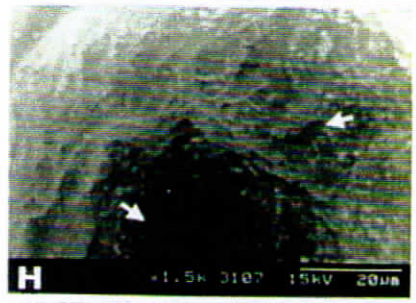

Foetal Calf Serum

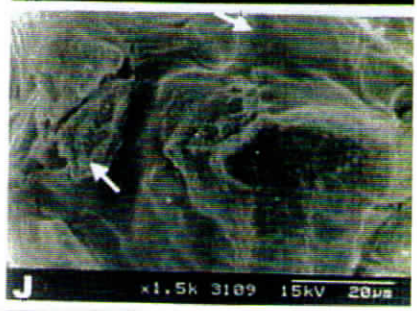

Rabbit Serum

Figure - IV-1

Scanning electron micrographs of HA granules subjected to *in vitro* dissolution studies after 12 h (A,C,E,G,I&K) & 24 h (B,D,F,H&J). The arrows indicate the surface changes after immersion.

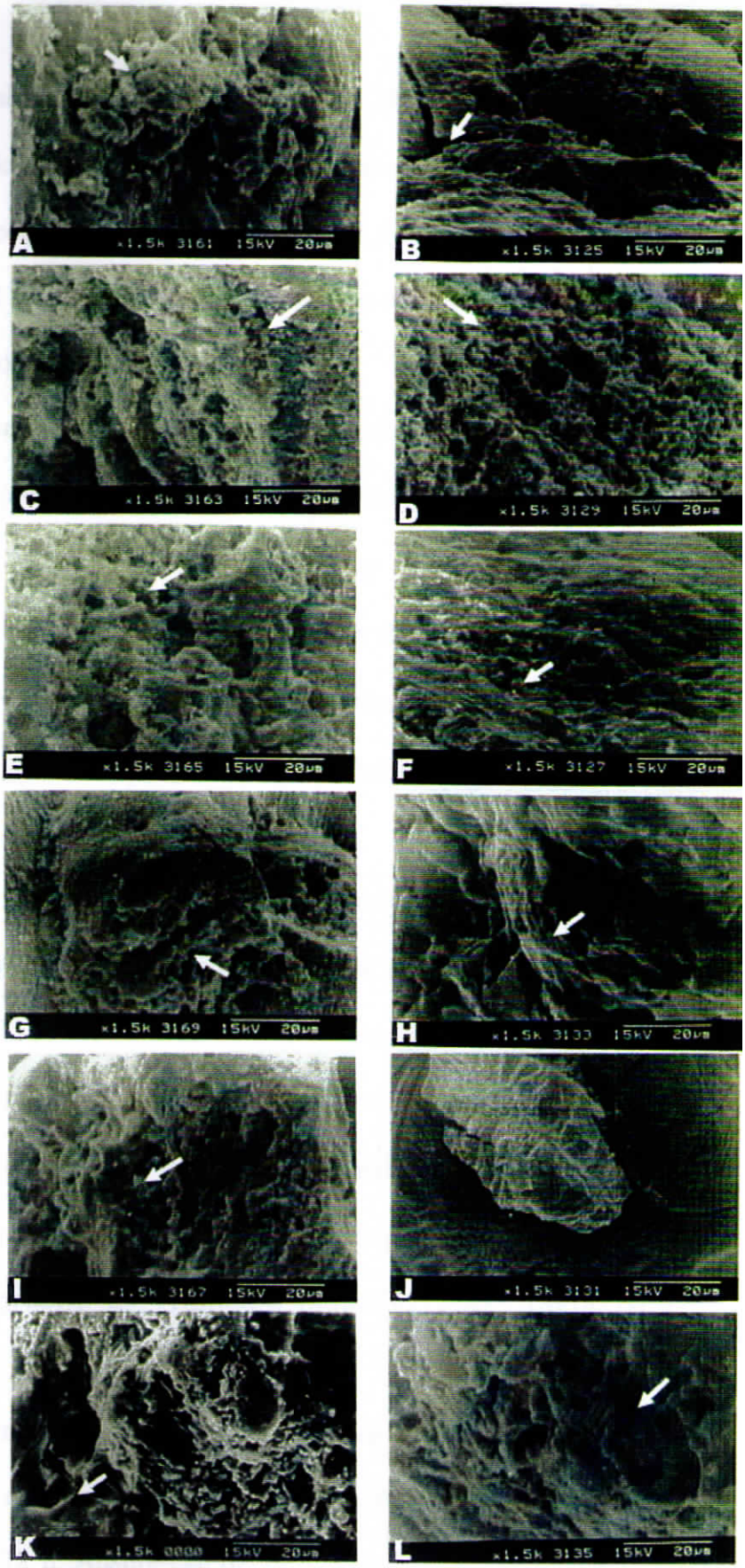

Figure -IV-2

Scanning electron micrographs of BGS granules subjected to *in vitro* dissolution studies after 12 h (A,C,E,G,I,K) & 24 h (B,D,F,H,J,L). The arrows indicate the surface changes after immersion.

BGS surface, after immersion in MEM (Figure IV.2 G & H) after 12 h seems to be intact with very few cracks of < 5 μm. The intergranular interface has opened up. Fine apatite-like deposits could be seen sparsely. After 24 h, the material surface has opened up completely and a thin coating of MEM is seen on the surface and within the pores. Apatite-like depositions were not seen.

BGS granules immersed in foetal calf serum (Figure IV. 2 I & J) after 12 h showed opening up of the pores with large cracks of > 10 μm on the periphery of the material. A thin coating of the protein could be seen on the material surface and within the pores > 5 μm. No apatite-like growth is seen on the material surface. After 24 h, the material surface showed large cracks of > 5 to 10 μm, with a thin coating of the protein on its surface and within the pores. But no apatite-like growth is seen on the material surface.

The surface of the BGS (Figure. IV.2 K & L) in rabbit serum showed cracks of >10 μm and the opening of the intergranular interfaces, and a fine deposit of the apatite-like substances could be seen on the material surface and with in the pores of > 5 μm. After 24 h, the material surface showed intense cracking up of > 15 μm, and a thick coating of the protein could be seen on the material and within the pores of < 5μm. Apatite-like deposits could be seen with a thin coating of the protein matrix.

IV.1.1.3 Surface topography of Triphasic bioactive glass composite system (HABGS)

HABGS granules immersed in acetate buffer (Figure. IV.3 A & B) after 12 h, the intergranular interface on the surface had opened up. No large cracks could be seen on the surface after 12 h. Apatite-like deposits could be seen on the smooth phase of the material and not on the granular phase of the material. After 24 h, the intergranular interface of the material surface had opened up completely with few

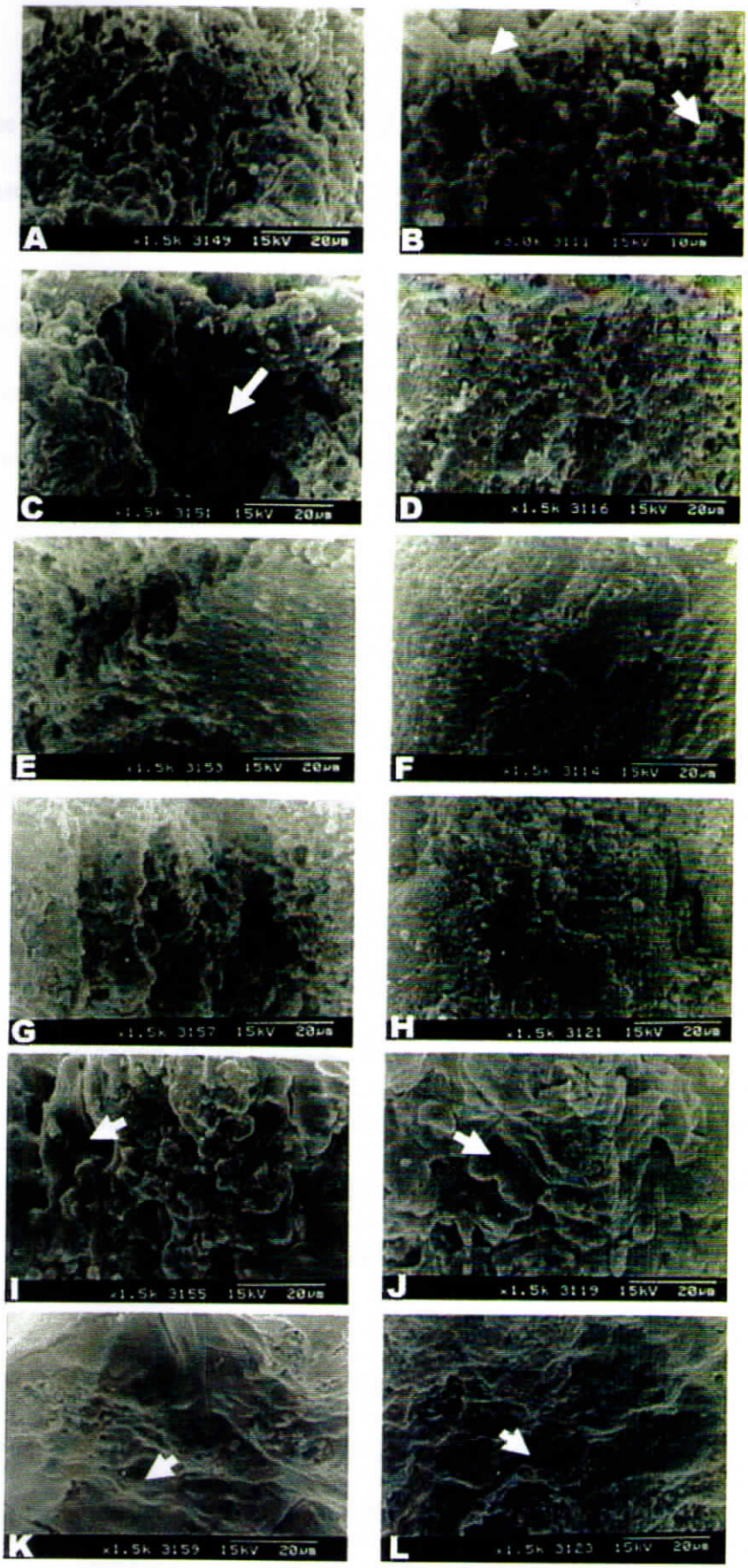

Figure -IV-3

Scanning electron micrographs of HABGS granules subjected to *In vitro* dissolution studies after 12 h (A,C,E,G,I&K) & 24 h (B,D,F,H,J&L) The arrows indicate the surface changes after immersion.

apatite-like deposits on the smooth phase of the material and with few cracks < 15 μm. The granular phase of the material also showed fine apatite-like deposits < 1 μm.

HABGS granules immersed in Tris-HCl (Figure.IV.3 C & D) after 12 h showed that the granular surface and the intergranular interface of the material had completely opened up, signifying that the material had undergone surface degradation. The pores of the granular phase were 10 to 20 μm in diameter, with few cracks on the smooth phase of the material. After 24 h, the granular phase of the material had also completely opened up. The pores were of the range of 5 to 20 μm. The smooth phase of the material showed a pit-like surface while the granular phase showed a ruffled-like surface.

HABGS granules immersed in SBF (Figure.IV.3 E & F) after 12 h showed no change in the smooth phase of the material except for a few pit-like surfaces. The granular phase of the material showed the intergranular interface has opened up, which could be due to active degradation of the material. The pores were of 5 μm to 20 μm. After 24 h the smooth phase of the material showed ruffled-like appearance on the periphery of the material. The granular phase of the material was normal and did not show much change. Fine deposits of apatite-like substances were seen on the surface of the material.

HABGS immersed in MEM (Figure.IV.3 G & H) after 12 h did not show any change on the smooth phase of the material. The intergranular interface of the material has opened up with large pores within the range of 10 to 20 μm. After 24 h the smooth phase of the material showed ruffled surfaces with cracks. The granular phase of the material remained the same as observed after 12 h. Apatite-like deposits could be seen on the material surface.

HABGS granules immersed in foetal calf serum (Figure.IV.3 I & J) after 12 h showed the smooth phase of the material with a thin coating of protein on the surface, and no cracks or pits were observed on the surface. The granular phase of the material did not show opening of the intergranular interface due to the protein deposit that had already penetrated the pores. Apatite-like deposits could be seen covered by a thin protein coat of 2 to 10 μm in diameter on the granular phase of the material. After 24 h the smooth phase of the material showed a thin coating of protein, and few cracks were seen on the periphery and at the boundaries between the smooth and granular phases. Apatite-like deposits were also observed. The pores of the granular phase of the material had opened up, but a thin protein matrix is seen on its surface, which might be preventing the degradation. The pores were of 2 to 20 μm in size.

HABGS in rabbit serum (Figure.IV.3K & L) after 12 h showed the smooth phase of the material with a thick coat of protein on the surface with apatite-like deposits. Pitting of the smooth surface was not seen. The intergranular spaces were filled with protein and large cracks were seen on the periphery of the material. After 24 h the smooth phase of the material showed a thick coating of the protein matrix on the surface. Apatite formation is seen sparsely. The granular phase of the material remained the same as observed at 12 h. But, the cracking of the material was observed only on the periphery of the material, with few pores of 2 to 5 μm in size on the surface.

IV.1.2 Biochemical Evaluation

IV.1.2.1 The pH of the simulated media before and after dissolution

Significant change in the pH was observed with HA, BGS and HABGS granules subjected to different media after 12 and 24 h (Table IV.1).

Table IV.1

Ceramics Used for Study	HYDROGEN ION CONCENTRATION OF THE MEDIUM																	
	ACETATE + SBF			TRIS-HCl + SBF			SBF			FC			MEM			RABBIT SERUM		
	Initial	12 hr	24 hr	Initial	12 hr	24 hr	Initial	12 hr	24 hr	Initial	12 hr	24 hr	Initial	12 hr	24 hr	Initial	12 hr	24 hr
HA	5.2	4.67	5.57	7.3	6.42	6.23	7.1	6.49	7.51	8.6	6.67	8.0	8.12	8.58	8.43	7.2	7.58	8.48
BGS	5.2	7.43	5.98	7.3	6.34	7.74	7.1	6.75	7.46	8.6	7.54	8.32	8.12	8.68	8.46	7.2	7.58	8.54
HABGS	5.2	7.83	5.63	7.3	7.06	7.69	7.1	6.82	7.46	8.6	8.33	8.48	8.12	8.32	8.69	7.2	8.64	8.53

Table IV.2, shows the sequence of the increase and decrease of pH after 12 and 24 h with HA, BGS and HABGS granules in different media. The difference in the pH observed was calculated by subtracting the pH value observed at 12 and 24 h from the initial pH value (before immersion). The value thus obtained would give possible information with regard to the decrease/increase in the pH/hour. This data could be considered for understanding the initial changes that are expected to take place with the bioactive ceramic granules in an *in vivo* situation.

After immersion of HA, BGS and HABGS granules in acetate buffer (pH 5.2), significant change in the pH of the acetate buffer was observed, which could be due to the bioactive nature of the material. HA in acetate buffer after 12 h showed decrease in pH from the initial pH to 4.67 with an approximate decrease of 0.04 pH/hour and after 24 h the pH again increased to 5.57 at the rate of 0.07 pH/hour. BGS showed increase in the pH to 7.43 after 12 h, an increase of 0.18 pH/hour. After 24 h the pH dropped from the initial increase of 7.43 to 5.98, a decrease of 0.12 pH/hour. HABGS immersed medium showed an increase in the pH to 7.83 after 12 h, an increase of 0.21 pH/hour. And after 24 h the pH dropped down to 5.63 a decrease of 0.18 pH/hour (Table IV.2 A).

The initial pH of the Tris-HCl with SBF medium was 7.3. HA after immersion showed a decrease in the pH after 12 h to 6.42, a decrease of 0.07 pH/hour and after 24 h the pH continued to decrease to 6.23 at the rate of 0.01 pH/hour. BGS granules immersed medium also showed a decrease in the pH after 12 h to 6.34, a decrease of 0.08 pH/hour and after 24 h the pH increased to 7.74, an increase of 0.116 pH/hour. With HABGS granules the pH reduced marginally to 7.06 after 12 h, a decrease of 0.02 pH/hour and after 24 h the pH increased to 7.69, an increase of 0.052 pH/hour (Table IV.2 B).

The initial pH of the simulated body fluid (SBF) medium was 7.1. After 12 hrs of immersion with HA, the pH decreased to 6.49, a decrease of 0.50 pH/hour and after 24 h the pH increased to 7.5, an increase of 0.084 pH/hour. BGS also showed decrease in the pH after 12 h to 6.75, a decrease of 0.029 pH/hour and after 24 h the pH increased to 7.46, an increase of 0.059 pH/hour HABGS granules immersed medium also showed decrease in the pH after 2 h to 6.82, a decrease of 0.023 pH/hour and after 24 h the pH increased to 7.46, an increase of 0.053 pH/hour (Table IV.2 C).

The initial pH of Minimum Essential Medium (MEM) was 8.12 before immersion of the granules. After immersion of HA, the pH increased to 8.58 after 12 h, an increase at the rate of 0.03 pH/hour and after 24 h the pH dropped marginally to 8.43, a decrease of 0.01 pH/hour. BGS immersed medium also showed an increase in the pH after 12 h to 8.68, an increase of 0.04 pH/hour and after 24 h the pH dropped down to 8.46, a decrease of 0.01 pH/hour. After 12 h of immersion of HABGS in MEM, marginal increase in the pH from 8.12 to 8.32 was observed, an increase of 0.01 pH/hour and after 24 h the pH further increased to 8.69, at the rate of 0.03 pH/hour (Table IV.2 D).

Table.IV.2

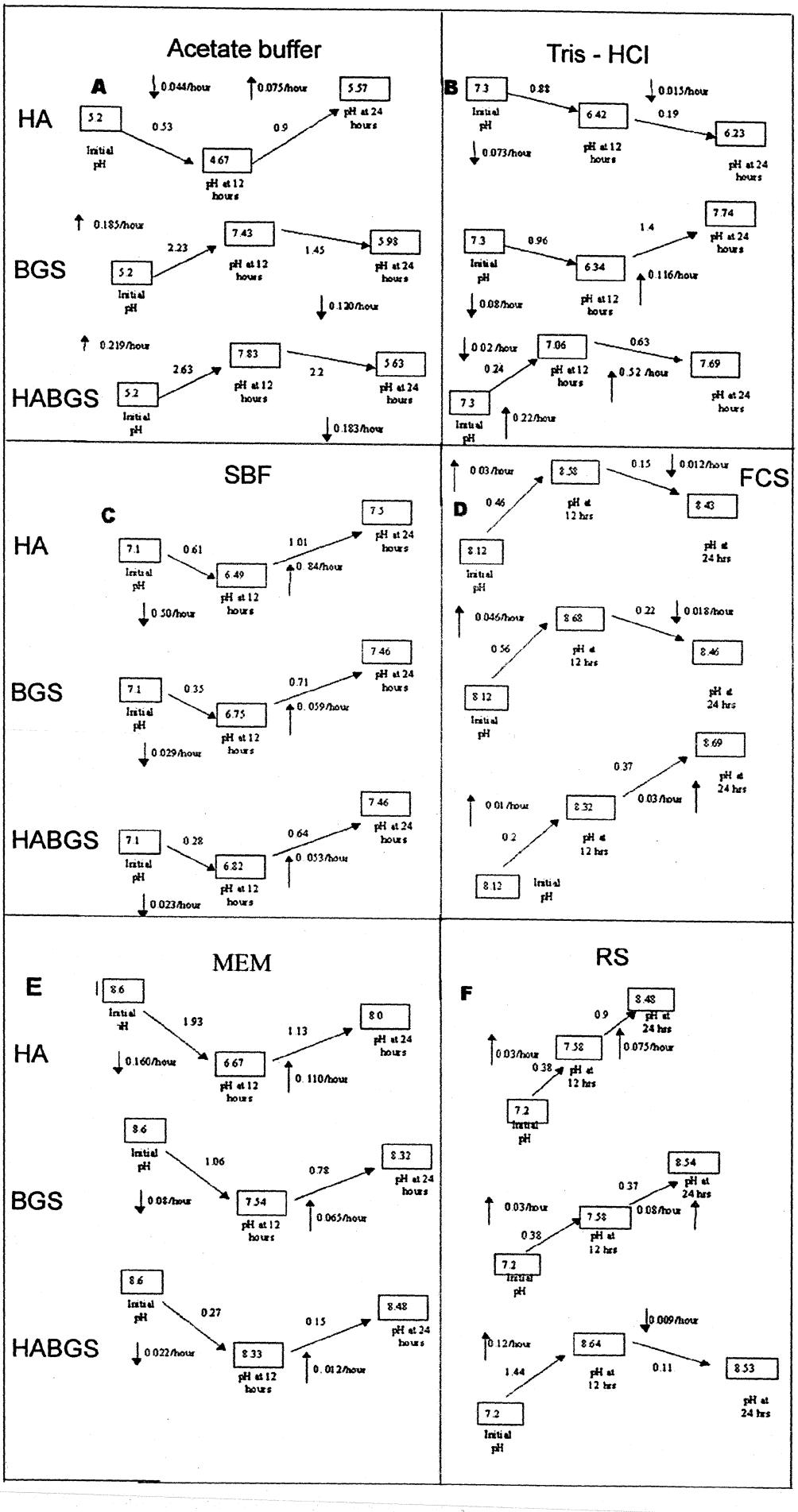
Acetate buffer
A
HA
3.2
Initial pH
0.044/hour
0.53
4.67
pH at 12 hours
0.075/hour
0.9
5.57
pH at 24 hours
BGS
0.185/hour
5.2
Initial pH
2.23
7.43
pH at 12 hours
1.45
5.98
pH at 24 hours
0.120/hour
HABGS
0.219/hour
5.2
Initial pH
2.63
7.83
pH at 12 hours
2.2
5.63
pH at 24 hours
0.183/hour
Tris - HCl
B
7.3
Initial pH
0.88
6.42
pH at 12 hours
0.073/hour
0.19
6.23
pH at 24 hours
0.015/hour
7.3
Initial pH
0.96
6.34
pH at 12 hours
0.08/hour
1.4
7.74
pH at 24 hours
0.116/hour
7.3
Initial pH
0.24
7.06
pH at 12 hours
0.22/hour
0.02/hour
0.52/hour
0.63
7.69
pH at 24 hours
SBF
C
HA
7.1
Initial pH
0.61
6.49
pH at 12 hours
0.30/hour
1.01
0.84/hour
7.5
pH at 24 hours
BGS
7.1
Initial pH
0.35
6.75
pH at 12 hours
0.029/hour
0.71
0.059/hour
7.46
pH at 24 hours
HABGS
7.1
Initial pH
0.28
6.82
pH at 12 hours
0.023/hour
0.64
0.053/hour
7.46
pH at 24 hours
FCS
D
0.03/hour
0.46
8.12
Initial pH
8.58
pH at 12 hrs
0.15
0.012/hour
8.43
pH at 24 hrs
0.046/hour
0.56
8.12
Initial pH
8.68
pH at 12 hrs
0.22
0.018/hour
8.46
pH at 24 hrs
0.01/hour
0.2
8.12
Initial pH
8.32
pH at 12 hrs
0.37
0.03/hour
8.69
pH at 24 hrs
MEM
E
HA
8.6
Initial pH
0.160/hour
1.93
6.67
pH at 12 hours
1.13
0.110/hour
8.0
pH at 24 hours
BGS
8.6
Initial pH
0.08/hour
1.06
7.54
pH at 12 hours
0.78
0.065/hour
8.32
pH at 24 hours
HABGS
8.6
Initial pH
0.022/hour
0.27
8.33
pH at 12 hours
0.15
0.012/hour
8.48
pH at 24 hours
RS
F
0.03/hour
0.38
7.2
Initial pH
7.58
pH at 12 hrs
0.9
8.48
pH at 24 hrs
0.075/hour
0.03/hour
0.38
7.2
Initial pH
7.58
pH at 12 hrs
0.37
8.54
pH at 24 hrs
0.08/hour
0.12/hour
1.44
7.2
Initial pH
8.64
pH at 12 hrs
0.009/hour
0.11
8.53
pH at 24 hrs

The initial pH of foetal calf serum was 8.6. After 12 h of immersion of HA in the foetal calf serum the pH of the medium decreased to 6.67, a decrease of 0.160 pH/hour and after 24 h it increased to 8, an increase of 0.11 pH/hour. BGS after immersion showed the same trend, as HA where the pH dropped to 7.54 after 12 h, a decrease of 0.08 pH/hour and after 24 h the pH was 8.32, an increase of 0.06 pH/hour. With HABGS granules the pH showed a marginal decrease after 12 h to 8.33, a decrease of 0.02 pH/hour and after 24 h the pH was 8.48, an increase of 0.01 pH/hour (Table IV.2 E).

The initial pH of the rabbit serum was 7.2 before immersion. HA after 12 h immersion in the medium showed an increase in the pH to 7.58, an increase of 0.03 pH/hour and after 24 h the pH increased further to 8.48, at the rate of 0.07 pH/hour. BGS showed an increase in the pH as that of HA, after 12 h the pH increased to 7.58, an increase of 0.03 pH/hour and after 24 h the pH showed further increase of 8.54, an increase of 0.08 pH/hour. HABGS granules after immersion showed an increase in the pH to 8.64 after 12 h, an increase of 0.12 pH/hour and after 24 h the pH decreased to 8.53, at the rate of 0.009 pH/hour (Table IV.2 F).

IV.1.2.2 Protein

There were significant changes in the protein content in the media with foetal calf serum, minimum essential medium and rabbit serum before and after immersion of 12 and 24 h (Table IV.3).

The initial protein content of MEM was 2.17 g/dL. After 12 h of immersion with HA, the protein content in the medium decreased to 1.41 g/dL and remained stable at 1.44 g/dL after 24 h. BGS granules immersed in MEM medium showed decrease in the protein content in the medium to 1.22 g/dL after 12 h and remained stable after 24 h at 1.26 g/dL. HABGS granules immersed in the MEM also showed

the same trend as that of HA and BGS, where the protein content dropped to 1.21 g/dL after 12 h and thereafter remained stable at 1.11 g/dL after 24 h. This decrease in the protein concentration is directly proportional to the adsorption of the proteins on the material.

Table IV.3

Material with Medium	Initial (g/dL)	12 hours (g/dL)	24 hours (g/dL)
HA + Minimum Essential Medium	2.17	1.41	1.44
HA + Foetal Calf Serum	7.57	3.84	3.45
HA + Rabbit Serum	6.23	8.05	7.9
BGS + Foetal Calf Serum	7.57	3.86	3.6
BGS + Minimum Essential Medium	2.17	1.22	1.26
BGS + Rabbit Serum	6.23	7.07	6.21
HABG + Foetal Calf Serum	7.57	4.25	2.89
HABG + Minimum Essential Medium	2.17	1.21	1.11
HABG + Rabbit Serum	6.23	6.83	6.18

The initial protein content of the foetal calf serum was 7.57 g/dL. After 12 h of immersion with HA the protein content was 3.84 g/dL and after 24 h it showed 3.45 g/dL. BGS granules immersed in foetal calf serum after 12 h showed 3.86 g/dL of protein in the medium and after 24 h the protein content in the medium was 3.6 g/dL. HABGS granules after immersion in foetal calf serum also showed decrease of the protein content to 4.25 g/dL after 12 h and after 24 h the protein content in the medium further reduced to 2.89 g/dL. The decrease in the protein content in the medium can be construed to the adsorption of the protein on the material.

The initial protein content of the rabbit serum was 6.23 g/dL. After 12 h of immersion in HA, the protein content of the medium was 8.04 g/dL and after 24 h it showed 7.9 g/dL. The decrease in the protein was very marginal. BGS granules immersed in rabbit serum showed 7.07 g/dL of protein after 12 h, and after 24 h the protein content in the medium was 6.21 g/dL. There was a gradual decrease in the

protein content observed after 24 h with BGS. HABGS granules immersed in rabbit serum showed a protein content of 6.83 g/dL after 12 h and after 24 h the protein content in the medium was 6.18 g/dL. HABGS showed continued adsorption of protein on the material even after 24 h.

IV.1.2.3 Calcium and Phosphorus

Significant change in the calcium and phosphorous content in the media (Table IV. 4) were observed before and after immersion. pH definitely influenced the release and uptake of calcium and phosphorous from/on HA (Figure IV. 4), BGS (Figure IV. 5) and HABGS (Figure IV. 6) granules into/from the media.

Table IV.4

Material in Medium	Calcium Before immersion (mg %)	Calcium 12 hrs (mg %)	Calcium 24 hrs (mg %)	Phosphorous Before immersion (mg %)	Phosphorous 12 hrs (mg %)	Phosphorous 24 hrs (mg %)
HA + Ac + SBF	4.65	1.95	5.95	2.18	Not detected	0.04
HA + Tris + SBF	0.125	5.57	3.62	2.7	1.8	Not detected
HA + SBF	9.81	8.39	3.6	2.56	3.14	1.75
HA + FC	12.45	9.3	10	5.62	4.81	4.81
HA + MEM	9.03	5.99	4.99	0.199	3.62	3.75
HA + RS	18.88	4.9	9	6.54	11.73	5.65
BGS + Ac+SBF	4.65	26.86	30.03	2.18	0.86	0.7
BGS +Tris+ SBF	0.125	14.98	19.05	2.7	1.29	0.58
BGS + SBF	9.81	5.99	8.99	2.56	2.19	2.17
BGS + FC	12.45	10.1	11.46	5.62	4.97	4.15
BGS + MEM	9.03	5.22	11.42	0.199	3.89	2.89
BGS + RS	19.41	12.12	10.38	4.46	8	4.17
HABG + Ac+SBF	4.65	27.87	28	2.18	1.08	2.33
HABG +Tris+ SBF	0.125	11.8	19.86	2.7	1.16	0.9
HABG + SBF	9.81	15.4	7.45	2.56	2.23	2.23
HABG + FC	12.45	11.25	9.4	5.62	3.7	3.72
HABG + MEM	9.03	4.79	9.79	0.199	2.72	2.39
HABG + RS	17.3	27.87	9.93	4.49	8.6	4.05

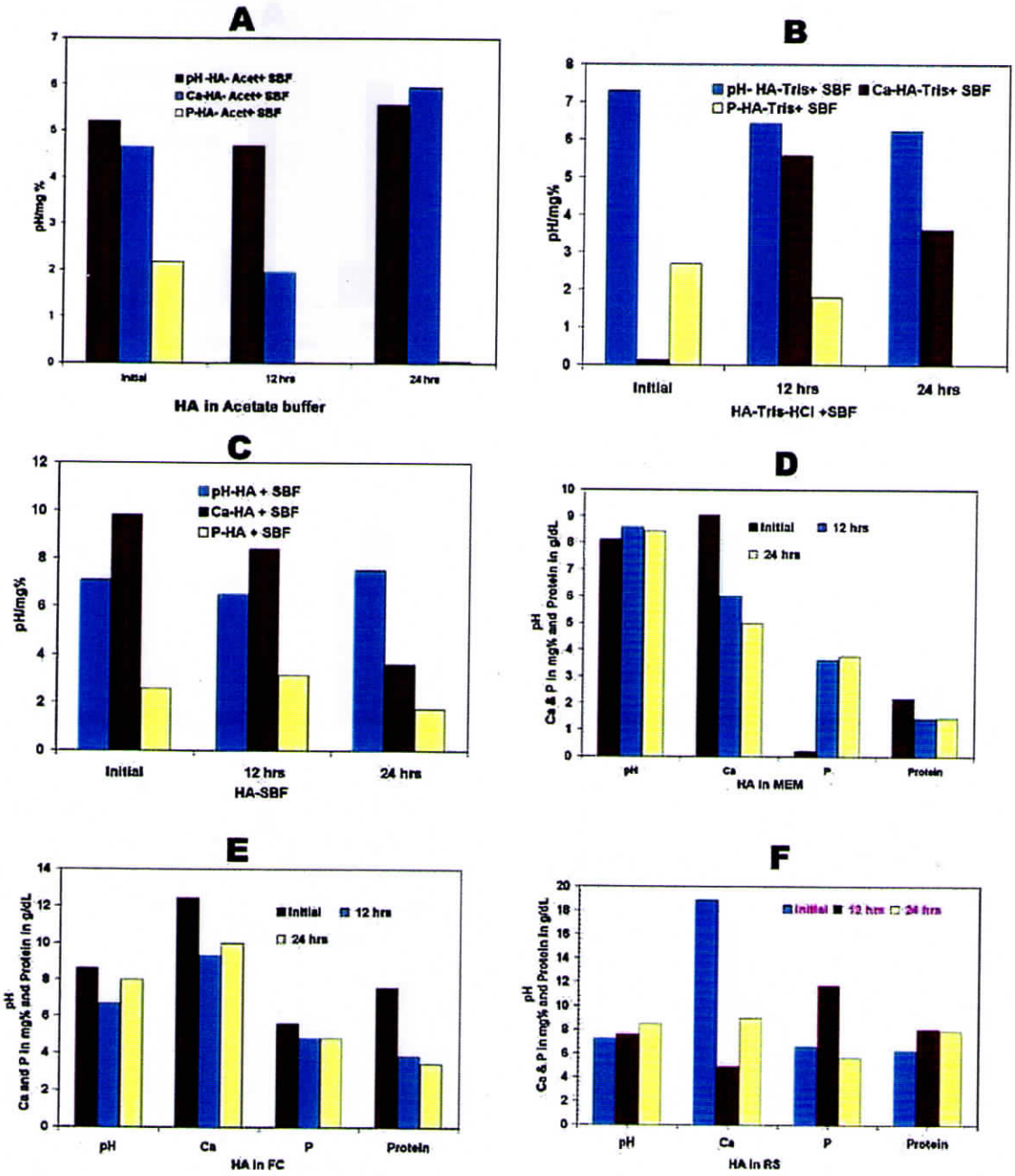

Figure -IV-4

Estimation of pH, calcium (Ca), phosphorous (P), and protein content of *in vitro* simulated media, after immersion with HA in A- Acetate buffer; B - Tris- HCl buffer; C- Simulated body fluid (SBF); D-Minimum essential medium (MEM); E- Foetal calf (FC) serum and F- Rabbit serum (RS), to study the extent of material dissolution after 12 and 24 hours.

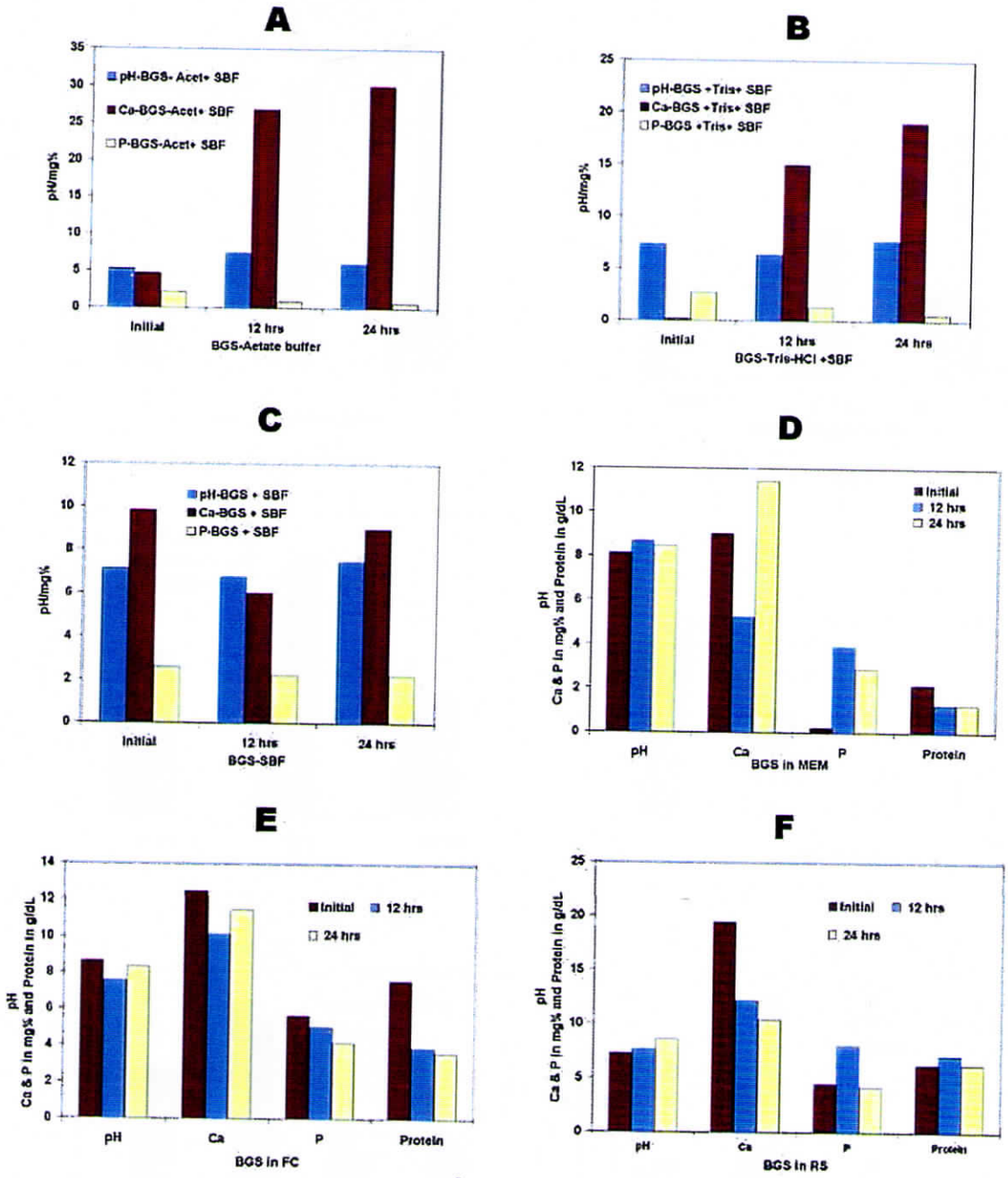

Figure - IV-5

Estimation of pH, calcium (Ca), phosphorous (P), and protein content of *in vitro* simulated media, after immersion with BGS in A- Acetate buffer; B - Tris- HCl buffer; C- Simulated body fluid (SBF); D-Minimum essential medium (MEM); E- Foetal calf (FC) serum and F - Rabbit serum (RS), to study the extent of material dissolution after 12 and 24 hours.

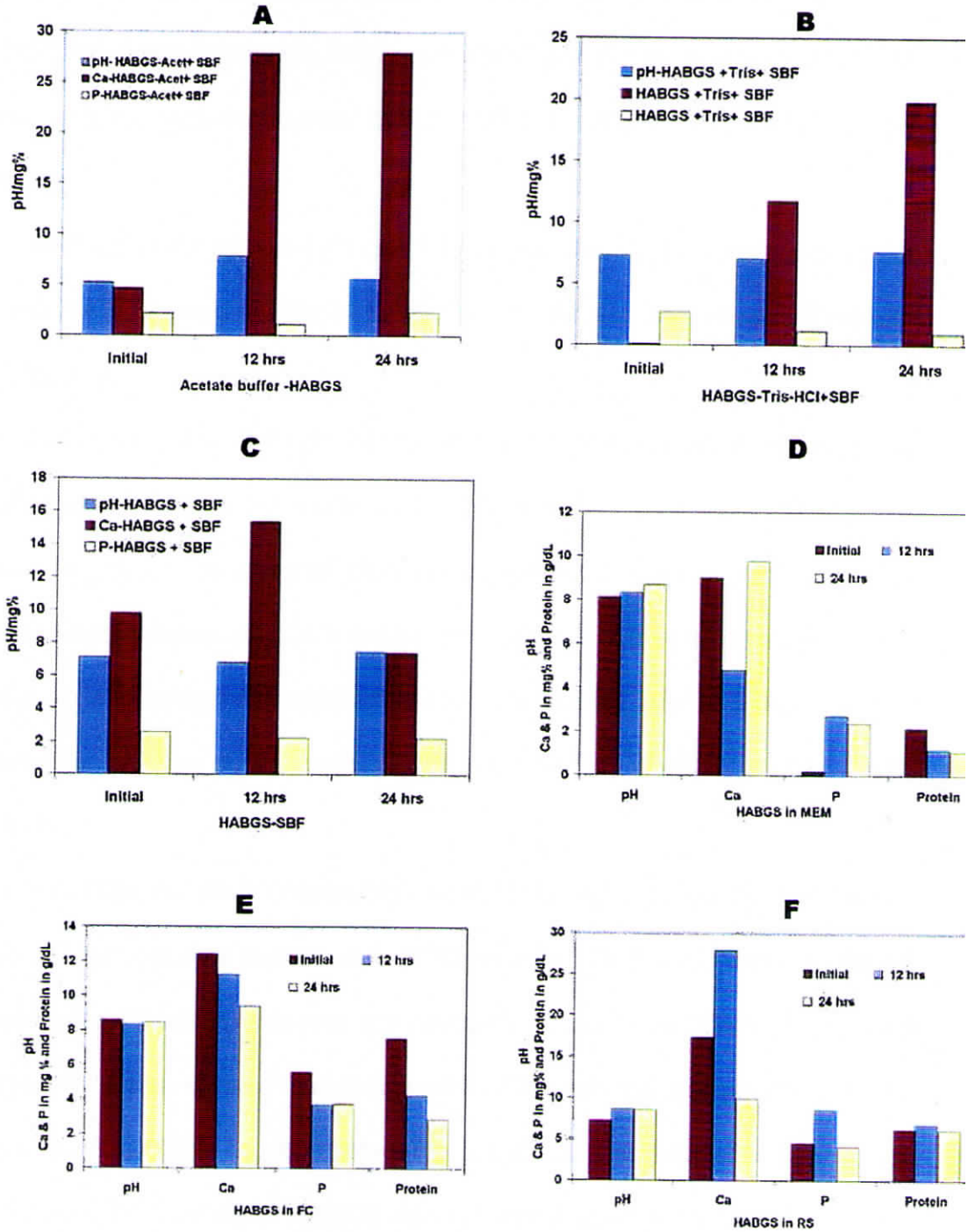

Figure -IV-6

Estimation of pH, calcium (Ca), phosphorous (P), and protein content of *in vitro* simulated media, after immersion with HABGS in A- Acetate buffer; B - Tris- HCl buffer; C- Simulated body fluid (SBF); D-Minimum essential medium (MEM); E- Foetal calf (FC) serum and F- Rabbit serum (RS), to study the extent of material dissolution after 12 and 24 hours.

Calcium and phosphorous uptake or release was slow with HA and faster with BGS and HABGS granules. BGS and HABGS granules showed quick release of calcium in acidic medium (Acetate buffer – pH 5.2), whereas HA showed a slow release.

SBF buffered with Tris-HCl (pH 7.3) showed increased calcium release with BGS and HABGS granules after 24 h, whereas HA showed slow release of calcium even after 24 h.

HA immersed in SBF (pH 7.1) showed stable calcium content and increased phosphorous release into the media after 12 h. But, after 24 h more calcium and phosphorous uptake was observed. BGS showed increased uptake of calcium after 12 h and release of calcium after 24 h without much change in the phosphorous content. HABGS showed increased calcium release into the medium after 12 h and uptake of calcium after 24 h, the phosphorous content in the medium remained unaltered even after 24 h.

HA, BGS and HABGS immersed in MEM showed a similar trend of calcium uptake and phosphorous release after 12 h, and after 24 h a moderate release of calcium and uptake of phosphorous was observed. HA, BGS and HABGS immersed in foetal calf serum showed moderate uptake of calcium and phosphorus from the medium at 12 and 24 h. In rabbit serum calcium uptake was more after 12 and 24 h with HA and BGS, whereas HABGS showed high calcium release after 12 h and uptake of calcium after 24 h. The phosphorous release was high with HA, BGS and HABGS granules immersed in rabbit serum after 12 h and after 24 h more uptake of phosphorous from the medium was observed.

IV.1.3 Fourier Transform Infrared Spectroscopy (FT -IR)

The IR spectra of HA (Table IV.5), BGS (Table.IV.6) and HABGS (Table. IV.7) after 24 h of immersion in the simulated media are summarized below. The changes in the spectra after immersion were conspicuous with respect to the functional groups. Silicate peaks were observed only with BGS and HABGS granules, while carbonate and phosphate peaks were observed with HA (Figure. IV.7 A-F), BGS (Figure IV.8 A-F) and HABGS (Figure.IV.9 A-F) granules.

IV.1.3.1 Hydroxyapatite

(Table IV.5)

Functional Groups & (Vibrational) modes	HA-Control (cm^{-1})	HA-Acetate Buffer (cm^{-1})	HA- Tris-HCl (cm^{-1})	HA- SBF (cm^{-1})	HA- MEM (cm^{-1})	HA-FCS (cm^{-1})	HA-RS (cm^{-1})
OH	3570 630	3569 3429	3568 3432 630	3570 3430 631	3569 3432 631	3568 3432 631	3570 3441
C=O		1622		1622	1627	1637	1638
CO_3^{2-} ν_3		1592 1455	1588	1461 1400 1380	1410	1461 1405 1378	1399
ν_2		803					
PO_4^{3-} ν_3	1092 1044	1047	1103 1045	1096 1045	1091 1045	1102 1042	1088 1045
ν_1	960	969 939 907	957 945	957	959	958	960
ν_4	600 568	643 580 560	600 567	600 567	600 569	668 600 568	599 568
ν_2		476	469 425	469	472	469	472
C-H		2960 2924	2957 2925	2924 2853	2923 2853	2923 2853	2923 2853
N-H					784	781	777

Figure - IV-7

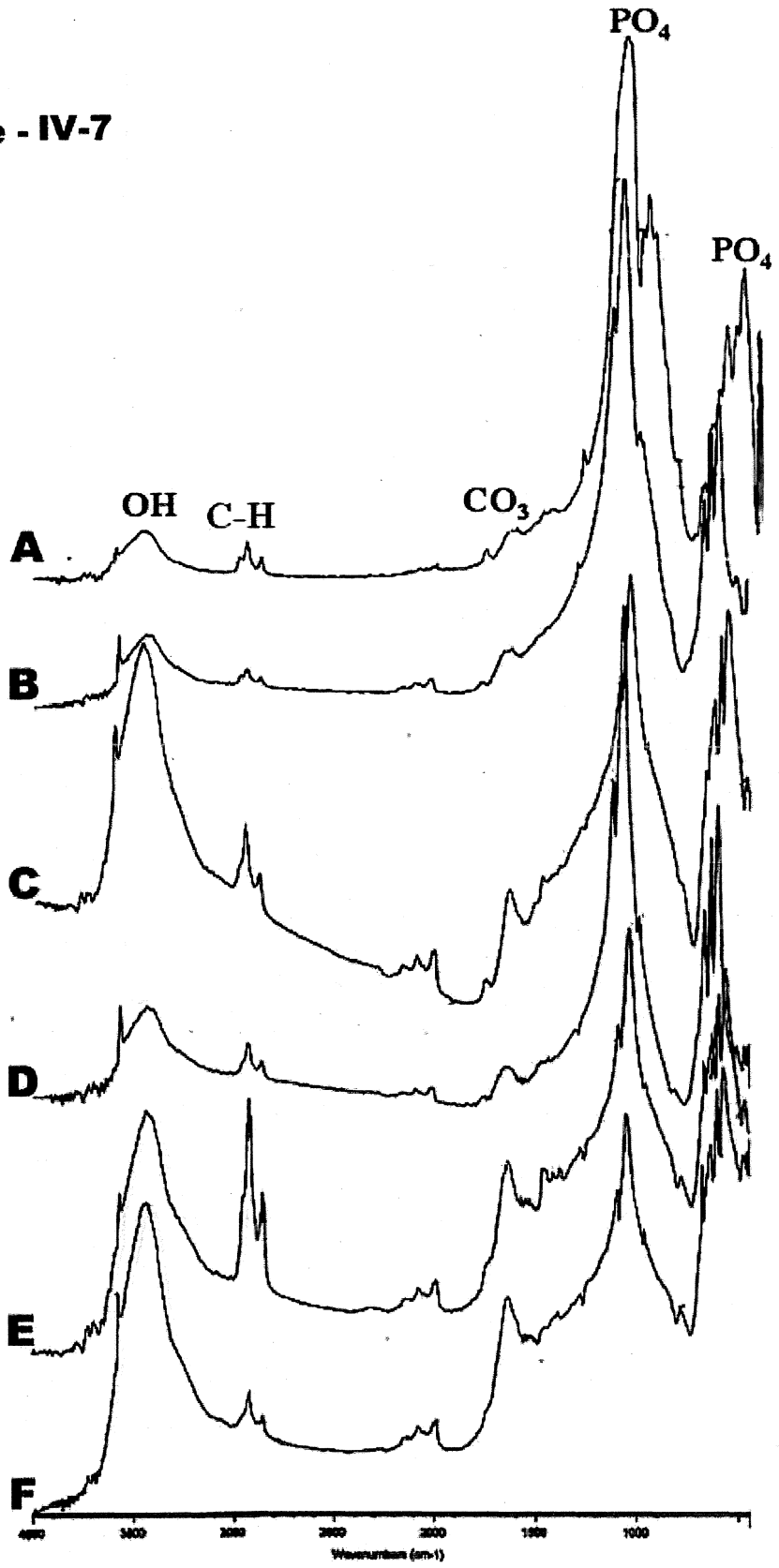

FT-IR spectra of HA granules subjected to in vitro simulated studies at 24 hours: A- Acetate buffer, B - Tris-HCl buffer; C- simulated body fluid (SBF); D - minimum essential medium (MEM); E - foetal calf serum and F - rabbit serum. Change in the hydroxyl group (OH), and phosphate groups (PO_4) and the appearance of C-H group, carbonate (CO_3) were observed after immersion.

IV.1.3.2 Bioactive glass system

(Table IV. 6)

Functional Groups & (Vibrational) mode	BGS-Control (cm^{-1})	BGS-Acetate buffer (cm^{-1})	BGS-Tris-HCl (cm^{-1})	BGS-SBF (cm^{-1})	BGS-MEM (cm^{-1})	BGS-FCS (cm^{-1})	BGS-RS (cm^{-1})
OH		3433	3426	3424	3432	3415	3420
C=O		1624	1625	1628	1619	1648	1650
CO_3^{2-}		1480	1433	1430		1538	1540
ν_3		1462 1445					1451 1401
ν_2				853	853	875	799
PO_4^{3-}	1117	1138	1060	1055	1051	1052	1085
ν_3	1051 1022	1058 1026 1005	1024 969	1023 976	1024 977	1023 976	1075 1024 976
ν_1	938	935 941 908	939 906	938 907	938 907	938 906	939 906
ν_4	581 554	610 600 569 508	683 644 618 588 557 525	683 625 553	683 644 555 519	683 643 554 518	683 644 625 595 555 513
ν_2	429		477	477	478	477	477
C-H		2923 2824	2924 2853	2924 2852	2924 2853	2925 2854	2923 2853
N-H		780					
Si-O-Si (str)	1117 –716	1138-778					
Si-O(str)	1117-1051	1138-1026					
2 NBO	1022-938	1005-935	1024-939	1026-938	1024-938	1023-938	1024-939
P-O (crystalline)		610-600					
P-O (bend amorphous)	581-554	600-559	588-525				595-555
Si-O (bend)		554-425	557-477	553-477	555-478	554-425	555-477

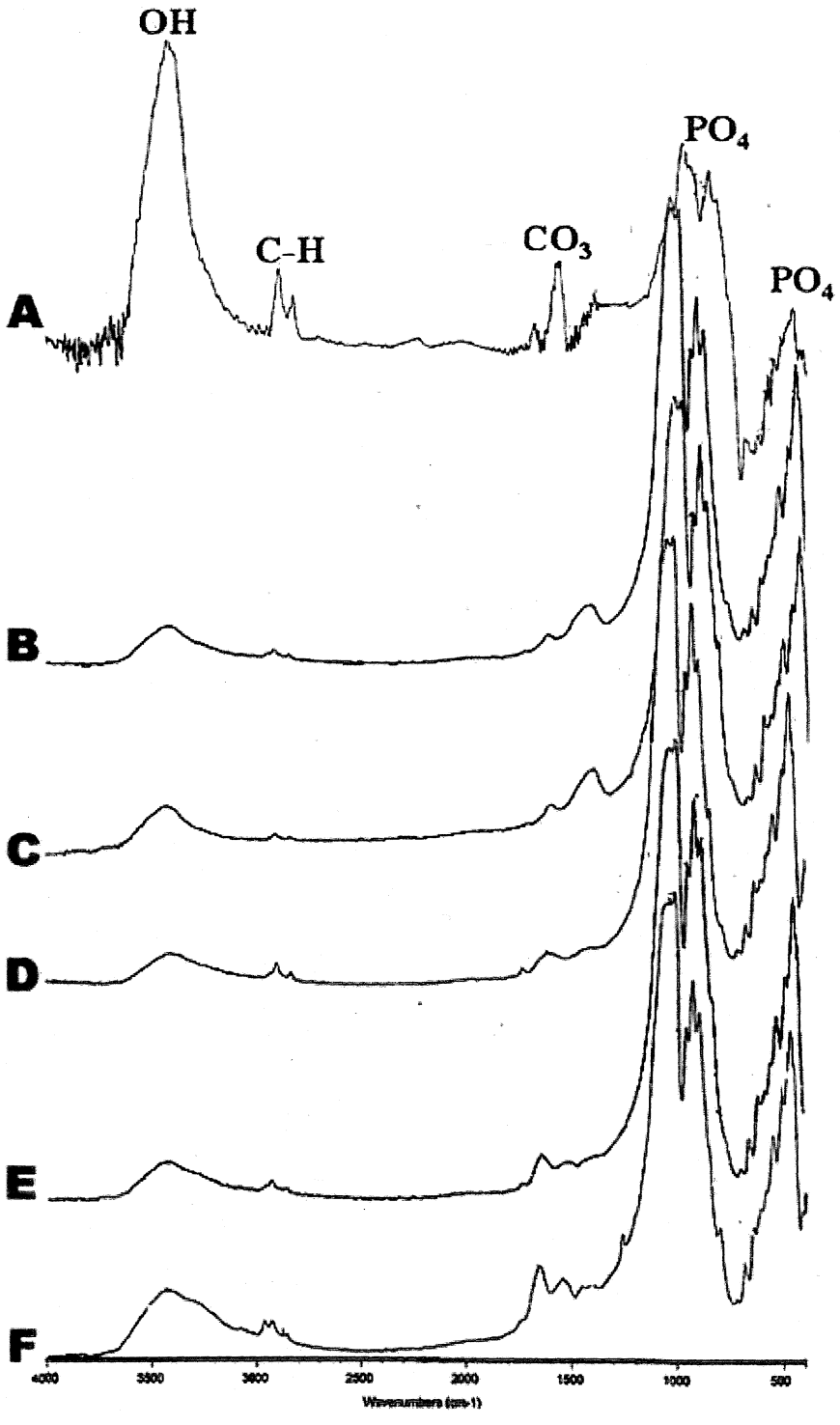

Figure -IV-8

FT-IR spectra of BGS granules subjected to *in vitro* simulated studies at 24 hours: A- Acetate buffer, B - Tris-HCl buffer; C- simulated body fluid (SBF); D - minimum essential medium (MEM); E - foetal calf serum and F - rabbit serum. Change in the hydroxyl group (OH), and phosphate groups (PO_4) and the appearance of C-H group, carbonate (CO_3) were observed after immersion.

IV.1.3.3 Triphasic bioactive glass composite system (HABGS)

(Table IV.7)

Functional Groups & (Vibrational) modes	HABGS-Control (Cm^{-1})	HABGS-Acetate Buffer (Cm^{-1})	HABGS-Tris-HCl (Cm^{-1})	HABGS-SBF (Cm^{-1})	HABGS-MEM (Cm^{-1})	HABGS-FCS (Cm^{-1})	HABGS-RS (Cm^{-1})
OH		3421	3432	3431	3431	3432	3432
C=O		1726 1627	1738 1627	1626	1626	1637	1637
CO_3^{2-} ↑ ν_3 ν_2 →		1447	1447	1447	1446	1452	1459
PO_4^{3-} ν_2	1118 1053	1054 1022	1050 1024	852 1064 1020	851 1053 1020	825 1048 1024	857 1068 1021
ν_3	1022		976	976	976	976	976
ν_1	938	941 906	940 904	938 905	937 906	938 904	937 905
ν_4	610 588 551	681 669 649 550	680 670 648 557 525	675 669 645 555 510	672 646 553 510	669 648 555 500	682 669 645 554
ν_2	430	476	475	476	476	475	476
C-H		2924 2852	2922 2853	2923 2853	2923 2853	2924 2854	2926 2872
N-H							
Si-O-	1118-716						
Si(str)							
Si-O(str)	1118 -1053						
2 NBO	1022-938	1022-941	1024-940	1020-938	1020-937	1024-938	1021-937
P-O (crystalline)							
P-O (bend amorphous)	588-551						
Si-O (bend)	551-430	550-476	557-475	555-476	553-476	555-475	554-476

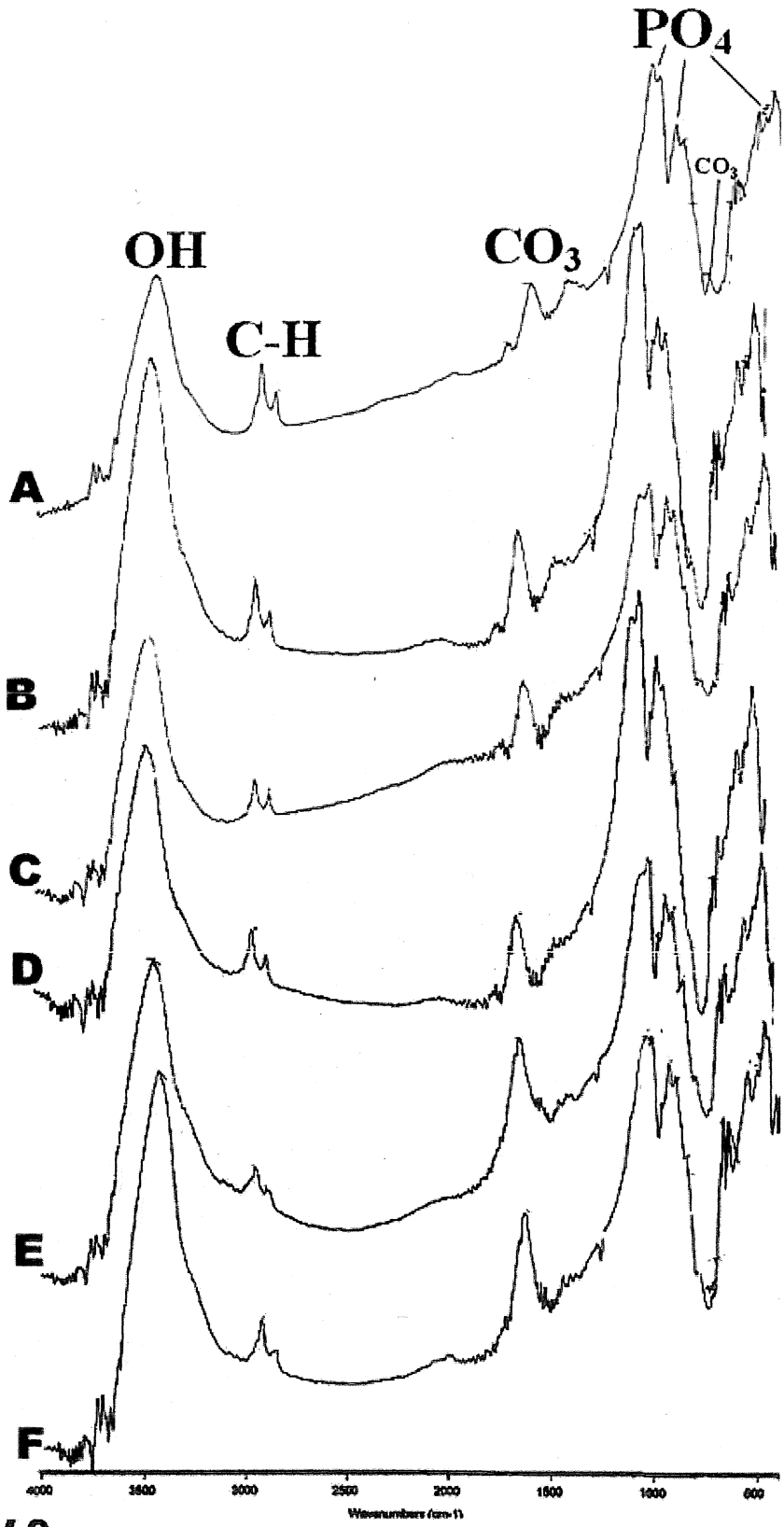

Figure -IV-9

FT-IR spectra of HABGS granules subjected to *in vitro* simulated studies at 24 hours: A- Acetate buffer, B - Tris-HCl buffer; C- simulated body fluid (SBF); D - minimum essential medium (MEM); E - foetal calf serum and F - rabbit serum. Change in the hydroxyl group (OH), and phosphate groups (PO_4) and the appearance of C-H group, carbonate (CO_3) were observed after immersion.

IV.1.4 Image Analysis

No significant change in the granule morphology (size) was observed between the control granules (before immersion) and the granules immersed in different media after 24 h. The surface changes that occurred after 12 and 24 h after dissolution did not produce any significant change in the size of the granules. (Table.IV.8).

Table IV.8

Medium	HA	BGS	HABG
	Control (0.526 ± 0.07)	**Control** (0.462 ± 0.005)	**Control** (0.5273 ± 0.02
	24 hours	**24 hours**	**24 hours**
Acetate+SBF	0.4669 ± 0.05	0.4601 ± 0.007	0.509 ± 0.03
Tris-HCl +SBF	0.4943 ± 0.03	0.5286 ± 0.03	0.5012 ± 0.02
SBF	0.4829 ± 0.02	0.4745 ± 0.045	0.4875 ± 0.001
MEM	0.5526 ± 0.005	0.439 ± 0.027	0.4995 ± 0.013
FC	0.5107 ± 0.06	0.4795 ± 0.011	0.5142 ± 0.05
RS	0.4929 ± 0.009	0.4925 ± 0.02	0.5932 ± 0.02

IV.1.5 *In Vitro* - Simulated Studies: Discussion

The sequence of physicochemical changes that occur when materials are subjected to an *in vitro* environment that are destined to occur on a material surface *in vivo* are expected to coincide with the changes (Hayakuna *et al.*, 1990; Daculsi *et al.*, 1989). This would in turn enlighten all possibilities to meticulously modify the "nearly-ideal" material to withstand the conditions in the hostile biological environment.

Formation of a biologically equivalent apatite surface, which is a common characteristic of bioactive materials, can be reproduced *in vitro* by immersion experiments using a simulated physiological solution that mimics the typical ion concentrations of body fluids.

This study observed the interaction of HA, BGS and HABGS materials in various physiological solutions. We designed a simulated body fluid, with different pH such as acidic, less alkaline and highly alkaline media in which the material response towards apatite formation was studied. Using this method, considerable evidence has been obtained revealing the mechanisms of surface reactions, which include dissolution, precipitation and ion exchange of calcium and phosphate accompanied by adsorption and incorporation of biological molecules as reported by Kokubo et al., (1990) and El-Ghannam *et al.*, (1997) .

The changes understood from these studies would immensely help in identifying and ascertaining the material response in the physiological media during their initial hours of contact and the influence of the pH and protein concentrations.

After immersion of HA in acetate buffer /Tris-HCl /SBF the pH showed some increase or decreased. This could be due to the slow reaction of the HA with the

medium. The continued proton consumption (H^+) and calcium deposition may lead to an undersaturated medium and hence the decrease in the pH. The increase in the pH might be due to the dissolution of HA, which is evident from the increase in the calcium and phosphate in the medium. de Groot et al., (1987) has reported that regardless of the crystalline phase, HA will continue to dissolve as long as it is subjected to an undersaturated environment. Surface topography of the material remained intact with exceptions of degradation only in the pore regions and edges of the granules.

Combination of X-ray diffraction, infrared and chemical analyses of synthetic and biological apatites showed that the CO_3 in biological apatites is incorporated in the structure principally as CO_3 for PO_4 coupled with Na for Ca substitution (Elliot 1974 and Le Geros 1981). Thus, biological apatites can be better described as carbonate hydroxyapatite (CHA) approximated by: (Ca, Mg, Na, X) $_{10}$ (PO_4, HPO_4, CO_3) $_6$ (OH, F, Cl) $_2$ (Karg *et al.,* 1981 and Le Geros *et al.,* 1991).

FT-IR spectrum of HA prior to immersion in the acetate /Tris-HCl/ SBF, after 24 h showed the $^-$OH peaks were observed around 3569 cm^{-1}. The hydroxyl peak present in the spectrum of carbonated apatite is weaker in intensity than that in commercial HA powders (Rehman and Bonfield 1997).

C-H peaks were observed in all the HA material after immersion in the medium between 2853 to 2960 cm^{-1} and their function is not clear.

Theoretically, there are four vibrational modes for carbonate and phosphate ions, ν_1, ν_2, ν_3, and ν_4 and all these modes are Raman and Infrared active and are observed for all the spectra of carbonated apatite and hydroxyapatite powders (Nelson and Featherstone, 1982). The carbonate ν_4 peaks have very low intensity and are seldom seen in the IR spectrum (Ei Feki *et al.,* 1991) and ν_2 and ν_3 have strong

vibrational modes in the IR spectra of bone and carbonated apatites (Rehman and Bonfield 1997). The carbonate apatite peaks (CO_3) of HA were observed between 1622 cm^{-1} to 1378 cm^{-1} were assigned to ν_3 mode of carbonate and the peak at 803 cm^{-1} observed only with acetate buffer was assigned to ν_2 mode of carbonate. The intense ν_3 peaks were thought to be responsible for totally obscuring the ν_1 carbonate peaks (Nelson and Featherstone, 1982). Hence, the ν_1 carbonate peaks were not observed with any of our material after dissolution experiments.

The ν_3 and ν_2 vibrational mode of the carbonate ions were assigned to surface carbonate ions, rather than to carbonate ions in the lattice of phosphate ions and the distribution of the carbonate ν_3 sites depending on the maturation and formation of apatite crystals (Rehman and Bonfield 1997). Phosphate ν_4 peaks of HA were observed at 600 cm^{-1} and 560 cm^{-1}. Shifts in the phosphate peaks were directly proportional to the changes observed in the medium, which might have formed some complex with different functional groups of material.

The spectrum of synthetic carbonated hydroxyapatite has two well defined peaks for the ν_3 sites centered at 1649 cm^{-1} and 1470 cm^{-1}, whereas synthetic commercial hydroxyapatite has three sites for ν_3 vibrational mode centered at 1648 cm^{-1}, 1454 cm^{-1} and 1419 cm^{-1}, for the carbonate ions (Rehman and Bonfield 1997).

In the carbonated apatite spectra a single intense ν_3 peak for the PO_4^{3-} is present at 1046 cm^{-1}, whereas in the hydroxyapatite spectra, the ν_3 peak has three different sites present at 1096 cm^{-1}, 1085 cm^{-1} and 1056 cm^{-1}, for the PO_4^{3-} ions (Rehman and Bonfield 1997). HA immersed in the simulated media without protein

and protein rich media after 24 h revealed PO_4 peaks from 1047 – 1042 cm^{-1}. Which directly correlates with the observations made for carbonated apatite material.

The occupancy of the ν_2 sites is considered to occur competitively between the ^{-}OH and carbonate groups at the interface of the growing crystal, whereas occupancy of the ν_3 sites depends on competition between the phosphate and carbonate ions (Le Geros et al., 1987; Elliot et al., 1985). Biological mineralization leads to substitutions i.e. carbonate substitutions in the synthetic apatites are classified as Type A: CO_3 for OH or Type B: CO_3 for PO_4 (Bonel *et al.*, 1964; Le Geros *et al.*, 1971; Elliot 1974).

This splitting of the ν_4 vibrational peak indicates the low site symmetry of molecules, as two and three observed peaks confirm the presence of more than one distinction site for the phosphate group (Young, 1974). This observation directly correlates with HA after immersion shows more than one phosphate peak.

The presence of ν_2 and ν_3 vibrational modes of carbonates in carbonated apatite may contribute to the decrease of hydroxyl ions in the spectrum, which is evident from the spectrum after 24 h. Hence, CO_3 substitution for phosphate (Type – B) is ruled out for HA in acetate /Tris-HCl/ and SBF and the apatite formed after 24 h in these media is hydroxycarbonate apatite (HCA).

The pH of the medium increased with HA after 24 h in MEM and rabbit serum, whereas in the alkaline, protein rich FCS the pH continued to decrease even after 24 h. The decrease or increase in the pH did not alter the protein adsorption on the material surface with MEM, FCS or rabbit serum even after 24 h, confirmed by the biochemical evaluation. The protein adsorption on the material surface is further confirmed by the SEM and FT-IR analysis, which revealed thick depositions of protein matrix as small and large flake-like deposits and some amide peaks were

peaks were identified at 1655 to 1555 cm^{-1} and the peak at 781 cm^{-1} could be assigned to N-H peak suggesting that protein adsorption on the material surface. The FT-IR spectra revealed apatite peaks at 1637 cm^{-1} to 1378 cm^{-1}, which could be due to the ν_3 vibrational mode of carbonate ion (Le Geros *et al.,* 1987). The ν_3 has peak split in four peaks centered at 1637, 1461, 1405 and 1378 cm^{-1} respectively. The ν_2 carbonate peak was not observed. The presence of ν_3 vibrational modes of carbonates in carbonated apatite did not contribute to the decrease of hydroxyl ions in the spectrum, which is evident from the spectrum after 24 h. The high ^{-}OH and the carbonate apatite peaks suggest that the apatite formed could be an amorphous hydroxycarbonate apatite.

The presence of proteins did not inhibit apatite formation, and the apatite formation is observed as early as 24 h with HA in FCS, MEM and rabbit serum. Several theories have been put forward to explain the protein adsorption on the material and apatite formation or inhibition on HA. Freely dissolved negatively charged proteins such as serum albumin and osteocalcin are known as crystallization inhibitors (Hardy and Furedi 1979; Hauschka and Carr 1982) in bone and are also known to bond to HA.

The inhibiting effect of serum proteins on HA nucleation and growth in vitro has also been described extensively (Martin *et al.*, 1994). Non-collagenous proteins could bind selectively to different faces of the crystal, preventing further growth of these faces while allowing others to grow at a rate limited only by the solution activity of the participating ions (Addadi and Weiner 1985;Boskey, 1996). In fact, these proteins could control crystal growth by binding phosphorylated amino acid groups to the Ca^{2+} ions on the surface of HA. These inhibitor agents could bind to crystal faces if the strereochemical structure were

compatible between the crystal and the inhibitors (Addadi and Weiner 1985). Recent results have indicated that acidic proteins are adsorbed preferentially on the (100) face of HA crystals and thus regulate the shape and size of the precipitates.

Hence, the composition of any solids deposited on the surface of calcium phosphate implants would largely be determined by the surrounding media (Jarcho 1981). It has been reported that the dissolution-reprecipitation behaviour was typical of most synthetic calcium phosphate ceramics (CPCs) immersed in protein-free solution with ion content similar to that of plasma (Radin and Ducheyne, 1993 & 1994).

Moreover, the concentration of calcium and phosphorous in the media and the availability of nucleation sites on the material are essential factors for the precipitation on less soluble HA. Furthermore, according to Radin and Ducheyne (1996), the precipitate that formed on the surface is not a biologically equivalent HA, but a precursor phase with lower calcium and phosphorous ratio than 1.67 and the initiation for precipitation reactions on HA is a slow process impeded by protein adsorption on the material surface (Radin and Ducheyne, 1993). This could explain why in an *in vivo* situation, the formation of bone mineral surface layer is delayed on HA.

FT-IR data suggests that, when serum proteins adsorbs on the coating surface it is likely that the adsorbed proteins may prevent degradation of sintered crystals, which is required for formation of new phases via solution-mediated physicochemical reactions.

Differences in the sintering temperature of HA ceramic will cause differences in crystallinity (crystal size), which will also affect its dissolution process and differences in *in vivo* performance (Niwa *et al.*, 1980).

The acid environment will cause partial dissolution of the macrocrystals of the Ca-P materials. This dissolution will raise the level of concentrations of calcium and phosphate ions in the microenvironment causing precipitation, the extent of dissolution being influenced by the composition of the ceramic and the size of micro- and macroporosity which influences the surface area supporting the theory of dissolution.

Microcrystals of CO_3 apatite may form directly by precipitation or indirectly by initial formation of other Ca-P phases, e.g. dicalcium phosphate dihydrate, DCPD, $CaHPO_4.2H_2O$; Octacalcium phosphate, OCP, $Ca_8H_2\ (PO_4)_6.\ 5H_2O$; amorphous calcium phosphate, ACP; and subsequent transformation of any of these non-apatitic phases to apatite (Le Geros *et al.*, 1983; Le Geros *et al.*, 1989; Le Geros, 1990).

Materials prepared by a sol-gel process are more bioactive than the materials of the same compositions prepared by other methods (Li et al., 1994). BGS was prepared by a sol-gel route and has the following chemical composition BGS-AW type -CaO 45 %, SiO_2 34 %, P_2O_5 16 %, and MgO 5 %. Certain hydroxyl groups such as SiOH and TiOH remaining in the sol-gel prepared materials are assumed to promote hydroxyapatite generation by providing sites for calcium phosphate nucleation (Li P et al., 1992).

For glasses with up to about 53 mole % of SiO_2, HCA crystallization occurs very rapidly on the glass surface within 2 h while glasses with SiO_2 content between 53 and 58 mole % of SiO_2 require two to three days to form both the amorphous calcium phosphate layer and to crystallize HCA. Compositions with > 60% SiO_2 do

not form a crystalline HCA layer even after four weeks in SBF (Hench and LaTorre, 1992).

Even the P_2O_5 free CaO, SiO_2 binary glasses formed the apatite layer *in vitro* as well as *in vivo* (Ohura *et al.,*), whereas the CaO, P_2O_5 -based glasses did not. This behaviour is in contrast to the conventional expectation, at least within the glass-forming compositional region.

In spite of it, only the CaO, SiO_2 based glasses formed the apatite layer, which decreased the ionic activity product of the fluid. This behaviour is due to a peculiar surface structure of the CaO, SiO_2-based glasses, which provides favourable sites for apatite nucleation. The CaO, SiO_2-based glasses form a silica hydrogel layer prior to the formation of the apatite layer. It is probable that this hydrated silica induces apatite nucleation. This is confirmed by the observation that a pure silica gel, prepared by the sol-gel method, formed bone-like apatite on it when soaked in simulated body fluid at pH 7.4 (Li *et al.,* 1992).

The increase in pH of BGS in acetate buffer, Tris-HCl and SBF after 24 h coincided with the increase in calcium release whereas the phosphorous was comparatively lower. The increase in the pH could be due to the proton uptake from the medium on to the material and followed by release of calcium ions by the material into the medium. pH definitely plays a significant role in the formation of different ionic complexes. BGS immersed in acidic and alkaline pH showed different calcium phosphate release rates. It has been reported that cations enhance the formation of silica phosphate complex (Murashov and Leszcynski 1999). Although calcium and phosphate ions can be adsorbed on the silica surface at pH 7.4, calcium adsorption was stronger than phosphate adsorption on BGS, because phosphate content remained unchanged even after 24 h.

Iler *et al.*, (1975) proposed that one H^+ is released for each Ca^{2+} adsorbed. Ca^{2+} could be attracted by the negative charge of the silanol and the H^+ would be liberated when the Ca^{2+} is adsorbed. Calcium adsorption increases when the pH and Ca^{2+} concentration in the suspension increase. According to Li and Zhang (1990), the negatively charged surface of a glass attracts calcium ions from the solution, leading to their accumulation within the glass solution interface.

The BGS granules showed surface cracks of ~15 μm and the intergranular interface has opened after immersion in acetate, Tris-HCl and SBF. These surface changes are due to the influence of pH on the BGS leading to increased release of calcium into the medium. These observations are confirmed by the works of Regi *et al.*, (2000) reported that glass soaked in SBF released high amount of Ca^{2+} during the first 24 h reaching values of 410 ppm. A significant decrease in Ca^{2+} concentration in SBF occurred, showing values of 65 ppm for Ca^{2+} at 3 days and after 1 week the Ca^{2+} concentration reached 35 ppm.

The CaO, SiO_2 based glasses release an appreciable amount of calcium, whereas the CaO, P_2O_5 based glasses releases phosphates. Both types of ions increase the ionic activity product of the apatite in the surrounding fluid. The magnitude of the increase is almost equal between the CaO, SiO_2 based glasses and the CaO, P_2O_5 based glasses (Ohtsuki *et al.*, 1992) (Figure.IV.11).

The solution surrounding the surface is, therefore, supersaturated and causes nucleation of apatite. It is also reported that pores present in pure silica, prepared by the sol-gel method, are nucleation sites for apatite (Pereira *et al.*, 1995). Carbonate peaks were observed between 1480 and 1445 cm^{-1} and were assigned to ν_3 mode and the ν_2 carbonate peaks were observed only in SBF at 853 cm^{-1}. The peak at 780 cm^{-1} could be due to the ν_2 vibrational modes for the carbonate ions (Walters *et al.*, 1990),

Figure-IV-10

STAGE ***Reaction stages of a bioactive glass implant***

1 Rapid exchange of Na^+ or K^+ with H^+ or H_3O^+ for solution:

$$Si - O - Na^+ + H^+ + OH^- \longrightarrow Si - OH^+ + Na^+ (solution) + OH^-$$

2 Loss of soluble silica in the form of $Si(OH)_4$ to the solution, resulting from breaking of Si -O- Si bonds and formation of Si-OH (silanols) at the glass solution interface:

$$Si - O - Si + H_2O \longrightarrow Si - OH + OH - Si$$

3 Condensation and repolymersiation of a SiO_2-rich layer on the surface depleted in alkalis and alkaline-earth cations:

$$O - Si(O) - OH + HO - Si(O) - O \longrightarrow O - Si(O) - O - O - Si(O) - O + H_2O$$

4 Migration of Ca^{2+} and PO_4^{3-} groups to the surface through the SiO_2 rich layer forming a $CaO-P_2O_5$ rich film on top of the SiO_2 rich layer, followed by growth of the amorphous $CaO-P_2O_5$ -rich film by incorporation of soluble calcium and phosphates from solution

5 Crystallisation of the amorphous $CaO-P_2O_5$ film by incorporation of OH^-, CO_3^{2-} or F^- anions from solution to form a mixed hydroxyl, carbonate, fluorapatite layer.

Adopted from Larry L. Hench-Introduction to bioceramics

Figure-IV-11

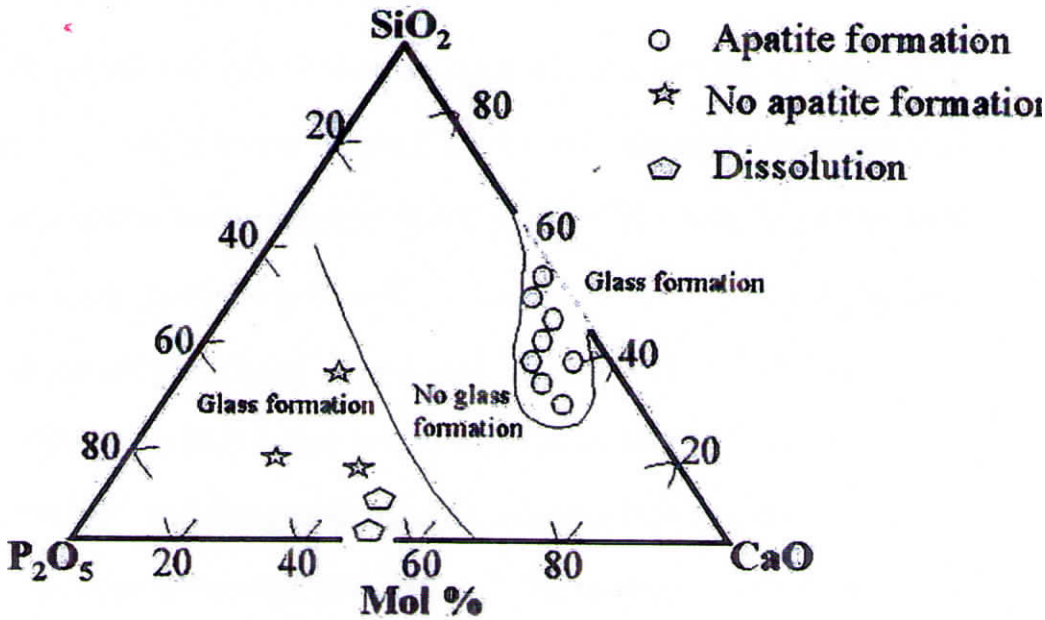

Compositional dependence of apatite formation on glasses in the syst CaO-SiO2-P2O5 in simulated body fluid (30 days) -

Adopted from Ohtsuki et al., 1991

Figure-IV-10

STAGE ***Reaction stages of a bioactive glass implant***

1 Rapid exchange of Na^+ or K^+ with H^+ or H_3O^+ for solution:

$$Si - O - Na^+ + H^+ + OH^- \longrightarrow Si - OH^+ + Na^+ (solution) + OH^-$$

2 Loss of soluble silica in the form of $Si(OH)_4$ to the solution, resulting from breaking of Si -O- Si bonds and formation of Si-OH (silanols) at the glass solution interface:

$$Si - O - Si + H_2O \longrightarrow Si - OH + OH - Si$$

3 Condensation and repolymersiation of a SiO_2-rich layer on the surface depleted in alkalis and alkaline-earth cations:

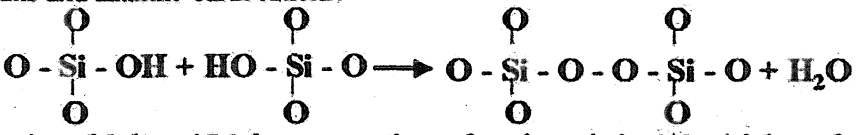

4 Migration of Ca^{2+} and PO_4^{3-} groups to the surface through the SiO_2 rich layer forming a $CaO-P_2O_5$ rich film on top of the SiO_2 rich layer, followed by growth of the amorphous $CaO-P_2O_5$ -rich film by incorporation of soluble calcium and phosphates from solution

5 Crystallisation of the amorphous $CaO-P_2O_5$ film by incorporation of OH^-, CO_3^{2-} or F^- anions from solution to form a mixed hydroxyl, carbonate, fluorapatite layer.

Adopted from Larry L. Hench-Introduction to bioceramics

Figure-IV-11

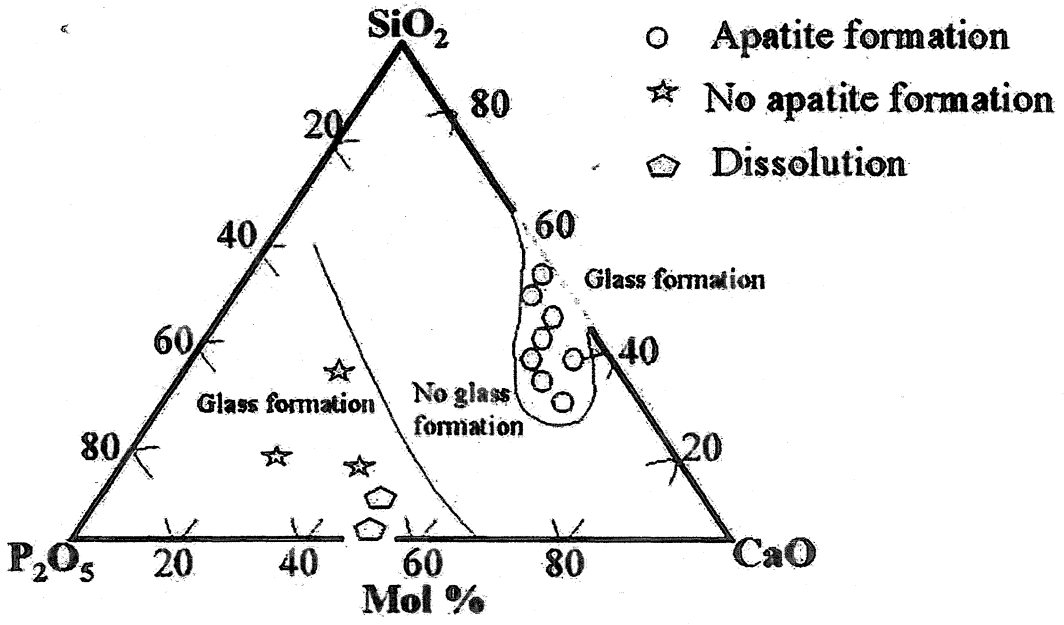

Compositional dependence of apatite formation on glasses in the system $CaO-SiO_2-P_2O_5$ in simulated body fluid (30 days) -

Adopted from Ohtsuki et al., 1991

which was observed only in acetate buffer and not in Tris-HCl or SBF. The apatite formed with BGS may be Type – B apatites, where the PO_4 groups were substituted by CO_3. This is confirmed by the biochemical changes observed in the medium after immersion for phosphate and peak shifts observed in the phosphate group after immersion in acetate, Tris-HCl and SBF media.

The ν_3 phosphate mode appeared as three peaks at 1117, 1051 and 1022 cm^{-1}. The peak observed at 935 - 905 cm^{-1} were assigned to ν_1 mode of phosphate. Minor peaks of P-O crystalline were observed at 610 - 600 cm^{-1} and 569 - 508 cm^{-1} in BGS immersed in acetate buffer. This could be due to the addition of P_2O_5 to the glass was shown to eventually cause the amorphous calcium phosphate film to develop into a crystalline hydroxyapatite layer (Gross *et al.*, 1998). The crystalline P-O peaks were not observed in BGS subjected to Tris-HCl or SBF media, only amorphous P-O peaks were observed between 600 - 525 cm^{-1}.

FT-IR spectra on the BGS revealed sharp ^{-}OH peak at 3433 cm^{-1} after 24 h whereas, the ^{-}OH peak was not observed in raw BGS samples. The presence of the ^{-}OH group signifies the formation of Si-OH complex. The peaks at 1138 to 1026 cm^{-1} could be due to the Si-O stretch of the wollastonite ($CaO.SiO_3$), which showed a significant shift from the original control peak at 1117 - 1022 cm^{-1}. The Si-O-Si stretch was observed in BGS before immersion between 1117 to 716 cm^{-1} is shifted to 1138 to 778 cm^{-1}. This change was observed only with BGS in acetate buffer. The Si-O bend was observed between 557- 425 cm^{-1}. The significance of the stretch and bend is not clear and extensive FT-IR studies have to be carried out to understand the chemical stability of these bonds under different physiological solutions.

The pH of BGS in FCS and rabbit serum showed decrease in pH after 12 h and after 24 h the pH started increasing. Whereas in MEM there was an increase in the pH after 12 h and remained unaltered even after 24 h. The increase or decrease in the pH did not influence the calcium ions release or adsorption. Glass ceramic, immersed in a simulated physiological solution, caused an increase in calcium and phosphate concentration in solution prior to the subsequent decrease associated with the calcium-phosphate precipitation (Kokubo *et al.*, 1990). This decrease in pH and the stable calcium and phosphate ions in the medium suggest that, the proton (H^+) release and calcium adsorption was slow and the protein adsorption on the material surface might have prevented further release of calcium and phosphate from the material surface. Effect of proteins on the formation of surface reaction layers on bioactive glass was analyzed using atomic force microscope (AFM) in bioactive glass 45S5 surface during immersion in protein-free buffer solution and protein containing culture medium. When immersed in serum free solutions, AFM showed that the surface of bioactive glass reacted non-uniformly. After 5 min of immersion, the glass surface showed a rough texture due to the formation of particles on the surface. With increasing immersion time, the particles increased in size and number. Unlike the reaction on the substrates immersed in serum-free solution, a uniform layer of globules, presumably proteins covered the substrates immersed in serum containing solutions. As the immersion time increased, the density of globules increased and the layer thickened.

SEM of the material surface showed surface-cracks on the periphery and in the center of the material and thin glossy protein coatings appeared on the surface and as well as within the pores (> 5 to 10 μm). Apatite-like deposits of < 1 μm could be seen on the material surface, that was confirmed by the FT-IR spectra of BGS

immersed in MEM, FCS and rabbit serum. The $\nu_3 CO_3$ peaks between 1648 and 1400 cm^{-1} and ν_2 peaks between 853 - 875 cm^{-1} confirmed the apatite formation by 24 h. Serum proteins adsorbed on the BGS surfaces at the early stages of the solution-mediated BGS reactions. Formation of a crystalline carbonated HA layer was delayed up to three or more days in solution with plasma ions. And again, in the presence of serum, only amorphous surfaces composed of Si, Ca and P were observed for any time up to seven days of immersion (Radin *et al.*, (1997).

The ^{-}OH peaks were observed between 3420 - 3415 cm^{-1} after 24 h for BGS immersed in MEM, FCS and rabbit serum. The presence of the ^{-}OH group signifies the formation of Si-OH complex. Using *in vitro* modeling results, it was suggested that this phenomenon was related to the presence of hydroxyl (Si-OH and Ti-OH) or carbonyl groups (C-OH) at the material surfaces (Li *et al.*, 1994).

Si-O bend was observed in all the samples after immersion between 555 – 477 cm^{-1}. C-H peaks were seen at the 2923 and 2824 cm^{-1} region and their significance is not clear.

The ν_3 PO_4 peaks were observed between 1117 to 976 cm^{-1} and ν_1 peak between 938 - 906 cm^{-1}. The ν_4 PO_4 peaks were observed between 610 - 513 cm^{-1} and the ν_2 peaks are seen between 429 – 477 cm^{-1}. Amorphous P-O peaks were observed between 595 – 555 cm^{-1} in rabbit serum but not in MEM or FCS immersed BGS. FT-IR analysis showed that, in the serum free solution, crystalline hydroxyapatite was formed by transformation from the initially formed amorphous calcium phosphate. In contrast, immersion in serum-containing solutions only produced an amorphous calcium phosphate.

However, given that the *in vitro* modeling studies did not address the mechanisms by which Ca and P containing phases form on hydroxylated surfaces,

definitive word as to whether this question can be reduced to a purely inorganic event, is still needed. In fact, it would appear than an event without intervening biological components is a strained concept for, essentially, an organic reaction sequence at the surface of bioactive glasses (Figure IV.1). In fact, serum proteins do have a major effect on the properties of the surface reaction layer.

Radin *et al.*, (1997) already demonstrated, using one-parametric variations in solution composition that the surface reactions on bioactive glass 45S5 were exquisitely dependent upon the modeling conditions. The solutions used were tris buffer, tris buffer complemented with plasma electrolyte and or serum and serum. After a short immersion (3 h) a crystalline, carbonated hydroxyapatite (c-HA) layer formed only in tris. Reaction surfaces of different structures, morphology and composition were observed in all other solutions after either short-and long -term immersions. They comprised two layers with the layer in contact with the bulk consisting mainly of Si; the outer layer was composed of Si, Ca, and P, was amorphous and had a Ca/P ratio of about 1.

Given the repeated observation of the absence of crystalline hydroxyapatite when proteins co-adsorb, it is unlikely that, *in vivo*, adsorption of biological molecules will take place subsequent to the transformation of an amorphous calcium-phosphate rich layer to carbonated apatite (Hench , 1991). The observation suggests that serum proteins adsorb in tandem with the occurrence of solution-mediated reactions leading to formation of a silica gel. Amorphous calcium-phosphate phases accumulate in this Si-rich matrix.

A significantly different behaviour between immersion in serum protein free and serum protein containing solutions was also observed in experiments intended to model silicon dissolution from bioactive glass particles (Radin *et al.*, 1999).

Bioactive glass granules can be internally hollowed out leading to shells of calcium phosphate in which osteogenesis can be observed (Schepers *et al.*, 1991).

Bioactive glass granules were immersed under integral (no solution exchange during the experiment, thereby simulating stagnant fluid conditions) or differential conditions (conditions simulating continuous fluid flow *in vivo*) in tris-buffered solution complemented with either plasma electrolyte (TE) or with electrolyte and 10% serum (TES-10). Only when solution was continuously replenished, thereby avoiding Si saturation in solution, and only when the solution contained serum proteins, was full Si dissolution from the core of the granules observed (Radin *et al.*, 1999). This result was ascribed to the different structure and composition of the surface reaction layer that formed in the presence of serum. In the serum free solution, the carbonated hydroxyapatite surface protects the glass from further corrosion. In contrast, the reaction layer formed in serum containing solutions does not offer sufficient protection from continued corrosion. This surface reaction layer is slightly porous and comprises proteins, silica and amorphous calcium phosphate (Radin *et al.*, 1999). In the presence of serum proteins, the apatite formation extensively delayed, a finding, which is consistent with other data on the effect of proteins on nucleation and crystal growth of apatite (Martin and Brown 1994; Radin and Ducheyne 1996).

Solutions more closely approaching the physiological state, the maturation of amorphous calcium phosphate to crystalline hydroxyapatite does not take place readily. The proteinaceous layer, which adsorbs onto the glass interfaces with the solid to liquid interaction of the amorphous calcium phosphate layer. Whereas, amorphous calcium phosphate can form exclusively as the result of physicochemical phenomena in the solid glass phase, it is suggested here that adsorbed serum proteins

impede the nucleation and growth reactions by which it would transform to carbonated apatite. The reactions in the glass are not blocked, however, as Ca and P diffusion leads to a continuously thickening of the Ca-P rich zone under the adsorbed protein layer. The adsorption of the protein layer may also be critical in terms of providing attachment sites for bone cells such as osteoblasts and their progenitors.

The concentration of serum proteins at the glass surface transformed to calcium phosphate, served to enhance the expression of the osteoblast phenotype. Measurement of protein that adsorbs from the tissue culture medium, a greater quantity of serum proteins adsorbed onto the calcium phosphate coated glass than onto the untreated BGS. However, a yet larger amount absorbed onto stoichiometric HA, which was used concurrently (El-Ghannam *et al.*, 1999). This was surprising, as *in vivo* results clearly documented a more intense bioactive effect for BGS than HA (Hench 1988; Schepers *et al.*, 1991). Thus, we reasoned that the effect of the serum protein adsorption treatment was related to the species that adsorbed and found, in fact, significantly different absorption profiles for untreated BGS, calcium phosphate coated BGS and stoichiometric HA (El-Ghannam *et al.*, 1999).

The time required for formation was shortest with the two glass ceramics, longer with TCP and longest with HA. It can therefore be assumed that the formation rate corresponds to the dissolution rate of the materials. This result is consistent with the results for bioglass (Hench *et al.*, 1971).

Triphasic Bioactive Composite System (HABGS)

HABGS is a novel material synthesized in our Institute and literature evidence for this composite material is not available and hence, the interpretations were made based on the comprehensive understanding of individual materials (HA and BGS) of the composite.

HABGS in acetate buffer + SBF showed an increase in the pH from 5.2 to 7.83 which could be due to the rapid release of ions into the medium, which is evident from the increase of calcium and decrease of phosphorous at 12 h. The high release of the Ca^{2+} could be due to the biphasic nature of the material. The BGS material in acetate buffer also showed the same trend of high calcium release and phosphate uptake. Whereas, in the acetate buffer of HA at 12 h, the $Ca^{2+}$and PO_4^{3-} uptake increased rather than the release, with a decrease in pH. This suggested that the HABGS composite material released more Ca^{2+} as that of BGS while uptake of PO_4^{3-} was less and this change in the calcium and phosphate might have favoured the increase in pH. The pH at 24 h reduced this change, which is online with that of the BGS immersed in acetate buffer at 24 h. The decrease in the pH of the buffer could be due to the supersaturation, precipitation and deposition of the ions that was released from the material at 12 h on the composite material. However, the Ca^{2+}/PO_4^{3-} ions continue to be stable at 28 mg% and 2.33 mg%. This suggested that the material is still continuously releasing Ca^{2+} and PO_4^{3-} ions into the medium, due to the acidic nature of the medium. SEM of the ceramic granules revealed that the intergranular openings and few apatite-like substances (< 1 um) were seen on the smooth phase of the material while the granular surface opened up at 12 h. By 24 h, further opening of the material surface was observed with few cracks < 15 μm in width and apatite-like deposits of < 1μm are seen both in the smooth surface and granular surface. Supersaturation and precipitation of the ions from the medium led to deposits on the surface, and the large cracks on the material surface indicated areas from where the ions must have been released continuously into the medium. FT-IR of the granules showed a high absorption peak for ^{-}OH at 3421cm^{-1}, whereas the OH peak is absent in HABGS control material. This confirmed the water absorption by

the material and the formation of Si-OH complex. The ν_3 carbonate peaks were observed at 1627 and 1447 cm^{-1}. The presence of the $^-$OH peak and CO_3^{2-} confirmed that the apatite formed is a HCA. The ν_2 of CO_3^{2-} were not observed in HABGS, whereas the ν_3 peaks were more prominent. Control peaks at 1118 to 716 cm^{-1} were assigned to the Si-O-Si stretch. After immersion the peak at 1118 cm^{-1} was not detected. So it could have formed complexes with Na^+ or K^+ from the acetate-SBF medium. The peak at 716 cm^{-1} showed a peak shift to 795 cm^{-1}, which could be due to the hydrolysis reaction and could have also formed a complex with the Si-OH (silanol). The ν_3 phosphate modes appeared as three peaks at 1054, 1022, 941 and ν_1 PO_4 peak was observed at 906 cm^{-1}. A peak split has occurred into 941 and 906 cm^{-1} after immersion at the ν_1 of the PO_4^{3-} in control at 938 cm^{-1}. This may be due to the release of the phosphate ions from the material at 24 h and formation of complexes with the newly formed apatite, which is usually seen in HCA layer on a 45S5 bioglass (Nelson and Featherstone 1982). The ν_4 phosphate peak at 588 (P-O bend amorphous) in control was not observed after 24 h of dissolution, rather three new peaks were observed at 681, 669 and 649 $cm^{-1}$and there was a small shift of 551 (P-O bend amorphous) in control to 550cm^{-1}. The phosphate ν_1 peak was observed in the region of 476cm^{-1} and is a stronger peak than ν_4 as observed in HA with acetate buffer at 24 h. The peak that is observed at 551-430cm^{-1} in control could be assigned to Si-O (bend) has shifted to 550-476 cm^{-1} after 24 h. C-H peaks were observed in HABGS granules subjected to dissolution in all the buffers between 2852-2926 cm^{-1}.

In HABGS subjected to Tris-HCl + SBF, the pH decreased from 7.3 to 7.06 at 12 h. The decrease in the pH was minimal when compared to the HA and BGS. The change in the pH did not inhibit the calcium and phosphate release from the material, as calcium (11.8 mg%) and phosphorous (1.16 mg%) were estimated at 12 h. Surface

topography revealed that the material had completely opened up with pores of 10 to 20 μm and a few cracks were seen on the smooth phase of the material. At 24 h, the pH increased to 7.69, which was in parallel to the observations made with BGS material but not with HA. The simultaneous release of Ca^{2+} and the uptake of PO_4^{3-} might have favoured this increase. SEM of the surface depicted the reduction of the pore size to 5-20 μm. FT-IR of the granules after dissolution confirmed the presence of the high absorption peak for OH^- at 3432cm^{-1} and at 1280 cm^{-1}. This could be due to the water absorption by the material and formation of Si-OH complex. The ν_3 carbonate peaks were observed at 1627 and 1447 cm^{-1}. The presence of the OH^- peak and CO_3^{2-} confirmed that the apatite formed is a HCA. The ν_2 of CO_3^{2-} were not observed in HABGS, whereas the ν_3 peaks are more prominent. Control peaks at 1118 to 716 are assigned to the Si-O-Si stretch. After immersion the peak at 1118 cm^{-1} was not detected and must have formed complexes with Na^+ or K^+ from the Tris-HCl + SBF medium and the peak at 716 showed a peak shift to 784 cm^{-1}. This could be due to the hydrolysis reaction and could have formed a complex of Si-OH (silanol). The ν_3 phosphate modes appeared as three peaks at 1050, 1024, 976 and two ν_1 peaks at 940 and 904 cm^{-1}. This may be due to the nucleation of the phosphate ions from the medium on to the material after 24 h and formation of complex with the newly formed apatite, which is usually seen in HCA layer on a 45S5 bioglass (Nelson and Featherstone 1982). The P-O bend amorphous peak was not observed between 588 – 551 cm^{-1} after immersion. The phosphate ν_2 peak was observed in the region of 475 cm^{-1} and has a stronger peak than ν_4. The peak that is observed at 551-430 cm^{-1} in control could be assigned to Si-O (bend) has shifted to 525 - 475 cm^{-1}.

HABGS subjected to SBF showed a decrease of pH at 12 h, which was observed for HA and BGS materials also and could be due to the proton consumption

and Ca^{2+} release. The Ca^{2+} release from the material was confirmed from the amount of Ca^{2+} in the medium. Whereas, the PO_4^{3-} concentration did not decrease even after 12 h. There were no significant changes on the surface topography of the granules at 12 h (pores of 5-20 μm) indicating dissolution of ions. The pH at 24 h increased and could be due to the supersaturation and precipitation of the ions, but the calcium decreased to 7.45 mg% while phosphorous ions was stable at 2.23 mg% at 24 h. This trend was also observed in BGS subjected to SBF at 24 h and suggested that parallel events are occurring between the BGS and HABGS. The material surface at 24 h revealed a ruffled-like appearance on the smooth surface and fine apatite-like deposits on the entire surface of the material. FT-IR of the granules showed a high absorption peak for OH^- at 3431cm^{-1}, whereas the ^-OH peak is absent in HABGS control material. This confirmed that water absorption by the material and formation of Si-OH complex. The ν_3 carbonate peaks were observed at 1626 - 1300 cm^{-1} and these peaks could be assigned to the surface CO_3^{2-} ions, rather than to CO_3^{2-} ions in the lattice of phosphate ions. The major peak was stationed at 1626 cm^{-1} and several minor peaks from 1626 to 1300 cm^{-1}. The distribution of the CO_3^{2-} ν_3 sites depends on the maturation and formation of apatite crystals (Rehman and Bonfield 1997). The presence of the ^-OH peak and CO_3^{2-} confirmed that the apatite formed is a HCA. The ν_2 of CO_3^{2-} were observed in HABGS at 852 cm^{-1}. It is suggested that the ν_2 sites are considered to competitive between the ^-OH and CO_3^{2-} at the interface of the growing crystal, whereas occupancy of the ν_3 sites depends on competition between the phosphate and carbonate ions (Le Geros *et al.*, 1987; Elliot *et al.*, 1985). Control peaks at 1118 to 716 are assigned to the Si-O-Si stretch. After immersion the peak at 1118 cm^{-1} was not detected and could have formed complex with Na^+ or K^+ from the SBF and the peak at 716 cm^{-1} showed a peak shift to 783 cm^{-1} and small peak at 725

cm^{-1}. This could be due to the hydrolysis reaction and could have formed a complex of Si-OH (silanol). The ν_3 phosphate modes appear as three peaks at 1064, 1020, 976 and ν_1 PO_4 peaks at 938 and 905 cm^{-1}. The P-O bend crystalline and P-O bend amorphous peaks were absent after the immersion of HABGS in SBF medium.

The ν_4 PO_4 were observed at 675, 669, 645, 555 and 510 cm^{-1}. The splitting of the ν_4 vibrational peaks indicated the low site symmetry of molecules, confirm the presence of more than one distinction site for the phosphate group (Young 1974). The phosphate ν_2 peak was observed in the region of 476 cm^{-1} and has a stronger peak than ν_4. The peak that is observed between 555, - 476 cm^{-1} could be assigned to Si-O (bend).

In HABGS subjected to FCS, the initial pH of the medium reduced marginally from 8.6 to 8.33 at 12 h. But, the pH of HA in FCS reduced to acidic 6.67 while BGS remained at pH 7.54. This decrease in the pH in HA may be due to the increased adsorption of protein and reduced Ca^{2+} release and phosphate uptake from the medium on to the material. The BGS and HABGS showed almost the same trend in calcium release whereas, the PO_4^{3-} release from the BGS was more than from HABGS at 12 h. The surface of the HABGS showed a thin protein coating, but the intergranular space did not open up much perhaps due to the covering of the protein matrix. Apatite-like deposits of 2-10 μm in size were observed covered by a thin matrix of protein. At 24 h, the pH continued to increase to 8.69. Whereas, in HA and BGS at 24 h the pH reduced from the pH value at 12 h. The Ca^{2+} reduced to 9.4 mg% at 24 h, which indicated precipitation and deposition of the Ca^{2+} on to the material surface. The PO_4^{3-} level remained same as that observed at 12 h. The decrease in the Ca^{2+} ion release and the continued protein adsorption onto the material from the

medium might have favoured the increase in the pH, since HA is formed at pH values greater than pH 8 (Bako and Kotsis, 1992).

FT-IR of the granules after immersion showed a high absorption peak for ^{-}OH at 3432cm^{-1}, whereas the OH peak is absent in HABGS control material. This confirmed that water absorption by the material and formation of Si-OH complex. ν_3 Carbonate peaks were observed at 1637 to1300 cm^{-1}. The presence of the ^{-}OH peak and CO_3^{2-} confirmed that the apatite formed is a HCA. The ν_2 of CO_3^{2-} was observed in HABGS at 825 cm^{-1}, these peaks could be assigned to the surface CO_3^{2-} ions, rather than to CO_3^{2-} ions in the lattice of phosphate ions and the ν_3 has a major peak at 1637 cm^{-1} and several minor peaks from 1637 to 1300 cm^{-1}. The distribution of the CO_3^{2-} ν_3 sites depends on the maturation and formation of apatite crystals (Rehman and Bonfield 1997). It is suggested that the ν_2 sites are considered to competitive between the OH^{-} and CO_3^{2-} at the interface of the growing crystal, whereas occupancy of the ν_3 sites depends on competition between the phosphate and carbonate ions (Le Geros *et al.*, 1987; Elliot *et al.*, 1985). Control peaks at 1118 to 716 are assigned to the Si-O-Si stretch. After immersion the peak at 1118 cm^{-1} was not detected and the peak at 716 cm^{-1} showed a peak shift to 784 cm^{-1} and small peak at 705 cm^{-1}. This could be due to the hydrolysis reaction and could have formed a complex of Si-OH (silanol). The phosphate modes appeared as three ν_3 peaks at 1048, 976 and ν_1 peaks at 938 cm^{-1} and 904 cm^{-1}. The peak at 1118 cm^{-1} is lost after immersion in buffer and could have formed complex with Na^{+} or K^{+} from the FC medium. The P-O bend amorphous and P-O bend crystal were absent in HABGS after immersion in FCS. The phosphate ν_2 peak was observed in the region of 475 cm^{-1} and has a stronger peak than ν_4. The peak that is observed between 500 - 475 cm $^{-1}$ could be assigned to Si-O (bend).

In HABGS subjected to MEM showed an increase in the pH, online with the HA and BGS at 12 h. The increase in pH followed the decrease in the Ca^{2+} ions in the medium and an increase in the PO_4^{3-} ions in HA, BGS and HABGS materials at 12 h. The protein concentration in the medium reduced by 50% in the medium as observed in HA, BGS and HABGS. The intergranular spaces on the surface of the material opened up with pores of 10 to 20 μm in width. At 24 h the pH increased from 8.32 to 8.69. This increase in the pH is followed by release of Ca^{2+} ions into the medium (9.79 mg%) and PO_4^{3-} uptake from the medium (2.29 mg%) at 24 h. But in BGS and HA at 24 h the pH reduced from 12 h. The protein concentration in the medium did not show much change at 24 h. This confirmed that protein adsorption had ceased once the medium attained supersaturation. FT-IR of the granules showed a high absorption peak for ^{-}OH at 3431cm^{-1} and at 1275 cm^{-1}, whereas the OH peak is absent in HABGS control material. This confirmed the water absorption by the material and formation of Si-OH complex. ν_3 carbonate peaks were observed at 1626 to1300 cm^{-1}. The presence of the ^{-}OH peak and CO_3^{2-} confirmed that the apatite formed is a HCA. The ν_2 of CO_3^{2-} was observed in HABGS at 851 cm^{-1}, whereas the ν_3 peaks are more prominent at 1626 to1300 cm^{-1}, these peaks could be assigned to the surface CO_3^{2-} ions, rather than to CO_3^{2-} ions in the lattice of phosphate ions. The distribution of the CO_3^{2-} ν_3 sites depends on the maturation and formation of apatite crystals (Rehman and Bonfield 1997). It is suggested that the ν_2 sites are considered to competitive between the OH^{-} and CO_3^{2-} at the interface of the growing crystal, whereas occupancy of the ν_3 sites depends on competition between the phosphate and carbonate ions (Le Geros *et al.*, 1987; Elliot *et al.*, 1985). Control peaks at 1118 to 716 are assigned to the Si-O-Si stretch. After immersion the peaks at 1118 and 716 cm^{-1} were not detected. The peak at 1118 cm^{-1} is lost after immersion in buffer, and

could have formed complex with Na^+ or K^+ from the MEM medium. The ν_3 phosphate modes appeared as three peaks at 1053, 1020, 976, and the ν_1 PO_4 peaks at 937 and 906 cm^{-1}. A peak split has occurred at the ν_3 of the PO_4^{3-} in control at 938 cm^{-1}. Phosphate ν_4 peaks were observed at 672, 646, 553 and 510 cm^{-1}. The splitting of the ν_4 vibrational peaks indicated the low site symmetry of molecules and confirmed the presence of more than one distinction site for the phosphate group (Young 1974). The phosphate ν_2 peak was observed in the region of 476 cm^{-1} and has a stronger peak than ν_4. The peak that is observed at 553 - 476 cm^{-1} could be assigned to Si-O (bend).

HABGS subjected to rabbit serum showed increase in the pH from 7.2 to 8.64 at 12 h. Whereas in HA and BGS a marginal increase in the pH after 12 h immersion in rabbit serum was observed. The increase in the pH is due to increased release of Ca^{2+} ion and PO_4^{3-} uptake. In HA and BGS the Ca^{2+} uptake and PO_4^{3-} release was more and hence the pH was less alkaline. The protein adsorption on the material surface after 12 h in HA, BGS and HABGS material was less and suggested that specific protein molecules alone were adsorbed on to the material surface. In *in vitro* the protein adsorption on to the material surface at the physiological pH was very less and than *in vivo* the reason for this dissimilarity is yet to be fully understood. Morphologically, the surface of the material showed a thick coating of protein with apatite-like deposits and presence of large cracks. After 24 h the pH showed a moderate decrease to 8.53. But, in HA and BGS granules subjected to rabbit serum after 24 h showed an increased pH. The decrease in the pH was parallel to the decrease in the Ca^{2+} and PO_4^{3-} ions in the medium. This suggested that calcium and phosphate ions had undergone supersaturation in the medium and deposition of the ions onto the material surface has started. The same mechanism was observed for HA

and BGS granules after 24 h in rabbit serum. The protein concentration in the medium decreased moderately after 24 h. The surface of the material did not change much when compared with the 12 h material surface. FT-IR of the granules showed a high absorption peak for ^{-}OH at 3432cm^{-1}, whereas the OH peak is absent in HABGS control material. This confirmed that water absorption by the material and formation of Si-OH complex. Carbonate peaks was observed at 1637 - 1300 cm^{-1}, these peaks could be assigned to the ν_3 peaks of the CO_3^{2-}. The presence of the ^{-}OH peak and CO_3^{2-} confirmed that the apatite formed is a HCA. The ν_2 of CO_3^{2-} was observed in HABGS at 857 cm^{-1}, whereas the ν_3 peaks are more prominent at 1637 - 1300 cm^{-1}, these peaks could be assigned to the surface CO_3^{2-} ions, rather than to CO_3^{2-} ions in the lattice of phosphate ions. The distribution of the CO_3^{2-} ν_3 sites depends on the maturation and formation of apatite crystals (Rehman and Bonfield 1997). It is suggested that the ν_2 sites are considered to competitive between the OH^- and CO_3^{2-} at the interface of the growing crystal, whereas occupancy of the ν_3 sites depends on competition between the phosphate and carbonate ions (Le Geros *et al.*, 1987; Elliot *et al.*, 1985). Control peaks at 1118 to 716 are assigned to the Si-O-Si stretch. After immersion the peak at 1118 cm^{-1} was not detected and the peak at 716 cm^{-1} showed a peak shift to 791 cm^{-1}. This could be due to the hydrolysis reaction and could have formed a complex of Si-OH (silanol). The ν_3 phosphate modes appear as three peaks at 1068, 1021, 976 and ν_1 PO_4 peaks at 937 and 905 cm^{-1}. The peak at 1118 cm^{-1} is lost after immersion in buffer, which could have formed complex with Na^+ or K^+ from the rabbit serum. The P-O (bend crystal) and P-O (bend amorphous) peaks were absent after the immersion in rabbit serum. The phosphate ν_2 peak was observed in the region of 476 cm^{-1} and had a stronger peak than ν_4. The peak that is observed at 554 - 476 cm^{-1} could be assigned to Si-O (bend).

CONCLUSION

Hydrogen ion concentration (pH) has definitely played an important role in understanding the inert/active nature of the material in different media with different pH and ionic concentrations with the protein free medium and protein containing medium. This preliminary investigation on the three materials revealed the possible cascade of reactions that it might undergo in an *in vivo* situation. The influence of pH on the material in different media directly depended on the materials physicochemical property. This is evident from the changes observed at 12 and 24 h in the medium by biochemical analysis, on the material surface by SEM, and from the FT-IR analysis. Hypothesis of the possible cascade of reactions that might take place in apatite formation with glass/glass-ceramic materials is given in Figure.IV.12.

The change in the pH after immersion of HA, BGS and HABGS materials in Acetate Buffer, Tris-HCl buffer, Simulated Body Fluid, Foetal Calf Serum, Minimum Essential Medium, and Rabbit Serum, showed increase and decrease of pH at 12 and 24 h irrespective of the type of material. Except for HA in Acetate (12 hrs) and Tris-HCl buffer (24 hrs), the gross changes in the pH were same for all the three materials in all the medium. But, the increase or decrease in the pH values between the three materials immersed in same medium at different time interval was not the same only the trend in increase and decrease of the pH was corresponding. The influence of the pH contributed to the release or uptake of calcium and phosphate ions from the material to the medium or from the medium to the material. The release of calcium and phosphate varied with different buffers and with different materials. HA was the least dissoluting material when compared to BGS and HABGS in all the medium. This is in support of the observations made by several other investigators. Even though BGS and HABGS are two different materials with different calcium

phosphate ratios, the initial degradation and release of calcium and phosphate and the change in the pH was identical. The influence of protein on the material was definite in all the three materials. But, the release and uptake of calcium and phosphate from the material did not reduced significantly in HA, BGS and HABGS even when the protein adsorption was 50% in FC and MEM and only 10% in rabbit serum on to the material surface. It is hypothesized that protein adsorption on the material surface will not change or inhibit the release of calcium and phosphate. This is confirmed by our experiments also. But, the major finding is that different material responds to these proteins in different way. This is evident from our observations that, the amount of calcium and phosphorous released or adsorbed was different from different material with the same type of serum at different time intervals. The surface apatite formation was observed in SEM and confirmed by our FT-IR studies that the type-B carbonated apatite was formed in all the material surface. But, the crystallization of the HCA is prominent only in BGS and HABGS material in all the media. The mechanism of apatite formation is schematically explained in (Figure.IV.12).

From these observations we conclude that:

a) Material property has a definite role in bringing out changes in the pH of the surrounding media during the initial periods and the pH also influenced the material to be less active or to react vigorously. The sequence of material response to different pH are as follows:

   i) Acid pH: HA<BGS<HABGS

   ii) Physiological pH: HA<BGS<HABGS

   iii) Highly alkaline pH: HA<BGS<HABGS

Initial response of the material to simulated body fluid (*In Vitro*)

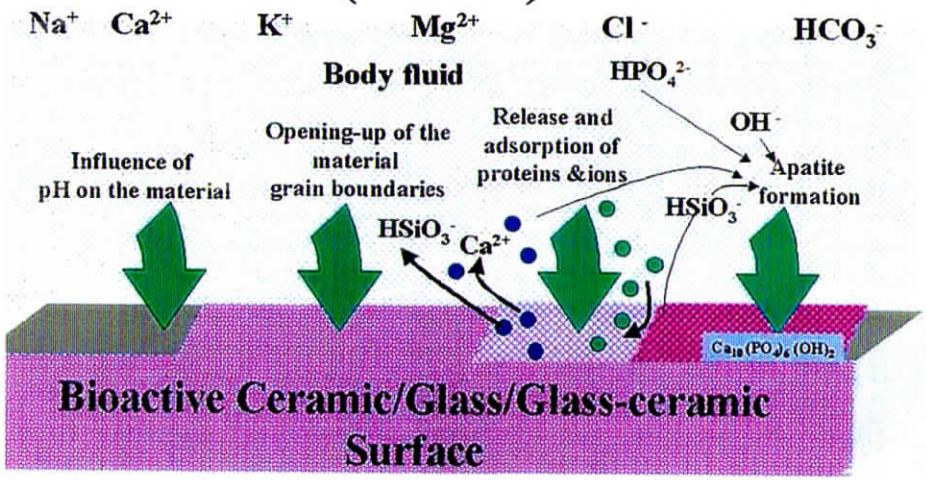

Figure -IV-12

Schematic diagram showing the possible cascade of reactions that might take place after the immersion of bioactive ceramics in simulated body fluid

b) The pH influence on the material favored the release or uptake of the ions. Based on the release and uptake of ions in different pH they are categorised as follows:

i) Acid pH :HA<HABGS<BGS

ii) Physiological pH :HA<BGS<HABGS

iii) Highly alkaline pH: HA< HABGS< BGS

c) Surface "Hydroxyl Carbonate Apatite" was formed in all the three materials subjected to different media. Based on these initial changes one can predict the early response of these materials in an *in vivo* situation.

IV.2 *In Vitro* – Cell Culture Studies

IV.2 *IN VITRO* -CELL CULTURE STUDIES

IV.2.1 Cytotoxicity: MTT assay (Cell viability)

With MTT assay 80 % of the L929 fibroblast cells in contact with the HA, BGS and HABGS material extract showed good viability similar to that of the control.

IV.2.2 Cells in direct contact with materials

HA, BGS and HABGS granules did not show any signs of toxicity embarrassment after 24 h in contact with L929 cells. Cells spread centripetally from the granules to form a monolayer on the glass coverslip. They showed the same morphology in comparison with the negative control (Figure.IV.13A-D).

IV.2.3 Cytocompatibility

SEM examination of HA seeded with L929 fibroblast cells (Figure.IV.13 E) revealed good anchorage, attachment, adhesion, spreading and cell growth (cell phenomenology) in the vicinity of the granules. Cells were elongated, cuboidal or polygonal in shape and actively colonized the surface either in singles or in rosettes. Cells were aligned in a way that the long axis is either parallel or at right angles to the edge, being thickly populated at the edges of the glass coverslip. The surface of HA under SEM showed the material to be intact and the intergranular interface has opened up in few areas and dicalcium phosphate dihydrate (DCPD) -like crystals were seen on the surface as rosettes after 48 h.

SEM revealed very few elongated fibroblast cells adhered on the BGS material (Figure.IV.13 F) surface after 48 h. The cells were more concentrated only on the smooth surface of the material but not on the rough surface.

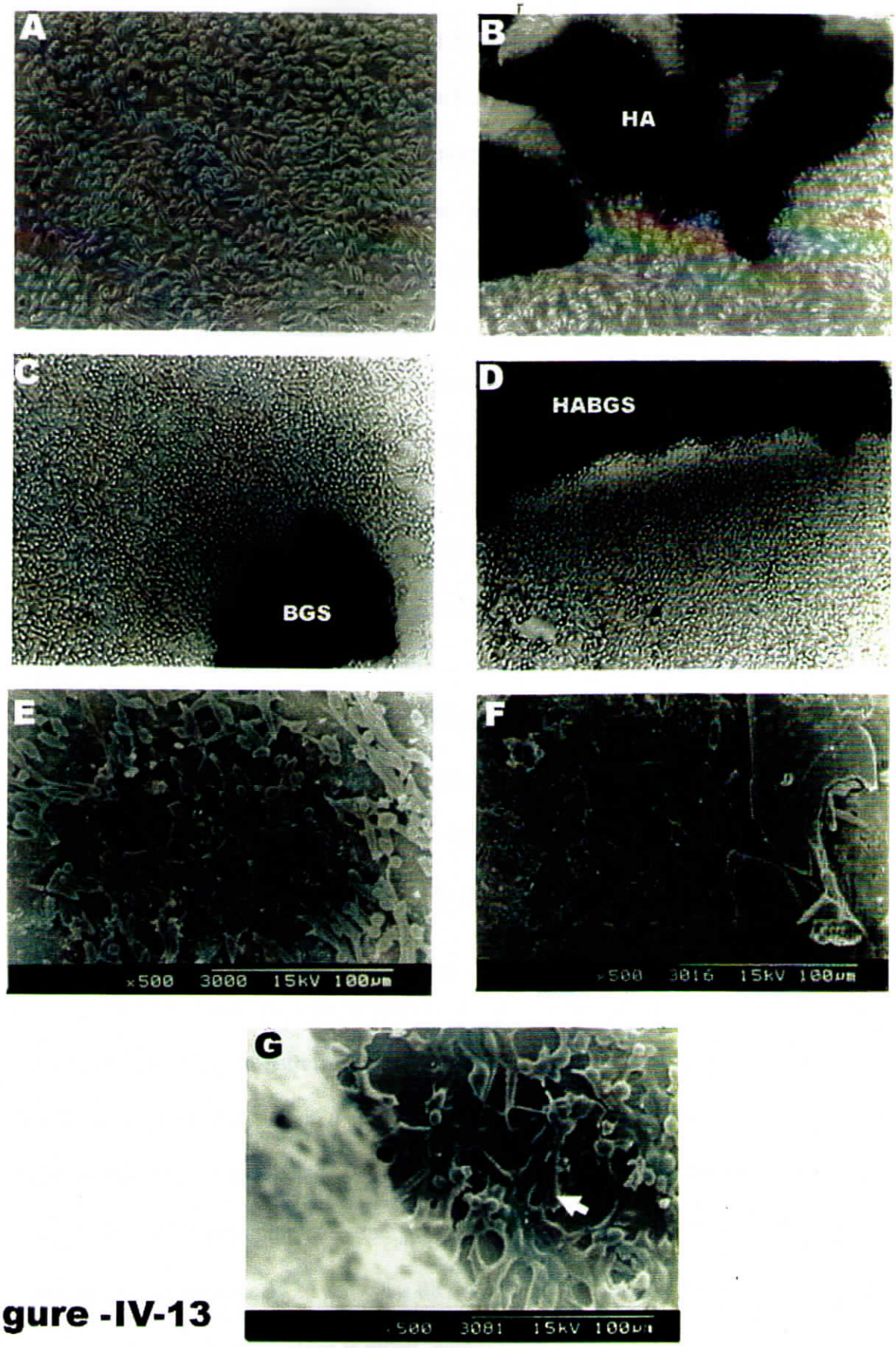

Figure -IV-13

Photomicrographs of L929 fibroblast cells – A- seeded on coverslip; in direct contact with – B- HA; C- BGS and D- HABGS granules after 48 hours.

Scanning electron micrographs of bioactive ceramic discs seeded with L929 fibroblast cells: E - HA; F- BGS and G - HABGS after 48 hours. Arrows denote fibroblast cells.

The surface of the BGS was found to be deposited with extracellular matrix forming an interlace of fibers on the surface. Prior to immersion in the culture medium the surface of the BGS showed intact grain boundaries. Macrocracks of 30 μm were observed on the surface. These macrocracks may be due to the non-uniformity in the particle packing during the *green* compaction. After subjecting to the culture medium, the material surface showed micropores, which may be due to the release of the calcium and phosphate ions from the material. The material seeded with the L929 fibroblast cells showed opening up of the grain boundaries and recrystallization of calcium phosphate on the surface of the material after 48 h.

HABGS seeded with L929 fibroblast cells (Figure.IV.13G) showed a monolayer of cells that adhered on to the material surface after 48 h. The material surface was intact and did not show any macrocracks. Micropores observed on the material surface upon immersion in the medium showed the widening of the surface pores. Cells that spread well on the material were observed only on the smoother phase of the material, but not adjacent to the opened up pores. Few crystal deposits were observed on the smooth surface of the material.

IV.2.4 Osteoblast cells

MG 63 osteoblast cells seeded on the HA, BGS and HABGS discs showed distinct cell attachment patterns on the surface of the materials after 48 h. Osteoblast cells were seen well adhered and spread on the glass coverslip, and the cell boundaries were clearly visible (Figure1V.14 A). Osteoblast cells on HA surface (Figure.IV.14 B) had completely merged with the surface after 48 h except for a few nodule-like protrusions of 20 μm were observed, the cell boundaries were not clearly visible and the material surface is intact, without any surface cracks.

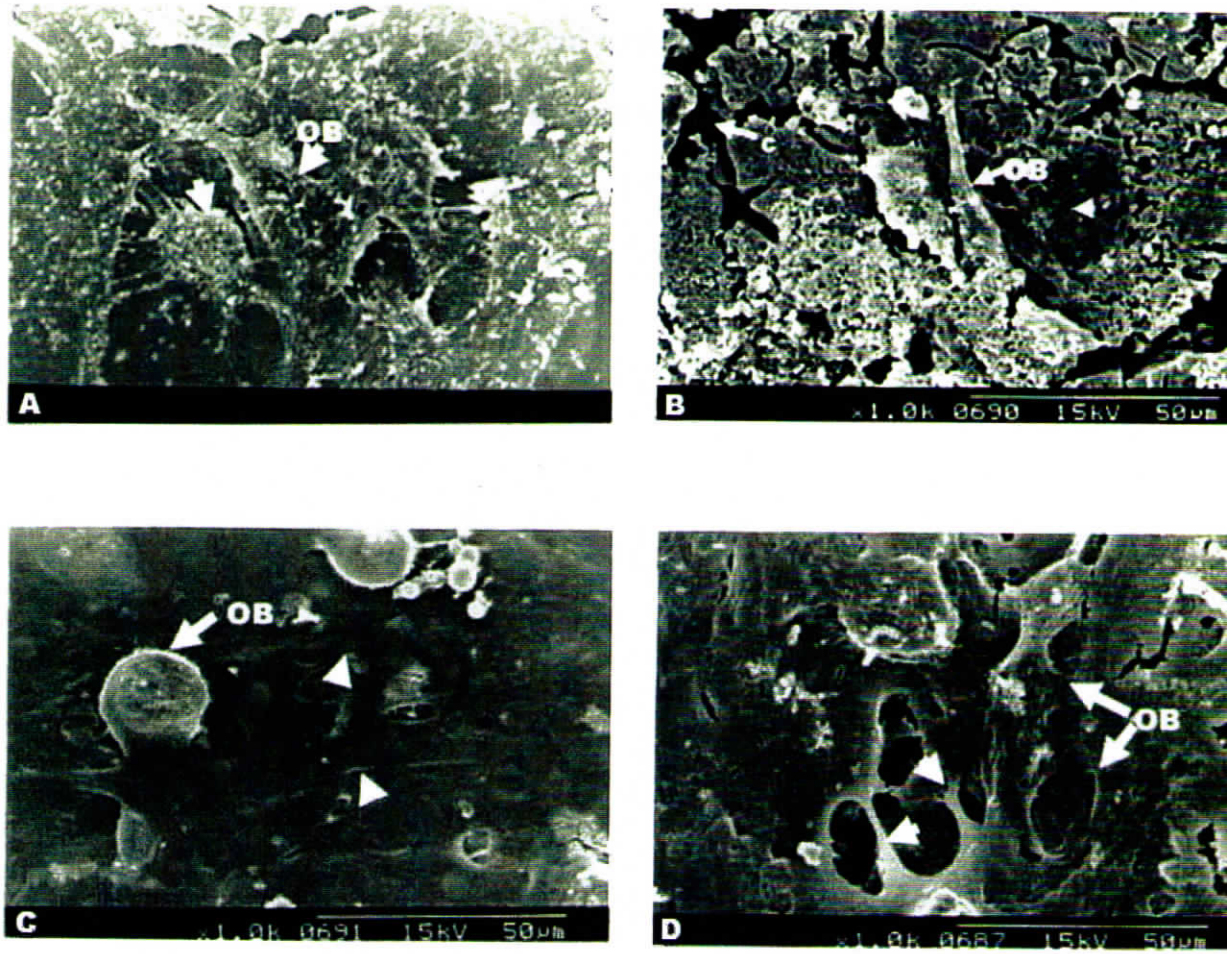

Figure -IV-14

Scanning electron micrographs of osteoblast cells(MG-63)seede on A - coverslip; B- HA; C- BGS and D- HABGS discs after 48 hou On HA and HABGS discs osteoblast cells (OB) showed good adh ion compared to cells on BGS disc . Arrow heads show the spr ding of osteoblast cells on the material surface.

Cells seeded on BGS (Figure.IV.14C) showed intense cracks of 10 – 20 μm in diameter and the surface pores had opened up and very few osteoblast cells were seen adhered to the material surface. The osteoblast cells that adhered on to the material surface showed elongated spindle morphology. Osteoblast cells seeded on the HABGS (Figure.IV.14D) material had merged with the surface completely and very few interconnecting cell processes could be seen. The material surface was intact without any macro cracks but showed surface pores of 5 to 6 μm in diameter after immersion into the medium.

IV.2.5 *In Vitro* – Cell Culture Studies: Discussion

In vitro models have proven to be valuable tools for testing and screening candidate biomaterials. The ideal material should act as a good scaffolding material and the material should degrade with time in a controlled fashion without leaving any toxic residue and must be excreted by normal physiological mechanism. Since, different types of calcium phosphate materials are required for different application such as resorbable materials for endosseous dental implants and load-bearing type for vertebral prosthesis, the physicochemical property of these materials will be highly variable. Hence, *in vitro* studies are essential to test the materials before *in vivo* application for their cytocompatibility and cytotoxicity.

In examining tissue responses to orthopaedic and dental implant materials, many *in vitro* studies of cell/substrate interactions have been done with fibroblast cells (Neupert and Vogel, 1984; Inoue *et al.,* 1987), chondrocytes (Rahn *et al.,* 1980), bone marrow cells (Verrier *et al.,* 1996), human osteoblast cells (Anselme *et al.,* 1997),macrophage (Fukuchi and Akao, 1995; Osyczka *et al.,* 1997).

Two mechanisms -cell mediated and dissolution- participate in the biodegradation and resorption of hydroxyapatite in the body, which is directly related to implant surface area. So porous HAP undergoes a significant degree of resorption. Cell-induced resorption or dissolution of the HAP ceramic crystals is frequently observed *in vitro* and *in vivo* (Daculsi et al., 1989; Orly et al., 1989). HA proved non-cytotoxic, as confirmed by the MTT assay, where 80% of L929 fibroblast cells showed good cell viability with HA extract even after 24 h. The fibroblast cells seeded on the material surface showed good adhesion and proliferation.

HA surfaces appear to be compatible with several cell types. The cells cause the dissolution of the HA ceramic crystals intra-cellularly by phagocytosis or extracellularly by producing an acid environment (Baron et al 1985, Le Geros et al., 1991, Daculsi et al 1989) which causes the partial dissolution of the HA ceramic crystals. HA allows the proliferation of fibroblasts (Orly et al., 1989) and cell do not seem to distinguish between HA and bone surfaces which indicates a significant similarity in the surface chemistry.

Cell adhesion comprises a sequence of events following cell attachment, cell spreading, organization of an actin cytoskeleton and formation of focal adhesions (Richard and Kyriacos, 2000). With cell adhesions on material surfaces the beneficial interactions with surfaces can be understood and in turn we are able to predict their behaviour to materials in an osseous site. HA mimics the extracellular matrix (ECM) by providing a structural component that will physically sustain tissue genesis. Cells adhered and proliferated on these discs and organized the ECM which conveyed mechanical and chemical stimuli, and other signals influencing cellular shape, actin cytoskeleton organization and transcription activity (Blaschke et al., 1994; Lelievre *et al.,* 1998; Chen et al., 1997) and consequently will engineer a functional tissue. This possibly may promote integration of the material with host tissue and potentially enhance tissue remodeling *in vivo.*

On the crystal level the dissolution of the ceramic HA crystals is non-site specific, i.e. dissolution is observed both on the surface and at the crystal core. In comparison, dissolution of biological apatite crystals is site specific, showing preferential dissolution of the crystal core (Le Geros and Le Geros, 1993).

The formation of carbonate-apatite crystals on HA surfaces is believed to be a dissolution-precipitation process of calcium and phosphate ions (Le Geros and Le

Geros, 1993). The role of bioactive ceramics is not a passive one but participatory, contributing to the formation of the carbonate apatite on surfaces and promoting the adhesion of matrix-producing cells and organic molecules as a result of surface chemistry and surface charges.

But for BGS, hydrated silica-gel layer forms on their surface by dissolution and polycondensation followed by precipitation of calcium and phosphate ions to form calcium phosphate (CaP) rich layer. In vitro the CaP layer is located on top of the silica gel whereas *in vivo* it is formed within the gel layer. This is ensued by crystallization into hydroxyl carbonate-apatite (Hench and Anderson, 1993, Hench,1991). The rate of formation of HCA is very rapid for BGS than HA among the present generation of bioactive materials (Hench 1994; Hench and West, 1996), which is responsible for the faster bone formation process in BGS. Reactions on material surfaces, including the formation of carbonate-apatite may be important in establishing the strong "bonding zone" at the bone-material interface unique to bioactive materials.

The material seeded with the cells showed opening up of the grain boundaries, perhaps due to the leaching of the substantial concentration of soluble silica followed by calcium and phosphate ions from the material which subsequently lead to dissolution, precipitation and crystallization of complex calcium phosphate precursor phases on the surface of the BGS disc in the cell culture medium. Another possibility is that cell induced acidification of the microenvironment may have occurred as a reaction to the presence of the calcium phosphate material (Evans *et al* 1984; Davies 1990) and the release of calcium and phosphate ions into the medium perhaps initiated the process of local degradation of the material and lead to precipitation and crystallization later.

BGS leaches rapidly at lower pH 3 to 5 and it is reported that pH of BGS surface remains high around 7.6 when in contact with the body fluids or in contact with the cells leading to less cell response on the material. So in normal body fluid at pH 7.24, the material leaches initially *in vitro* due to its bioactive nature but becomes stable once the supersaturation is attained (Matsuda *et al* 1987).

In short, the nature of the material (Klein *et al* 1990), the action of cells on the material (van der Meulen and Koerten 1994), the body fluids and pH (Matsuda *et al* 1987) influence the dissolution of the material. The pH change on the material surface contributes prominently to cell attachment and the expression of cells depended on the preparation of the glass-ceramic surface and a better cellular response *in vitro* was achieved when the glass surface was less reactive (Vrouwenvelder *et al* 1992; 1994). Hence, the process of cell spreading is influenced by the nature of the underlying substrate as reported by Maroudas (1975). All these possibilities, could be the reasons why only a small population of elongated fibroblast and osteoblast cells were seen adhered on the surface of the BGS material specifically noted more on the exposed regions of the grain boundaries of the disc. L929 fibroblast and MG 63 osteoblast-like cells spread centripetally from the granules to form a monolayer on the glass coverslip.

Reduced cell attachment on the BGS does not mean toxicity to the cells, since the MTT assay in our study did not indicate a loss of cellular viability (80% viability) with the BGS extract and the adhered cells on the BGS disc surface showed no growth retardation, confirming that the material is biocompatible. Besides, BGS granules did not show any signs of toxicity embarrassment after 24 h in contact with L929 cells and even when maintained in culture for 6 days (data not shown).

HABGS material with L929 fibroblast cells and MG 63 osteoblast-like cells showed good adhesion and spreading after 48 h. MTT assay proved that, more than 80% of cells were viable with HABGS.

The fibroblast cells were seen only on the smoother phase of the material but not in the rough surface. Hence, material surface also plays a major role in determining the cell adhesion. The rough surface may be due to the influence of the medium. Osteoblast cells after 48 h on HABGS disc were seen well spread and merged with the surface. This may be due to the smooth surface of the HABGS disc. The material surface was intact and did not change on the influence of the medium or cells even after 48 h.

The micropores seen on the material surface could be due to the influence of medium on the material. These micropores on a bioactive material may favour apatite formation. Material characteristics influence surface-related phenomenon such as cell adhesion and/or ingrowth and material degradation and these are often important parameters to monitor in biomaterial evaluation (Matlaga and Salthouse 1983; Taylor and Gibbons 1983).

Bioactivity may be related to the formation of carbonate apatite crystals *in vitro* (Hench and Andersson 1993; Hyakuna *et al* 1990) which may be related to biodegradation and in turn to solubility (LeGeros and Daculsi 1990; LeGeros *et al* 1991). This scenario mimics the *in vivo* situation of initiation of the biomineralization process by host cells for osteogenesis (Hench 1991b; 1994). So the formation of a biologically equivalent apatite on the ceramic surface, followed by adsorption and incorporation of biological molecules (Hyakuna *et al* 1989 and El-Ghannam *et al* 1999), for cell attachment, proliferation, differentiation and extracellular matrix

formation (Schepers *et al* 1993; Matsuda and Davies 1987, El-Ghannam *et al* 1995) comprise the events leading to the healing of the defect.

Studies of protein adsorption/desorption kinetics in bioactive substrates indicate that surface charge is an important variable (Lobel and Hench 1996, 1998). The rapid adsorption of calcium and phosphate ions on the silica gel layer of bioactive glasses shifts isoelectric points at physiological pH, and could implicate the process of osteoprogenitor cell differentiation and proliferation in *in vivo*.

cm^{-1}

IV.2.6 Conclusion

Based on the *in vitro* studies, bioactive ceramic granules HA, BGS and HABGS were proven non-toxic, and cytocompatible. The material cell and material medium influence will determine the cell adhesion and proliferation. L929 mouse fibroblast and MG 63 human osteoblast-like cells showed better adhesion and spreading on HA and HABGS, whereas with BGS very few cells were seen. From this observation it is understood that material property definitely influenced the adhesion of the cells. If the material is highly reactive, the time required for the cells to adhere, spread and proliferate will increase. The protein concentration in the medium would also decide on the fate of the material surface and the cell adhesion. It is hypothesized that in the cell culture medium definite protein concentration and cell seeding density has to be studied in broader aspect to understand the material - cell interaction, which may give some information with regard to the initial events of tissue-material response *in vivo*.

CHAPTERS – V

IN VIVO STUDIES

V.1 *In Vivo* – Heterotopic Implantation

V. *IN VIVO* STUDIES

V.1 *In Vivo* - Heterotopic Implantation: Results

V.1.1 Scanning Electron Microscopy

Scanning electron micrographs showed the presence of macropores and micropores on the material surface. The porosity of HA is >100 μm; BGS < 30 μm; HABGS < 30 μm and size of the granules were in the range of 300 to 350 μm (Figure.V.1A, D & G). FG coated HA granules showed a homogeneous coating of FG and the pores of the granules showed interconnecting FG matrix (Figure.V.1B & C). FG coated BGS (Figure.V.1E & F) and FG coated HABGS (Figure.V.1H & I) granules exhibited prominent interconnecting woven FG matrix on the surface and within the macropores and micropores of the granules. Cracks were observed on the surface of the coated granules.

V.1.2 Radiography

Calcium phosphate ceramics were opaque to X-rays and hence, new bone formed around the granules in the quadriceps muscle was not detected (Figure.V.2A). Hence, image analysis of the X-ray was performed to quantify the area of opaqueness with that of the FG coated granules and uncoated granules, which revealed that FG coated HA, BGS and HABGS surface area, had increased (Figure.V.2B) after implantation when compared to the uncoated granules.

V.1.3 Gross Appearance

The *in situ* position of the implant materials was maintained. There was no gross evidence of inflammation or necrosis around the implant sites and healing of the tissue was apparent.

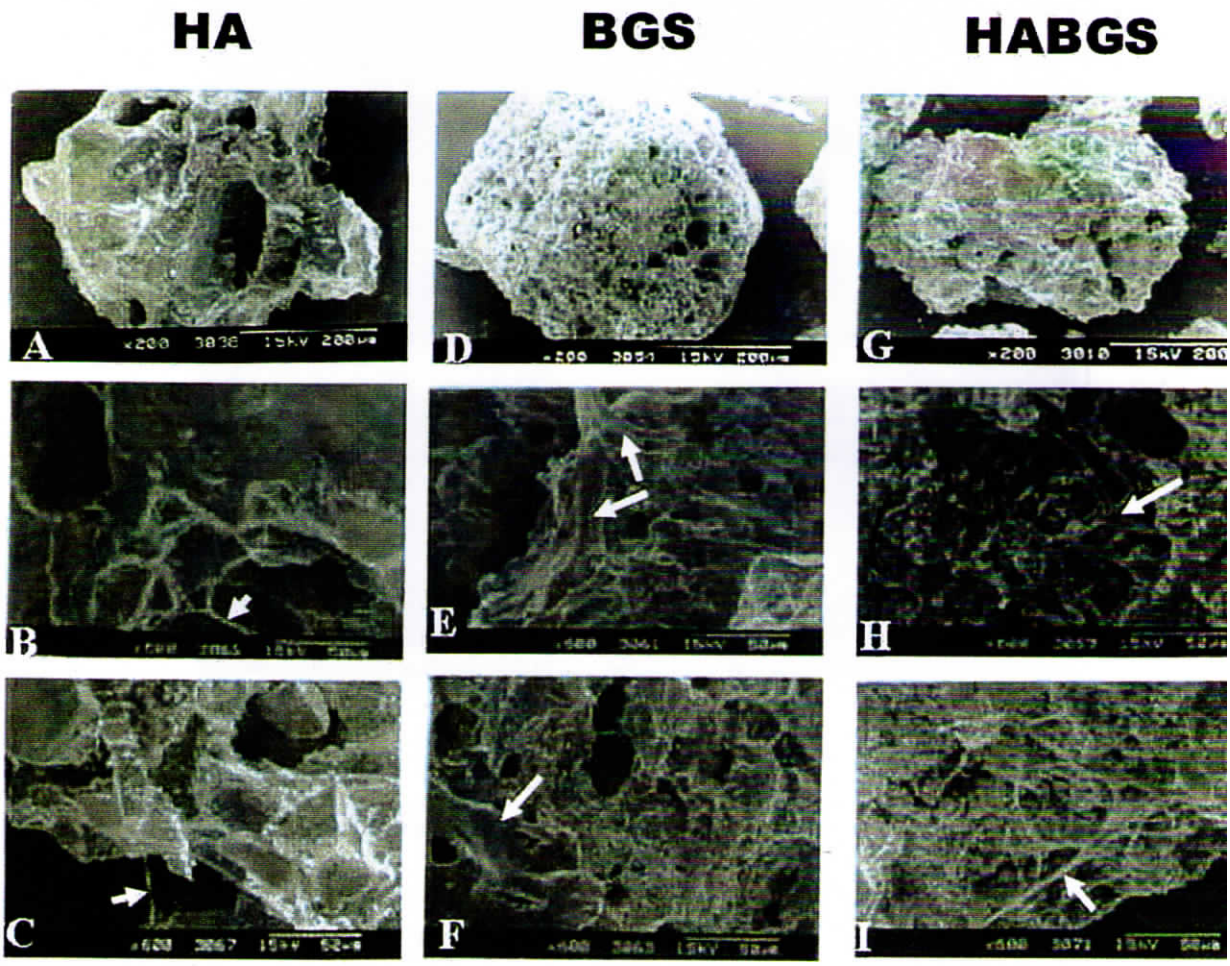

Figure - V-1

Scanning electron micrographs of bioactive ceramic granules, coated with fibrin glue (FG): A, D & G are uncoated HA, BGS and HABGS (control) ceramic granules. B, E & H are HA, BGS and HABGS coated with 2.5 mg of FG; C, F & I are HA, BGS and HABGS coated with 5 mg of FG. Arrows show the fibres of FG on the material surface after coating.

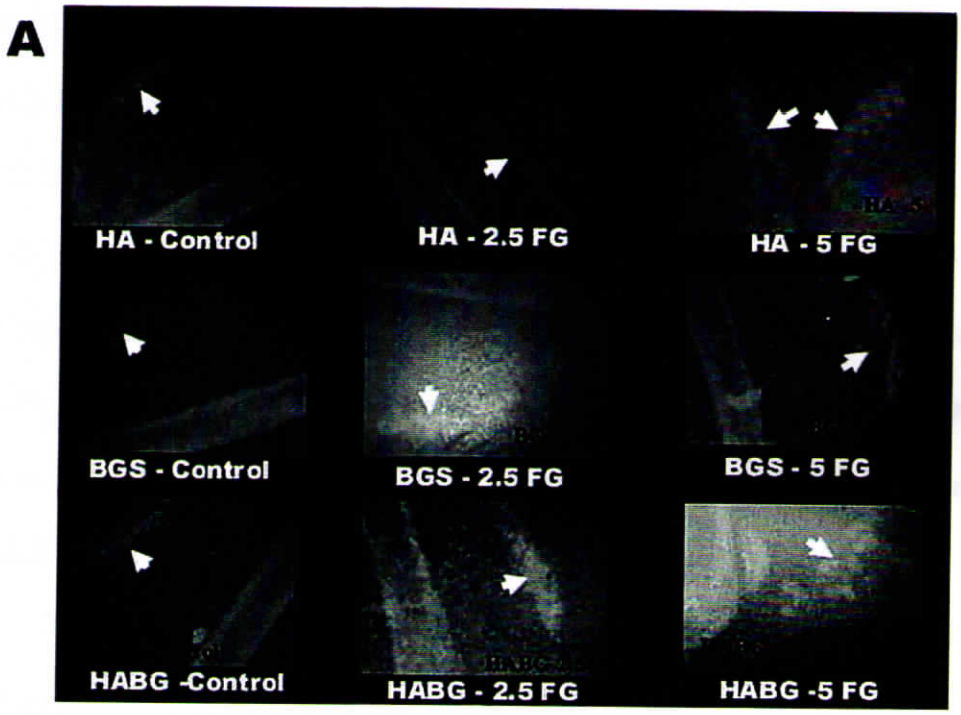

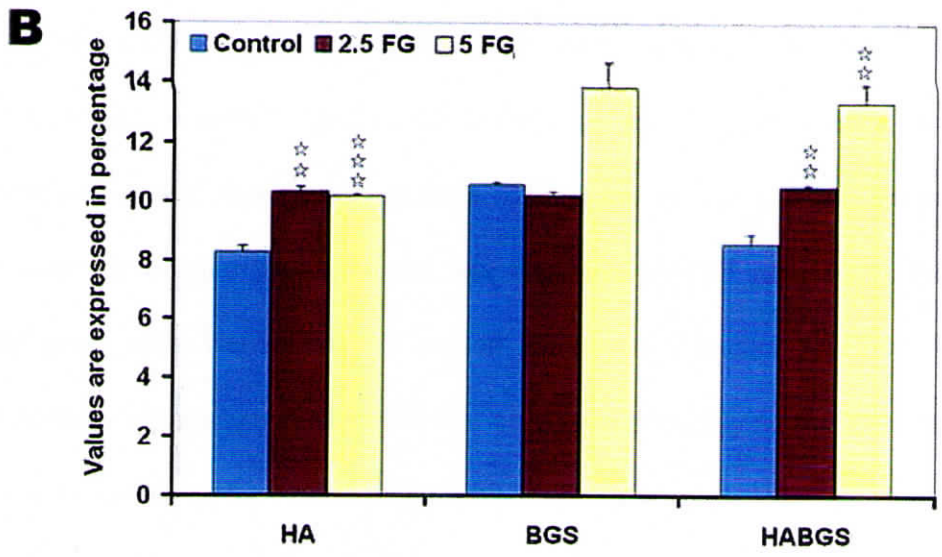

Figure -V-2

X- ray photomicrographs of ceramic granules implanted in mice quadriceps muscle after 28 days: A - HA, BGS and HAB-GS uncoated and FG coated granules, the implant area is marked by an arrow; B - Quantitative image analysis data of the X-ray photomicrograph.

V.1.4 Histological Evaluation (after 28 days)

V.1.4.1 Fluorescence Microscopy

FG coated BGS and HABGS showed active mineralizing yellow (tetracycline - Day 15) fluorescence areas and green (calcein blue - Day 24) fluorescence areas on post-implantation (Figure.V.4.C-F). However, this was not observed in FG coated HA (Figure.V.4.A & B). Fluorochrome labeled controls (HA, BGS and HABGS) (Figure.V.3.A-C) did not show any active fluorescence sites or mineralizing areas.

V.1.4.2 Light Microscopy

The geometry of the uncoated HA material (Figure.V.5A) is intact without any surface cracks (Figure.V.7B). The granules were surrounded by a thick connective tissue (Figure.V.5A, Figure.V.7A & B) around the material in some histological sections and loose connective tissue in other sections. The arrangement of the thick connective tissue was parallel to the ceramic surface, with close apposition against the ceramic granule. The pores of the ceramic granules were infiltrated by polymorphic cells and few fibroblast cells (Figure.V.7B). No foreign body giant cells were observed around the material except for few occasional monocytic macrophages. Osteoblast-like cells were seen around the material in areas where material surface are rough with small pits of > 30 μm in size. Neo-vascularization around the implant granules was observed. Cells are also seen adhered on to the surface of the ceramic granules. No osteoid deposition could be observed around the material.

Hydroxyapatite coated with 2.5 mg fibrin glue showed apparent difference in the tissue response when compared to the uncoated granules. The geometry of the granules was intact. The tissue response to the FG coated granules varied with regard to the amount of protein content coated on the granules.

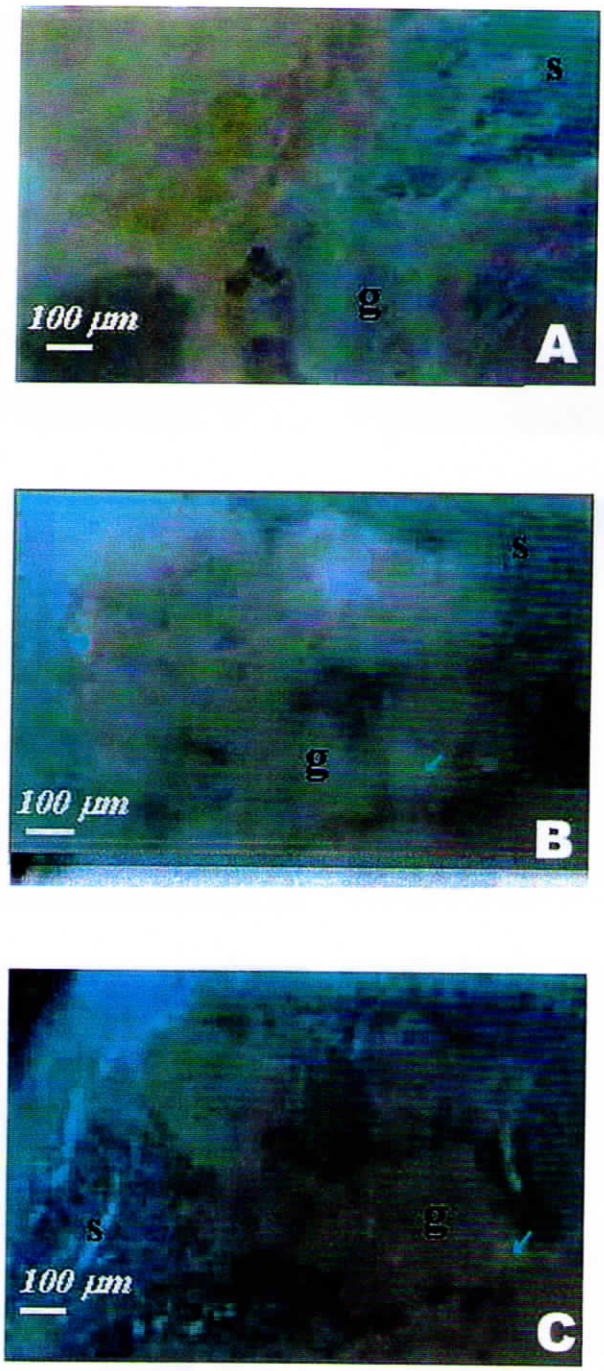

Figure-V-3

Fluorescence micrographs of uncoated bioactive ceramics implanted in mice quadriceps muscle after 28 days: A – HA; B - BGS; and C - HABGS. Mild fluorescence was observed wit BGS and HABGS (arrows), whereas no fluorescence was see with HA.

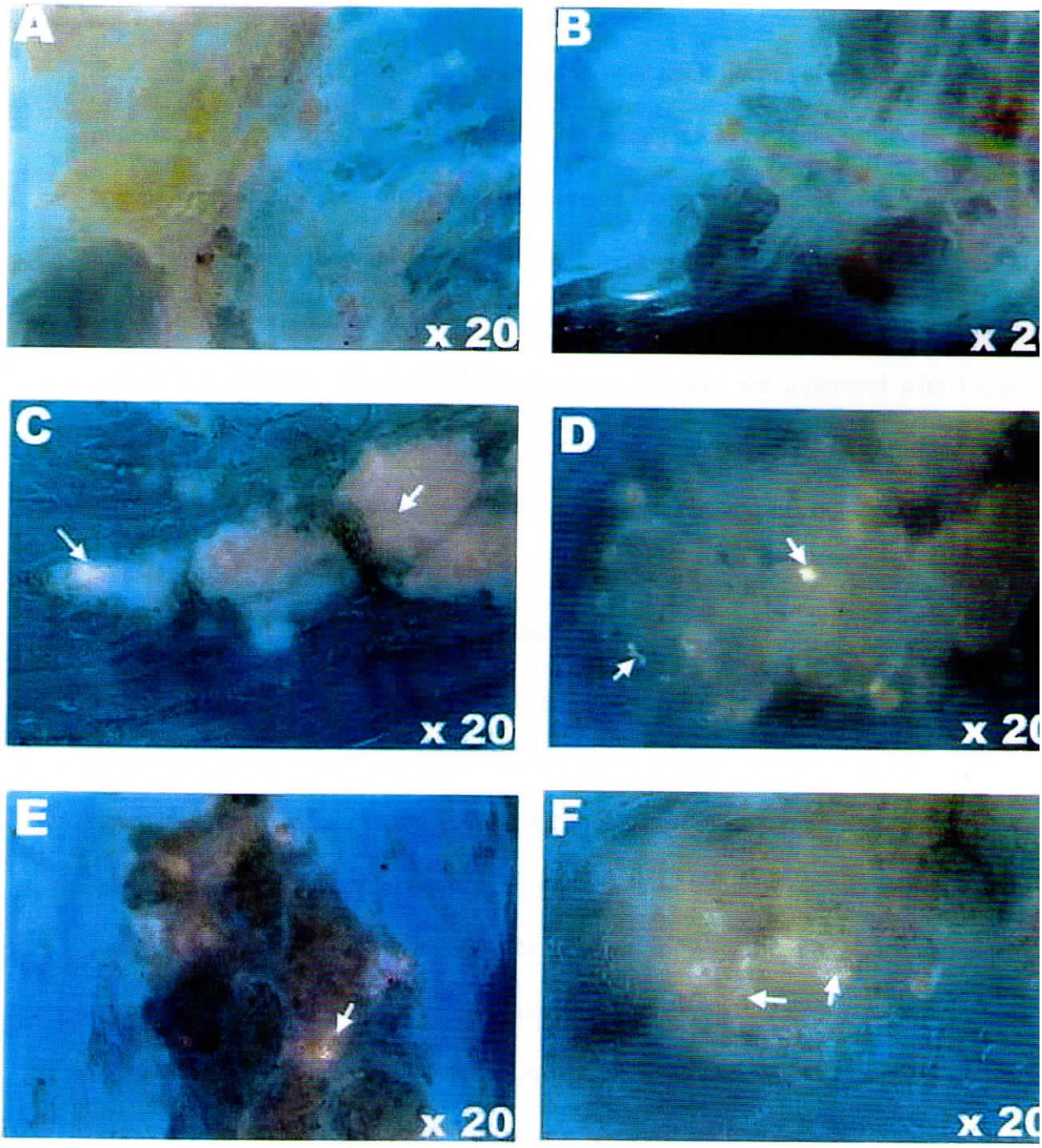

Figure -V-4

Fluorescence micrographs of bioactive ceramics coated with FG implanted in mice quadriceps muscle,after 28 days: A & B - HA coated with 2.5 mg and 5 mg FG; C & D - BGS coated with 2.5 mg and 5 mg FG; E & F - HABGS coated with 2.5 and 5 mg FG. The fluorescence areas are marked by arrows.

The 2.5 mg FG coated HA granules showed thick fibrous reaction around the material (Figure.V.5B, Figure.V.8A & B). No inflammatory reaction was observed in any of the sections. Few multinucleated foreign body giant cells were observed in close proximity to the implant surface. The arrangement of the connective tissue is parallel to the ceramic surface. Few polymorphic cells and fibroblast cells were seen around the granules. The pores of the ceramic granules are infiltrated with loose fibrous connective tissue. Neo-vascularization was observed away from the implant. No osteoblast-like cells were seen around the granules and no bone formation or mineralizing areas were observed in any of the sections.

HA coated with 5 mg FG showed better tissue response when compared to 2.5 mg FG. No thick fibrous capsules were seen around the granules, only loose connective tissue was seen parallel to the ceramic surface without apposition to the granules (Figure.V.5 C, Figure.V.6 A). A 20 μm gap was observed between the loose connective tissue and the granules. The gap was lined by mesenchymal cells and few osteoblast-like cells (Figure.V.5 C). No foreign body giant cells or inflammatory reaction were observed in any of the sections. Few fibroblast cells were observed in close proximity to the rough surface of the granules and within the pores of the ceramic granules. Neo-vascularization was observed adjacent to the implants and away from the implants (Figure.V.6A, Figure.V.8D). No osteoid deposition was observed.

The uncoated BGS granules had completely disintegrated (Figure.V.5D, Figure.V.7C & D) and did not show any well-defined woven bone. But, osteoid depositions (Figure.V.5D) were visible at the periphery of the implant.

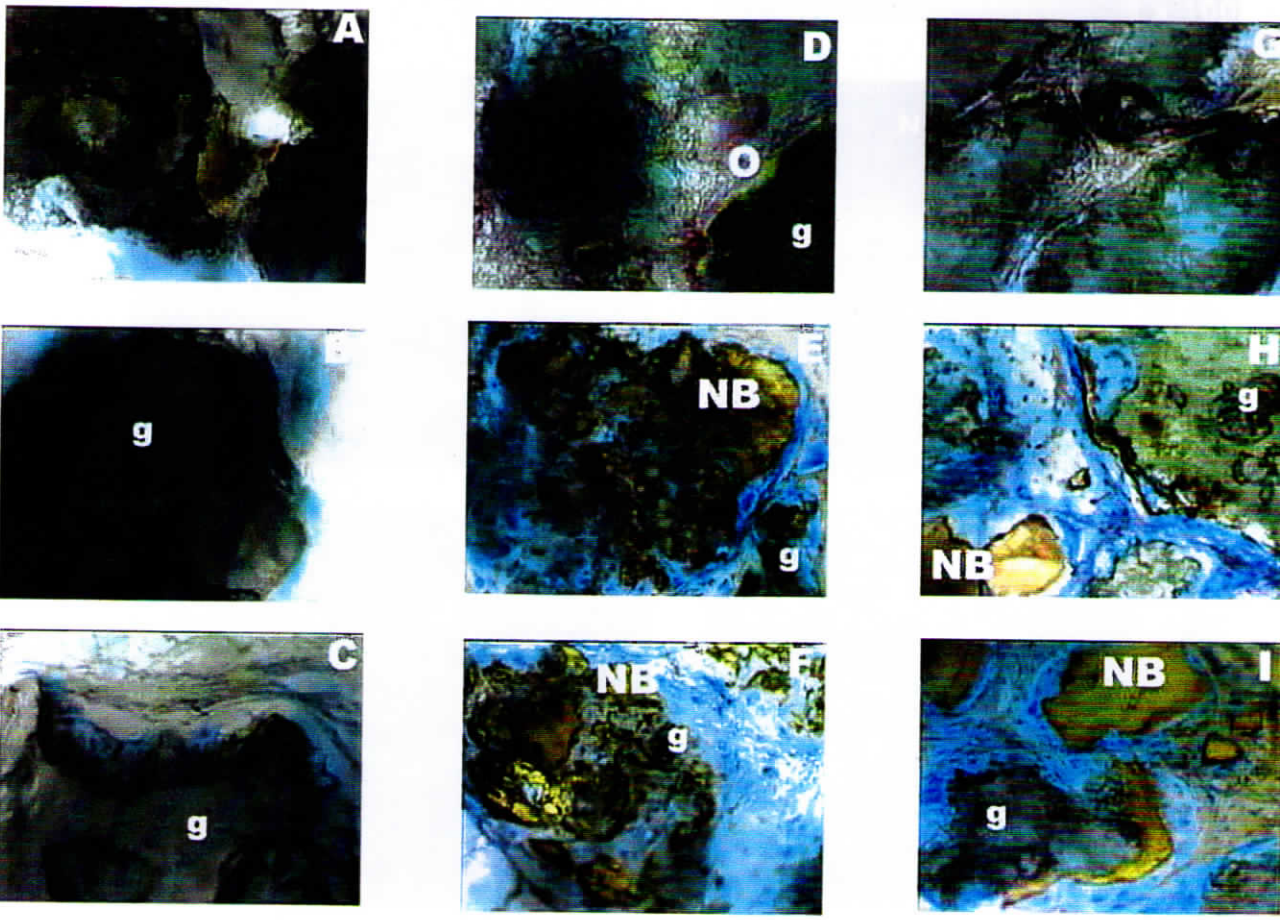

Figure -V-5

Light micrographs of FG and uncoated bioactive ceramic granules, after 28 days. A- HA uncoated, B- HA coated with 2.5mg FG, C- HA coated with 5mg FG, D - BGS uncoated, E - BGS coated with 2.5 mg FG, F - BGS coated with 5mg FG, G - HABGS uncoated, H - HABGS coated with 2.5 mg FG and I - HABGS coated with 5mg FG. Granules (g); osteoid (O); new bone (NB) & soft tissue (s). Arrows denote cracks on the material surface.

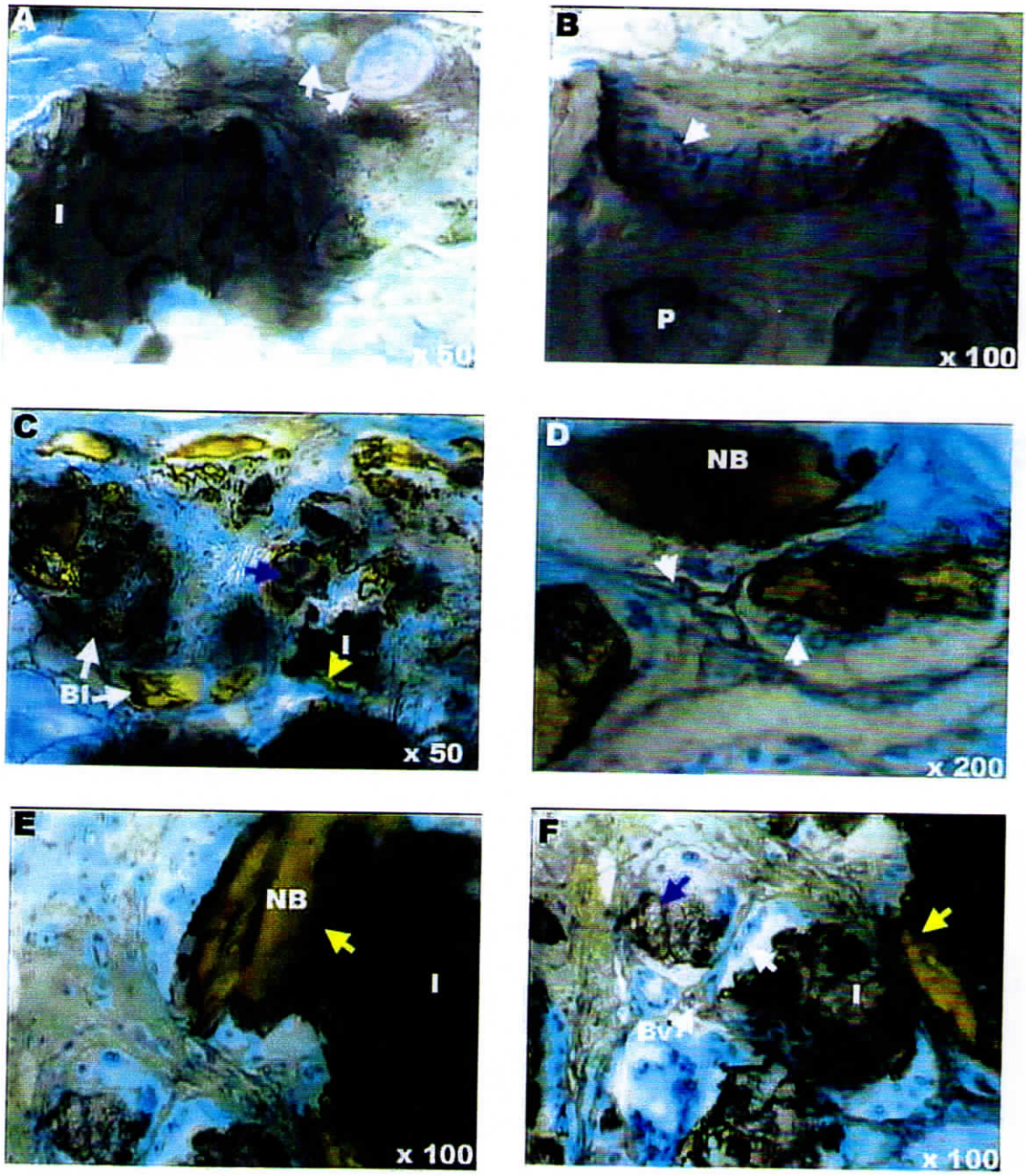

Figure -V-6

Photomicrographs of FG coated ceramic granules showing the tissue architecture after implantation in mice quadriceps muscle after 28 days. A & B - HA coated with FG, the implant (I) is surrounded by thin connective tissue, the tissue material interface and the pore (P) is infiltrated with mesenchymal cells (white arrow); C & D - BGS coated with FG; E & F - HABGS granules coated with FG. New blood vessels (Bv), were observed in the vicinity of the implants. Degraded implants are shown in blue arrow and new bone (NB) is seen closely apposed with the implant (Yellow arrow).

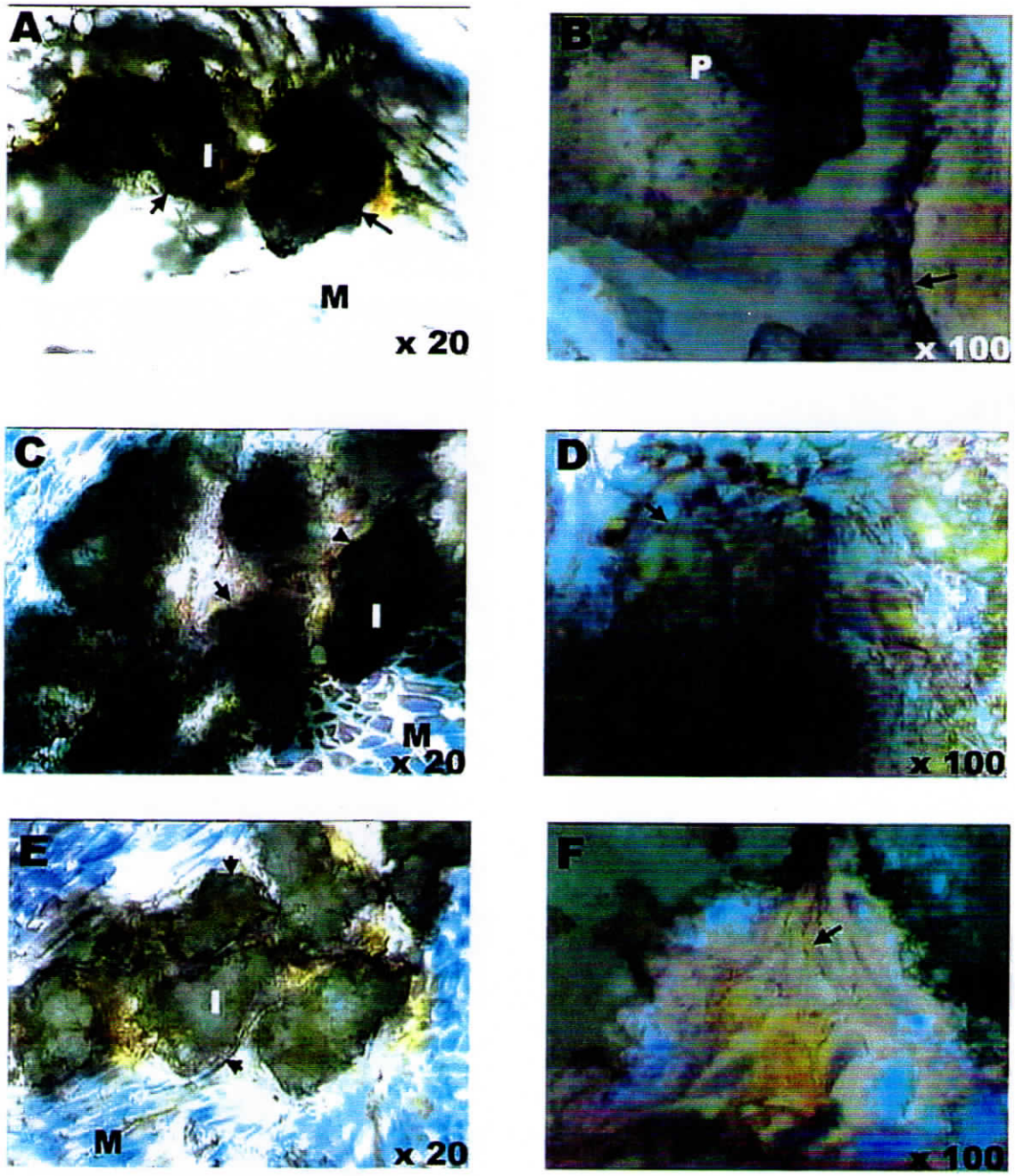

Figure -V-7

Photomicrographs of HA, BGS and HABGS uncoated granules implanted in mice quadriceps muscle after 28 days. A & B - HA implant (I) well apposed (arrow) to the muscle tissue (M), with infiltration of cells within the pores (P); C & D - BGS, disintegrated small particles of BGS granules are apposed to the muscle tissue, D- show mesenchymal cells and few yellow mineralizing zones; E & F - HABGS granules with a thin connnective tissue, mineralizing zones were not observed.

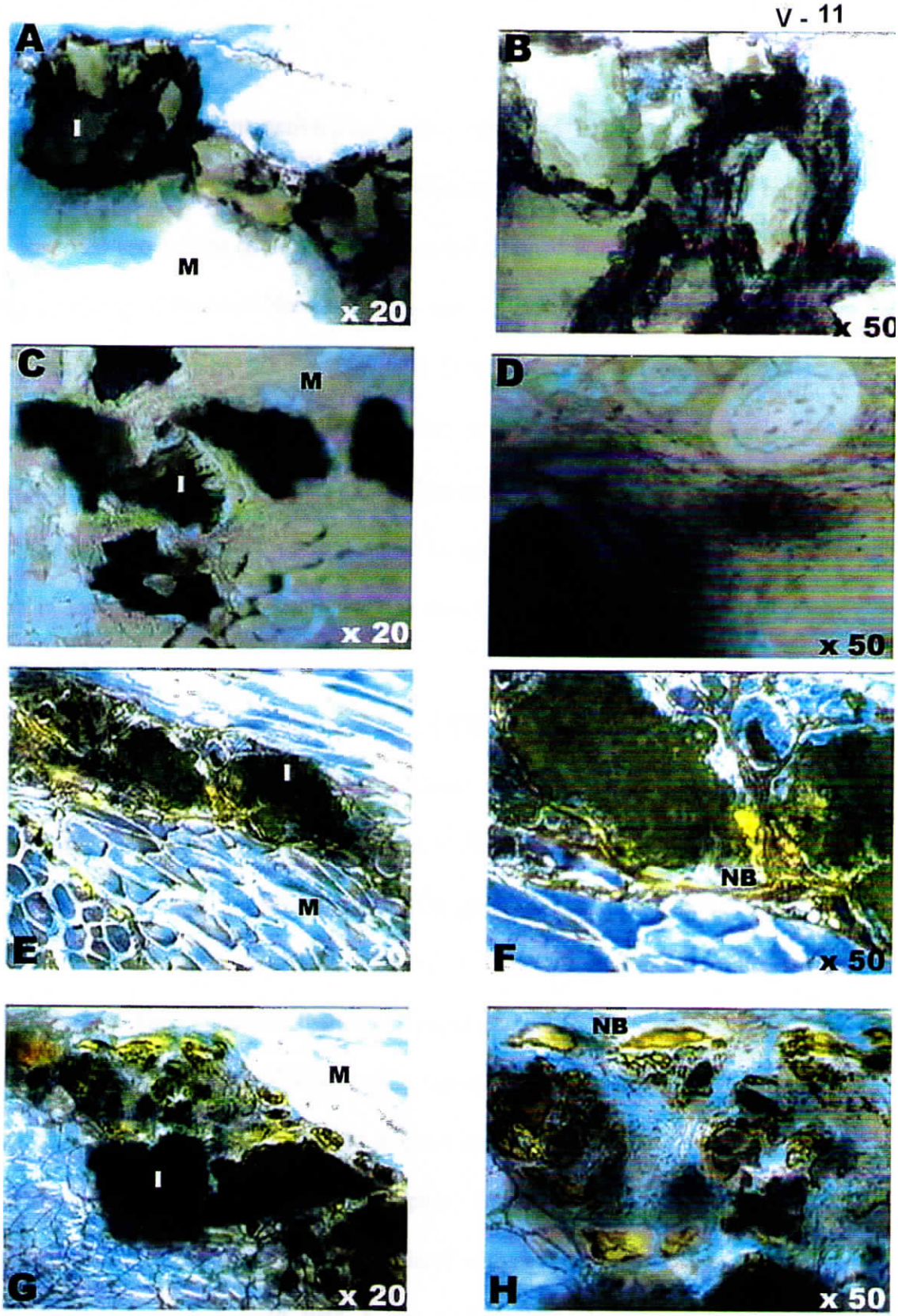

Figure -V-8

Photomicrographs of HA (A-D) & BGS (E-H) coated with FG implanted in mic quadriceps muscle after 28 days.A & B - HA coated with 2.5 mg FG and C & HA coated with 5 mg FG; E & F - BGS coated with 2.5 mg FG and G & H - BG coated with 5 mg FG. No adverse inflammation or fibrous tissue encapsulat was observed around these materials.
(I- Implant, NB - New bone, M - Muscle)

Implants underwent active degradation exhibiting large cracks, which were infiltrated by few fibroblast cells and osteoblast-like cells. No inflammatory reaction was observed around the granules. Neo-vascularization was observed in the vicinity of the implants. Osteoblast-like cells were seen in close proximity with the newly formed blood vessels. A 20 μm thick gel layer was observed around few BGS granules. Polymorphic cells around the implant could be seen with few foreign body giant cells and monocytic macrophages. Mesenchymal cells were seen lining the ceramic granules in close apposition as well as inside the cracks. A loose connective tissue is seen parallel in apposition to the ceramic granules, no fibrous tissue was observed in any of the sections observed.

Bone formation was observed with BGS coated with 2.5 mg of FG. The newly formed bone is an immature woven bone with osteoblast-like cells lining the implant and the newly formed bone (Figure.V.5E, Figure.V.8E & F). Mesenchymal cells were seen within the disintegrated BGS granules and on the periphery of the granules. The degradation of the granules is from the periphery to the center (Figure.V.8F). The connective tissue is arranged parallel to the implant surface. Few foreign body giant cells were seen around the implant where the degradation of the material is high. New bone is formed in close apposition with the granules and also seen as '*bone-islands*' adjacent to the implant. Bone is not formed throughout the granule but is seen randomly, always associated with new blood vessels around them.

BGS granules coated with 5 mg of FG showed pronounced new bone formation around the material and in close apposition to the material (Figure.V.5 F, Figure.V.8 G & H). The granules had undergone active degradation and were completely disintegrated into bits, infiltrated by mesenchymal cells, macrophages and foreign body giant cells (Figure.V.6 C). A thick loose connective tissue has

encapsulated the granules at 2 - 3 cell distance. The gap between the connective tissue and the granules is filled with loose matrix with degraded granules and cells. The bone is seen in close apposition with the granules and as *bone islands* (Figure.V.6 C & D) as observed with 2.5 mg FG. Neo-vascularization (Figure.V.6 D) is observed adjacent to the implant and also near the *bone islands*. Osteoblast-like cells were seen lining the newly formed bone (Figure.V.6 D).

The uncoated HABGS granules were intact in the middle without any cracks and the degradation of the granules was observed only on the periphery (Figure.V.5G). The granules were seen in close proximity to one another with loose connective tissue infiltrating the cracks on the periphery (Figure.V.7E & F). The connective tissue is seen in close apposition to the blunt phase of the ceramic granules. Degranulated areas were seen on the periphery of some granules indicating active degradation but no osteoclast-like/foreign body giant cells were seen in close proximity around these areas. No inflammatory cells were seen around the implanted granules. Few monocytic macrophages were observed around the granules, with fibroblast cells. Osteoblast-like cells were not observed. Neo-vascularization was observed away from the ceramic granules but not in close proximity to the ceramic granules. Mineralizing areas were observed at the close proximity of the implant without any well developed bone (Figure.V.7 F).

The HABGS granules coated with 2.5 mg FG showed cracks on the periphery. Thin loose connective tissue was seen encapsulating and infiltrating into the cracked surface of the granules (Figure.V.5H). The granules were not seen apposed with the loose connective tissues. There were 10 - 25 μm gap between the ceramic granules and loose thick connective tissue capsule. This gap is occupied by mesenchymal cells, osteoblast-like cells and few macrophages.

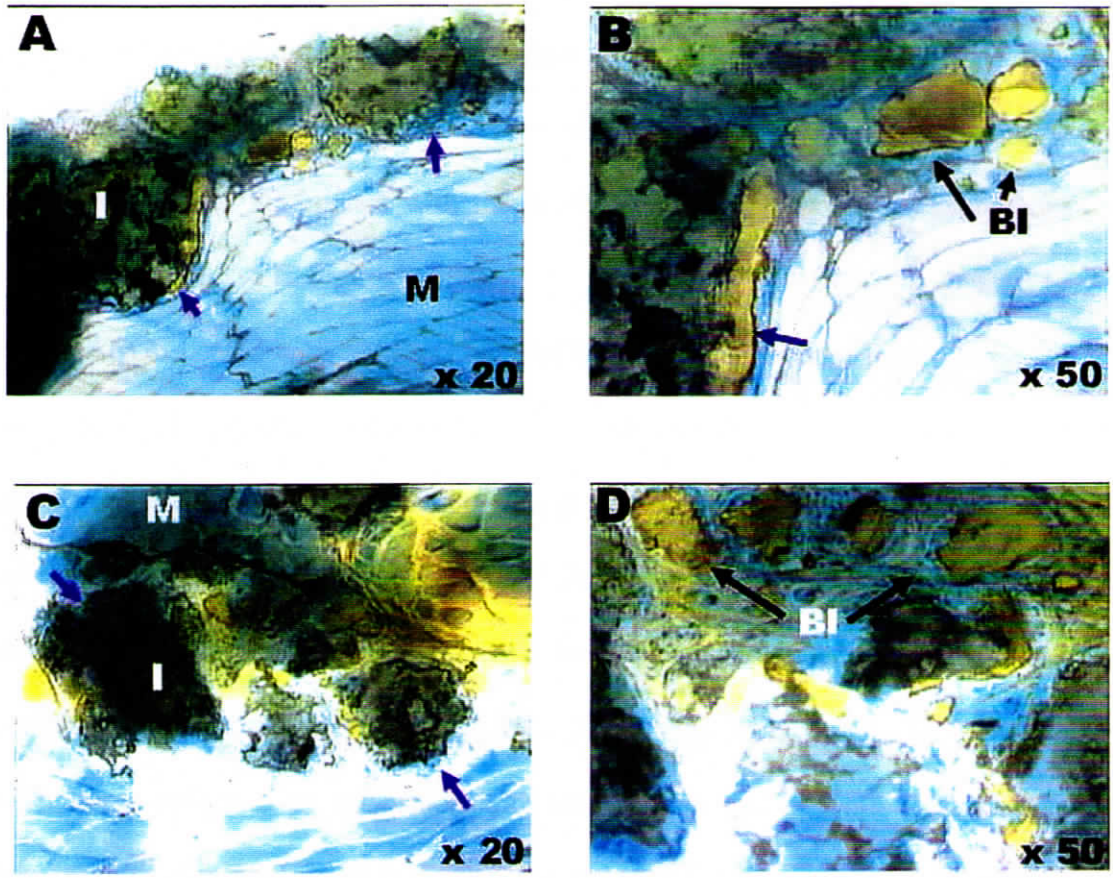

Figure -V-9

Photomicrographs of HABGS coated with FG implanted in mice quadricepsmuscle after 28 days. A & B - HABGS coated with 2.5 mg FG ; C & D - HABGS coated with 5 mg FG, seen closely apposed with the muscle (M) tissue (blue arrows) and the black arrows denotes the bone apposed to the implant (I) and bone islands (BI).

Bone is seen formed in close apposition with the ceramic granules and also as '*bone islands*' (Figure.V.9A & B). The newly formed bone was immature woven bone. No osteocytes were observed within the mineralized matrix. Only osteoblast-like cells and few fibroblast cells were seen lining the newly formed bone. No inflammatory reactions were observed in any of the sections. Neo-vascularization is observed adjacent to the implant with the newly formed bone as well as away from the implant (Figure.V.6 E, Figure.V.9 B).

HABGS coated with 5 mg FG showed better tissue response than 2.5 mg FG coated HABGS granules. The material has degraded and loose thin fibrous connective tissue is seen encapsulating the granules, and the newly formed '*bone islands*' (Figure.V.5I, Figure.V.9C & D). Within and surrounding the capsule, mesenchymal cells, osteoblast-like cells and few macrophages were observed. Neo-osteogenesis was observed with 5 mg FG. The newly formed bone is immature woven bone, seen in close apposition with the granules and as '*bone islands*'. The 'bone *islands*' were seen more in number when compared to the bone in apposition with the granules. Blood capillaries were seen around the implant and the bone islands (Figure.V.6 F).

V.1.5 QUANTITATIVE IMAGE ANALYSIS

V.1.5.1 Radiography

Image analysis of the implant zone revealed a significant difference between the uncoated ceramic granules and the FG coated ceramic granules (Figure.V.2B). The opaqueness of the implanted site was quantified with respect to the total area of the X-ray exposed. HA coated with 2.5 mg FG showed significant difference of $P < 0.01$ and 5 mg FG coated HA showed $P < 0.001$ when compared to the uncoated HA granules. BGS coated with 2.5 mg FG showed significant difference of $P < 0.10$

and 5 mg FG showed $P < 0.02$ when compared to the uncoated BGS granules. HABGS granules coated with FG also showed significant difference with 2.5 mg FG $P < 0.01$ and with 5 mg FG coated HABGS $P < 0.01$ to that of uncoated HABGS granules (TableV.1).

Table V.1

Material	Control (%)	2.5 FG (%)	5 FG (%)
HA	8.26 ± 0.20	10.3 ± 0.17	10.16 ± 0.08
BGS	10.56 ± 0.08	10.2 ± 0.11	13.83 ± 0.80
HABGS	8.56 ± 0.33	10.46 ± 0.08	13.33 ± 0.63

V.1.5.2 Stained Sections

Image analysis of the uncoated HA, BGS and HABGS granules and fibrin glue (FG) coated granules were carried out to quantify the percentage of new bone formed after 28 days post-implantation in the mice quadriceps muscle.

Quantitative image analysis of HA implanted in mice quadriceps muscle with and without FG after 28 days (Figure.V.10 A), revealed that the percent area of implant zone in uncoated HA was 32.92 ± 9.25, however some fibrous area of 9.09 ± 1.28 was observed around the implant. The implant zone with 2.5 mg FG coated HA was 40.33 ± 6.08 and with 5 mg FG coated HA 35.20 ± 6.19. No mineralizing areas were detected with HA uncoated and FG coated HA granules. The fibrous tissue was not detected with FG coated ceramic granules. Statistically no significant change was observed between the implant zone (IZ) and the soft tissue (ST) of HA uncoated and FG coated HA granules (Table.V.2)

Table V.2

Material	IZ (%)	ST (%)	MZ (%)	FZ (%)
HA-Control	32.92 ± 9.25	63.65 ± 8.38	0	9.09 ± 1.28
HA-2.5 FG	40.33 ± 6.08	59.67 ± 6.08	0	0
HA-5 FG	35.20 ± 6.19	63.73 ± 5.60	0	0

The percent area of the implant zone with uncoated BGS granules (Figure.V.10 B) was 49.82 ± 4.70 and the implant zone was comparatively less with 2.5 mg FG coated BGS granules 35.43 ± 3.14 and 5 mg FG coated BGS granules 39.72 ± 5.33. Statistically no significant change was observed between the implant zone (IZ) and the soft tissue zone (ST) of FG coated and uncoated BGS granules. Whereas, BGS coated with 2.5 mg FG and 5 mg FG mineralizing zone (MZ) showed statistically significant change compared to the uncoated BGS granules. The percent area of the mineralizing zone (MZ) with 2.5 mg FG coated BGS granules was $P < 0.10$ and with 5 mg FG coated BGS granules the significance was $P < 0.05$. No fibrous tissue (FZ) was detected with the uncoated BGS and FG coated BGS granules (Table.V.3).

Table V.3

Material	IZ (%)	ST (%)	MZ (%)	FZ (%)
BGS-Control	49.82 ± 4.70	46.21 ± 5.81	1.25 ± 0.44	0
BGS-2.5 FG	35.43 ± 3.14	57.11 ± 4.72	7.45 ± 2.37	0
BGS-5 FG	39.72 ± 5.33	46.84 ± 4.91	9.83 ± 1.94	0

FG coated HABGS granules after implantation showed a marked reduction in the percent area of the implant zone (IZ) when compared to the uncoated HABGS granules (Figure.V.10. C). The implant zone for uncoated HABGS granules was 55.48 ± 11.6, without any mineralizing zones and with 2.5 mg FG coated HABGS

granules the implant zone was 38.80 ± 4.62 and the mineralizing zone was 10.29 ± 2.87. HABGS coated with 5 mg FG had an implant area of 33.41 ± 6.23 with a mineralizing zone of 18.57 ± 5.80. The percent area of mineralizing zone was more in HABGS coated with 5 mg FG than 2.5 mg FG coated granules..Fibrous zone for uncoated HABGS granules was 8.74 ± 1.46, 2.5 mg FG coated granules also showed fibrous zone of 11.9 ± 1.22 and no fibrous zones were observed with 5 mg FG coated HABGS granules. No statistically significant change was observed for the percentage of new bone formed between 2.5 mg and 5 mg FG coated HABGS granules (Table.V.4).

Table V.4

Material	IZ (%)	ST (%)	MZ (%)	FZ (%)
HABGS-Control	55.48 ± 11.6	37.60 ±13.49	0	8.74 ± 1.46
HABGS-2.5 FG	38.80 ± 4.62	38.36 ± 5.07*	10.29 ± 2.87	11.9 ±1.22
HABGS-5 FG	33.41 ± 6.23	55.45 ± 5.80	18.57 ±8.50	0

V.1.5.3 Fluorescence Sections

Quantitative image analysis of the fluorescence sections was performed to analyze the percentage of mineralizing zone after tetracycline administration at Day 15 (Figure.V.11). HA uncoated and FG coated samples did not show any mineralizing zone. BGS uncoated showed a mere 0.922 ± 0.276 percent area of mineralizing zone. Whereas, 2.5 mg FG coated BGS granules showed 5.808 ± 0.35 and 5 mg FG coated BGS granules showed 4.629 ± 0.645 percent of mineralizing zone. HABGS uncoated granules showed mineralizing area of 2.746 ± 0.302 and 2.5 mg FG coated HABGS showed 2.545 ± 0.49 and 5 mg FG coated HABGS granules showed mineralizing areas of 7.275 ± 1.695 percent (Table.V.5).

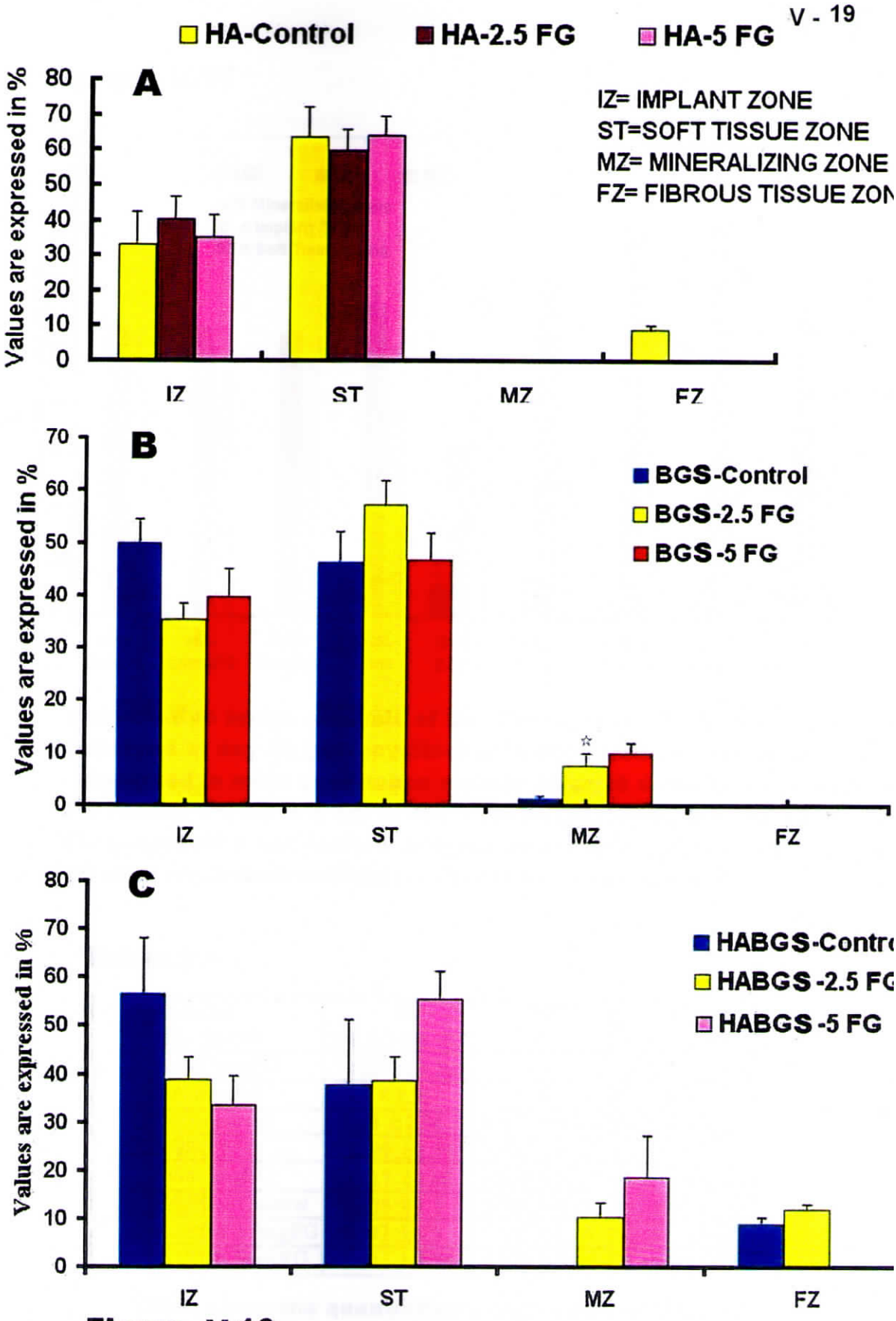

Figure -V-10

Image analysis of bioactive ceramic granules implanted in mice quadriceps muscle with and without FG after 28 days : A - HA; B - BGS and C - HABGS granules. Control (uncoated FG) is compared with 2.5 mg FG and 5 mg FG coated granules for the percentage of bone formed. Note : * = $p < 0.05$

Figure -V-11

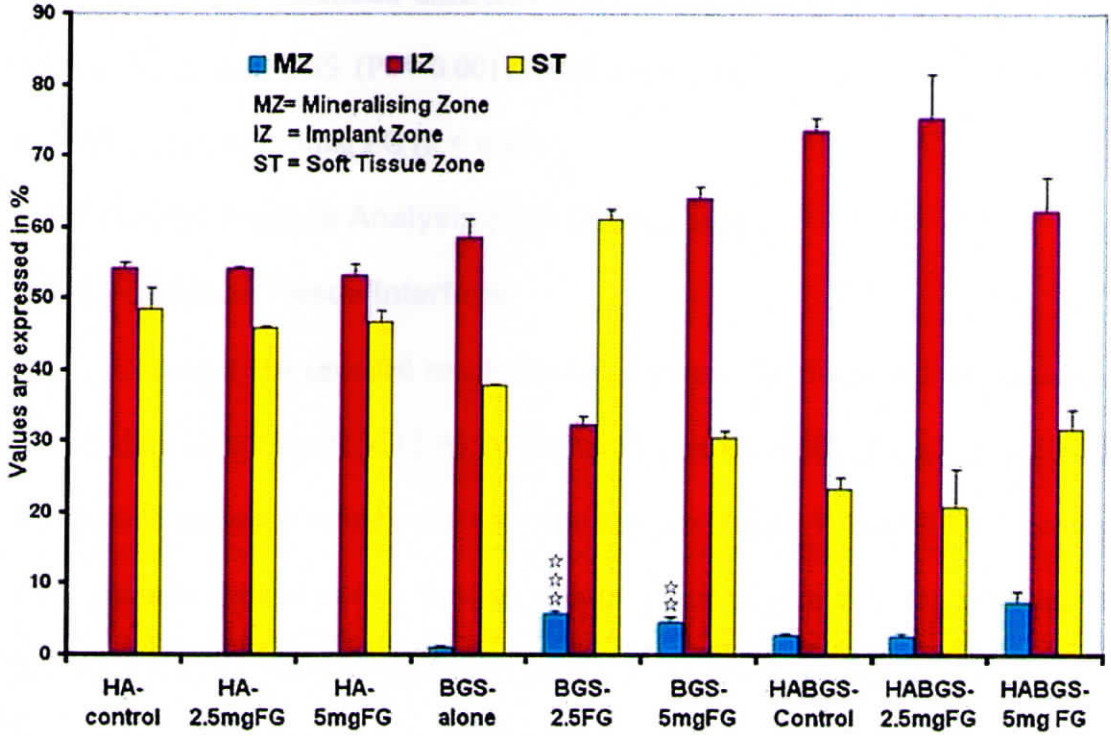

Quantitative image analysis of the percentage of mineralizing zones observed at day 15 (tetracycline) with uncoated and FG coated HA implanted in mice quadriceps muscle after 28 days. Uncoated HA an FG coated HA did not show any mineralizing areas but, uncoated and FG coated BGS and HABGS showed active mineralizing zones at day 15 after implantation. Note : = p < 0.01; *** = p < 0.001**

Table.V.5

Material	IZ	MZ	ST
HA-control	54.157 ±0.793	0	48.364 ±3.135
HA-2.5mgFG	54.186 ±0.264	0	45.813 ±0.264
HA-5mgFG	53.3 ±1.55	0	46.693 ±1.55
BGS-control	58.63 ±2.54	0.922 ±0.276	37.739 ±0.193
BGS-2.5FG	32.199 ±1.29	5.808 ±0.35	61.087 ±1.39
BGS-5mgFG	64.017 ±1.68	4.629 ±0.645	30.491 ±0.944
HABGS-Control	73.605 ±1.7	2.746 ±0.302	23.422 ±1.522
HABGS 2.5mgFG	75.291 ±6.3	2.545 ±0.49	20.692 ±5.44
HABGS 5mg FG	62.394 ±4.74	7.275 ±1.695	31.636 ±2.72

Table show the quantiative image analysis data of the stained sections of HA, BGS and HABGS uncoated and FG coated granules implanted in mice quadriceps muscle after 28 days.

Statistically significant difference in the mineralizing zone was observed with 2.5 mg FG coated BGS ($P < 0.001$), BGS coated with 5 mg FG ($P < 0.01$) and HABGS coated with 5 mg FG ($P < 0.10$).

V.1.6 Optical Surface Analysis (3 D- Luminance)

V.1.6.1 Material-Tissue Interface

Uncoated HA revealed rough interface between the tissue and the implant in the bonding zone (Figure.V.12 A). Whereas, HA coated with 2.5 mg FG and 5 mg FG showed smooth bonding surface without any gap (Figure.V.12 B & C). Uncoated BGS granules showed normal bonding with the tissue (Figure.V.12 D), whereas, the 2.5 mg and 5 mg FG coated granules showed large gap at the interface of the tissue and the implant (Figure.V.12 E & F), with HABGS coated and uncoated granules the bonding of soft tissue to the ceramic granules appeared to be normal (Figure.V.12 GI).

V.1.6.2 Bone-Tissue-Implant Interface

BGS uncoated granules were seen in close apposition with the newly formed osteoid, where a step-like appearance could be noticed (Figure.V.13 A). The FG coated (2.5 and 5 mg) BGS granules showed smooth bone apposition to the granules (Figure.V.13 B & C). HABGS control granules did not show any mineralized zones and hence the surface analysis was performed only for FG coated HABGS granules. The FG coated HABGS granules showed stable smooth interface (Figure.V.13 D), where the bone is seen in close apposition with the granules. But a gap was observed between the newly formed bone and the soft tissue (Figure.V.14 A).

V.1.6.3 Bone-Island Surface

The bone island is isolated from the soft tissue without any direct surface apposition (Figure.V.14 B).

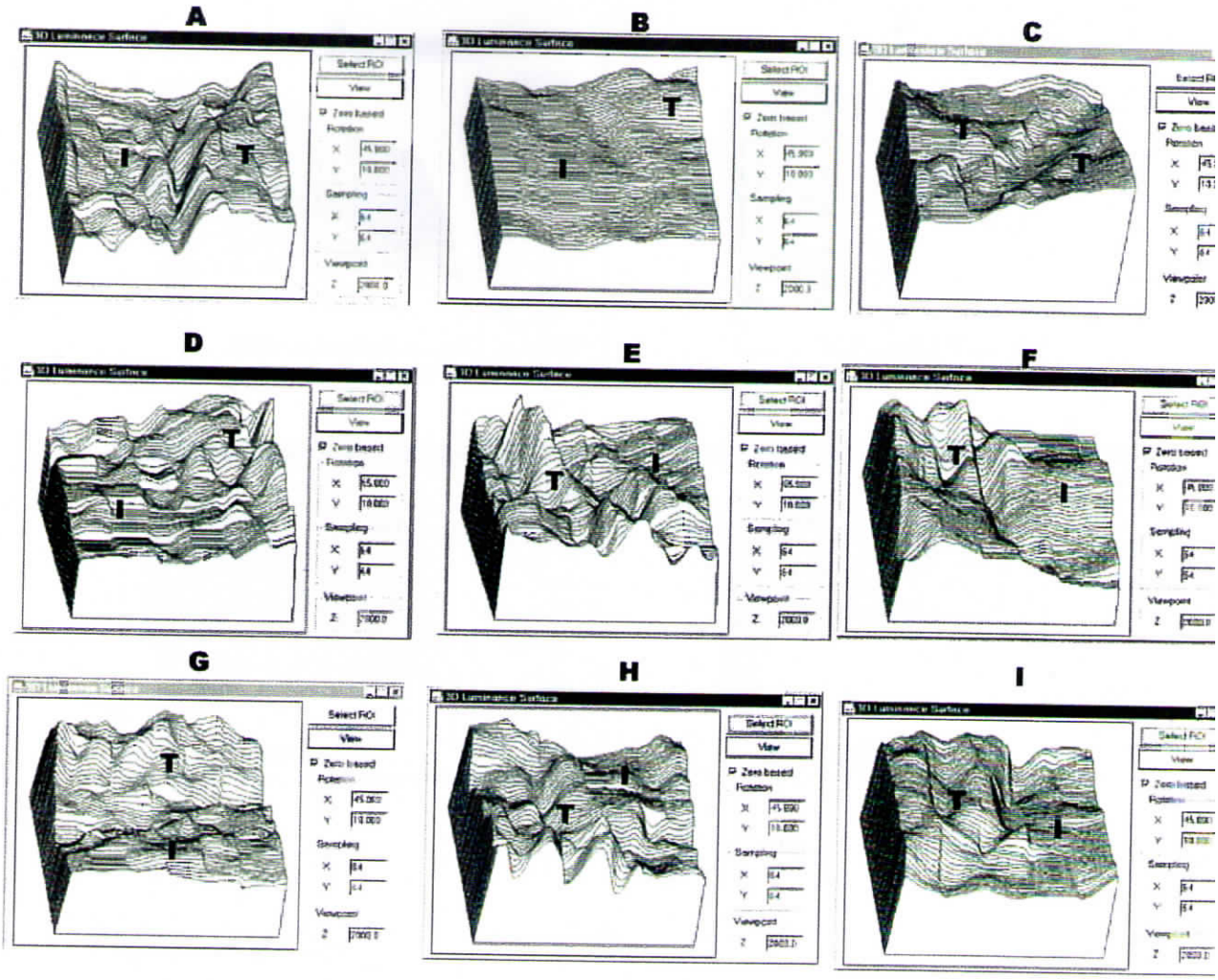

Figure - V-12

3- D surface luminance (Optimas Image Analysis Software) of the material tissue interface after implantation in mice quadriceps muscle, post-implantation - 28 days. A - HA uncoated; B - 2.5 mg FG coated & C - 5 mg FG coated HA; D, E & F - BGS uncoated and 2.5 and 5 mg FG coated surface; G, H & I - HABGS uncoated and 2.5 and 5 mg FG coated surface. The interface of the tissue (T) & the bioactive ceramic implant (I) is shown.

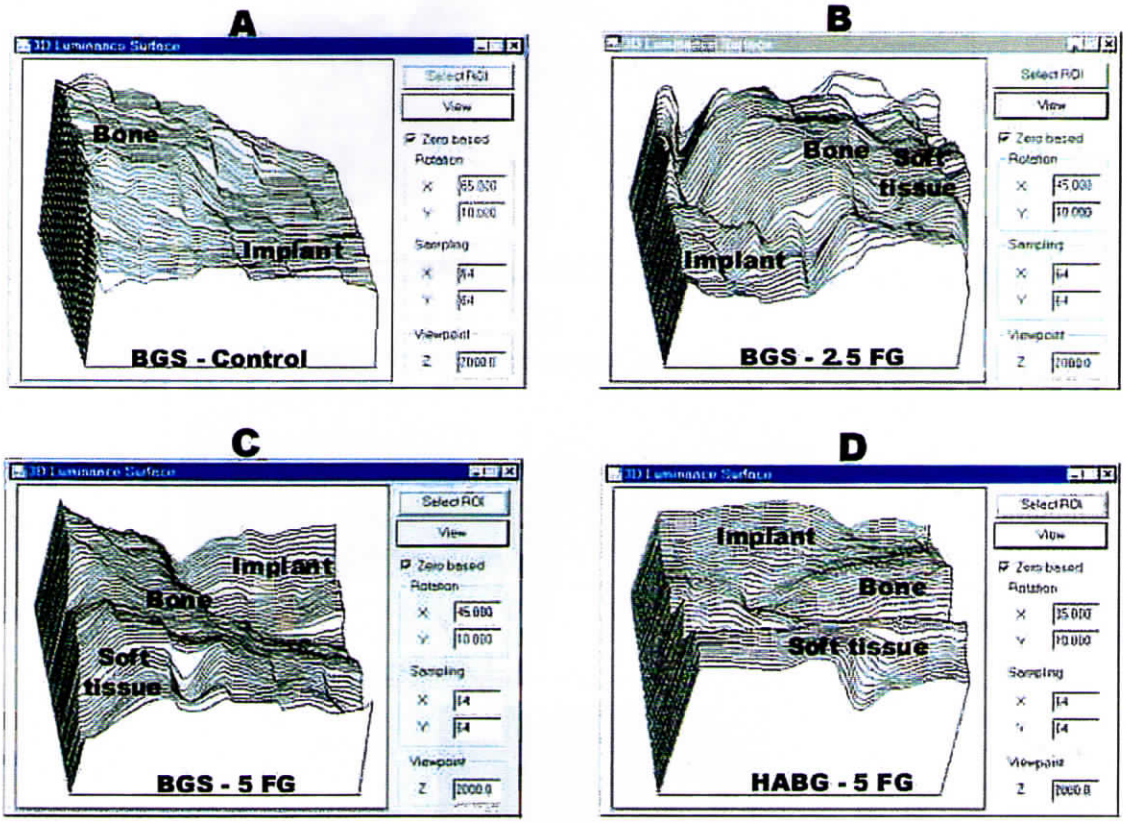

Figure -V-13

3 - D surface luminance image of BGS and HABGS granules implanted in mice quadriceps muscle after 28 days. A - BGS uncoated; B - BGS 2.5 mg FG coated; C - 5 mg FG coated and D - HABGS - 5 mg FG coated, stained sections. The implant-bone-soft tissue interface is shown.

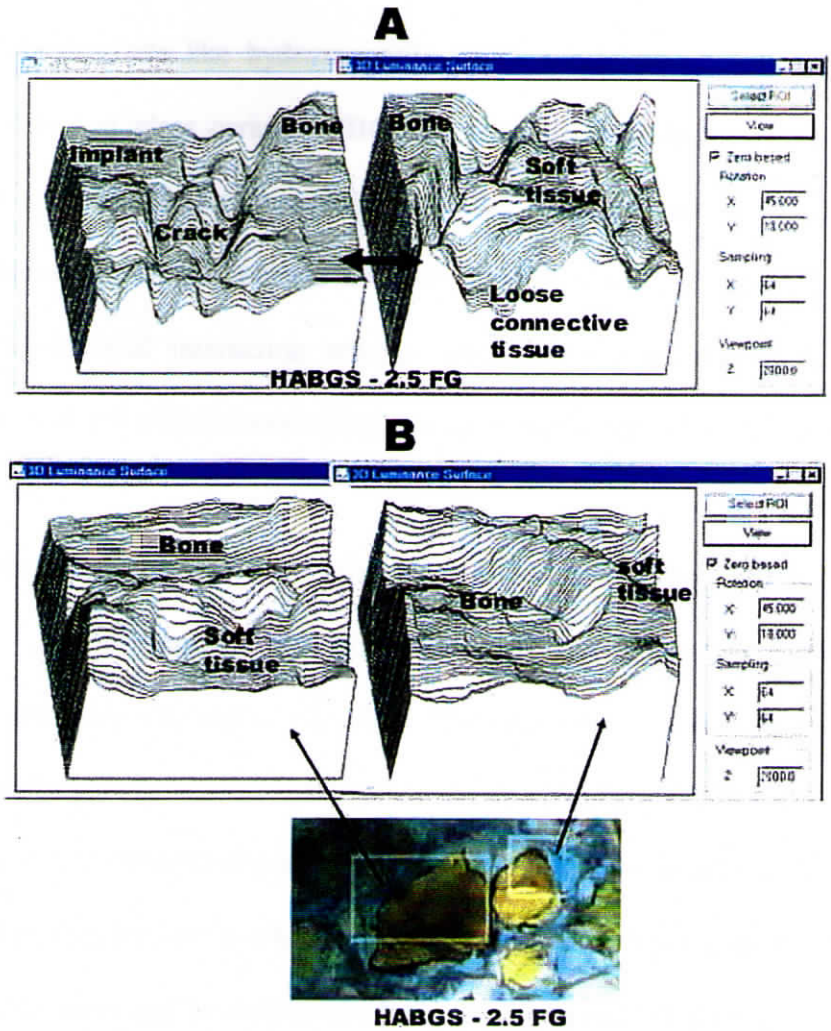

Figure -V-14

3 - D surface luminance image of HABGS granules implanted in mice quadriceps muscleafter 28 days. A & B - HABGS 2.5 mg FG coated; stained sections. The implant - bone - soft tissue interface and the interface between the soft tissue and bone is shown.

V.1.7 *In Vivo* - Heterotopic Implantation: Discussion

Synthetic grafts like hydroxyapatite (HA), tricalcium phosphate (TCP) and bioactive glass and glass ceramics (BG) are extensively studied for their bioactive property in *in vitro* and *in vivo* situations in order to understand the bioactive nature of these materials. The *in vitro* evaluation includes simulated body fluid studies, intended cell-material interaction studies while *in vivo* studies small and large animals are used for material evaluation, for its bioactive property at heterotopic and orthotopic sites.

Material response of HA, TCP and BG on the systemic influence, toxicity immunological action (Anderson, 1971), bonding (Hench, 1988), mechanical property (Holand *et al.*, 1985, Nakamura *et al.*, 1985), biodegradation, and its limited tissue response has been extensively investigated (de Groot, 1983; van Raemdonck *et al.*, 1984; Ducheyne and Lemons, 1988). This combination of *in vitro* and *in vivo* studies has led to a better understanding of surface reactions of bioactive ceramics in the body and their effects on bone formation and cell function.

Osteoconductive property of bioceramics in bone is well established but most investigators believe that calcium phosphates are devoid of intrinsic osteoinductive properties. The varied possible factors involved in this biological mechanism of heterotopic osteogenesis phenomenon include the type of ceramics, porous structure, phase composition, implantation site, the animal species, and therefore this phenomenon is not constantly observed.

X-ray images of HA, BGS and HABGS did not reveal much change after implantation. Calcium phosphate ceramics are opaque to X-rays and hence if any bone formed around could not be detected. Image analysis of the X-rays was done to

identify any change. The changes were compared with the initial or zero day of the ceramic granules implanted in the mice. The surface area for the BGS and HABGS granules alone showed some change whereas HA did not. This could be due to the material degradation or new bone formed around BGS and HABGS.

The difference between the bioactive and bioinert implants is their response to tissue in *in vivo*, by forming a bond with the host tissue. Bioactive implants showed stronger chemical bonding, whereas inert implants showed weaker mechanical bonding (Heimke, *et al.*, 1980). For glass ceramics, bonding with bone is dependent on the phosphorous concentration in the bulk material. A phosphorous concentration of between 2 and 6 % gave good bonding whereas, less phosphorous was associated with the presence of macrophages, and too high a concentration is thought to cause ectopic calcification (Clark *et al.*, 1976).

The *in vitro* simulated studies on HA, BGS and HABGS revealed that phosphate leaches more from the material by 12 hours in rabbit serum. After 28 days it was observed that HA granules implanted in the mice revealed thick connective tissue around the material that may favour strong bonding with the tissue and prevent micromotion. The absence of inflammatory reaction around the material suggests that the material is compatible with the host tissue. BGS and HABGS granules showed thin loose connective tissue bonding with the material, with a ~ 10 – 15 μm gap between the thin loose fibrous capsule and the implant. This could be due to the glassy phase observed around the material. This glassy phase is seen well integrated with the newly formed connective tissue. Where there is no glassy phase the connective tissue were seen bonded with the granule surface.

When the implant is successfully immobilized in the soft tissue during the experimental period, soft tissue adhesion to 45S5 was observed (Hench and Paschall,

1973). Crystalline glass ceramic Ceravital does not bond to soft tissues. Previous experiments have shown soft tissue-Bioglass® adhesion in sheep (Wilson and Nolletti), dogs (Wilson and Merwin, 1988), monkeys (Wilson *et al.*, 1987) and rats (Wilson *et al.*, 1981).

HA did not show any bone formation within the pores and only loose connective tissue with mesenchymal cells was observed, which suggested that osteoinduction has not taken place till 28 days. The pore size (100 to 120 μm) did not contribute to the early osteoinduction. The delay or absence of osteoinduction in HA could be due to the implantation duration. Whereas, BGS and HABGS granules are non-porous and the random pore size in these materials were in the range of 30 μm to 40 μm. Scanty mineralizing areas were observed in apposition to the implant and on the surface in some sections with BGS and HABGS granules. The material has cracked and fibroblast cells and few macrophages were observed without any osteoblast cells within the pores.

The observations made by early investigators revealed that porous material evoked different response based on the size of the pores. Pores lesser than 5 μm did not allow tissue ingrowth, pores that are 25 μm showed fibrous and vascular tissue, 40 μm pores showed limited mineralized bone ingrowth, pores of more than 100 μm led to variably deep ingrowth of bone, and pores larger than 500 μm showed rapid but incomplete filling with bone (van Blitterswijk *et al.*, 1986). Heughebaert *et al.*, (1988) reported that porous HA implanted in soft tissue in hamsters for 12 months favored bone formation by osteoinduction. Yamasaki *et al.*,(1990) reported that porous HA ceramic granules implanted in abdomen of dog resulted in heterotopic bone after 3 months.

HA, BGS and HABGS did not evoke any chronic inflammatory reaction, which is evident from the histological observations. The materials were seen well tolerated by the host tissue, with good tissue material bonding. It is well known that all implanted biomaterials encounter inflammation caused by the wound inflicted during surgery.

The first phase of wound reaction is the stage of hemostasis, followed by acute inflammation with dilatation of blood vessels, leukocyte infiltration and fibroblast proliferation. In the absence of any foreign body, the wound is eventually filled with scar tissue and regains approximately 70 % of its original strength after a period of 6 months and 2 years. Foreign body reaction is characterized by the presence of a capsule formed by parallel collagen fibers that encompasses a concentration of macrophages and foreign body giant cells (Coleman *et al.,* 1974). The severity of implant-associated chronic inflammation depends on several factors. The prime concern is the physicochemical property of the implant material. Some authors have reported that an implant material can affect the number of macrophages and foreign body giant cells at the site of implantation (Geret *et al.,* 1986). Unfortunately, it is not always clear whether these differences originate from structural or chemical characteristics, surface roughness (Salthouse and Matlaga, 1980), surface tension (Hench and Ethridge, 1982; Schakenraad *et al.,* 1986), chemical composition (Clark *et al.,* 1976), implantation site (van Blitterswijk and Grote, 1989). The implantation site is known to affect the inflammatory response to a biomaterial (van Blitterswijk *et al.,* 1985) due to micromotion (Hench and Ethridge, 1982; van Blitterswijk *et al.,* 1985), while vascularity and elastic modulus are also thought to play important roles in eliciting or minimizing the inflammatory response.

Surgical incision leads to breaking of the vessels and release of blood leading to a cascade of reactions in initiating a clot. Hence, the first blood-material interaction will be the adsorption of the protein molecules on the implant surface. HA, BGS and HABGS showed equal amounts of protein adsorption on the material surface as observed in our *in vitro* dissolution experiments. In the alkaline pH, the foetal calf serum protein adsorption was 50 % on HA, BGS and HABGS granules, whereas at normal pH in rabbit serum, the protein adsorption was 10% and all the three materials showed apatite formation by 24 hours as confirmed by FT-IR studies. From this study it is understood that pH definitely played a preferential role in deciding the adsorption of the type and amount of proteins irrespective of the material surface. But, the adsorption of the protein did not retard the release or uptake of calcium and phosphate ions but could possibly change surface properties which influences cell adherence (Schakenraad *et al.*, 1986). Protein adsorption might also influence ceramic degradation upon implantation, and significantly slow down the formation of a bone mineral surface layer (Radin and Ducheyne, 1994; 1996). Klein *et al.*, (1984) demonstrated a decrease of phagocytosis of hydroxyapatite and tricalcium phosphate by neutrophils after coating the material with serum, albumin or α- 2HS- glycoprotein. Subcutaneous implantation of HA has revealed the presence of serum protein fibronectin and IgG in guinea pig. Serum proteins adsorbed on the BG surface favored only an amorphous surface composed of Si, Ca and P until 7 days in serum (Radin *et al.*, 1997). Therefore, in the presence of serum proteins, the apatite formation is extensively delayed, a finding consistent with other data on the effect of proteins on nucleation and crystal growth of apatite (Martin and Brown, 1994; Radin and Ducheyne 1996).

With respect to the three materials implanted intramuscularly in the quadriceps muscle the healing of the tissue was normal. No chronic inflammation was observed around the material after 28 days with HA, BGS and HABGS granules. Few macrophages, neutrophils and foreign body giant cells were seen around the implant where the degradation of the material was prominent which is in conjunction with normal cell response after a wound infliction. This confirmed that the materials were less toxic and evoked minimal inflammatory reaction. Drobeck *et al.*,(1984) reported that hydroxyapatite discs and particles implanted subcutaneously in the rat showed only isolated macrophages at 7 and 24 days. Misiek *et al.*,(1984) gave a contradicting report to the earlier report by Drobeck (1984). He observed that the inflammation was seen even at 2 weeks after implantation with multinucleated cells in the granulation tissue enveloping both kinds of specimen. Furthermore, the particles were rimmed with macrophages. Similar inflammatory signs were observed even after 6 weeks. This differential inflammatory response to the ceramics could be due to the type of ceramics, the implant dimensions, the site of implantation, and the animal species. There seems to be no indication that the severity of the inflammation is correlated with the kind of ceramic used. The absence of any significant inflammatory reaction after long-term implantation is reported by several investigators for hydroxyapatite (Klein *et al.*, 1983; van Blitterswijk *et al.*, 1985), tricalcium phosphate (Klein *et al.*, 1983), glass ceramics (Hench and Ethridge, 1982; Hench, *et al.*, 1984; Ono *et al.*, 1990).

Neo-vascularization was observed around HA, BGS and HABGS granules. Thick connective tissue was observed in close apposition with HA granules, with

new capillaries and venules. BGS and HABGS also showed new capillaries and venules in close proximity to the implant granules.

HA, BGS and HABGS showed good cellular morphology and no necrosis was observed in all the sections observed. HA did not reveal any osteoblast or osteoblast-like cells even after 28 days of intramuscular implantation. BGS and HABGS granules showed osteoblast-like cells lining the granules where apatite- like deposits (approximately 15 μm) were formed. In the mineralizing zones these osteoblast- like cells were observed, but not in close apposition with the mineralizing zone. These mineralizing zones are seen in close apposition with the material surface. This could be due to the active reaction that is going on between the granule surface and the newly mineralizing area. The presence of the capillaries and venules around the material or in close proximity to HABGS and BGS granules might have favored the induction. Osteoblast cells seen around the implants might have originated either from the proliferation, differentiation and migration of the perivascular pericytes and endothelial cells or the mesenchymal stem cells or committed osteoprogenitor cells as observed in periosteal osteogenesis and bone fracture repair (Urist *et al.*, 1983; Brighton and Hunt, 1991; Diaz Flores *et al.*, 1992; and Ripamonti *et al.*, 1993). A delayed osteoinduction is observed in HABGS and BGS granules but not in HA granules.

Bonding of the tissue to the material surface decides the biocompatible, bioactive property of the material, which would ensure the mechanical stability of the implant *in vivo.*

Bioactive implants showed stronger chemical bonding whereas, inert implants showed weaker bonding (Heimke, *et al.*, 1980). The porosity of the material and the surface roughness of the material could decide the tissue attachment. HA being

porous showed loose fibrous tissue infiltration into the granules. Since the pores of the granules are not interconnected it is obvious that the penetration of the tissue will be only to the pore surface. The thick/thin fibrous connective tissue seen around the implanted HA is in close apposition with the surface of the granules, supported by the *in vitro* experiments where a thick monolayer of fibroblast cell/thin monolayer of osteoblast cells was observed attached on the HA surface. So it is obvious that fibroblast cells adhere more on the HA surface which perhaps depends on the type of protein that was adsorbed from the serum on to the material surface and also to the less reacting HA surface in the physiological media.

BGS and HABGS materials have almost similar tissue responses. Loose fibrovascular connective tissue was observed around the granules. The apposition of this connective tissue was observed only in the regions were there is no glassy phase or apatitic surface. The material has cracked and thin fibrous connective tissue could be seen infiltrating these cracks and prevented the movement of these granules. This is confirmed by the less inflammatory reaction in the vicinity of the materials.

HA, BGS and HABGS are known for their bioactive property due to the close chemical similarity to the bone tissue. The dissolution studies performed on these granules in various buffers indicated that the material response is broadly in favor of the pH. And it is well known that pH of the microenvironment plays a definite role in altering the bioactive property of the material which in turn will elicit an appropriate cell or tissue response.

The pH in turn should be stable to evoke a proper response, if not then there could be an aggressive reaction of the medium and the cells around the material. From our observations, the materials subjected to various pH, influenced the pH change by complex chemical reactions and evoked apatite deposition. This apatite

deposition is very crucial in evoking a proper cell response in *in vitro* and *in vivo*. The rate of bioactivity is directly proportional to the tissue response seen around the material *in vivo*. HA showed thick, loose connective tissue around the material surface in close apposition whereas, in BGS and HABGS the tissue bonding was observed in the areas where apatite deposition or "reactive zone" is not occurring.

Reactive Zone: *It is the interface between the reacting bioactive material surface and the active extra cellular matrix.*

For glass ceramics, bonding with bone is dependent on the phosphorous concentration in the bulk material. A phosphorous concentration of between 2 and 6 % gave good bonding. Bioglass® compositions containing from 42 to 52 mol% of SiO_2 can bond to soft tissues, in a sheep model, between 1 and 3 months. The composition containing 45 mol% has been previously bond to soft tissue (Wilson and Merwin, 1988). Substitution of CaF_2 for some of the CaO in 45S5 Bioglass® did not affect this ability. Hence it is concluded that chemical bonding to the tissue occurred initially via protein adsorption followed by the materials intrinsic property.

It is important to know the biodegradation property of the material before subjecting the material for the intended application. The sintering temperature, the chemical composition, the mechanical property of the material and the type of protein adsorption and cell response are the deciding factors in the biodegradation of the material.

The results from our dissolution studies revealed that HA material is less degrading in all the media at different pH. BGS and HABGS granules showed the same trend of material release of calcium and phosphate and the surface morphology and apatite formation after 12 and 24 hours. This is just an initial response of the

material to various media in *in vitro*. From these observations, the material degradation at an early period can be pictured in an *in vivo* situation.

Hydroxyapatite did not show any material degradation. BGS granules showed cracks and was completely disintegrated into particles of 50 to 60 μm in size. HABGS granules did not break up but the periphery of the granules showed intense degradation, and the center of the granules showed few cracks, infiltrated by cells. The behaviour of the granules *in vivo* correlated to the *in vitro* situation of the granules in different pH and protein concentration.

HA being granular, porous, irregular, moderately smooth did not evoke any chronic inflammatory reaction. Foreign body giant cells and macrophages could be seen where the surface of the material is irregular and rough and have small pits that are of 2 to 3 cell diameter. BGS and HABGS material showed cracks on the material surface, which could be due to the active degradation of the granules by the cells and the material itself breaks down after interacting with physiological fluid. BGS and HABGS granules are not macroporous and they have pores in the order of 30 to 40 μm in size, which is seen infiltrated by mesenchymal cells and few macrophages. No aggressive inflammatory action was observed around these pores and surface of the granules till 28 days.

It is well accepted that implant shape and surface structure have a direct influence on the biological performance of a biomaterial. Size is an important parameter, because above a certain size, particles can no longer be phagocytosed as a whole, which leads to frustrated phagocytosis. Surface texture affects tissue reactions, making them more severe for rough than for smooth surfaces (Salthouse and Matlaga, 1980). Implant shape definitely affects the tissue response. Round particles induce less unfavorable reactions than angular

materials (Salthouse and Matlaga, 1980; Misiek *et al.,* 1984). Another factor is the ratio of volume to surface area, which influences the reaction where a particulate induces a more severe reaction than a solid body. The effect of implant porosity has two lines of action: porosity has less effect on the natural course of a wound reaction (Krizek, 1983), on the contrary, porous implant has an unfavorable volume/surface ratio, which can lead to a more severe tissue reaction. Particulate ceramics cause more severe inflammatory response than a solid or macroporous body as observed with hydroxyapatite (Misiek *et al.,* 1984) and tricalcium phosphate. No significant increase in inflammatory response was observed when macroporous hydroxyapatite ceramic was compared with dense hydroxyapatite (van Blitterswijk *et al.,* 1985; Grote *et al.,* 1986). Since surface texture affects the inflammatory response associated with biomaterial implantation, it may well be that bioactive implant materials evoke different responses at different times after implantation due to material-specific changes in their surface structure. Glass ceramic and calcium phosphate ceramics implanted intramuscularly showed more macrophages and multinucleated cells at their interface than intraosseous implants due to the stretching of the muscle tissue with the implant (Klein *et al.,* 1983; 1983; van Blitterswijk *et al.,* 1986). Degradation and wear also affect the tissue response to a biomaterial. The inflammatory response found for rapidly degrading biomaterial was more severe than for a slowly degrading substance.

Calcium phosphate ceramic materials can be produced with varying Ca/P ratios. The Ca/P ratio for bone has been given as 1.77, for tooth it is dentine, 1.58, and for tooth enamel it is 1.64 (Drissens, 1980). The most commonly used calcium phosphate bioceramic material is hydroxyapatite, $Ca_{10}(PO_4)_6(OH)_2$. The rationale for using hydroxyapatite as a biomaterial is the advantage of using a material having

using hydroxyapatite as a biomaterial is the advantage of using a material having similar composition and crystalline structure as natural calcified tissues. Hydroxyapatite and other calcium-based ceramic materials can actively encourage bone regeneration at the surface of an implant. It has been postulated that the use of calcium phosphate ceramic biomaterials might replace the use of bone grafts in orthopaedic surgery. Glass and ceramic materials can be customized using wet chemical methods to produce materials with a wide range of mechanical properties (Le Geros *et al.* 1990; Ducheyne *et al.*1993,). Such materials can be made to have varying degrees of degradation and ionic release. Bioactive glasses having an interfacial response that can result in tissue bonding can be produced from mixtures of silica, phosphate, calcium, and sodium. Glass-ceramic containing crystalline oxyapatite and fluorapatite [$(Ca_{10}(PO_4)_6$- (O,F_2)] and β-wollastonite (SiO_2-CaO) in a MgO-CaO-SiO_2 glassy matrix (A-W type) was developed (Nakamura *et al.*, 1985). A-W glass-ceramic bonds to living bone, through a thin calcium and phosphorous rich layer that is formed at the surface of the glass ceramic (Nakamura *et al.*, 1985).

Materials of controlled surface activity (or biodegradability) showing direct bonding to bone have been termed "bioactive". Such glass compositions may allow release of ions conducive to osteogenesis. Bioactive glasses capable of forming chemical bonds may offer potential for long-term stabilization of implants. Strength of bioactive ceramic coatings is important due to the action of stress transfer from the implant prosthesis to surrounding tissues.

Fibrin Sealants (FS) or Fibrin Glue (FG) are biological adhesives derived from blood. These adhesive systems exploit the final stage of the coagulation cascade. Fibrinogen, the main structural protein in the blood responsible for forming clots, is proteolytically cleaved and converted into fibrin monomer by thrombin, a

serine protease that is converted from its inactive form by a factor Xa. The fibrin monomers assemble into fibrils, eventually forming fibers in a 3-D network. Another serine protease, Factor XIII, is proteolytically cleaved by thrombin in the presence of Ca^{2+} ions into an activated form. The activated Factor XIII (FXIIIa) then converts the noncovalent bonds between the assembled fibrin monomers into covalent bonds by transamination. This renders the fibrin gel less susceptible to proteolytic digestion by plasmin and also increases the overall strength and stiffness of the gel. The gel adheres to a variety of adherents such as collagen and cell surface receptors, most notably integrins. It is readily resorbed by enzymatic and phagocytic pathways.

FG is widely used in wound healing, it acts as a scaffold for migrating fibroblasts as well as a hemostatic barrier (Peacock, 1984), stimulates mesenchymal cells (Bruhn *et al.*, 1980), induces and promotes angiogenesis (Knighton *et al.*, 1982; Thompson *et al.*, 1985; Ono *et al.*, 1989) and also enhances formation of granulation tissue (Dinges *et al.*, 1986). The influence of FG on bone healing or as an inductive protein with bioceramics is debatable or quizzical and no proof exists concerning the osteogenic potential of FG (Schlag and Redl, 1987). So there are questions to be answered - a) Can FG influence neo-osteogenesis? b) Is early bone healing accelerated by the use of FG? The presence of factor XIII in FG is definitely known to sustain bone healing with systemic application (Claes *et al.*, 1985). Therefore, our interest was focused to study the combined effect of FG with bioactive granules on the osteoinductive potential of this biomaterial composite at an extraskeletal site in the mice model. Clinically fibrin is relatively non-antigenic (Peacock, 1984). The possibility of an immunological response was negligible in this study since there was no adverse reaction as similarly observed in other *in vivo* models using heterologous fibrin sealants (Sierra, 1993). The absence of any inflammation or the presence of a

few foreign body giant cells indicated that the ceramic implants were biocompatible and healing was uneventful with FG.

HA control and test implants did not reveal any active site of bone mineralization or osteoid deposition. Even though HA is bioactive it did not favour early biomineralization, but the uncoated HA triggered thick fibrous encapsulation around the implant granules, perhaps due to its very slow degradation property. However, in FG coated HA implants, FG delaminated from the HA coated surface and could have prevented the fibrous encapsulation. Histologically, there was no new bone formation with FG coated HA but FG favoured differentiation of osteoblast-like cells and neo-angiogenesis in the vicinity of the granules indicating that osteogenesis could be a delayed phenomenon for this less reactive material.

The uncoated HABGS and BGS control implants showed some primitive biomineralization on the periphery of the implant, which perhaps may be due to the delayed osteoinduction of the bare granules. On the contrary, FG coated with BGS and HABGS showed good healing response with neo-osteogenesis. Bone islands were seen around the implants as well as in/on the periphery of the implant, which could have been formed by the osteoinductive potential of the FG in unison with the material characteristics of the granules. In fact, BGS granules degraded faster than the HABGS granules. This may be due to the composite nature of the HABGS material having the HA phase which is a slow degrading one than BGS. Hence, the bone formation in BGS was within and on the periphery of the granules, whereas in the HABGS it was only on the periphery of the granules bone formation was observed. Our results are further convinced with the fluorochrome injected animals showing active bone mineralizing areas with FG coated BGS and HABGS granules. Tetracycline (yellow fluorescence) administered on Day 15 confirmed this incidence

of early bone formation and calcein labeling (green fluorescence) on Day 24 showed that bone formation is still in progress whereas the control group (HA, BGS and HABGS) did not show any fluorescence (mineralizing areas).

BGS and HABGS coated implants showed cracks on the material, which may be due to either the surface tension forces or the microacidic environment or both, created by the adsorbed FG onto the material. The FG matrix fiber is seen penetrating deep into the microcracks. In the initial hours after implantation the local acidic microenvironment at the defect site might have initiated the active dissolution of the BGS and HABGS thereby releasing the FG within it resulting in the induction of new bone. We also hypothesize that the calcium and phosphate ions leaching out of the granules with the FG, and the ion exchange reactions with the adjacent tissue provided the micromilieu that assisted the cellular differentiation and induction of osteogenesis in BGS and HABGS implants (Figure V.16).

The presence of multinucleated giant cells indicated their assistance in resorption of the degrading ceramics (Guillemin *et al.*, 1987; Daminen *et al.*, 1994) to pave way for *de novo* bone formation. Active osteoblast cells lining the periphery of the implants also indicated that bone formation is still in progress. With respect to HA, the material could have released ions very slowly and in turn, the release of FG is expected to be very slow to initiate new bone formation in the vicinity of the granules. This relates the fact that the phase composition of the material is an important criteria in the osteoinduction process that was definitely induced and hastened by the presence of FG. The speed of the formation and reprecipitation of the carbonated apatite on the surface of the bioactive materials *in vivo* (Hench, 1994) provides a propitious environment for mineralization around the implants at a very early period (Hench, 1991). This explains why the BGS and HABGS materials

induced new bone earlier and faster than HA. Osteogenesis is initiated at the ceramic surface and there is intimate bone apposition. Hench et al (1991) has proposed that the surface of bioactive materials affected cellular activity through the cascade of cell differentiation. Reported histological observations have also indicated that the amount of time required to first detect osteogenesis was shortened significantly by pretreatment of the bioactive ceramic implants with either fibronectin or laminin and the retention of cells within ceramics is augmented by the adsorption of the cell-binding proteins, but this effect varies depending on ceramic pore structure and /or chemical composition (Dennis *et al.*, 1992). So probably, the FG adsorbed BGS and HABGS allowed cell colonization and differentiation towards bone matrix synthesis.

The characteristics of fibrin, especially its stimulatory effect on mesenchymal cells, and its angiotropic effect suggest a FG-mediated enhancement of osteogenesis. Fibrin served as an adhesive for mesenchymal cells in the muscle to attach and differentiate in the composite ceramic environment and secondarily to reduce or prevent displacement of granules. Osteoblast cells seen around the implants coated with FG, might have originated either from the proliferation, differentiation and migration of the perivascular pericytes and endothelial cells or the mesenchymal stem cells or committed osteoprogenitor cells (Figure.V.15) as observed in periosteal osteogenesis and bone fracture repair (Urist *et al.*, 1983; Brighton and Hunt, 1991; Diaz-Flores *et al.*, 1992; Ripamonti *et al.*, 1993). It has been proposed that FG can improve osteogenesis in poorly angiogenic materials like ceramics (Wornom and Buchman, 1992) and as a carrier in BMP enhanced bone formation. Reddi and Huggins (1973) have reported that osteogenic transformation of fibroblasts was profoundly influenced by the geometry of the transformants.

Figure -V-15

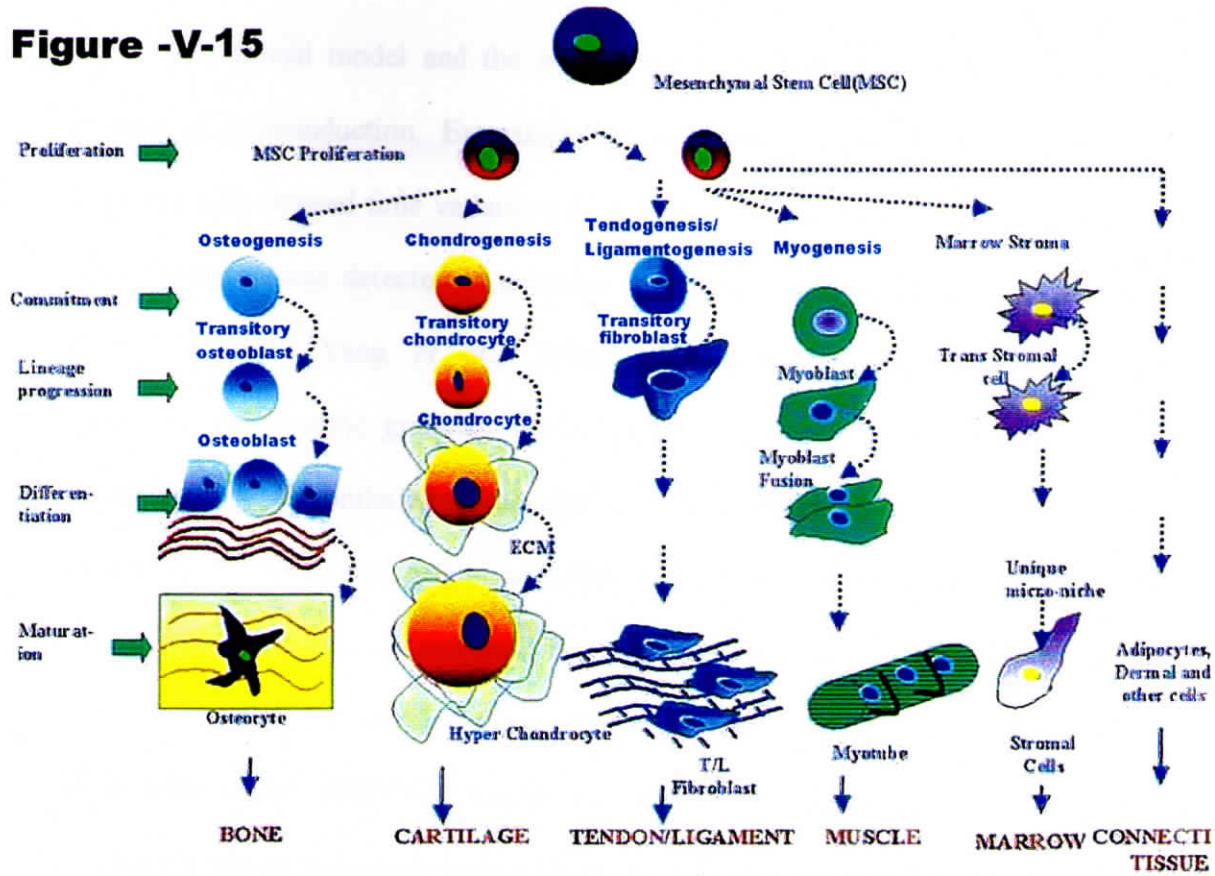

Schematic drawing of stem cell differentiation into different lineages

(Adopted from A.I.Caplan - The Mesengenic Process)

Figure -V-16

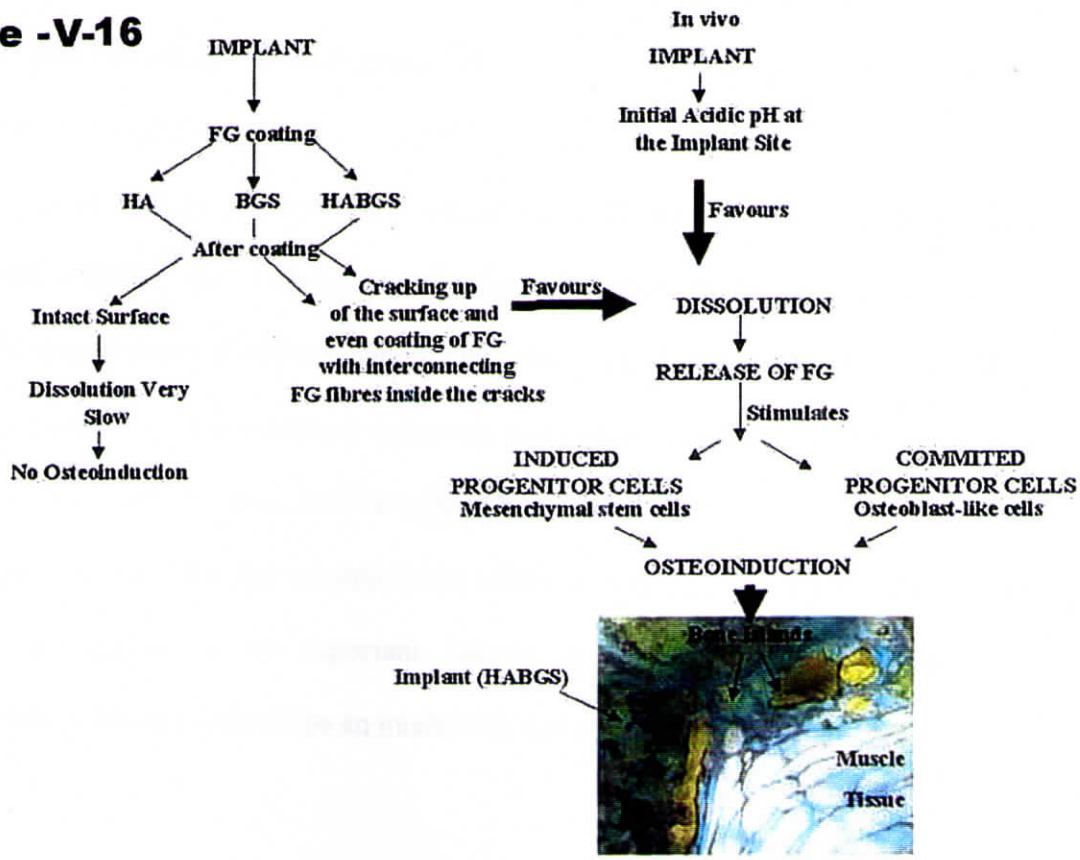

Schematic drawing of the possible mechanism by which FG coated ceramic granules favoured osteoinduction in mice quadriceps muscle after 28 days.

The animal model and the site of implantation be a factor in deciding the process of osteoinduction. Extraskeletally implanted porous HA-TCP ceramic in dogs and pigs showed time variations 45-60 days for bone formation. Histologically, bone formation was detected in ceramics, implanted in rabbits, goats and rats only after 120 days (Yang *et al.*, 1996). Subcutaneous implantation of porous hydroxyapatite ceramic granules in abdomen of dogs resulted in heterotopic bone formation only 3 months after implantation (Yamasaki *et al.*, 1990 and 1992). No influence of bone matrix gelatin and fibrin sealant was demonstrated histologically on early osteoinduction in rats until Day 21(Schwarz *et al.*, 1993). Kawamura and Urist (1988) noted a significant increase of ectopic bone formation in the mouse thigh with sealed BMP/NCP composite implants on post-implantation Day 21, despite the use of xenogenic human fibrin. So it is obvious that this phenomenon of osteoinduction is not constantly observed in different animal models and varies with the physicochemical characteristics of the biomaterial used in respective experimental systems.

In this study, FG-mediated enhancement of bone formation in mice were HABGS > BGS > HA with early bone induction by Day 15, not reported elsewhere. Further experiments of our engineered composites are to be tested at orthotopic sites to understand the FG-mediated induction and enhancement of bone formation to unravel this myth. In cases, involving large bone defects, a need to reduce the time is necessary to establish the ceramic-bone interface and bony ingrowth. Initiation of early osteogenesis is an important criteria in the application of bone repair technology, where FG could be an interesting and a promising candidate.

V.1.8 Conclusion

Atraumatic and atoxic osteosynthesis observed on Day 15 with the two-component FG-ceramic composite at a non-osseous site has proved to be successful in the mice model. Bone formation was accelerated by the presence of FG together with the favorable phase composition of BGS and HABGS non-porous granules at an ideal implantation site. So osteoinductive proteins and angiogenic factors can increase cell retention, which is a significant factor in promoting early differentiation of osteogenic cells and an important criteria for the design of osteogenic cell-ceramic constructs for tissue regeneration and repair.

V.2 *In Vivo*– Orthotopic Implantation

V.2 *In vivo* - Orthotopic Implantation: Results

V.2.I. X-ray

X-ray observation revealed the material integrated with the host bone after 3 and 6 months (Figure.V.17). The radioopacity of the defect after 6 months implantation was higher than the 3 months. The order of radioopacity of the three different implants in the tibia bone after 6 months was HA>HABGS>BGS.

V.2.2 Microradiography

HA material was seen well integrated with the host bone without any visible gap with the newly formed bone after 3 and 6 months, without any visible change in the size of the granules (Figure.V.18 A & B). BGS material after 3 months revealed visible gaps at the interface of the new bone and the granules, the granules size has reduced. The gaps seen at 3 months are completely replaced by new bone by 6 months (Figure.V.18 C & D). HABGS implanted bone specimen did not show any visible gaps after 3 and 6 months (Figure.V.18 E & F).

V.2.3 Microangiography

X-rays of the undecalcified bone did not reveal any blood vessels or capillaries around the implant after infusing barium sulphate and Indian ink through the femoral vein. Hence, bone was decalcified and the X-ray was taken. Under the microscope, the X-ray images revealed fine vessels (probably Volkmann's canal) filled with $BaSO_4$/Indian ink, evident as bright white streaks around the implant (Figure.V.19 A, B & C). Figure V.19 D, E and F showed normal bone with fine vessels adjacent to the implant.

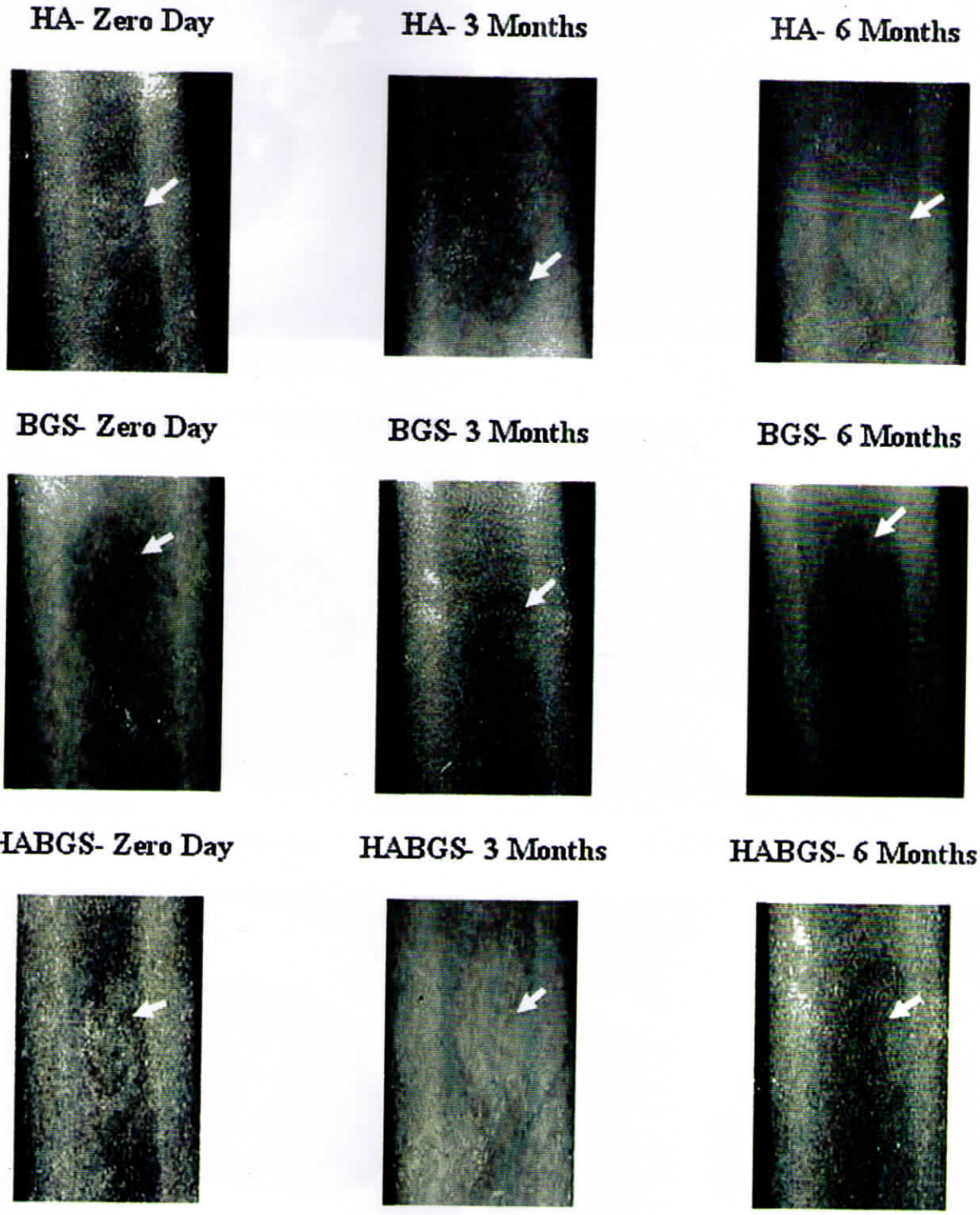

Figure -V-17

X-ray photomicrographs of bioactive ceramic granules implanted in rabbit tibia bone :The arrows indicate the defect site at zero day (immediately after implantation)and after 3 and 6 months.

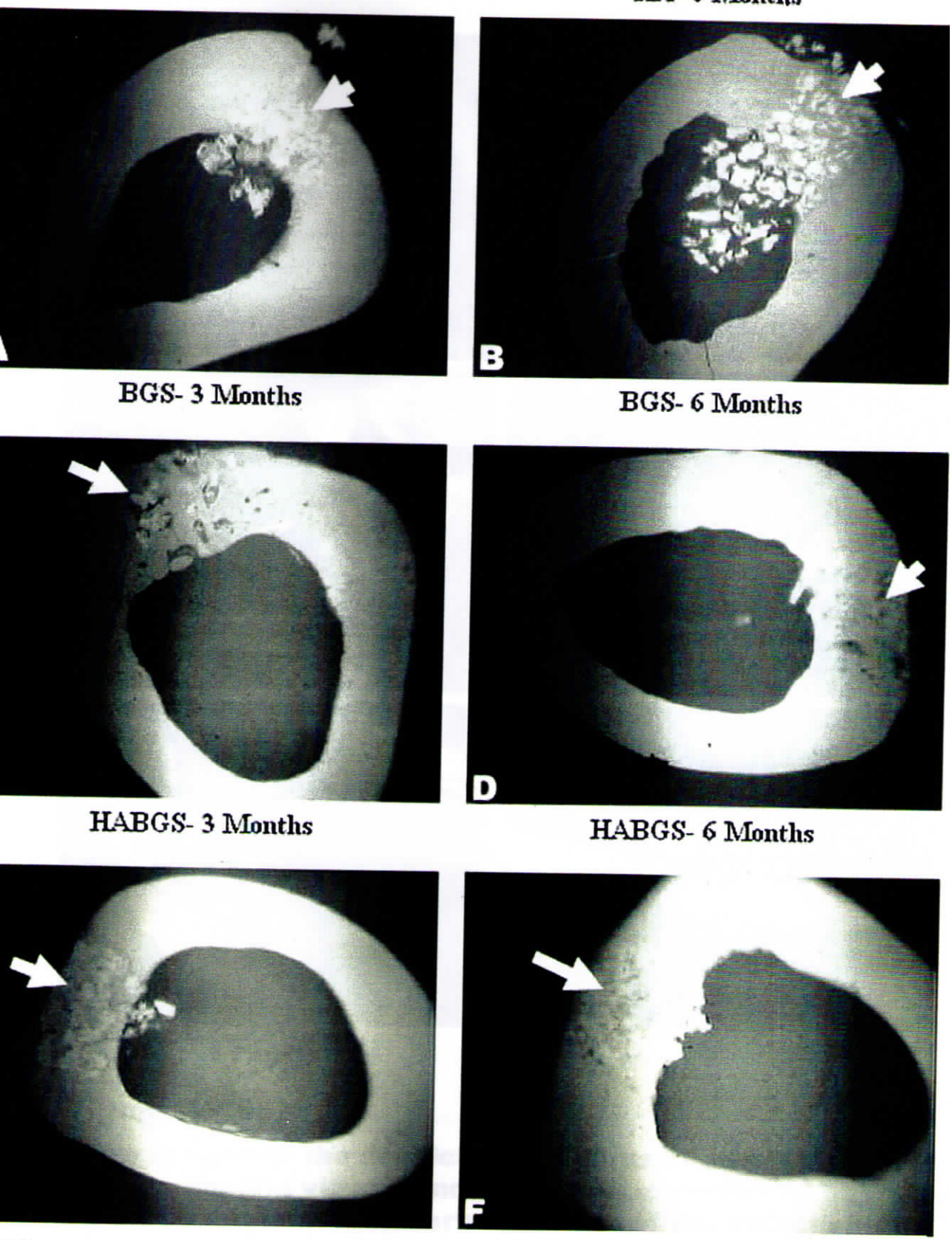

Figure -V-18

X-ray microradiographs of the cross-section of rabbit tibia bone with bioactive ceramic granules after 3 and 6 months: A, B & C - HA, BGS & HABGS after 3 months; D, E & F - HA, BGS and HABGS after 6 months . The arrows indicate the implant area.

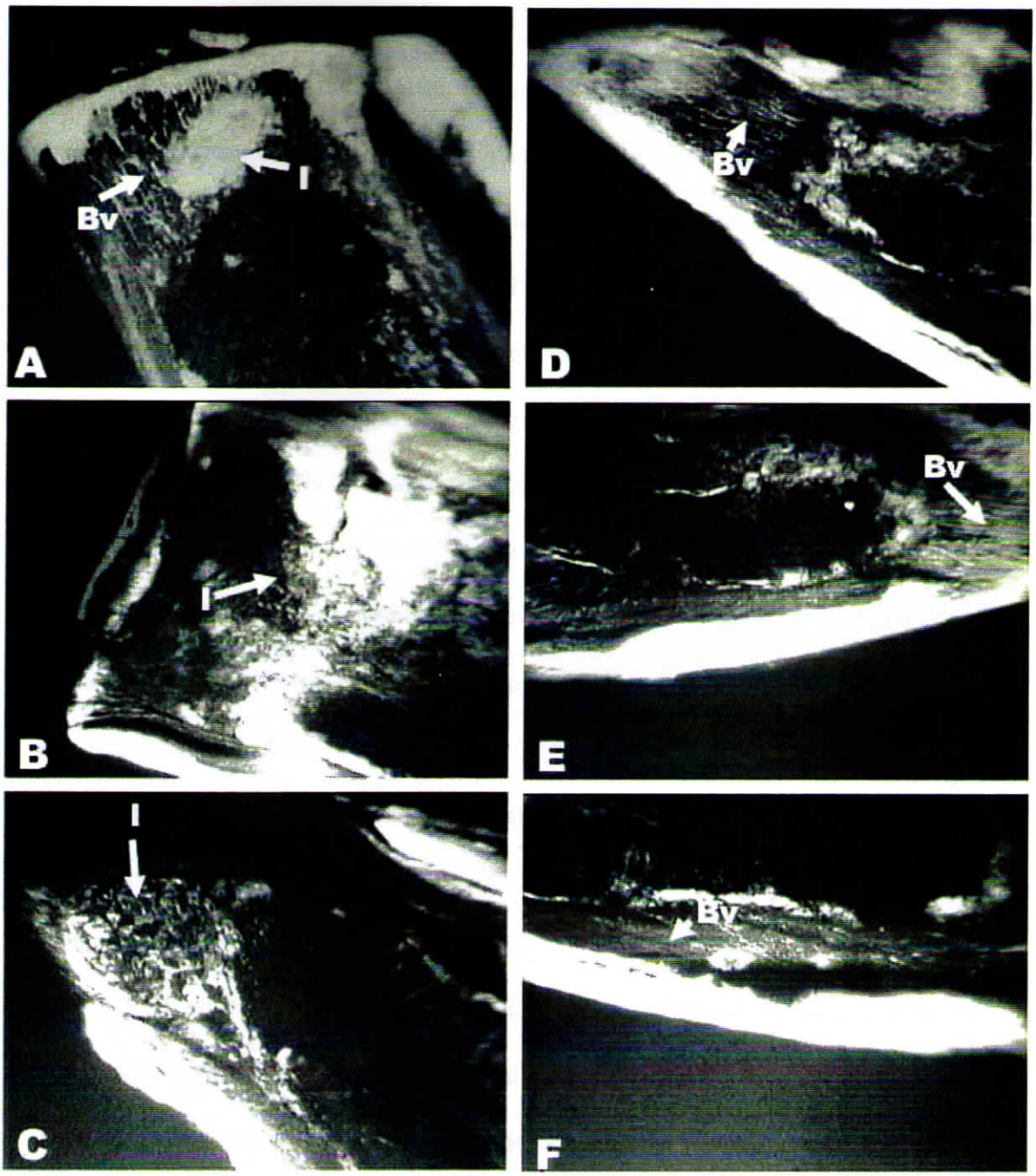

Figure -V-19

X-ray images of the decalcified sections of rabbit tibia bone with an implant viewed under light microscope and capture by a CCD camera. A - F serial sections of the defect site wit the implant (I), blood capillaries (Bv) probably the Volkmann canals are more radioopaque with barium sulphate.

V.2.4 Gross Evaluation

The *in situ* position of the implant material was maintained without any signs of macroscopic changes in the adjacent tissue. There were no gross evidences of inflammation or necrosis around the implant sites and good healing response was observed. The 3 and 6 months groups of HA, BGS and HABGS implanted in rabbit tibia bone did not show any visible gaps between the implant and the host bone under the stereomicroscope, and while sectioning the implant into thin slices of 100 μm the granules were seen tightly bonded to the newly formed bone and did not slip off.

V.2.5 Scanning Electron Microscope (SEM)

HA after 3 and 6 months showed good osseointegration with the newly formed bone and showed few gaps of 7 μm to 15 μm to be replaced by new bone. The implant material was intact even after 3 (Figure.V.20 A & B) and 6 (Figure.V.21 A & B) months. FG coated HA granules also showed good osseointegration with the newly formed bone and no gaps were observed between the new bone and the implant after 3 months (Figure.V.22 A & B).

BGS after 3 months (Figure.V.20 C & D) showed good osseointegration with the newly formed bone, and the material was seen cracked in the center possibly suggesting material degradation. The gaps between the newly formed bone and the implants were 15 μm to 25 μm after 3 months, and after 6 months (Figure.V.21 C & D) the material was completely replaced by bone with very few narrow gaps of 5 μm to 10 μm. FG coated BGS granules (Figure.V.22 C & D) did not show any gaps between the new bone and the implant and the healing was good at 3 months.

HABGS showed enhanced healing and good osseointegration with the newly formed bone. Few gaps of 10 μm to 20 μm were seen between the newly formed bone and the implant at 3 months (Figure.V.20 E & F). The six months group of

HABGS (Figure.V21.E & F) showed better osseointegration, very few granules are left to be replaced by the new bone, the interface between the host bone and the implant were at the range of 10 μm to 15 μm. FG coated HABGS granules (Figure.V.22 E & F) also showed the same trend as observed with FG coated HA and BGS granules. The healing was normal without any visible gaps between the newly formed bone and the implant granule. The implant granule was seen well osseointegrated with the newly formed bone.

V.2.6 Fluorescence Microscopy

Mineralizing zones were observed in HAP implanted animals (Figure.V.23 A & B) in the cortical region and in the interface of the new bone and the host bone and also in few areas of the periosteum and endosteum. Fluorescence was also observed in the pores of the implant and in the Haversian system of the mineralizing osteons. No fluorescence streaks (lines) were observed within the implant. HA coated with FG showed intense fluorescence of tetracycline (Figure.V.24 A) around and adjacent to the granules. The formation of new bone seems to be from the implant towards the host bone, which is confirmed by the alizarin complexone dye (Figure.V.24 B), showing fluorescence away from the implanted granules. The periosteum and the Haversian canal showed fluorescence with the alizarin dye that was administered after 2 months.

In BGS implanted animals, the fluorescence was observed in the cortical region and on the periphery of the implant, streak fluorescence was observed within the implants, at the interface region of the host bone and new bone (Figure.V.23 C & D). The periosteum and endosteal zones did not show much fluorescence. The Haversian canal and the surrounding osteons showed intense fluorescence.

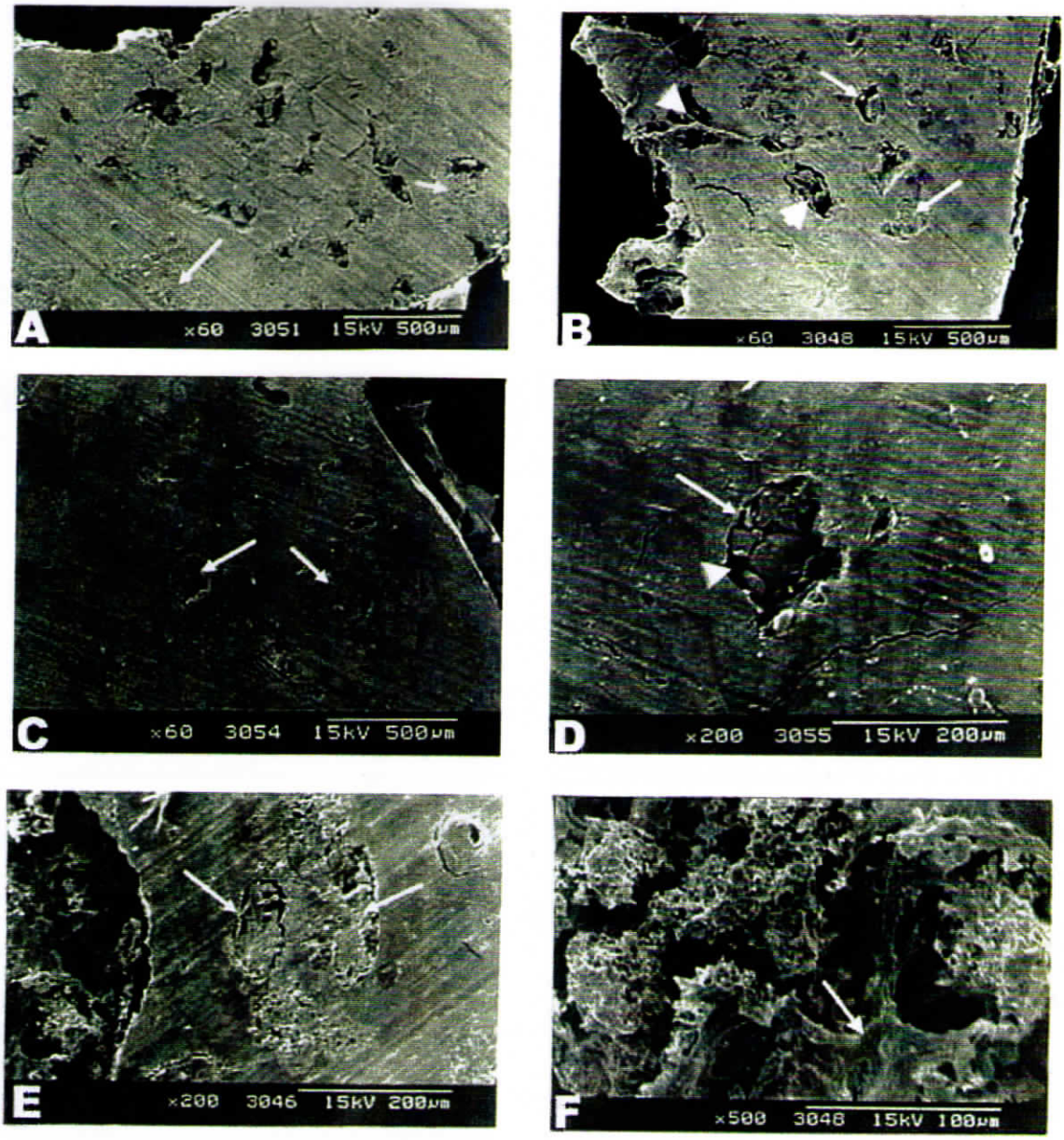

Figure -V-20

Scanning electron micrographs of bioactive ceramic granules: A &B - HA; C & D - BGS and E & F - HABGS; implanted in rabbit tibia bone after 3 Months. Implant well integrated (white arrow) with the new bone, the gaps that are seen within the defect (arrow head) are due to sectioning artifacts.

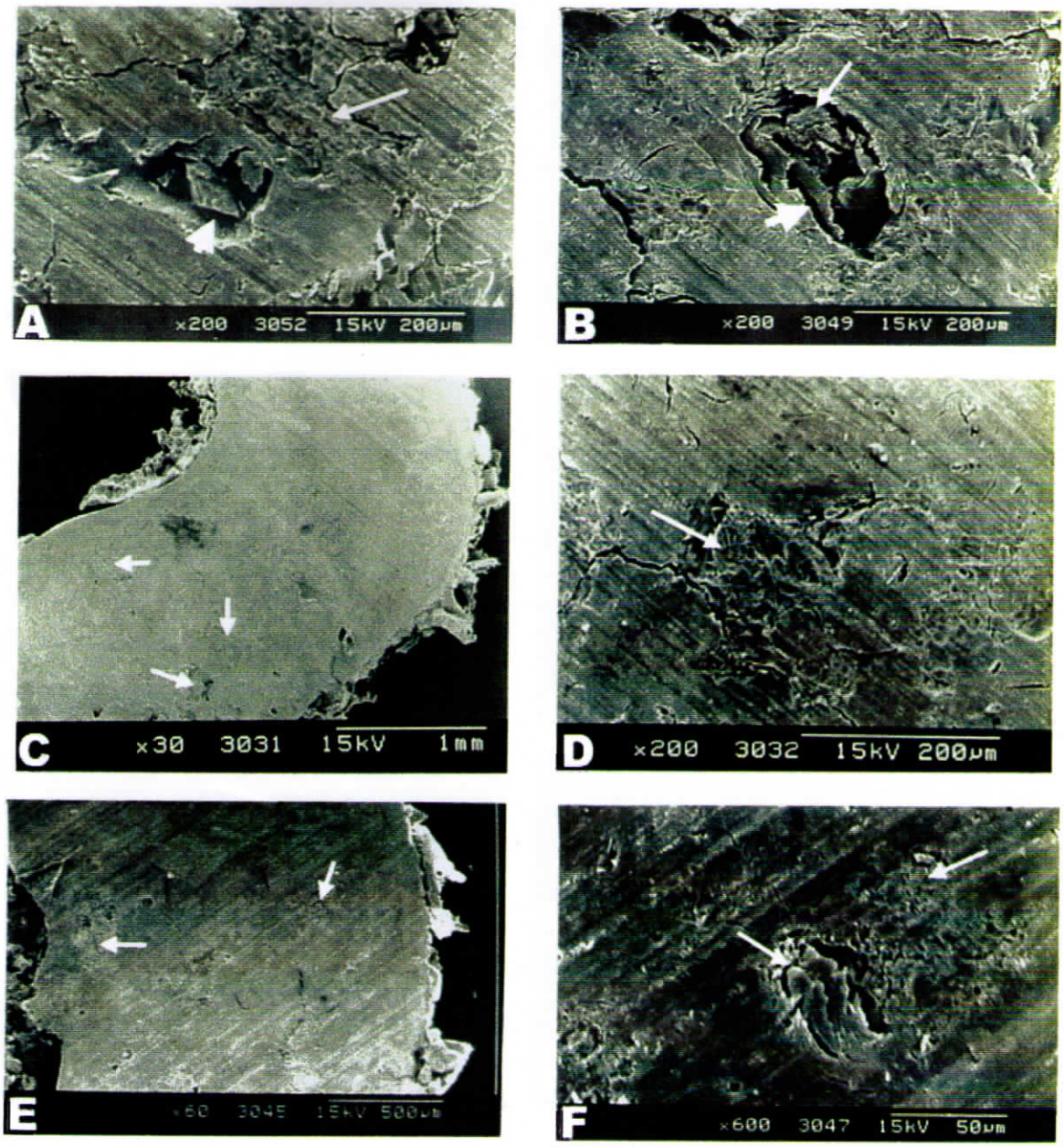

Figure -V-21

Scanning electron micrographs of bioactive ceramic granule of A & B - HA, C & D - BGS ;E & F - HABGS granules implante in rabbit tibia bone after 6 months: The granules are integra with newly formed bone (arrow), the arrow head show the ga caused due to sectioning artifact.

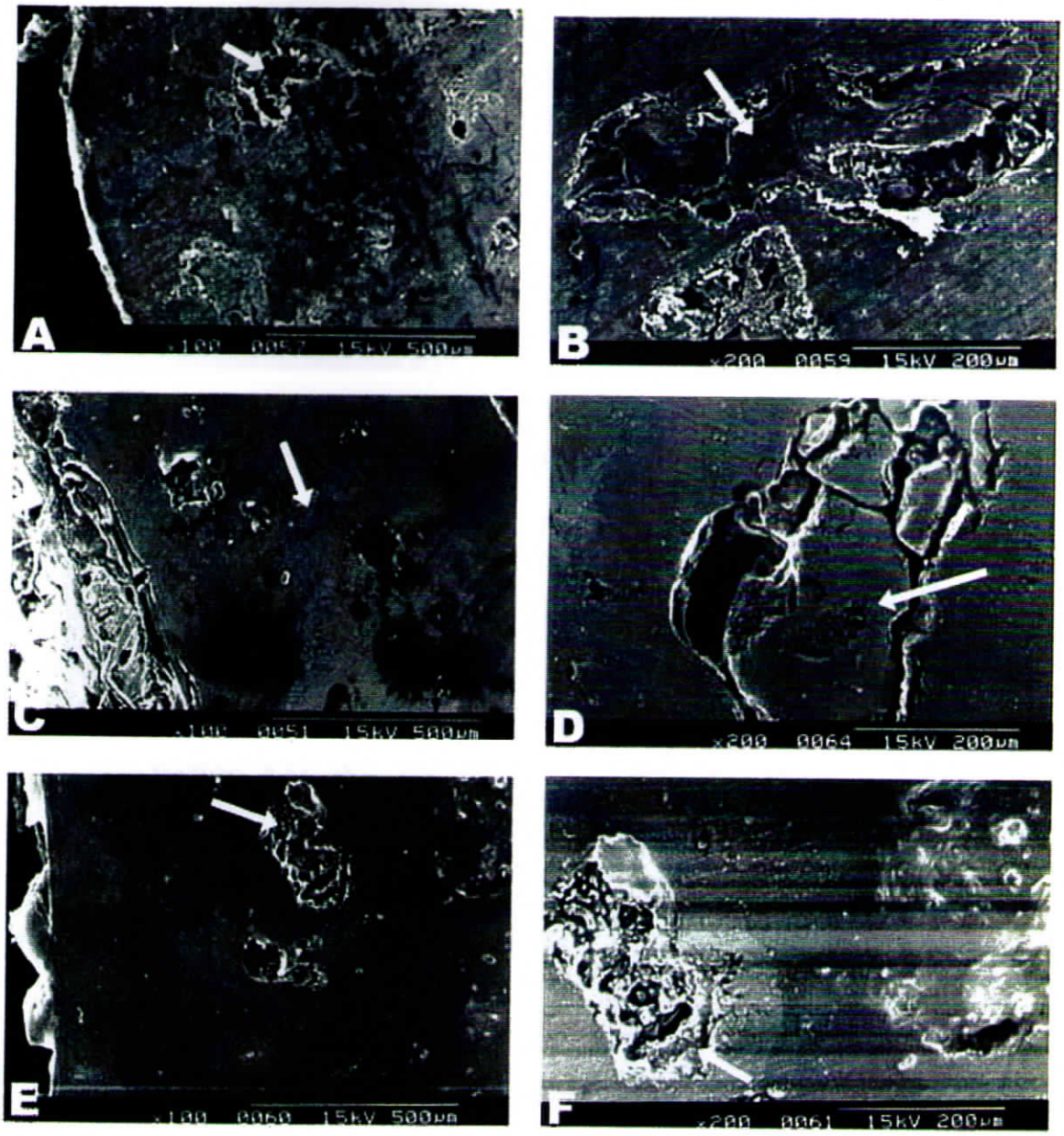

Figure -V-22

Scanning electron micrographs of FG coated bioactive ceramic granules implanted in rabbit tibia bone after 3 months. A & B - HA coated FG granules well apposed to the newly formed bone (arrow); C & D - BGS granules apposed to the new bone with visible gaps (arrow) of approximately 20 micrometers, the large gaps of more than 100 micrometers seen in D could be due to sectioning artifact; E & F - HABGS granules show active degradation and are in close apposition with the new bone, with few gaps (arrow) of about 10 - 20 micrometer.

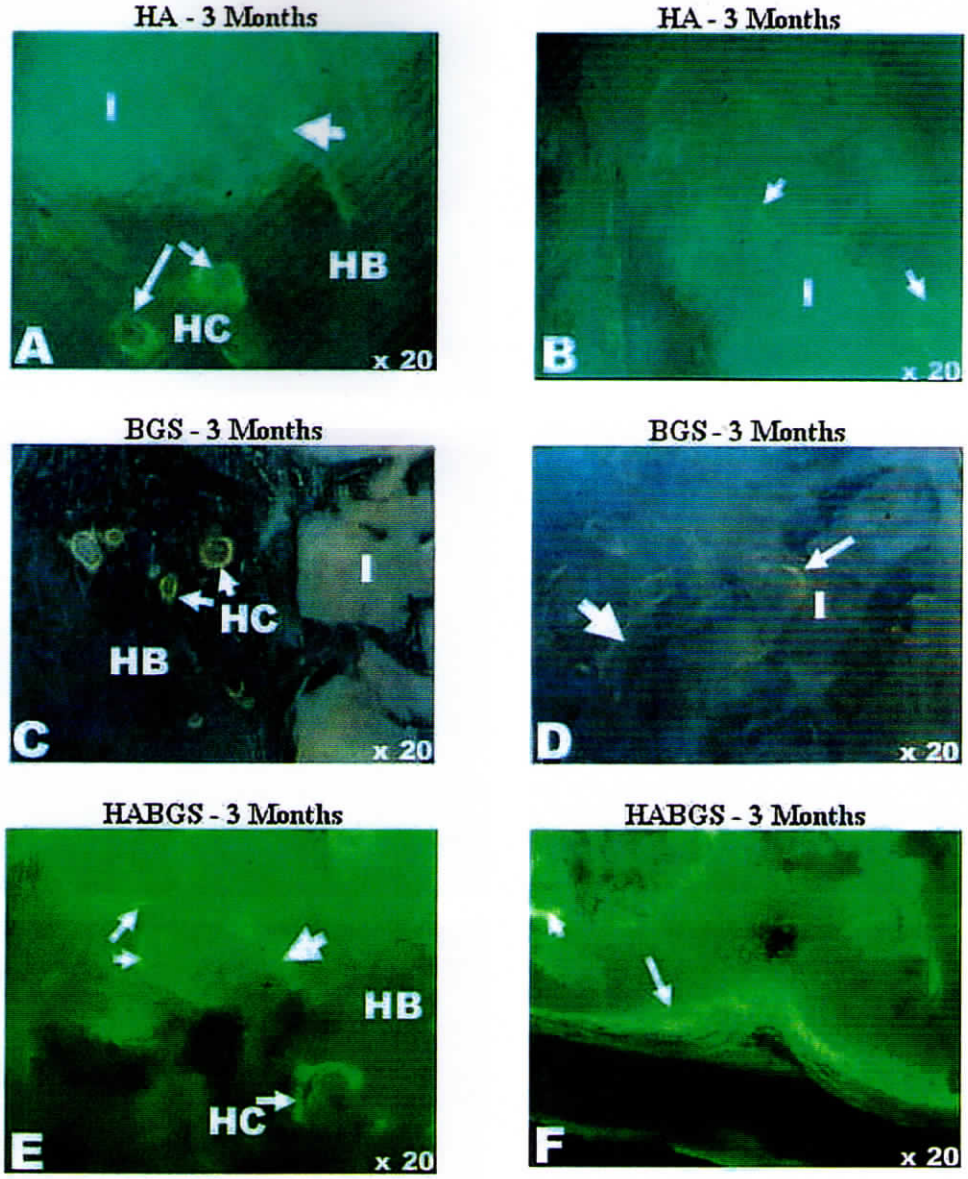

Figure -V-23

Fluorescence micrographs of bioactive ceramics implanted in rabbit tib bone after 3 months: A & B - HA, yellow fluorescence in the new bone in erface (thick arrow) and in Haversian canal (HC) adjacent to the host bo (HB) are the mineralizing zones; C & D - BGS, yellow fluorescence is inte se around the Haversian canals (HC) in C, and in the middle of the impla (I) and at the interface of the host bone and new bone (thick arrow) in D. E & F - HABGS, the fluorescence is intense at the implant new bone interf in E (big arrow head) and also in the HC and in the sub periosteal bone.

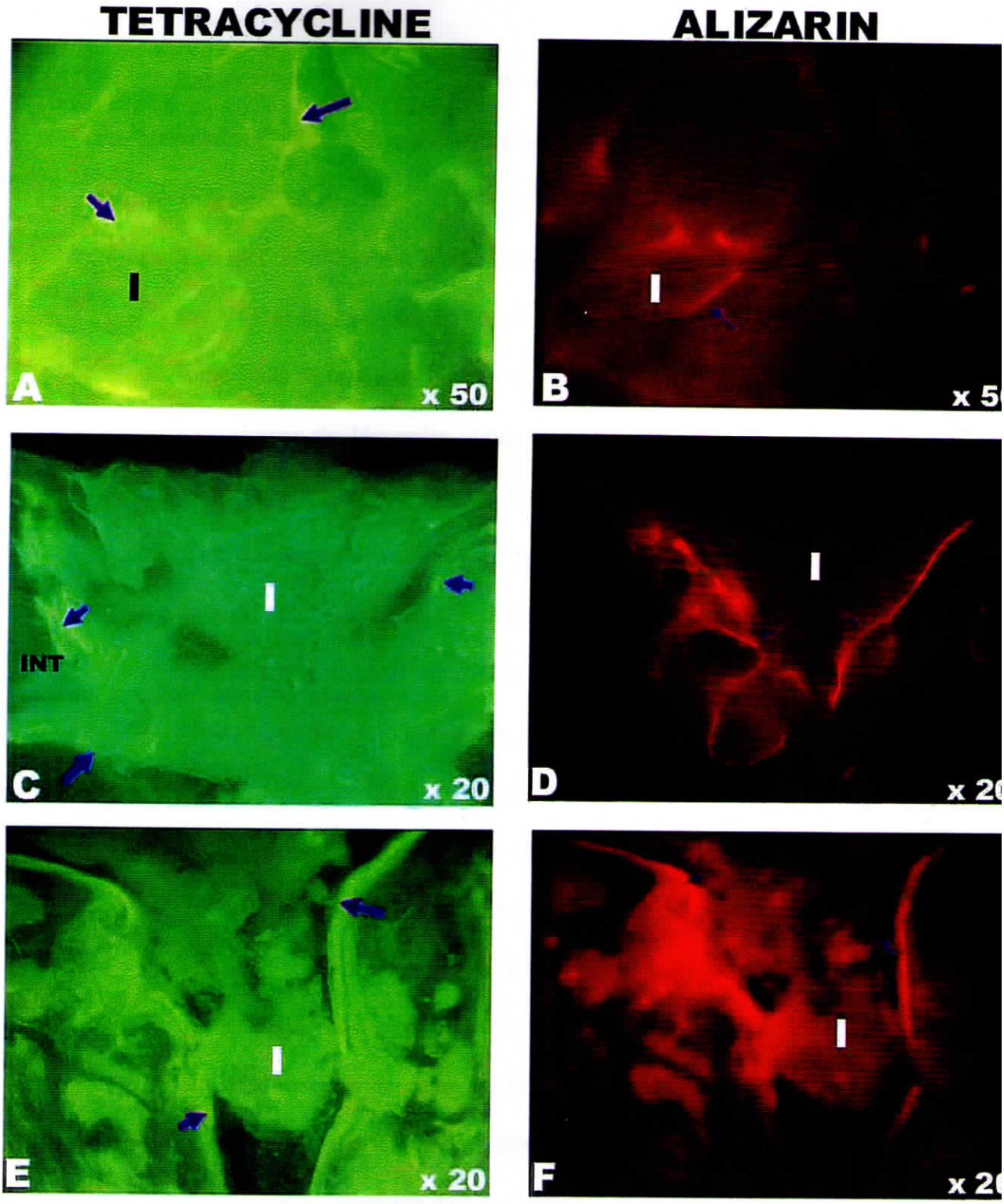

Figure -V-24

Fluorescence micrographs of FG coated bioactive ceramic granules implanted in rabbit tibia bone after 3 months: A, C & E - The yellow - tetracycline labeled, B, D & F - red - alizarin complexone; A & B - HA coated with FG, the arrow denotes the fluorescence around the implant; C & D - BGS coated FG granules, the yellow fluorescence is seen in C at the interface (INT) of the host bone and the new bone; D - the fluorescence within the implant (I); E & F - HABGS coated wi FG, the fluorescence is seen within the implant site as well as at the interface E and in F the alizarin red fluorescence is observed only within the defect (arro

The sequence of the healing of the defect with FG coated BGS implants, from the proximal end of the defect towards the distal end in the tibial bone is described as follows (Figure.V.25 A – H)

a. The section-1 adjacent to the defect in the proximal region did not showed any yellow fluorescence in the periosteal and the cortical region, except for some mild fluorescence in the endosteal region (Figure.V.25 A). Whereas, with alizarin the Haversian canals could be seen in the cortical region as well as in the periosteal zone (Figure.V.25 B).

b. The fluorescence was seen in the mid cortical region and in the endosteal zone of section-2, but not in the interface of the new bone and the host bone and in the periosteal zone (Figure.V.25 C). Alizarin, red fluorescence is observed in the periosteal and in the newly formed Haversian system, but not in the interface or the endosteal zone of the defect. (Figure.V.25 D).

c. The yellow fluorescence was observed only in the interface and in the endosteal regions but not in the periosteal zone in section-3 (Figure.V.25 E). Alizarin red fluorescence was observed within the cortical region and in the Haversian canal region, but not in the periosteal region or in the interface of the host bone and the newly formed bone (FigureV.25 F).

d. In section-4, the tetracycline labeling was seen in the interface and in few zones of the endosteum, but not in the cortical or periosteum (Figure.V.25 G). Alizarin red fluorescence was observed in the periosteum and in the cortical regions of the defect and also in the newly formed Haversian canals (Figure.V.25 H).

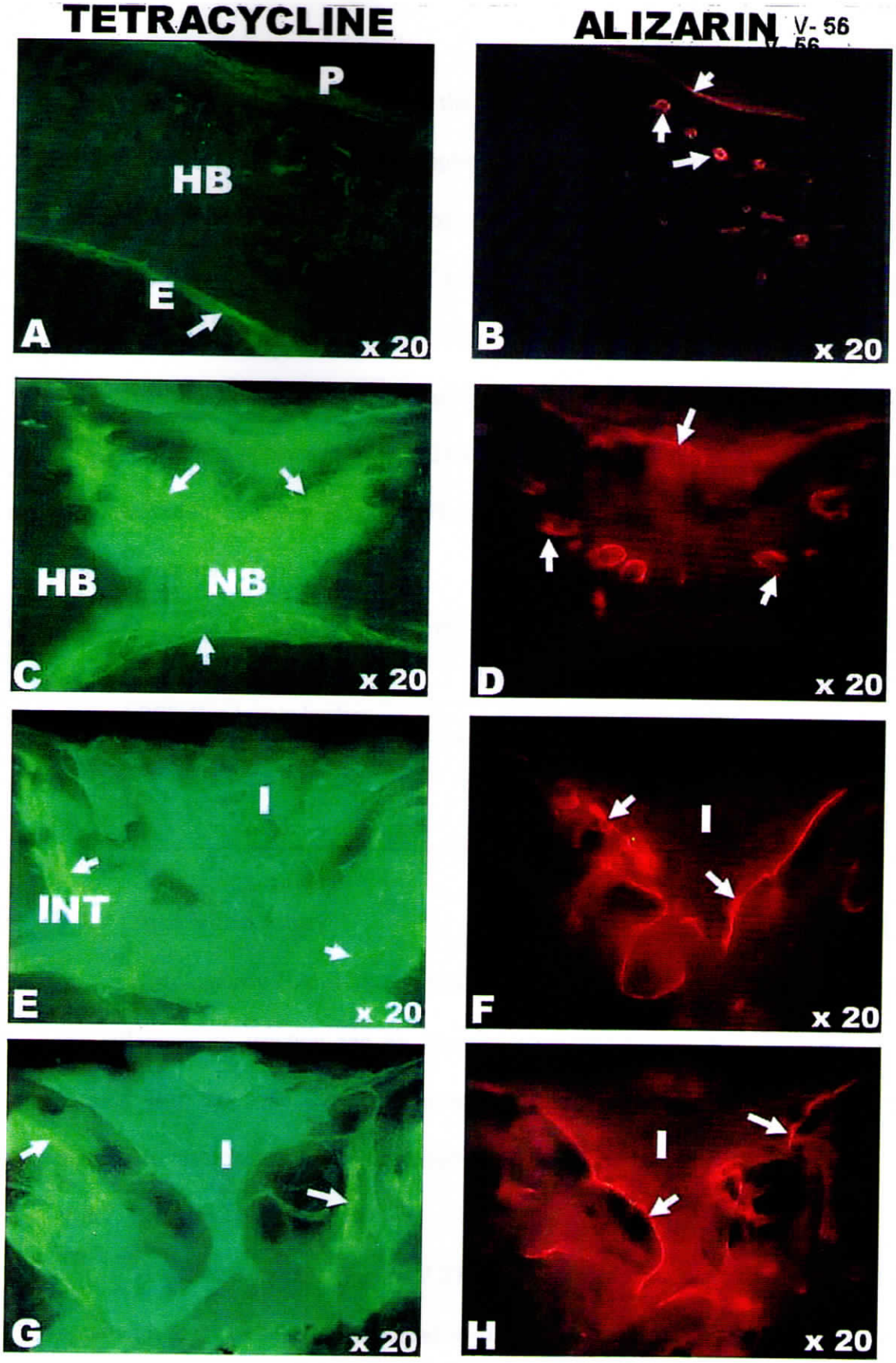

Figure -V-25

Fluorescence photomicrographs of the serial sections of BGS coated FG implanted in rabbit tibia bone after 3 months: A - H - mineralization pattern marked by arrows; HB =host bone, P = periosteum, E = endosteum, NB = new bone, I = Implant and INT = Interface of the bone.

Fluorescence was observed at the interface of the HABGS implants and the new bone, within the cracks of the implants and also in the periosteal and endosteal regions. The Haversian canal and the osteoid seams also showed intense fluorescence (Figure.V.23 E & F). HABGS coated with FG altogether showed a different kind of healing response when compared to that of FG coated HA and BGS. Fluorescence was observed in the periosteum, endosteum, in the mid cortical area and fluorescence streaks within the implant (Figure.V.24 E &F, Figure.V.26 A-D). Fluorescence was also observed in the newly developed Haversian system.

Healing pattern: (Table.V.6)

CERAMIC WITHOUT FG	CERAMIC WITH FG
HA: Host bone to Implant	HA: Implant to Host bone
BGS: Host bone to Implant	BGS: Implant to Host bone
HABGS: Host bone to Implant	HABGS: Mechanism possibly both ways: Host bone to Implant and from Implant towards Host bone

V.2.7 Light Microscopy

Histologically HA, BGS and HABGS showed good healing response without any inflammatory reaction and no fibrotic or necrotic tissues were observed at all periods. But, the bone formation pattern and the material degradation varied from material to material and from one period to another period.

V.2.7.1 Hydroxyapatite (HA)

HA after 3 months (Figure.V.27 A-F) was seen well integrated with the host bone with few gap left to be replaced by the new bone. The implants were lined with osteoblast cells and osteoblast-like cells and few fibroblast cells, no foreign body giant cells or osteoclast cells were observed. The periosteum and the endosteum area of the bone were completely closed.

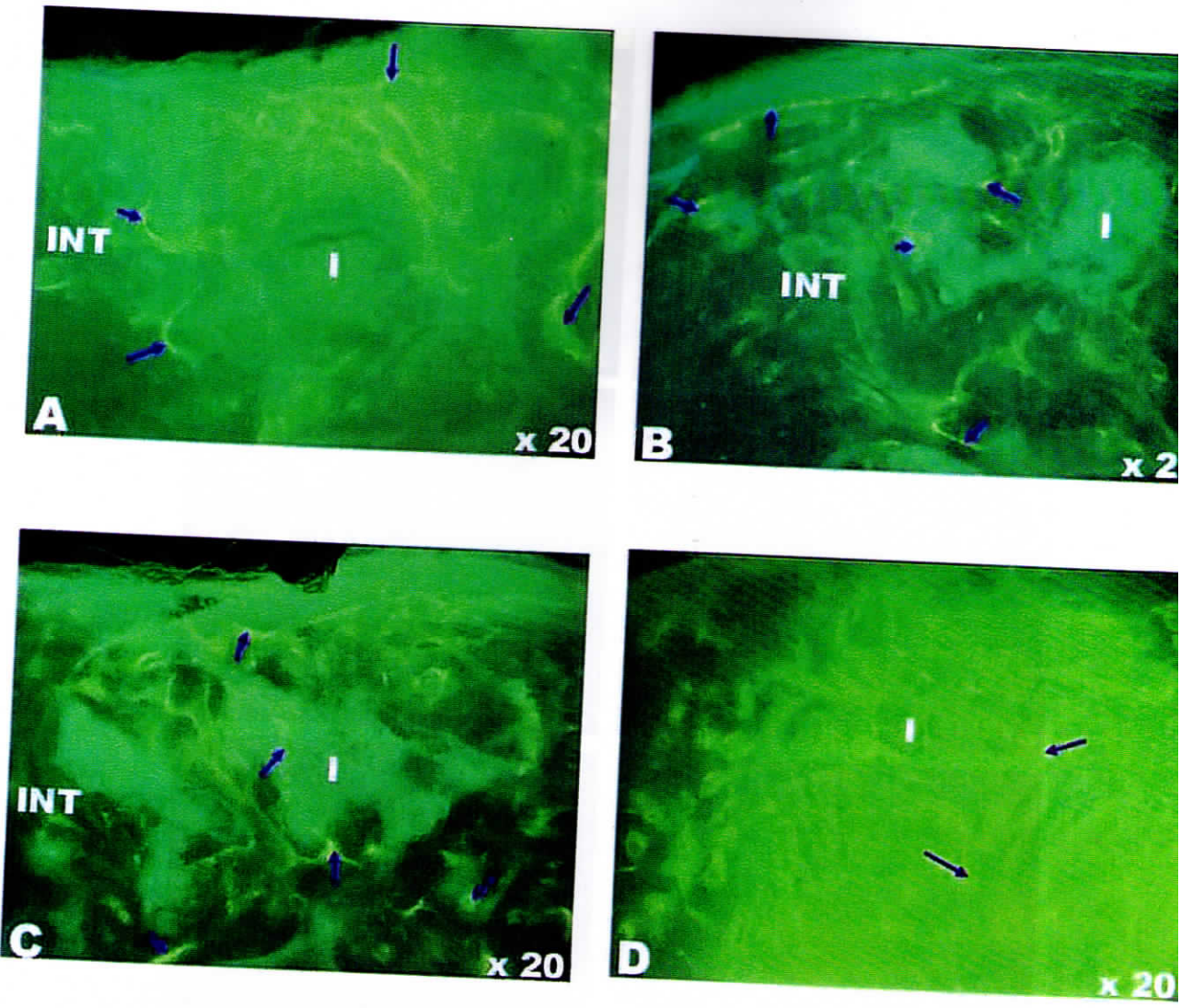

Figure -V-26

Fluorescence photomicrographs of the serial sections of FG coated HABGS granules implanted in rabbit tibia bone after 3 months. A - D - Tetracycline labeled, yellow fluorescence (arrows) around the implant (I) and in the interface (INT) denoting the mineralization pattern.

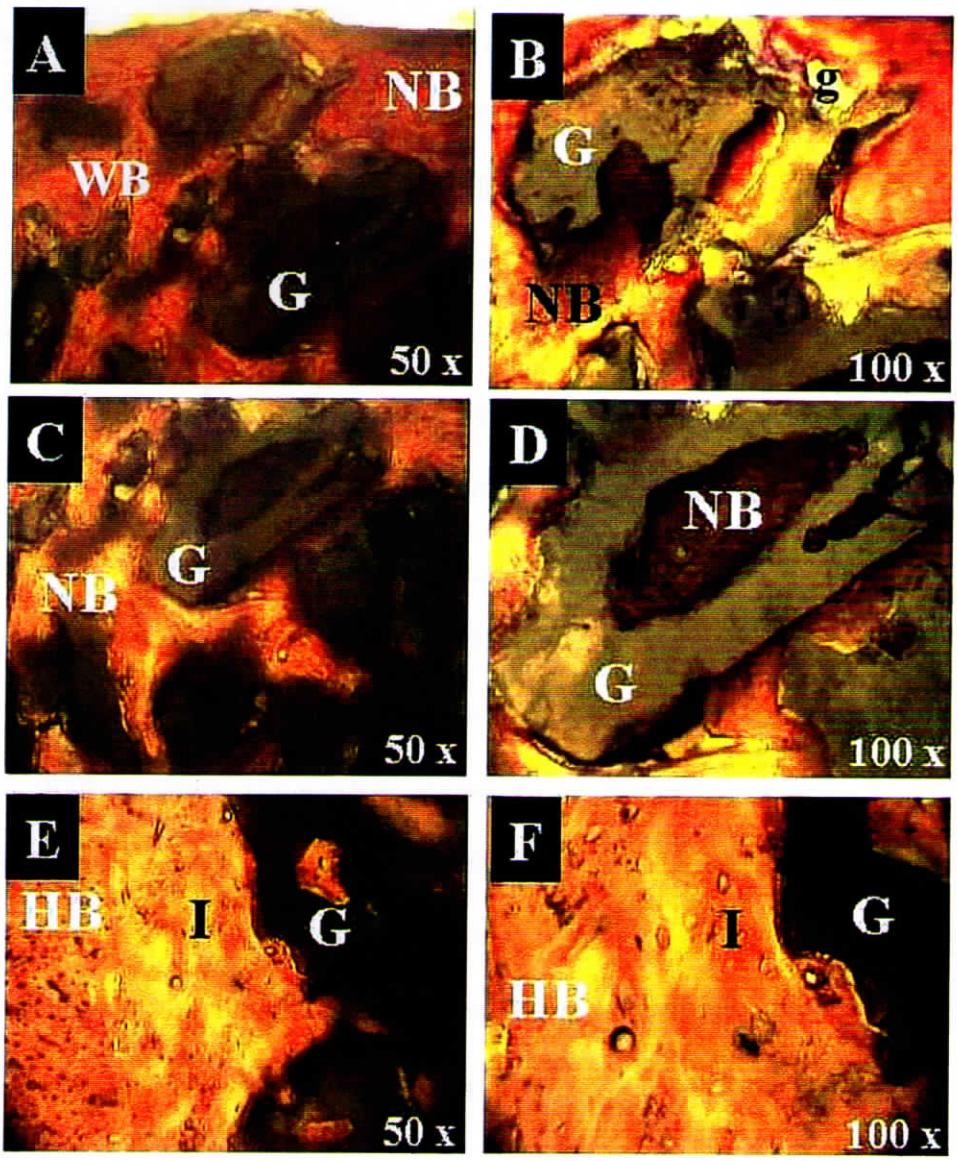

Figure -V-27

Photomicrographs of hydroxyapatite implanted in rabbit tibia bone after 3 months: A & B - the periosteal - cortical region, granule (G) is seen osseointegrated with the new bone(NB), few gaps (g) of 10-20 micrometer could be seen ;C & D - the implant in the mid cortical region and the new bone is seen within the pores of the granules; E & F - the implants in the new bone - host bone (HB) interface (I). Mature woven bone (WB) is seen around the newly formed bone after 3 months.

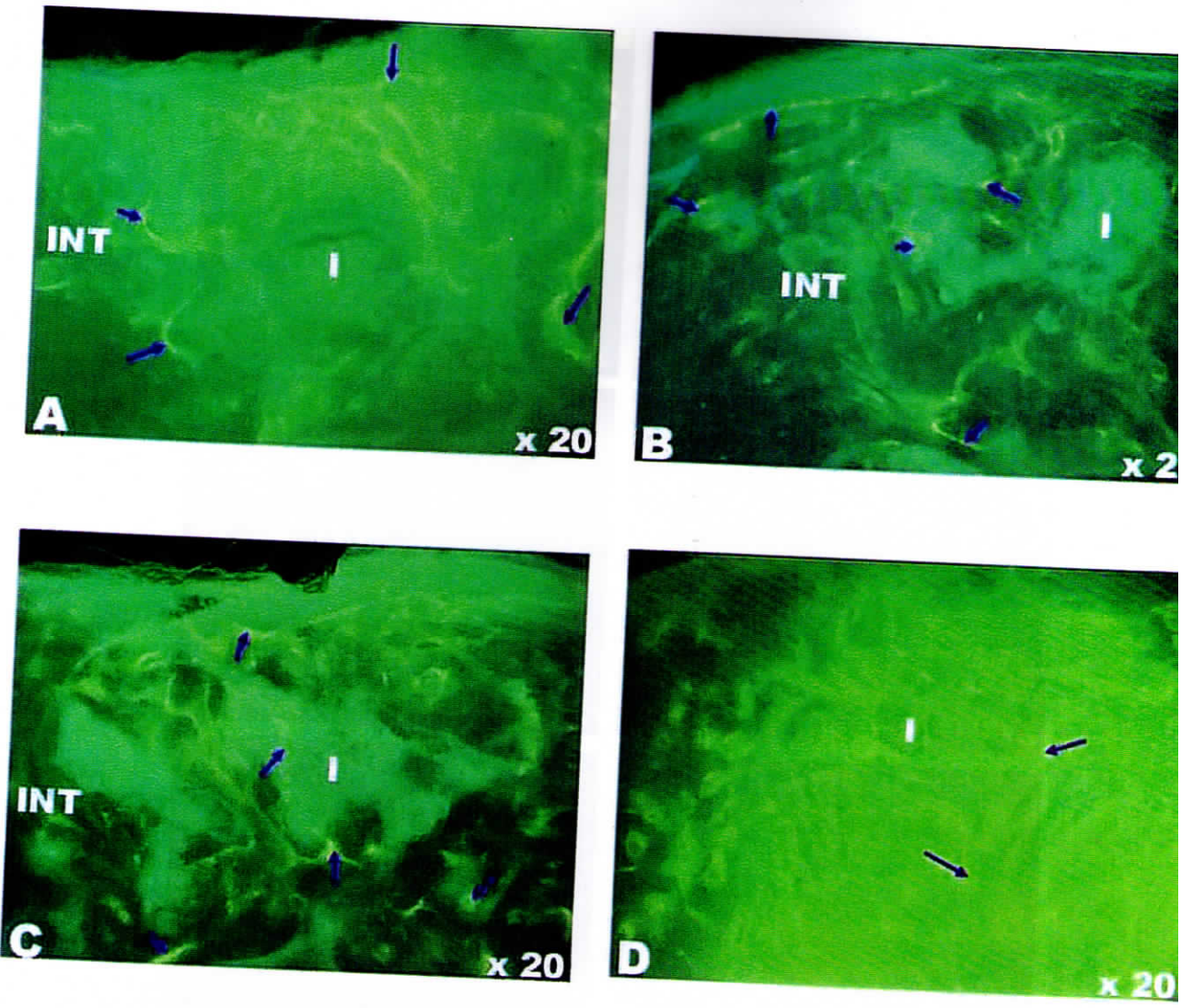

Figure -V-26

Fluorescence photomicrographs of the serial sections of FG coated HABGS granules implanted in rabbit tibia bone after 3 months. A - D - Tetracycline labeled, yellow fluorescence (arrows) around the implant (I) and in the interface (INT) denoting the mineralization pattern.

The new bone formed at the implant site was mature woven bone, the healing pattern in the cortical-periosteal implanted zone and the cortical-endosteal implanted zones were not the same. The cortical-endosteal implant zone was showing mature woven bone being transformed into lamellar type of bone, without any gaps and showed good osseointegration with the implant. Whereas, the cortical-periosteal implant zone showed mature woven bone with few gaps (Figure.V.27B). There were no gaps at the interface between the host bone and the newly formed bone. The pattern of bone formation at the interface was that of the mature woven bone, undergoing transformation into lamellar bone. The pores of the implant were completely replaced with mature woven bone.

HA after 6 months (Figure.V.28 G-L) was seen well integrated with the host bone without any gaps. The material seemed to be intact even after six months after implantation. Woven bone was completely replaced by lamellar bone in cortical-periosteal and cortical-endosteal zone. The periosteal zone of the implanted area showed good healing without any gap. Bone formation in the cortical-endosteal zone was compact without any gaps in the HA 3 month group. Whereas, HA- 6 months showed few gaps between the implant and the mature lamellar bone in the endosteal zone, lined by osteoblast-like cells. Well-developed Haversian system was observed around the implant in the cortical region. The pores of the implants in the cortical-endosteum and the cortical-periosteum zones showed mature woven bone.

HA coated with FG (Figure.V.29 A-F) showed better bone healing without any inflammatory reaction and fibrous encapsulation around the granules. The periosteum and the endosteal bone were completely closed without any visible gaps. Mature woven bone was seen formed within the defect.

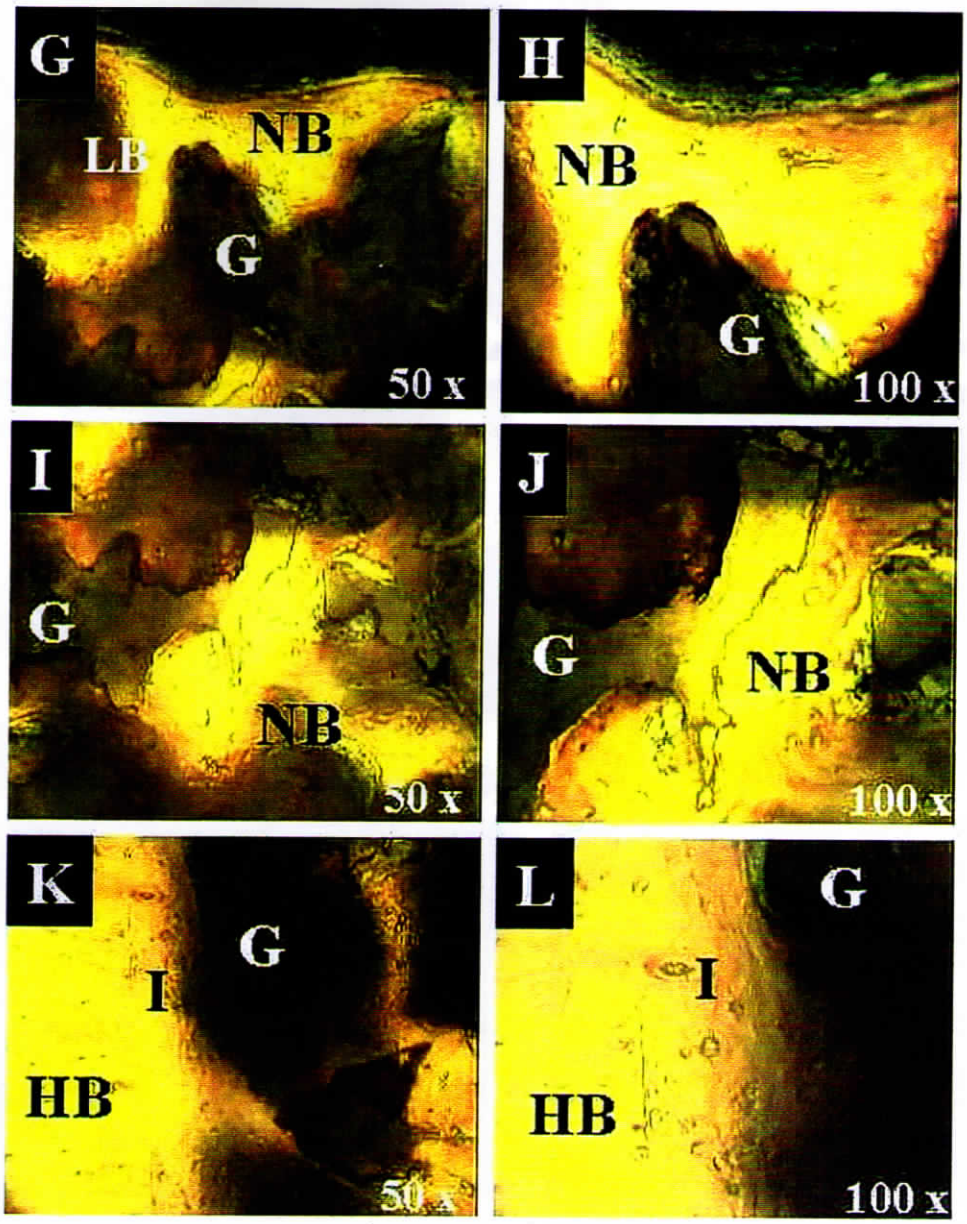

Figure -V-28

Photomicrographs of hydroxyapaite implanted in rabbit tibia bone after 6 months: G & H - the periosteal-cortical region of the Implant, where the implant is well integrated with matu lamellar bone (LB); I & J - the mid cortical region; K & L - th interface (I) between the host bone (HB) and the new bone (NB).

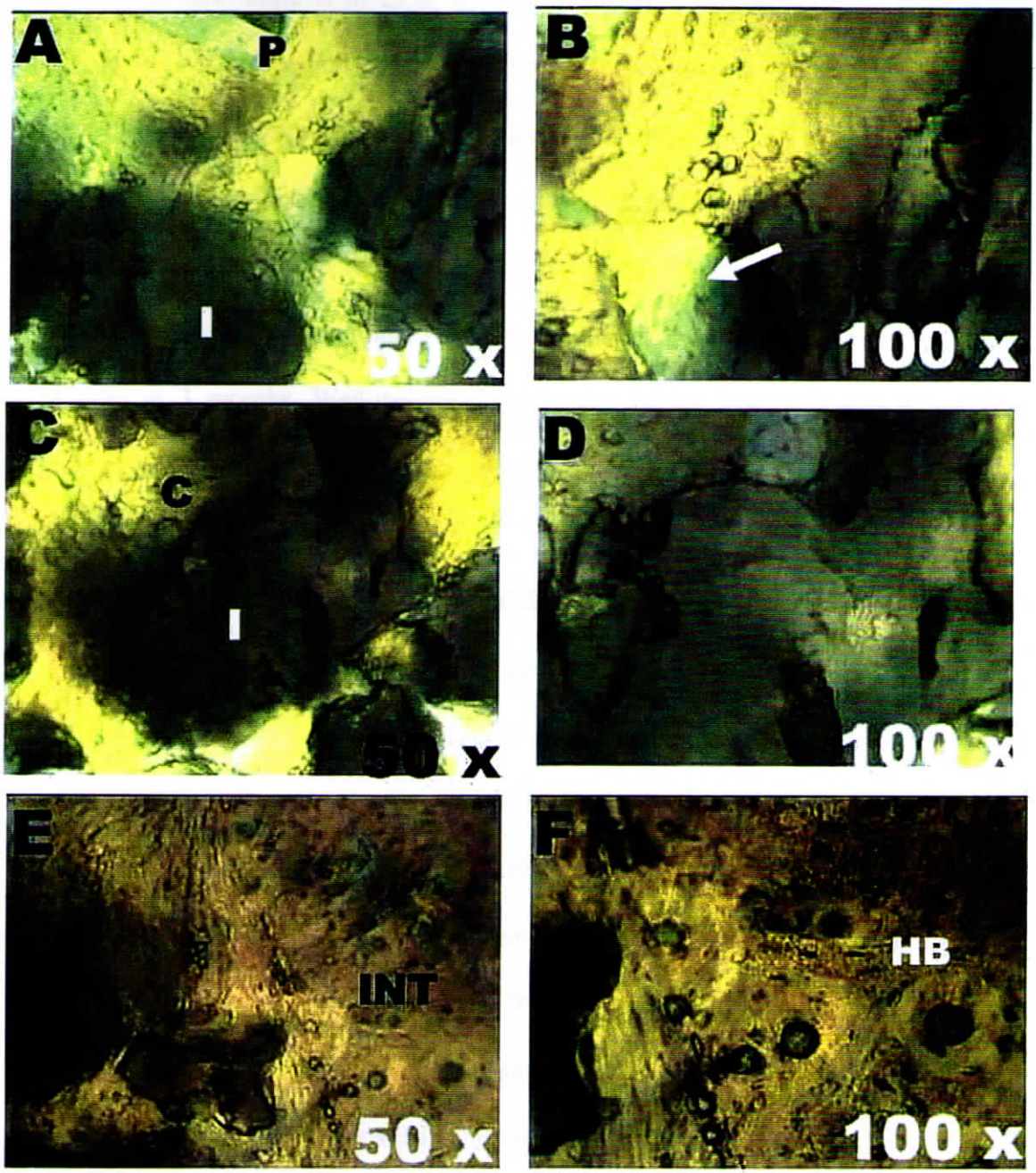

Figure -V-29

Photomicrographs of HA granules coated with FG (A-F) implanted in rabbit tibi bone after 3 months. The implant (I) and the new bone (NB) is well integrated, with few gaps of 50 - 80 micrometer (arrow) observed in the sub-periosteal reg (P), no such gaps were observed in the mid-cortical (C) and in the interface (IN of the host bone (HB) and the new bone(NB)

The new bone is in close apposition with the implant, without any visible gaps in the cortical region and also in the cortical-endosteal regions. But, few gaps were visible in the sub periosteal zone around the implant. There were no signs of any material degradation, or cracking of the implanted granules. Osteoblast and osteoblast-like cells were seen along with few fibroblast cells in the gaps that are yet to be replaced by the new bone. No foreign body giant cells or osteoclast cells could be seen at 3 months. Well-developed Haversian canals were observed around the implant site. The pattern of mature woven bone formed at 3 months was different from that of HA without FG.

V.2.7.2 Bioactive glass system (BGS)

BGS material after 3 months (Figure.V.30 A-F) was seen well integrated with the newly formed mature woven bone in the cortical-periosteal zone whereas, in the cortical-endosteal zone lamellar bone was observed with few gaps, lined by osteoblast cells and few mesenchymal/stromal cells. Well-developed Haversian canals were seen in the cortical-endosteal region. The material has undergone active degradation and the size of the implanted granules had reduced significantly. Interconnecting glossy canals (might be Volkmann's canals) were observed in the cortical-endosteal zone between the granules.

BGS granules after 6 months (Figure.V.31 A-F) were seen only as a shade, fully replaced by the mature lamellar bone in the mid-cortical region and cortical-endosteal regions. The BGS granules were well integrated with the newly formed lamellar bone in the sub periosteal region but, the material was intact and yet to be fully replaced by the new bone.

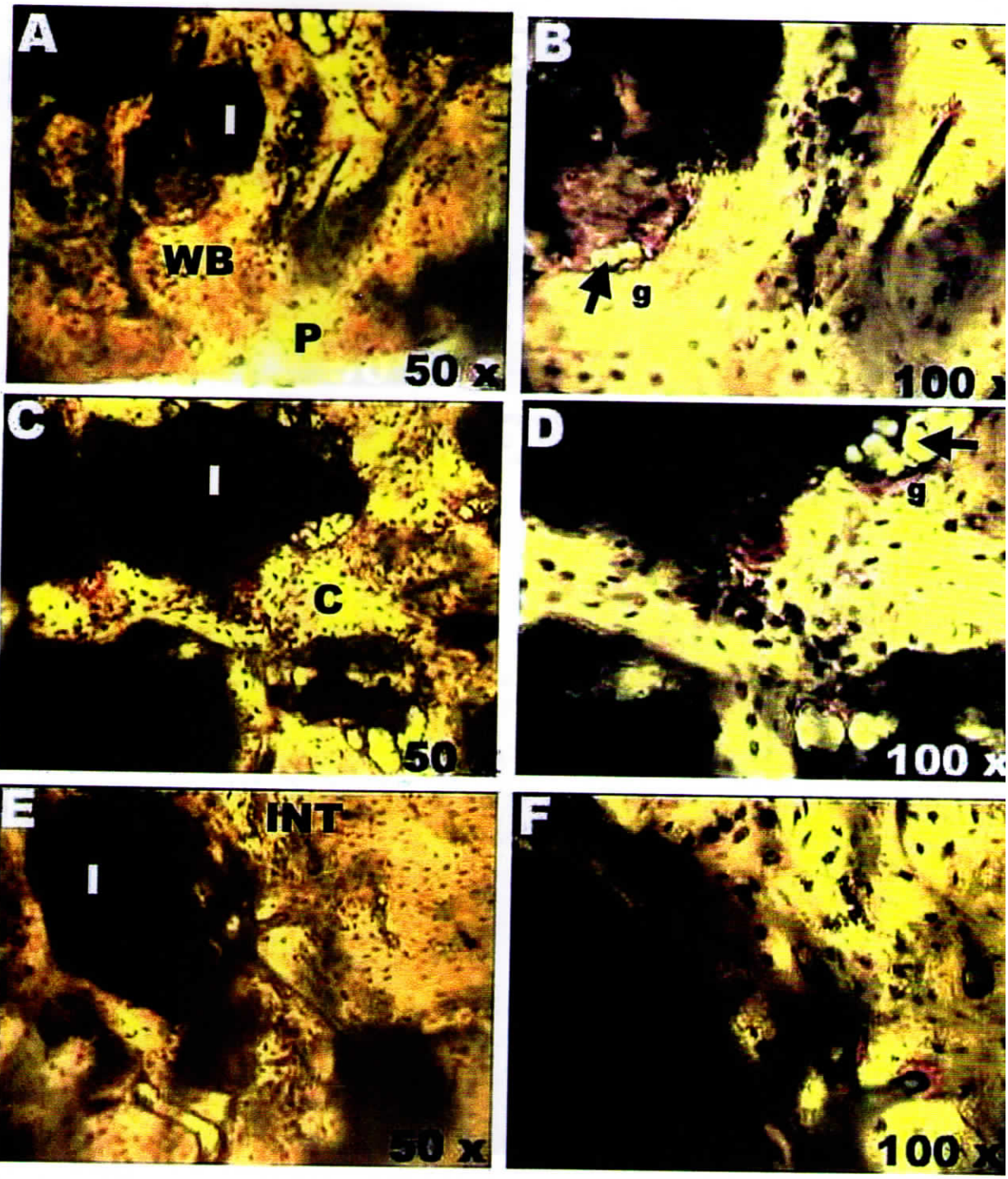

Figure -V-30

Photomicrographs of BGS implanted in rabbit tibia bone after 3 months. A &B - periosteal-cortical region (P) showed the implant (I) osseointegrated with the newly formed bone with few gaps (g) of approximately 10 to 20 micrometer. C & D - the mid-cortical (C) region with few gaps of 20 to 25 micrometer. E & F - the interface (INT) of the new bone and the host bone. Mature woven bone (WB) is seen after 3 months

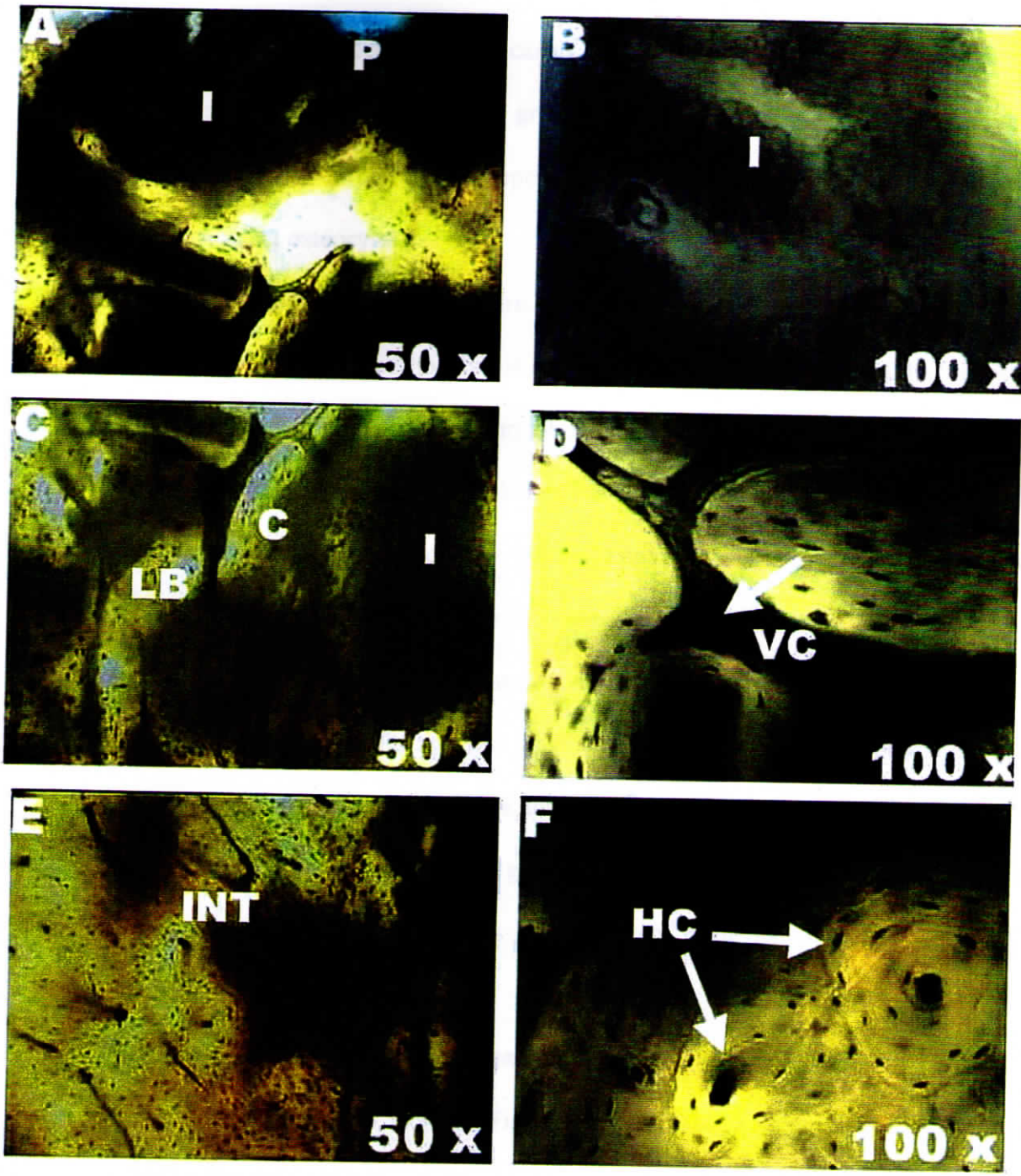

Figure -V-31

Photomicrographs of BGS implanted in rabbit tibia bone after 6 months: A & B - the periosteal-cortical region (P) where the implant is seen integrated with the newly formed bone without any gaps. C & D - the mid cortical region (C) where the implant is completely replaced by mature lamellar bone. E & F - the interface (INT) of the new bone and the host bone. Well developed Haversian canal (HC) and the Volkmann's canalwere seen aroun the implants

The interconnecting glossy canals (Figure.V.31 C & D) seen between the implant materials in BGS 3 months group were also seen in the six months groups. Haversian canals were well developed in the periosteal and endosteal zone with interconnecting osteocytes.

BGS coated with FG (Figure.V.32 A-F) showed good healing without any inflammatory reaction and no fibrous encapsulation was observed in all the sections. The endosteum and the periosteum of the defect are completely closed. Mature woven bone is seen around the implanted granules in the periosteum, cortical and the endosteal regions of the defect. The granules had cracked and disintegrated into small pieces showing signs of degradation visible with gaps (Figure.V.32 D) in between the granules in the cortical region as well as in the interface of the new bone and the host bone. Osteoblast cells and few mesenchymal/stromal cells were observed in the gaps between the implants and the mineralizing bone. No interconnecting glossy canals were observed between the granules as observed in uncoated BGS granules. The healing pattern of the bone is quite different from that of the uncoated BGS granules.

V.2.7.3 Triphasic bioactive glass composite system (HABGS)

HABGS after 3 months (Figure.V.33 A-F) showed good healing response without any inflammatory reaction or fibrous encapsulation. The periosteum and the endosteum of the bony defect were completely closed by 3 months enclosing the implant granules. Mature woven bone was seen around the implant granules. The implant material showed good osseointegration with the newly formed bone with few gaps in the periosteal and the cortical region of the defect. The gaps around the granules are lined with osteoblast cells and few mesenchymal/stromal cells. The material surface promoted new bone to grow on its surface.

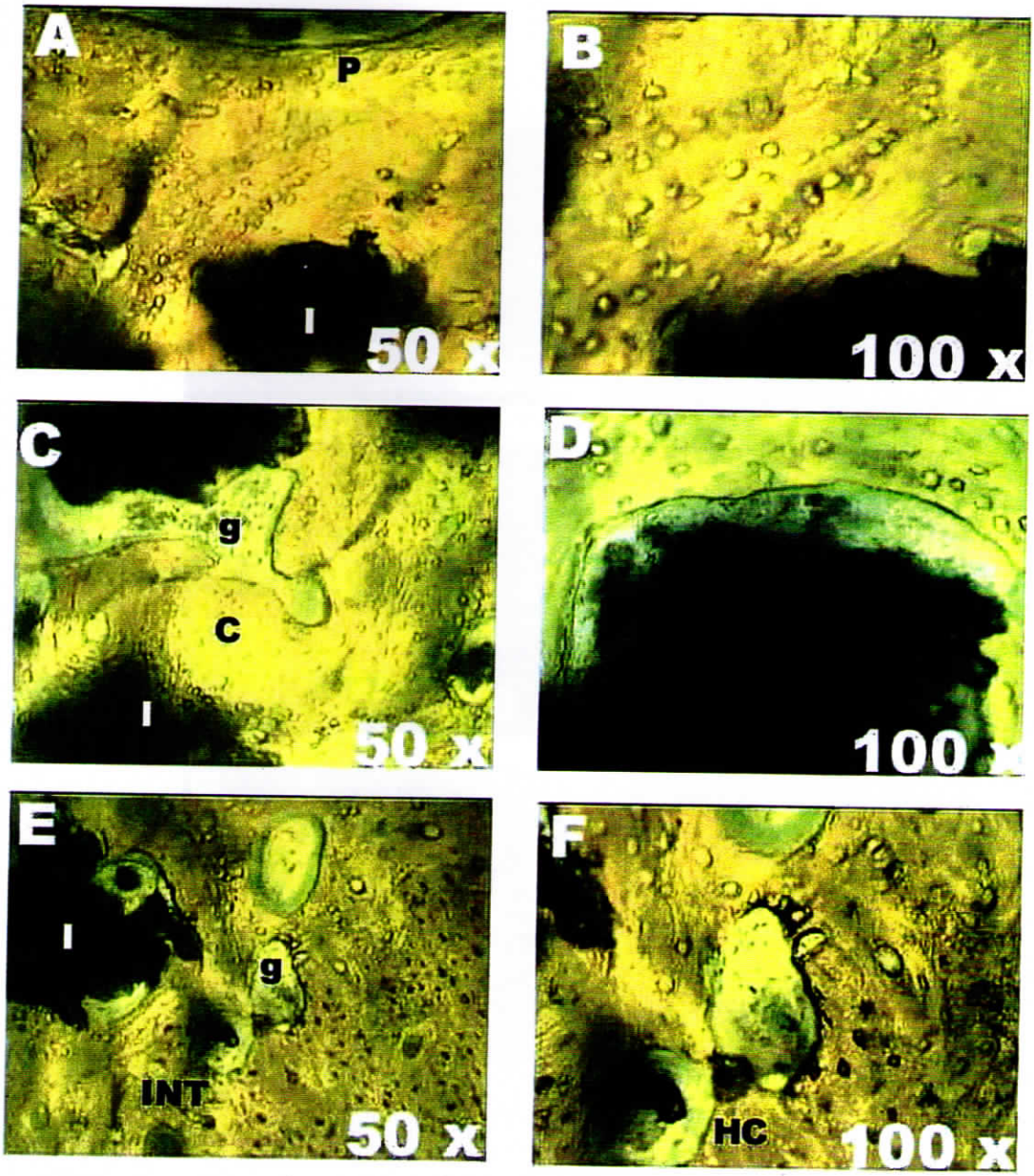

Figure -V-32

Photomicrographs of FG coated BGS granules implanted in rabbit tibia bone after 3 months. A &B - periosteal-cortical region where the implant (I) is seen osseointegrated with the new bone without any gaps (g), C & D - mid-cortical region (C) were gaps of approximately 40 to 50 micron width is seen between the implant and the new bone; E&F interface (INT) of the new bone and the host bone, the gap (g) is due to some remodeling process adjacent to the Haversian canal (HC)

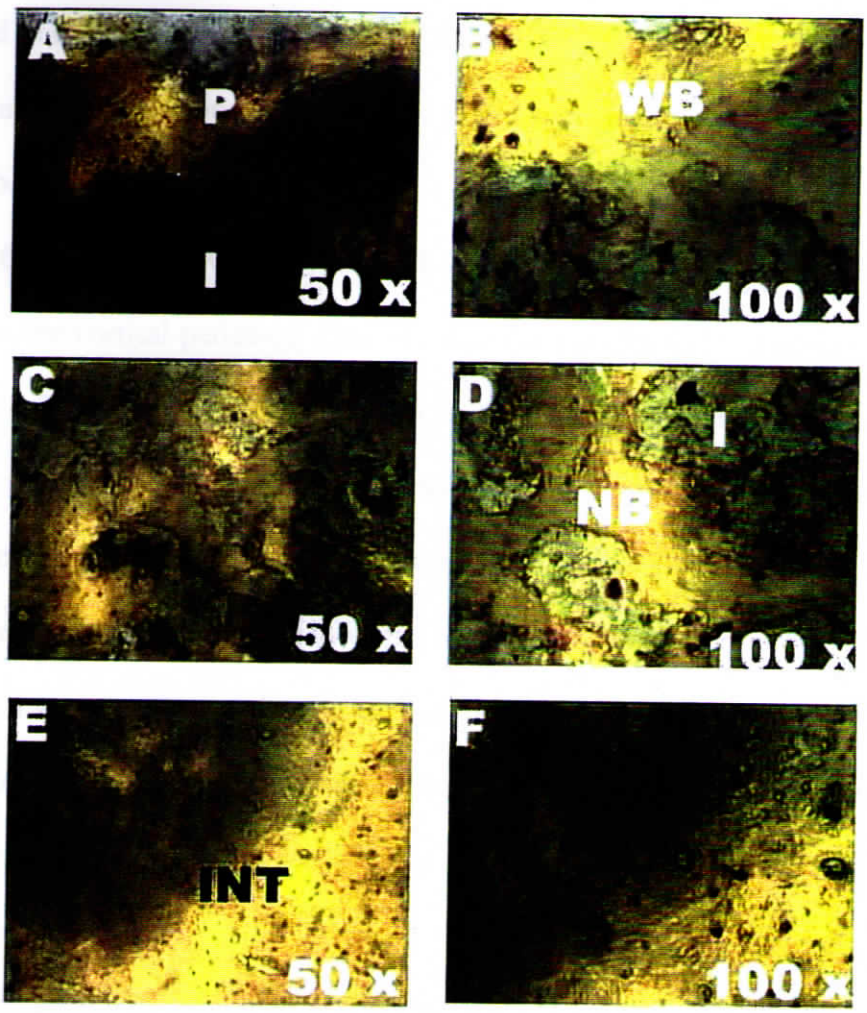

Figure -V-33

Photomicrographs of HABGS implanted in rabbit tibia bone 3 months: A & B - the periosteal region (P) where the implant (I) is seen well osseointegrated with the newly formed mature woven bone (WB), bone is also seen formed on the surface of the granules; C & D - the mid cortical region and E & F - the implant in the interface (I) between the host bone (HB) and the new bone (NB)

The interface between the host bone and the new bone was well integrated without any gaps. No osteoclast was observed in all the sections after 3 months. Newly formed Haversian canals were seen in the mid cortical region of the defect, but not seen in the cortical-periosteal region of the defect. No glossy interconnecting canals were observed between the granules.

After 6 months HABGS (Figure.V.34 A-F) implanted site showed mature woven bone in the cortical-periosteal zone and lamellar bone in the mid cortical and cortical-endosteal zone. Few gaps were seen in the cortical-periosteal zone to be replaced by new bone, lined by mesenchymal/stromal cells and osteoblast cells. Mature osteocytes and osteoid cement lines were seen on the material surface. and around the implant granules. Haversian canals were lined by endothelial cells inside and surrounded by interconnected osteocytes in the cortical-periosteal and cortical-endosteal zones and at the interface of the host bone and the new bone. Glossy interconnecting channels (may be Volkmann's canals) were observed between the granules after 6 months.

No inflammatory reaction was observed with FG coated HABGS granules after 3 months (Figure.V.35 A-F). Healing of the bone is normal. The periosteum and the endosteal region of the defect were completely closed by mature woven bone. The implanted granules had disintegrated into small pieces, infiltrated by mesenchymal/stromal cells and osteoblast cells lining the ridges of the granules and the newly formed bone (Figure.V.35 A & B). The newly formed bone was not in close apposition with implants in the cortical-periosteal region and the mid cortical region. Whereas, in the cortical-endosteal region the implants were seen closely apposed to the newly formed bone. Thick osteoid cement lines were seen around the implant granules in the mid cortical region.

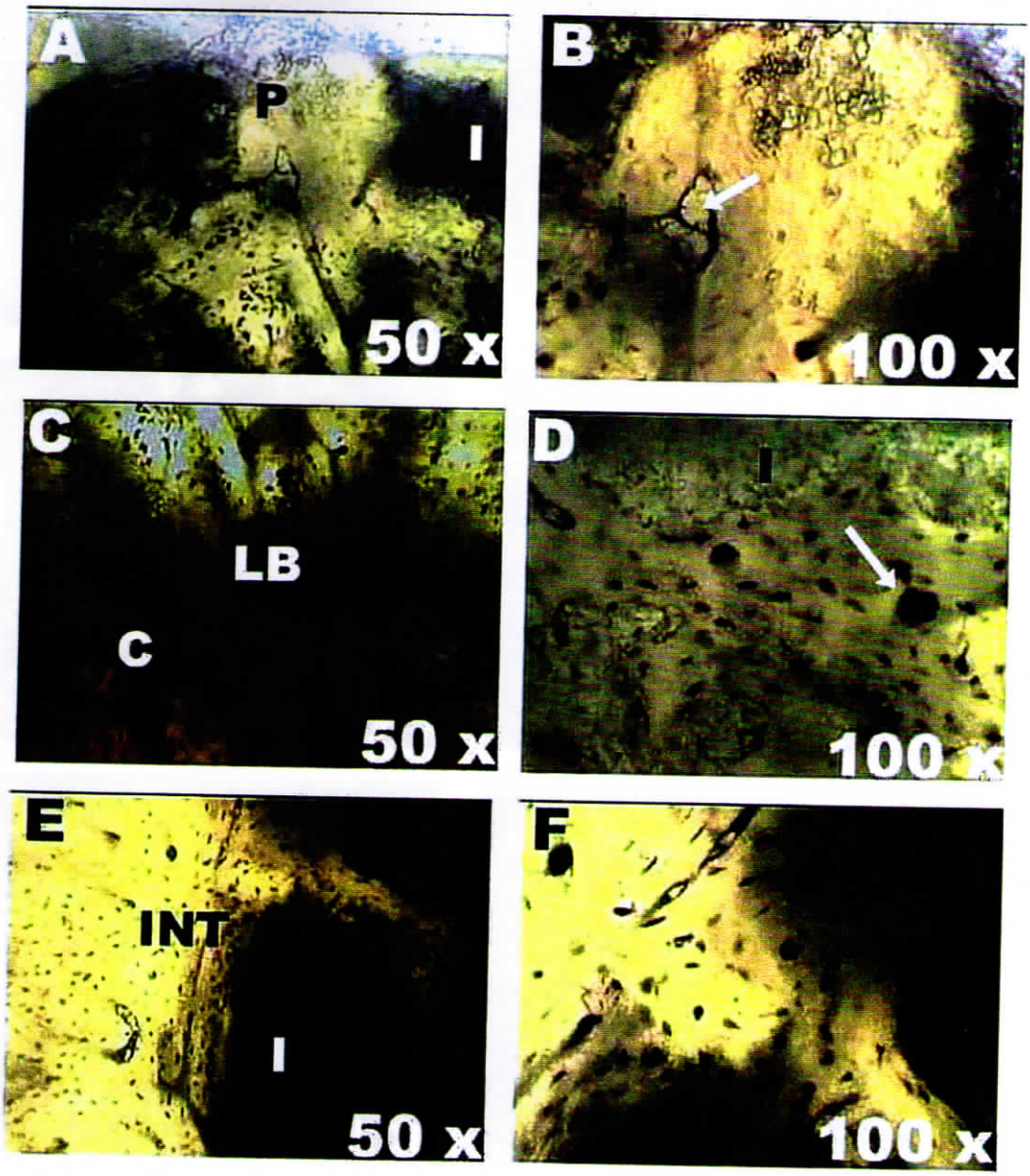

Figure -V-34

Photomicrographs of HABGS implanted in rabbit tibia bone after 6 months: A & B - implant in the sub-periosteal (P) region, in B the arrow denotes the gap within the lamellar bone (LB) undergoing remodeling; C & D - implant in the mid cortical (C) region, where the implant (I) is well osseointegrated with the new bone without any visible gaps, the arrow in D denotes the bone formed on the material surface showing Haversian canal; E & F - the implant (I) in the interface (INT) of the host bone and the newly formed bone.

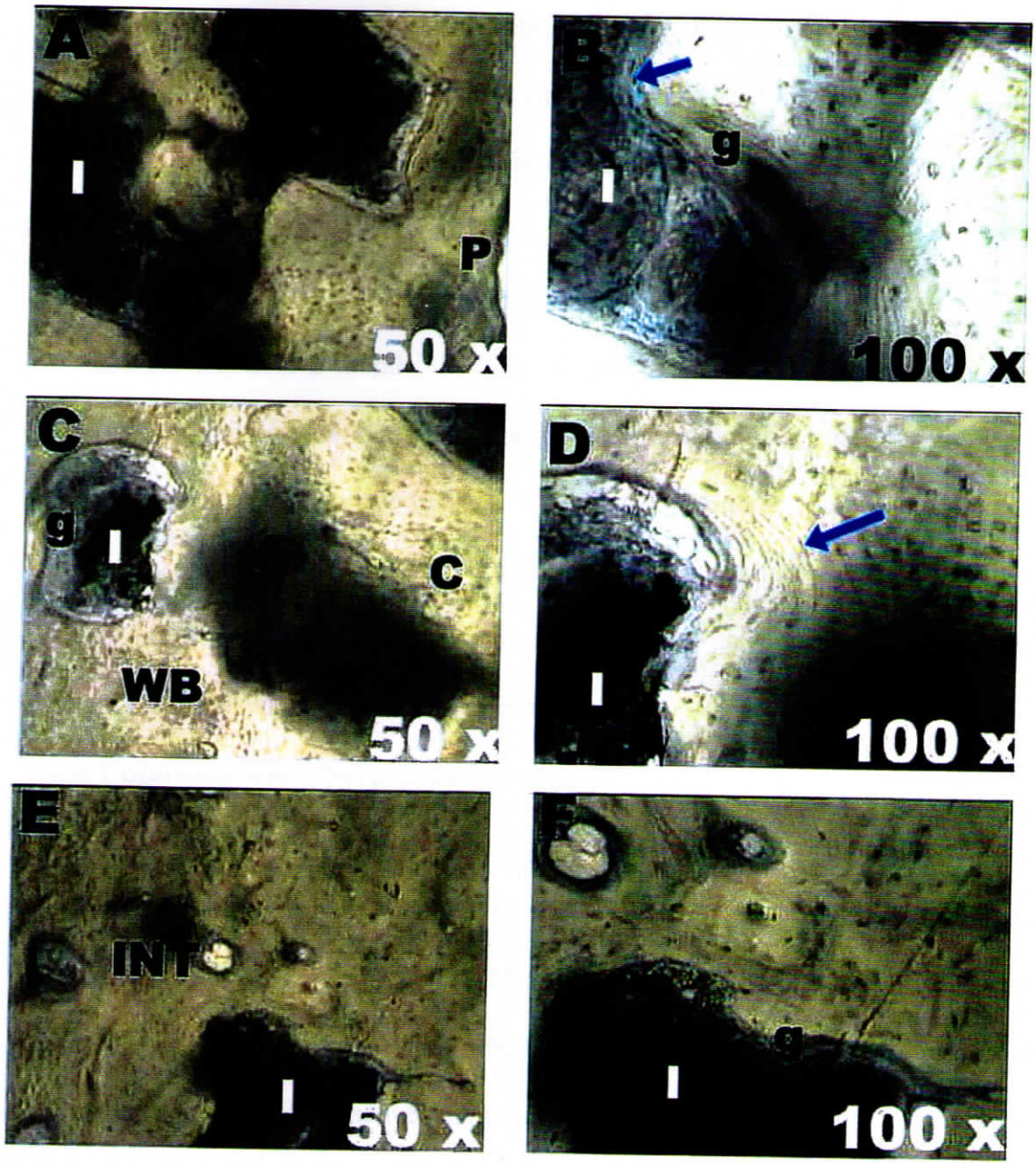

Figure -V-35

Photomicrographs of FG coated HABGS granules implanted in rabbit tibia bone after 3 months: A & B - subperiosteal region (P), the implant is seen not closely apposed with new bone and large gaps (g) of 20 -40 micron could be seen, lined by osteoblast cells (arrow); C & D -the mid cortical region (C), where mature woven bone (WB) seen around the implant, cement lines could be seen (arrow) around the implant; E& F- the implant in the interface (I), with few gaps (g) .

Mature woven bone is remodeled into lamellar bone in the cortical-endosteum and the mid-cortical regions of the defect. Well-developed Haversian canals were seen around the implant granules, lined internally by endothelial cells and externally by mature osteocytes.

In sham operated animals where the defect was without any implants, showed a delayed healing until 2 months, but after 3 months the defect was almost closed with few gaps. Fibrin glue alone implanted in the defect showed better healing with good vascularization (Figure.V.36 A, B & C) and by 3 months the healing of the defect was complete with few gaps (Figure.V.36 A). Mature woven bone was observed after 3 months with and without FG. The mineralization pattern was different for FG filled defects and for defects without FG (Figure.V.36 D).

V.2.8 Polarized Microscopic Observations

The polarized microscopic observations revealed a unique pattern of polarization of collagen within the defect and around the defect with HA, BGS and HABGS granules after 3 and 6 months (Figure.V.37 A – I). FG coated HA, BGS and HABGS granules after 3 months also showed the same polarization pattern as that of uncoated granules. The active mineralizing zones polarized in yellow colour (Figure.V.38 A-C). The yellow polarization was observed in close apposition with the granules where the surface of the granules is flat and perpendicular to the host bone. The polarization (yellow) at the interface between the host bone and the new bone was more in the proximal end rather than the distal end of the tibial bone. Small polarizing collagen fibers were seen perpendicular to the thick bundles of polarizing collagen fibers around the curves and pores of the granules. The active mineralized areas of the bone are shown in blue colour (Figure.V.38 - schematic diagram).

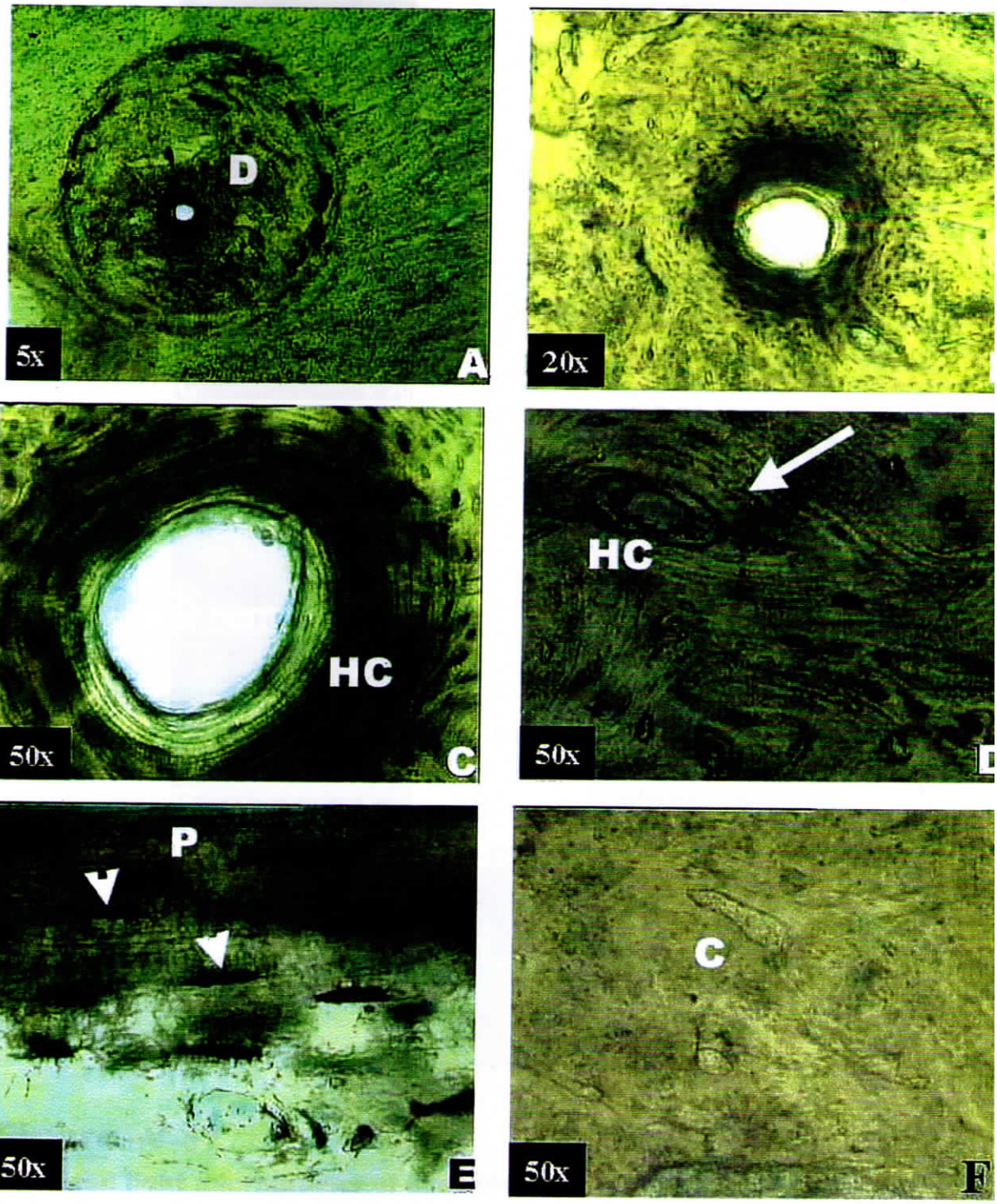

Figure - V-36

Photomicrographs of longitudinal section, A-C and cross section D-F, of rab tibia bone filled with FG alone after 3 months. Defect (D) is completely heal without any gap. A - C shows a central Haversian cannal (HC); D - a "loop" r eralisation pattern around the Haversian cannal (HC); E - the periosteum (P and the arrows denote the osteocytes arranged perpendicular to the mid c ical bone ; F - mid cortical region (C). No gaps were observed in the defect.

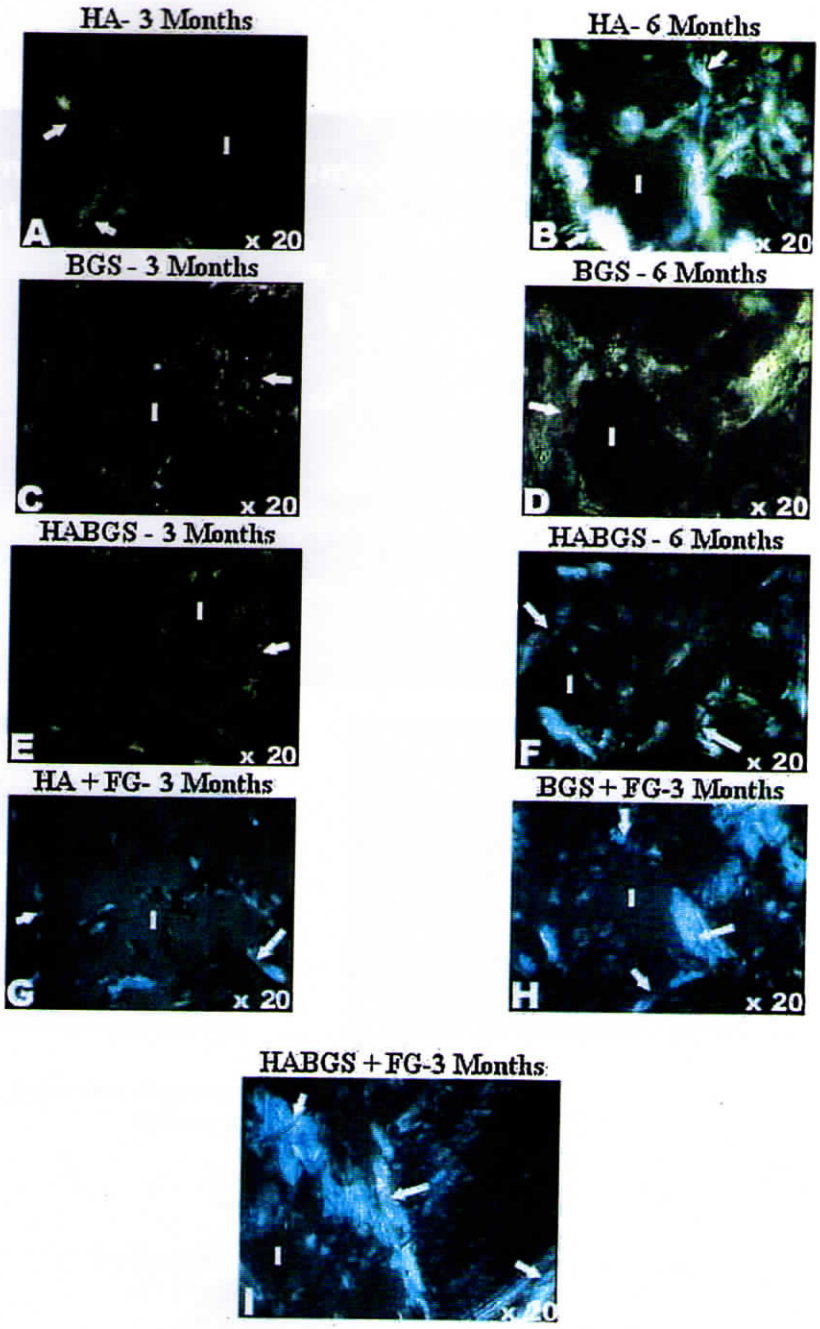

Figure -V-37

Polarized light micrographs of uncoated and FG coated HA, BGS and HABGS granules implanted in rabbit tibia bone after 3 and 6 months. A,C & E- HA, BGS and HABGS after 3 months; B, D & F-HA, BGS and HABGSafter 6 months;G, H & I - HA, BGS and HABGS coated with FG. after 3 months.
The arrow denotes the polarizing area around the implant (I), the the intensity of the polarizing area is high around the implant and in the interface of the host bone and new bone with HA, BGS and HABGS after 6 months and also with FG coated HA, BGS and HABGS after 3 months.

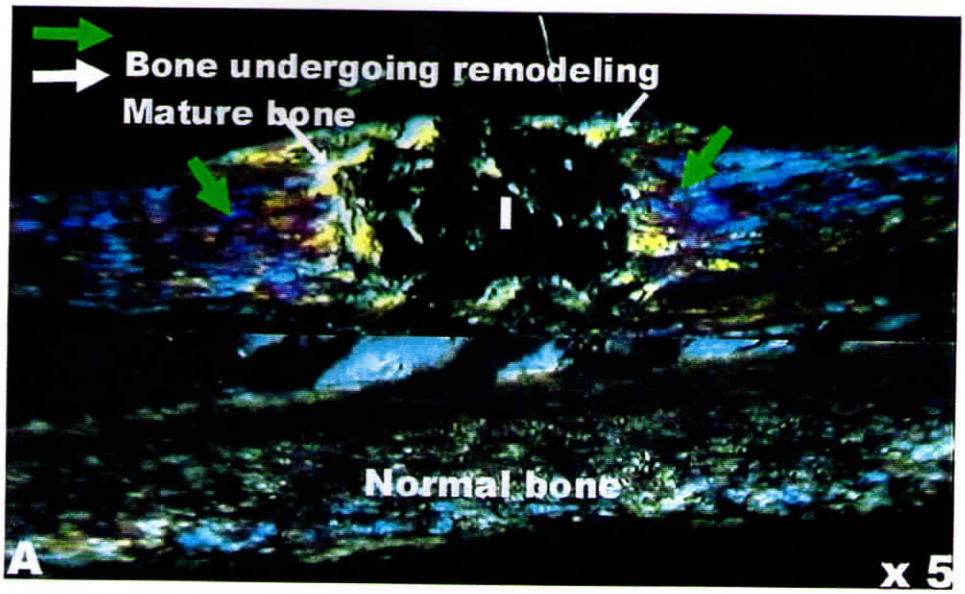

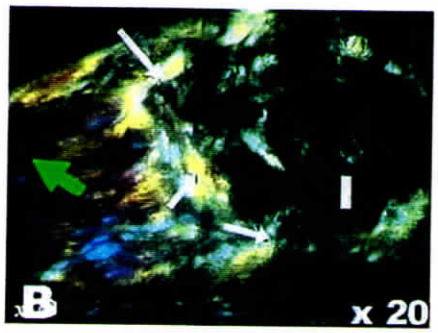

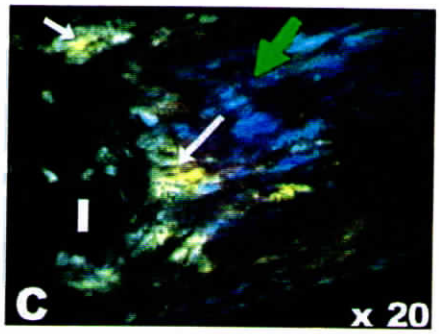

Schematic diagram showing the polarizing zones in bone after implantation

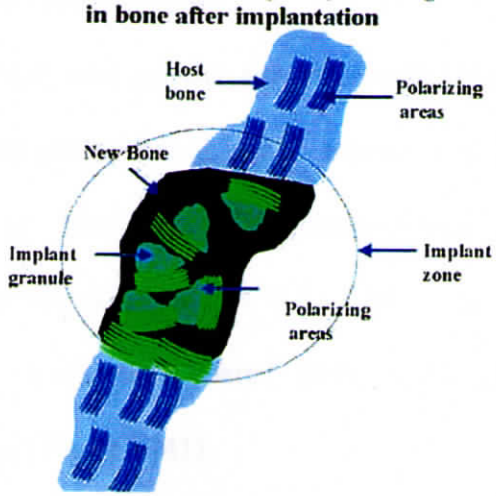

Figure -V-38

Polarized light micrographs of rabbit tibia bone with an implant: A, B & C - show bone undergoing remodeling (white arrow) and mature bone (green arrow).

The schematic diagram shows the orientation of collagen bundles around the implant where the mineralized collagen around the implant are arranged perpendicular to the normal bone collagen

V.2.9 BIOCHEMICAL ANALYSIS

V.2.9.1 Calcium

The calcium level in the serum did not show much variation after implantation, when compared to the serum calcium values before implantation with HA after 3 and 6 months and also with FG coated HA after 3 months. BGS uncoated and FG coated samples did not reveal any significant change in the serum calcium level before and after 3 and 6 months. HABGS implanted after 3 months showed a significant difference of $P < 0.001$. Whereas, the 6 months and 3 months FG coated HABGS groups did not reveal any significant change in serum calcium level after implantation (Figure.V.39)

V.2.9.2 Phosphorous

The serum phosphorous levels of uncoated and FG coated HA, BGS and HABGS did not show any statistically significant change for serum protein before implantation and after 3 and 6 months implantation (Figure.V 40).

V.2.9.3Alkaline Phosphatase

Serum ALP was normal for HA and HABGS uncoated and FG coated implanted animals even after 3 and 6 months and did not show any statistically significant change. Uncoated BGS granules after 3 months showed significant change in the serum ALP of $P < 0.01$. But, 6 months uncoated BGS implanted animals and 3 months FG coated BGS implanted animals did not show any significant change (Figure.V.41).

V.2.9.4 Acid Phosphatase

Serum ACP was normal for uncoated HA, BGS and HABGS animals and FG coated granules even after 3 and 6 months. Statistically no significant change was observed for serum ACP before and after implantation (Figure.V.42).

V.2.9.5 Protein

The serum protein of uncoated and FG coated HA implanted animals did not show any significant change after 3 and 6 months. The serum protein of uncoated BGS after 3 months showed statistically significant change of $P< 0.01$. But, no significant change in serum protein content was observed for uncoated BGS after 6 months and FG coated BGS after 3 months. Serum protein of uncoated HABGS and FG coated HABGS granules did not reveal any significant change after 3 and 6 months (Figure.V.43).

V.2.9.6 Creatinine

Serum creatinine for uncoated and FG coated HA, BGS and HABGS granules implanted in rabbit tibia showed normal serum and urine creatinine. Statistically no significant change was observed for serum creatinine before and after implantation. (Figure.V.44).

V.2.9.7 Radioimmunoassay (RIA)

Serum PTH and calcitonin in rabbit implanted with uncoated and FG coated HA, BGS and HABGS granules after 3 and 6 months did not show any statistically significant change (Table.V.7)

Table V.7

Material	3-Months		6-Months		3-Months-FG	
	PTH	CT	PTH	CT	PTH	CT
Sham	12.35 ± 2.55	157.5 ± 39.61	Not observed			
HA	38.55 ± 8.57	123.7 ± 32.4	21.52 ± 7.99	149 ± 32.1	22.62 ± 6.31	159.7 ± 17.09
BGS	25.47 ± 10.88	109 ± 22.69	21.65 ± 5.56	75.92 ± 16.9	15.05 ± 0.41	154.7 ± 9.96
HABGS	12.82 ± 1.24	64.6 ± 17.29	21.22 ± 3.87	97.18 ± 34.9	15.42 ± 0.20	110.2 ± 15.22

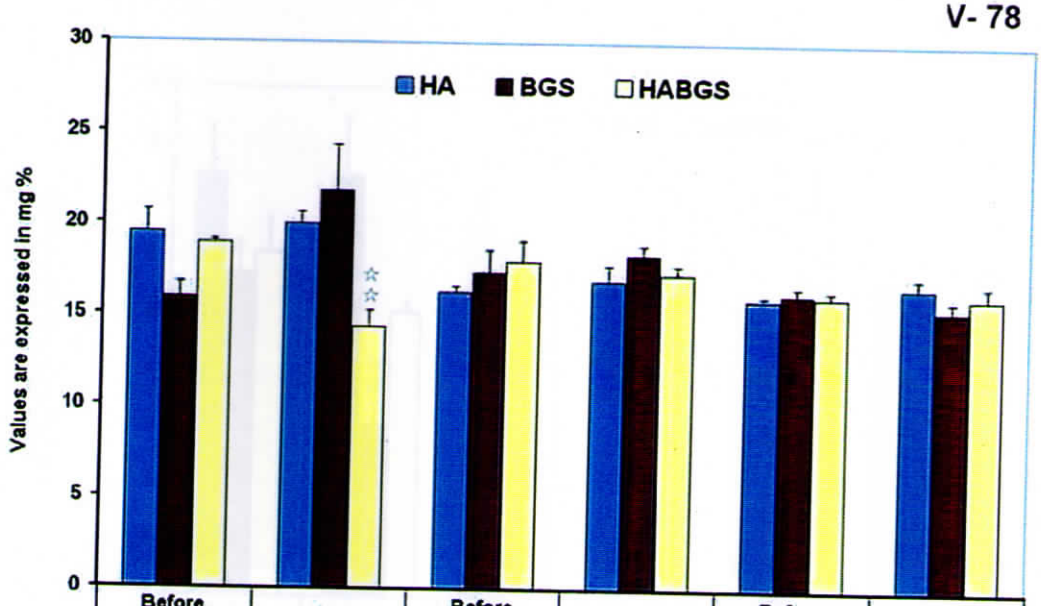

	Before Implantation 3 M	After Implantaion	Before Implantation FG-3 M	After Implantation	Before Implantation 6 M	After Implantation
HA	19.51	19.95	16.27	16.93	15.93	16.67
BGS	15.94	21.84	17.38	18.32	16.2	15.38
HABGS	18.94	14.37	18.03	17.32	16.12	16.08

Figure -V-39

Serum calcium in rabbit implanted with bioactive ceramic granules in tibia bone before and after 3 & 6 months. Significant change was observed in rabbit implanted with uncoated HABGS granules after 3 months(=P < 0.01). No significant change was observed in any other groups**

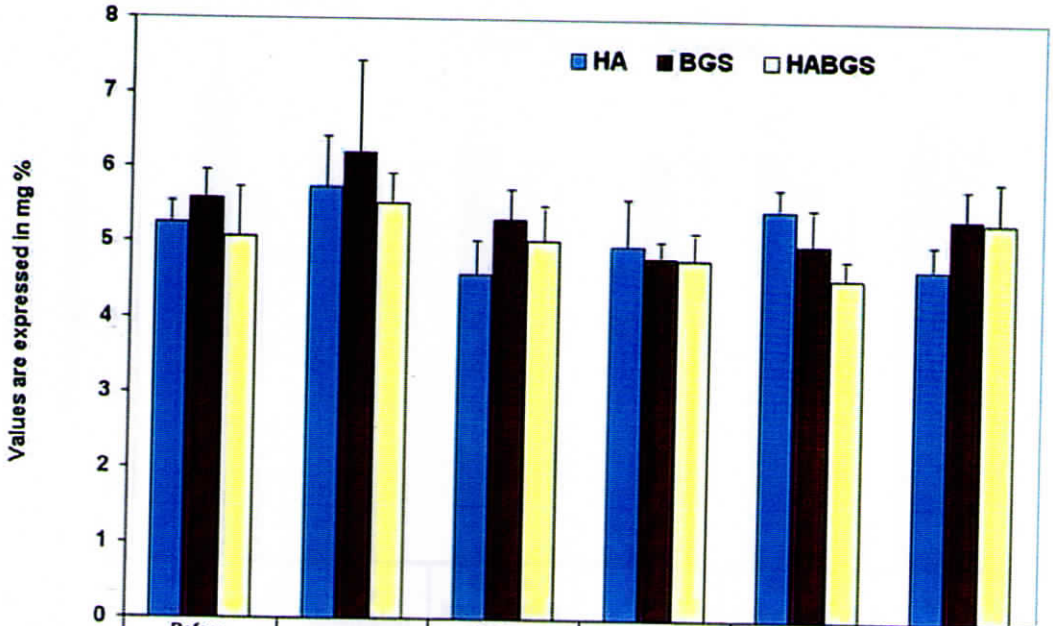

	Before Implantation 3 M	After Implantaion	Before Implantation FG-3 M	After Implantation	Before Implantation 6 M	After Implantation
HA	5.26	5.75	4.58	4.97	5.46	4.69
BGS	5.59	6.22	5.33	4.82	5.01	5.38
HABGS	5.08	5.53	5.04	4.8	4.56	5.32

Figure -V-40

Serum phosphorous in rabbit implanted with bioactive ceramics granules in tibia bone before and after 3 & 6 months. No significant change was observed in all the groups.

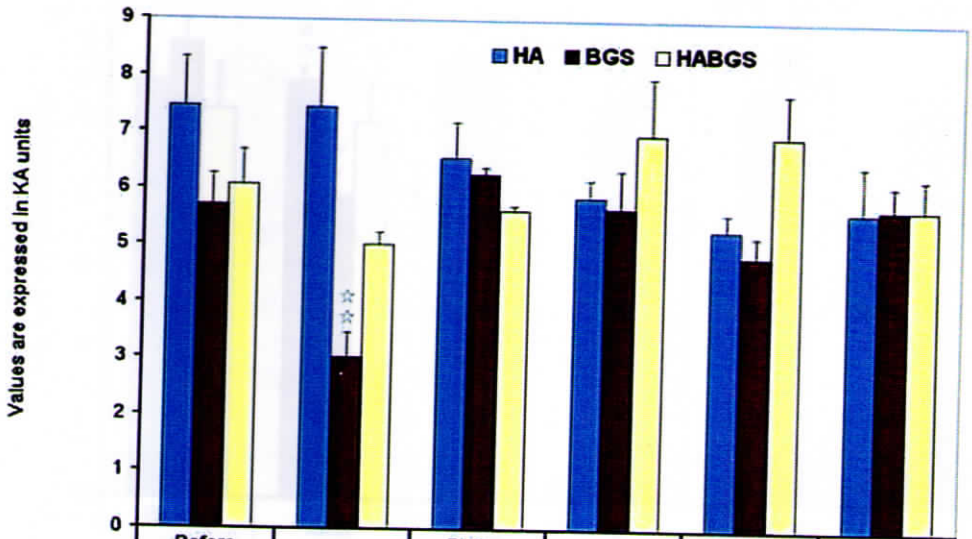

	Before Implantation 3 M	After Implantaion	Before Implantation FG-3 M	After Implantation	Before Implantation 6 M	After Implantation
HA	7.46	7.45	6.56	5.86	5.29	5.64
BGS	5.72	3.02	6.26	5.67	4.83	5.69
HABGS	6.08	5.02	5.63	6.99	6.95	5.7

Figure -V-41

Alkaline phosphatase activity in rabbit serum implanted with bioacti ceramics cgranules in rabbit tibia bone before and after 3 & 6 month Significant change in the BGS implanted group was observed after 3 months(= P < 0.01), but no significant change was observed in ot groups.**

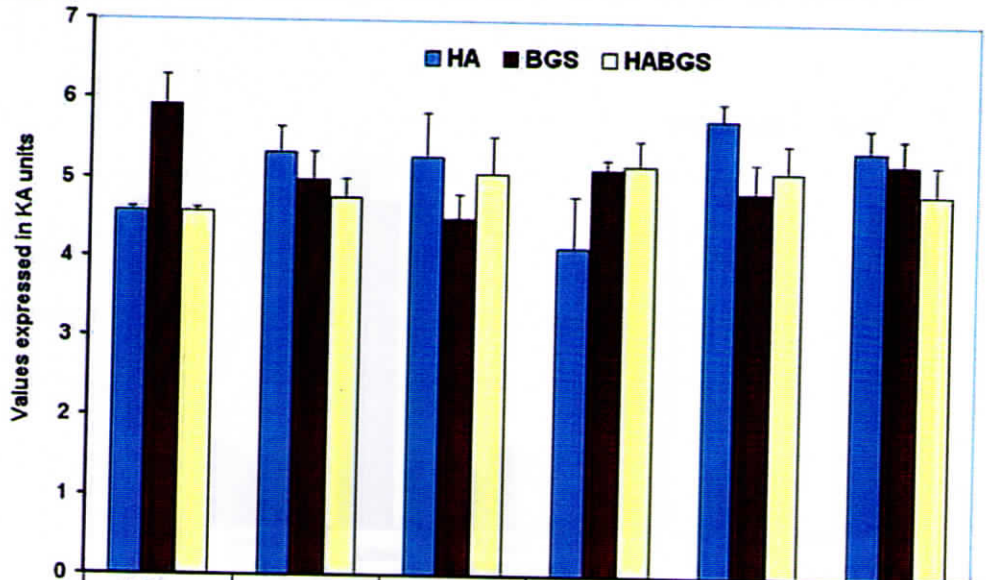

	Before Implantation 3 M	After Implantaion	Before Implantation FG-3 M	After Implantation	Before Implantation 6 M	After Implantation
HA	4.58	5.33	5.29	4.15	5.78	5.4
BGS	5.93	5	4.51	5.14	4.86	5.24
HABGS	4.58	4.76	5.07	5.19	5.12	4.87

Figure -V-42

Acid phosphatase activity in rabbit serum implanted with bioactive ceramics in rabbit tibia bone before and after 3 & 6 months. No significant change was observed in any of the groups

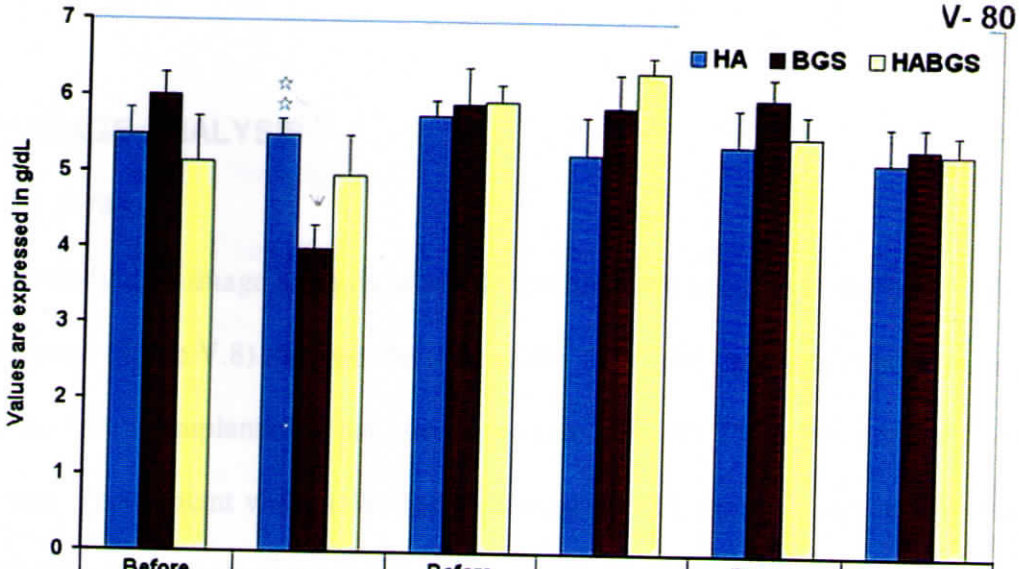

	Before Implantation 3 M	After Implantaion	Before Implantation FG-3 M	After Implantation	Before Implantation 6 M	After Implantation
HA	5.49	5.49	5.76	5.25	5.4	5.19
BGS	6.02	4	5.91	5.88	6.02	5.37
HABGS	5.14	4.96	5.94	6.35	5.52	5.31

Figure -V-43

Serum protein in rabbit implanted with bioactive ceramic granules in tibia bone before and after 3 and 6 months. Significant change in the HA (3 months) implanted gropup was observed (= P < 0.01) but no significant change was observed in other groups**

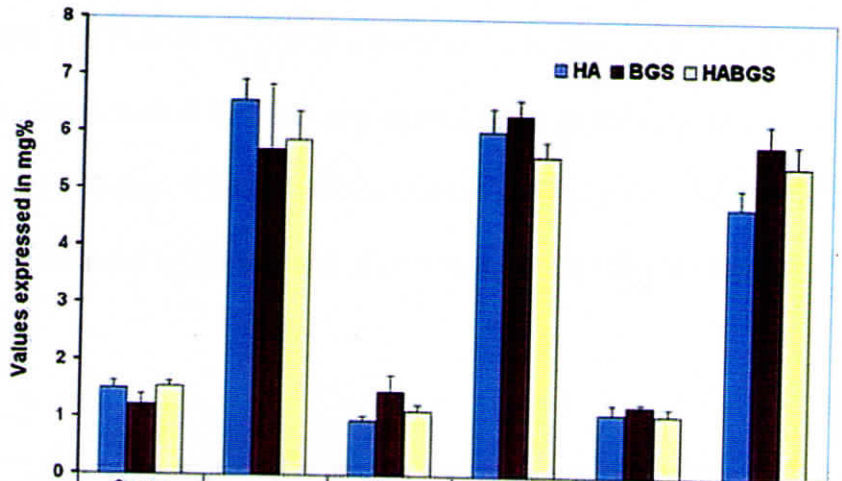

	Serum 3 M	Urine	Serum FG-3 M	Urine	Serum 6 M	Urine
HA	1.51	6.57	0.97	6.03	1.11	4.74
BGS	1.22	5.69	1.48	6.33	1.25	5.83
HABGS	1.54	5.87	1.13	5.6	1.09	5.48

Creatinine level in serum and urine after implantaion

Figure -V-44

Creatinine activity in rabbit serum and urine implanted with bioactive ceramic granules in rabbit tibia bone after 3 & 6 months

V.2.10 IMAGE ANALYSIS

V.2.10.1 X-ray

Quantitative image analysis of the X-ray (based on opacity) of the rabbit tibia cortical bone (Table.V.8) showed the total width (TW) for the cortical bone as 6.6 mm at the time of implantation but after 3 and 6 months the TW of the cortical bone was 6 mm. The implant width (IW) had increased for HA from 2.2 mm at zero day (immediately after implantation) to 2.9 mm after 3 months and increased further to 3.2 mm after 6 months.

The TW of the BGS implanted cortical bone at zero day was 6 mm but after 3 months the TW increased to 6.3 mm and retained the original cortical thickness of 6 mm even after 6 months. The IW of the BGS at zero day was 3 mm and after 3 months the IW remained same at 3 mm and after 6 months the IW reduced to 2.8 mm.

The TW of HABGS implanted cortical bone at zero day was 5.5 mm but after 3 months the TW increased to 7 mm and again after 6 months the TW of the cortical bone decreased to 6 mm. The IW of HABGS at zero day was 3.2 mm and after 3 months the IW reduced to 2.5 mm and after 6 months a moderate increase of 2.7 mm was observed.

Table V.8

Material	TW Zero day (mm)	IW Zero day (mm)	TW 3 Months (mm)	IW 3 Months (mm)	TW 6 Months (mm)	IW 6 Months (mm)
HA	6.6	2.2	6	2.9	6	3.2
BGS	6	3	6.3	3	6	2.8
HABGS	5.5	3.2	7	2.5	6	2.7

V.2.10.2 Implant Vs New bone

The amount of new bone formed with respect to the implants will decide on the quality of the implant, which is directly proportional to the bioactive nature of the implant. Image analysis of the implant site was carried out to quantify the amount of new bone formed with respect to uncoated HA, BGS and HABGS granules at two different times (3 and 6 months), and FG coated HA, BGS and HABGS granules after 3 months (Table.V.9).

The cortical thickness of the implants and the size of the granules directly correlated with the amount of new bone around the implant. Uncoated HA after 3 months revealed 71.4 % of bone for 28.6 % of implant, after 6 months the new bone around the implant was 67.9 % for 32.1% of implant. FG coated HA after 3 months showed 70.23 % new bone for 29.77 % of implant.

BGS implanted in cortical bone revealed 84.2 % of bone for 15.8 % of implant after 3 months, and after 6 months the percentage of new bone formed was 80.5 % for 19.5 % implant. FG coated BGS granules showed 72 % of new bone for 28 % implant after 3 months.

HABGS after 3 months showed 72.1 % of new bone for 27.9 % of implant. The 6 months group showed 74.5 % of new bone for 25.5 % of implant. FG coated HABGS granules showed 65.2 % of new bone for 34.8 % of implant.

Table V.9

Group	Granule Size (μm)	Percentage (%)		Cortical Thickness (mm)
		Bone	Implant	
HA-3M	168.2 ± 17.9	71.4	28.6	1.221 ± 0.034
HA-6M	246.2 ± 18.4	67.9	32.1	1.322 ± 0.029
HA +FG –3M	184 ± 7.50	70.23	29.77	1.242 ± 0.029
BGS-3M	169.8 ± 11.47	84.2	15.8	1.728 ± 0.09
BGS-6M	150.2 ± 15.6	80.5	19.5	0.923 ± 0.01
BGS + FG –3M	162 ± 13.6	72	28	1.120 ± 0.043
HABGS-3M	172 ± 8.62	72.1	27.9	1.098 ± 0.015
HABGS-6M	154 ± 13.30	74.5	25.5	1.015 ± 0.024
HABGS + FG –3M	158 ± 11.16	65.2	34.8	1.117 ± 0.056

V.2.10.3 Osteocytes

Osteocytes in the mineralized matrix were measured to compare the size of the osteocytes in the newly mineralized bone to that of the osteocytes in mature mineralized matrix (Table.V.10). Statistically significant change $P < 0.05$ in the size of osteocytes was observed in sham (defect alone without the implant) with FG. Whereas, no significant change in the size of the osteocyte was observed with sham alone. FG coated HA showed significant change of $P < 0.01$. Whereas, uncoated HA did not show any significant change in the size even after 3 and 6 months. Uncoated and FG coated BGS implant site showed significant difference of $P < 0.10$ after 3 months. The 3 and 6 months group implanted with uncoated HABGS did not show any significant change in the size of the osteocyte. Whereas, FG coated HABGS implanted site showed a significant change of $P < 0.001$ after 3 months.

Table V.10

Group	Osteocytes (μm)	
	Cortical (Implanted zone)	Interface (Host and New Bone)
Sham without FG- 3M	12.46 ± 0.42	12.43 ± 0.43
Sham with FG - 3M	9.86 ± 0.184	10.76 ± 0.290
BGS-3M	12.56 ± 0.30	11.6 ± 0.414
BGS-6M	11.9 ± 0.44	11.36 ± 0.36
BGS with FG –3M	11.9 ± 0.44	10.96 ± 0.19
HA-3M	11.4 ± 0.25	10.96 ± 0.29
HA-6M	10.9 ± 0.23	10.86 ± 0.20
HA with FG –3M	11.6 ± 0.23	10.5 ± 0.17
HABGS-3M	10.66 ± 0.22	11.06 ± 0.20
HABGS-6M	10.73 ± 0.19	10.7 ± 0.16
HABGS with FG –3M	12.8 ± 0.29	11.06 ± 0.19

V.2.10.4 Rate of Mineralization

The rate of mineralization is calculated based on the fluorescence emitted by the mineralizing bone. Tetracycline and alizarin complexone dye was administered at one month interval after implantation. The rate of mineralization was observed between the implant and the new bone and was found to be different for uncoated and FG coated HA, BGS and HABGS granules. Bone mineralization with uncoated HA showed 3 μm/day and with FG coated HA the mineralization rate was 3.3 μm/day. Uncoated BGS showed 2.8 μm/day and FG coated BGS 6.6 μm/day. Uncoated HABGS showed a mineralization rate of 3 μm/day whereas, FG coated HABGS showed 4.3 μm /day.

The mineralization rate was also quantified for the Haversian canals, where active mineralization is in progress during the administration of dyes. The difference in the uptake of the dye lead to an understanding of, the role of Haversian canals in the process of mineralization. The Haversian canals seen around the host bone/new

bone interface picked up either tetracycline or alizarin. The rate of mineralization between two Haversian canals was 1 μm/day.

V.2.11 X-Ray Diffraction (XRD)

V.2.11.1 Hydroxyapatite (Figure.V.45)

The XRD spectrum of raw HA sintered granule powder showed sharp crystalline apatite [Ca_{10} $(PO_4)_6$ $(OH)_2$] peaks at an angle 22°, 23°, 25.5°, 26.1°, 26.9°, 28.2°, 29°, 31.8°, 32.3°, 33°, 34.1°, 39.3°, 39.8°, and 42°and few minor brushite peaks (Ca $HPO_4.2H_2O$) were also observed at 21.3°, 36.6°, 35.5°, 37.5° and 40.5°.

The spectrum of tibia bone powder (non-sintered) showed amorphous apatite peaks at 23°, 26.1°, 31.9°, and 43.8°, brushite peaks at an angle 21.3°, 23.6°, 37.5° 41.8° and 42.5°.

The mixing of the bone powder and the sintered HA granule resulted in peaks that were different from that of the normal bone as expected. The apatite peaks were observed at an angle 21.8°, 26.1°, 26.8°, 29.2°, 32°, 32.4°, and 33.3°, 34.1° and brushite peaks at 21.3°, 36.6°, 40.2°, 40.5° and 42.5°.

The spectrum of HA implanted in tibia bone after 3 months showed amorphous peak. Apatite peaks were observed in the following regions after implantation at an angle 21.8°, 26.2°, 26.8°, 29.2°, 32.2° and 32.8°. Brushite peaks were observed at 21.3°, 23.8°, 29.7°, 35.5°, 40°, 40.4°, 41.8° and 42.3°.

The peaks observed with FG coated HA implanted in tibia bone after 3 months showed amorphous peaks. Apatite peaks were observed at an angle 26.3°, 26.8°, 29.4°, 32°, 33.3° and 42° and brushite peaks were observed at an angle 21.3°, 23.6°, 34.4°, 37.4°, 40.1°, 40.5° and 42.5°.

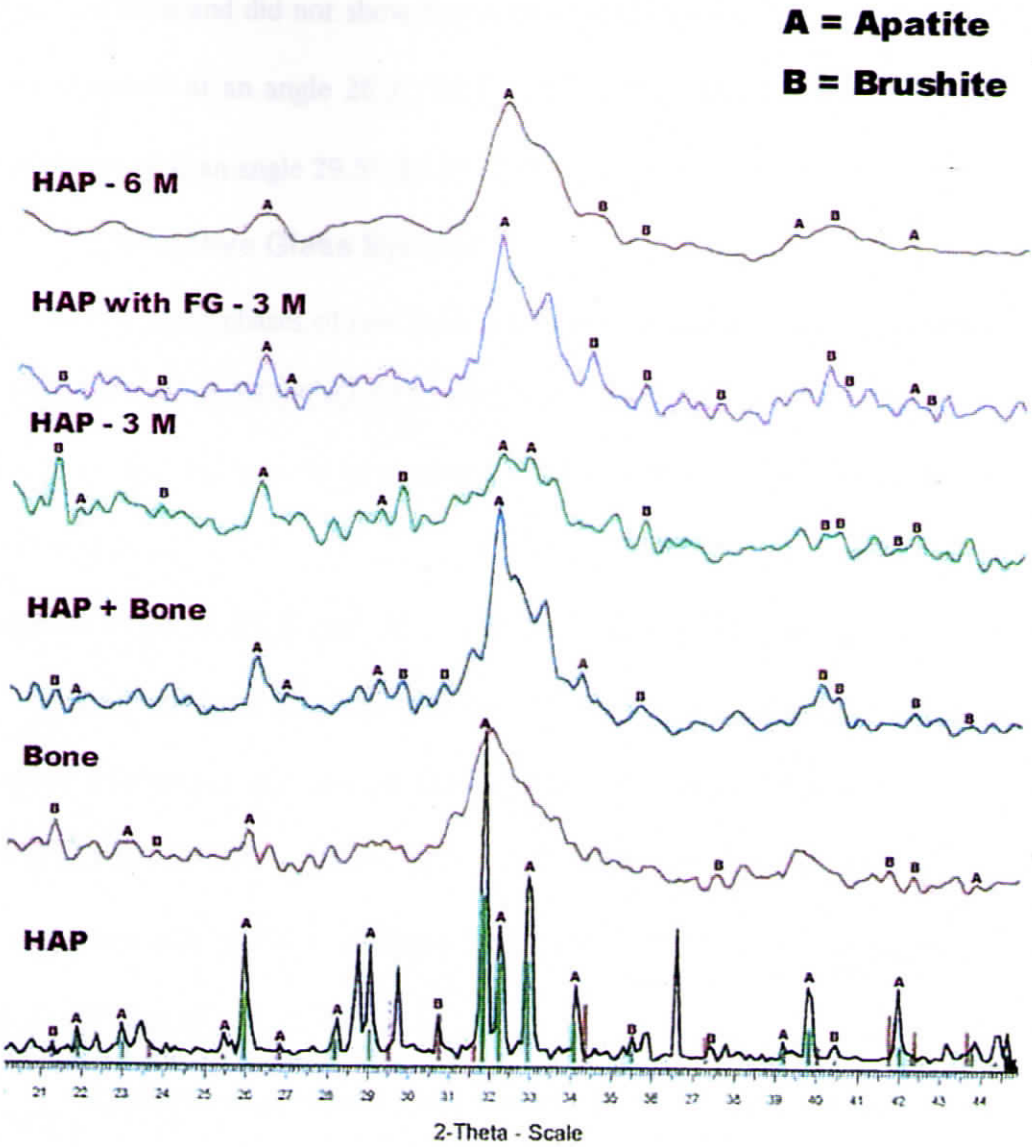

Figure -V-45

X-ray diffraction (XRD) spectra of raw HA sintered granule powder, raw bone powder, mixed HA and bone powder and HA 3 & 6 months after implantation in rabbit tibia bone. The major peaks observed were apatite (A) of the material and bone and few minor peaks of brushite (B) of bone. The green bar denotes the apatite [$Ca_{10}(PO_4)_6(OH)_2$] ; brown bar denotes the brushite [$Ca_2(PO)_4 \cdot 2H_2O$] peak on the x-axis.

HA implanted in tibia bone after 6 months showed amorphous peaks as that of normal bone and did not show any crystalline HA peaks. Amorphous apatite peaks were observed at an angle 26.3°, 32.1°, 32.9°, 39.2° and 42°. Brushite peaks were also observed at an angle 29.5°, 34.4°, 35.5° and 40.1°.

V.2.11.2 Bioactive Glass System

The major phases of raw BGS granules were apatite ($Ca_{10}(PO_4)_6(OH)_2$) and wollastonite ($CaO.SiO_2/CaO.SiO_3$) and whitlockite ($Ca_3(PO_4)_2$). The spectrum of the BGS sintered powdered granules were crystalline. The apatite phases were identified at 22°, 22.8°, 26°, 28.3°, 31.9°, 36.5°, 39.3°, the wollastonite phase at an angle 23.2°, 25.5°, 27.1°, 29°, 30°, 28.5°, 40.1° and the whitlockite phase at 31.3°.

The spectrum obtained with raw BGS and bone powder (Figure.V.46) was slightly amorphous and showed apatite peaks at an angle 22.1°, 23.1°, 26°, 28.2°, 29.1°, 31.9°, 33°, 34.1°, 35.8°, 39.2°, 39.9°, 40.5°, 43.8°, 44.3°, 46.5°, 48.4°, 49.4° and wollastonite peaks at an angle 23.5°, 25.6°, 27.1°, 30.3°, 36.5°, 38.8°, 39.2°, 41.5°, 45° and 45.7°.

Amorphous spectrum was observed 3 months (Figure.V.47) after implantation in the tibia bone. The apatite peaks were observed at an angle 25.5°, 26.4°, 32.2°, 33.1°, 34.1°, 39.9°, 40.5°, 42°, 44.4°, 46.6°, the wollastonite peaks were observed at an angle 23.4°, 25.5°, 28°, 38.5°, 39.1°, 46.7° and periclase (MgO) at 36.9° and 42.9°.

The spectrum of BGS coated with FG after 3 months (Figure.V.47) implantation in tibia bone showed amorphous peaks. The apatite peaks were observed at an angle 22°, 25.5°, 26.4°, 28.2°, 29.1°, 32.2°, 34.1°, 39.9°, 40.2°, 41.9°,

44.4°, 46.5°, 48.6°, 49.4°, wollastonite peaks were observed at an angle 22.5°, 27°, 27.8°, 28.8°, 38.5°, 39.1°, 41.4°, 45°, 45.6° and periclase at 36.9°.

BGS after 6 months (Figure.V.47) of implantation in the tibial bone showed an amorphous spectrum. The apatite peaks were observed at an angle 26°, 32.3°, 32.7°, 35.5°, 39.2°, 40.1°, 42°, 44.4°, 46.8° and 48°, wollastonite peaks were observed at an angle 23.4°, 27.1°, 27.9°, 28.8°, 30°, 36.4°, 38.2°, 41.4° and periclase peaks were observed at 36.9° and 42.9°.

V.2.11.3 Triphasic Bioactive Composite System (HABGS)

XRD spectrum of the raw HABGS powder revealed the granules to be crystalline (Figure.V.48). The apatite peaks were observed at an angle 22°, 25.5°, 26°, 29°, 31.9°, 39.4°, 38.6° and 45.2°, wollastonite peaks were observed at an angle 26°, 25.5°, 27.1°, 29°, 30.1°, 32.6°, 33°, 35.4°, 36.5°, 38.6°, 43.6°, 46° and whitlockite peaks were observed at an angle 28.3°, 31.3°, 34.6°, 37.6°.

Immediately after mixing the raw bone powder and the HABGS powder (Figure.V.48), the spectrum revealed crystalline peaks, consisting of apatite peaks observed at an angle 22°, 25.5°, 32.3°, 33.1°, 35.5°, 39.1°, 42°, 46.7°, 48.6°, wollastonite peaks were observed at an angle 25.5°, 31.6°, 34.9°, 37.6°, 40.3°, 44.2°, 45.1°, 47.4° and whitlockite peaks at an angle 28.2°, 31.6°, 34.9°, 37.6°, 40.3°, 44.2°, 45.1° and 47.4°.

The spectrum obtained with HABGS after 3 months (Figure.V.49) implantation showed amorphous peaks and apatite peaks were observed at an angle 22°, 23°, 27°, 32.3°, 32.9°, 38°, 42.3°, 44.3°, 45.1°, 46.6°, 48.3°, 49.4°, wollastonite peaks were observed at an angle 25.5°, 30.1°, 35.4°, 41.6°, 44.7° and whitlockite peaks were observed at an angle 26.1°, 28.2°, 31.4°, 34.5°, 40.2° and 47.2°.

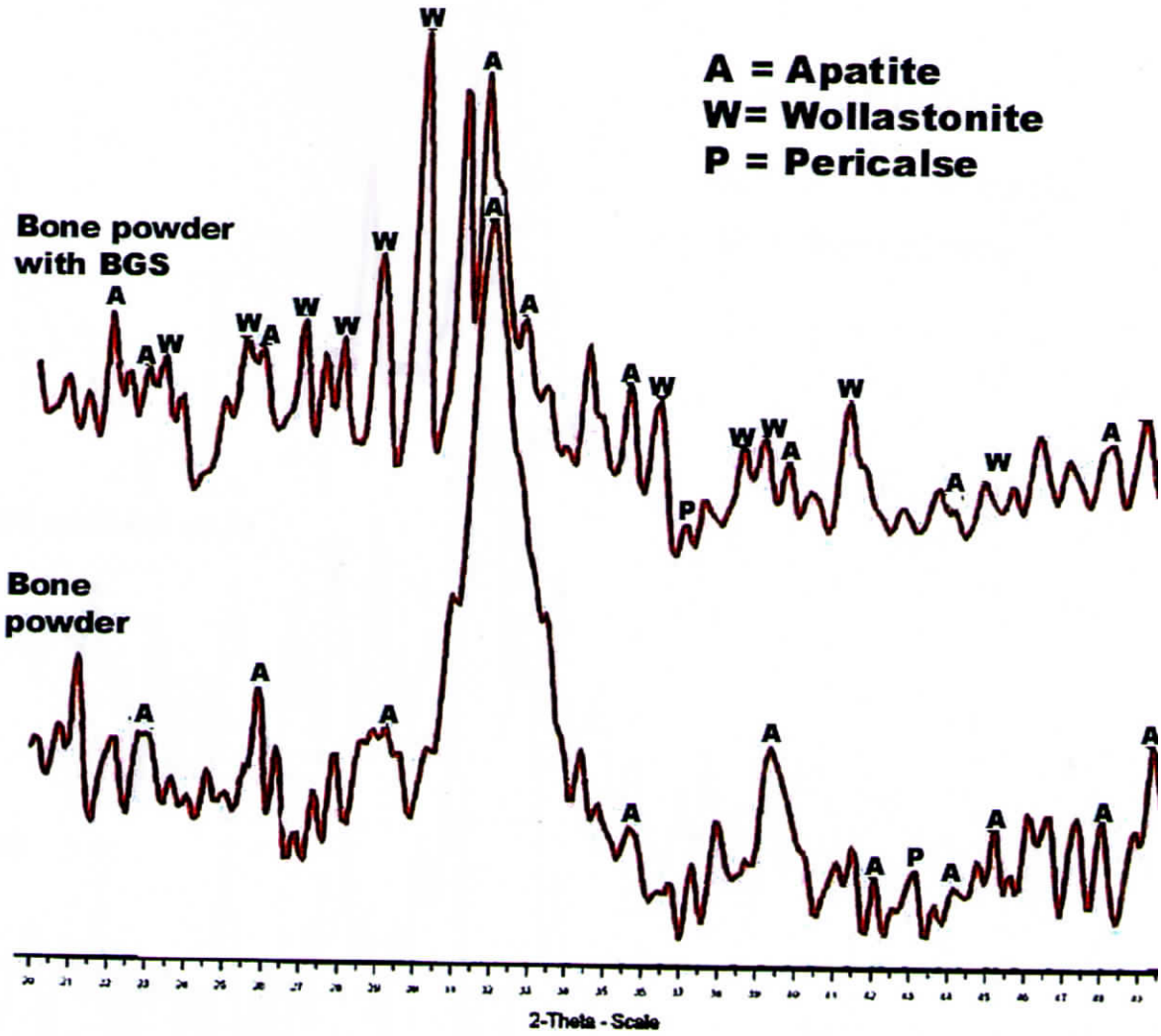

Figure -V-46

X-ray diffraction (XRD) spectra of raw bone powder and BGS wi raw bone powder of rabbit tibia bone. The major peaks that are observed were the apatite (A) peaks of the material and bone, t wollastonite (W)peaks of the material and periclase (P) of bone.

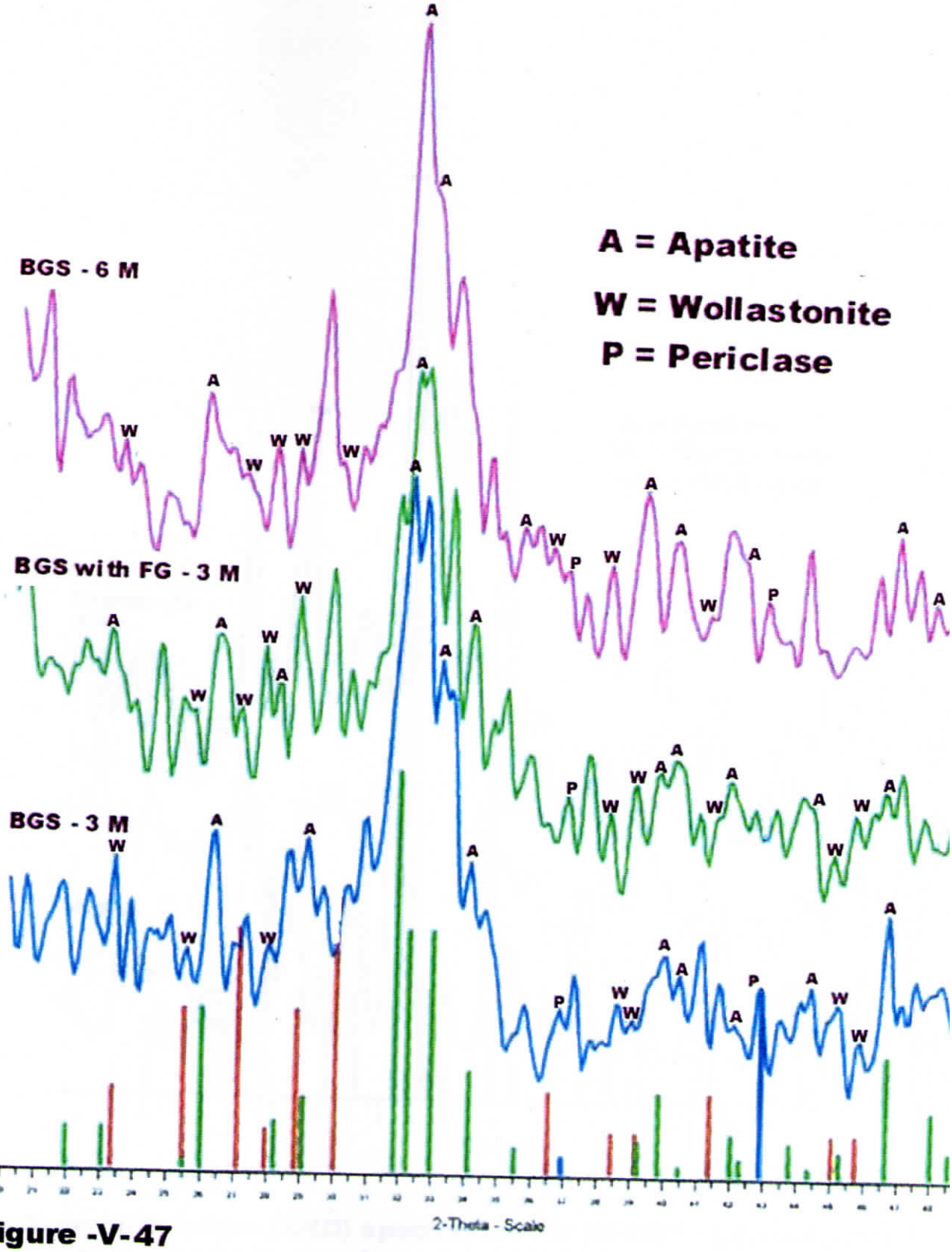

Figure -V-47

X-ray diffraction (XRD) spectra of BGS after implantation in rabbit til bone after 3 & 6 months. The major peaks that are observed were apatite (A) peaks of the material and bone and the wollastonite (W) peaks of the material and periclase (P) of bone. The green bar denot apatite ($Ca_{10}(PO_4)_6(OH)_2$); brown bar denotes wollastonite (CaO SiC CaO SiO_3) and blue bar - periclase (MgO) on the x-axis of the graph.

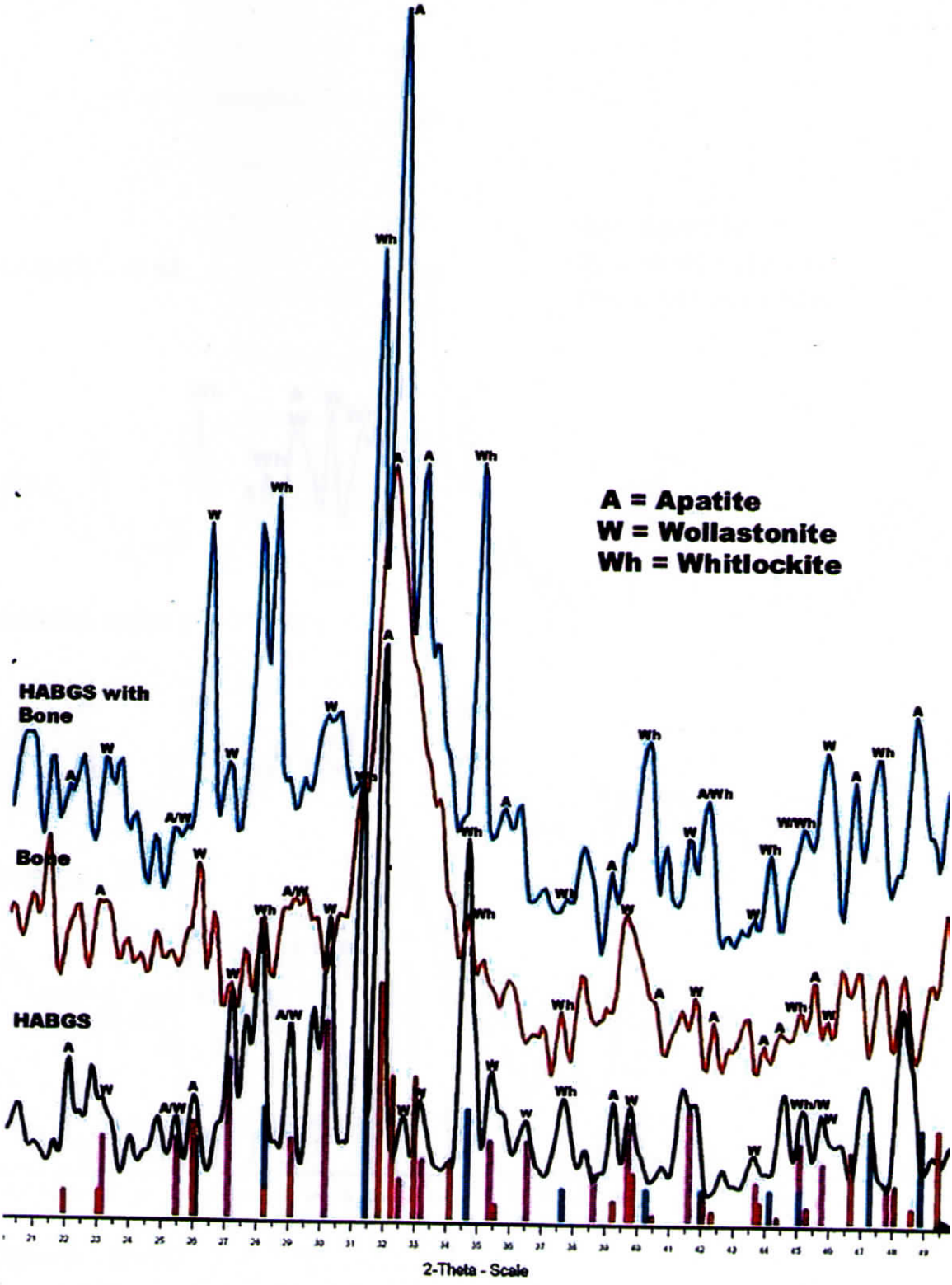

Figure -V-48

X-ray diffraction (XRD) spectra of raw HABGS sintered granule powder, raw bone powder, mixed HABGS and bone powder of rabbit tibia bone. The major peaks that were observed are apatite (A), wollastonite (W) and whitlockite (Wh) peaks of the material and bone. The brown bar denotes the apatite [$Ca_{10}(PO_4)_6(OH)_2$]; purple bar- Wollastonite [$CaO\ SiO_2/CaO\ SiO_3$] and blue - Whitlockite (tricalcium phosphate [$Ca_3(PO)_4$]).

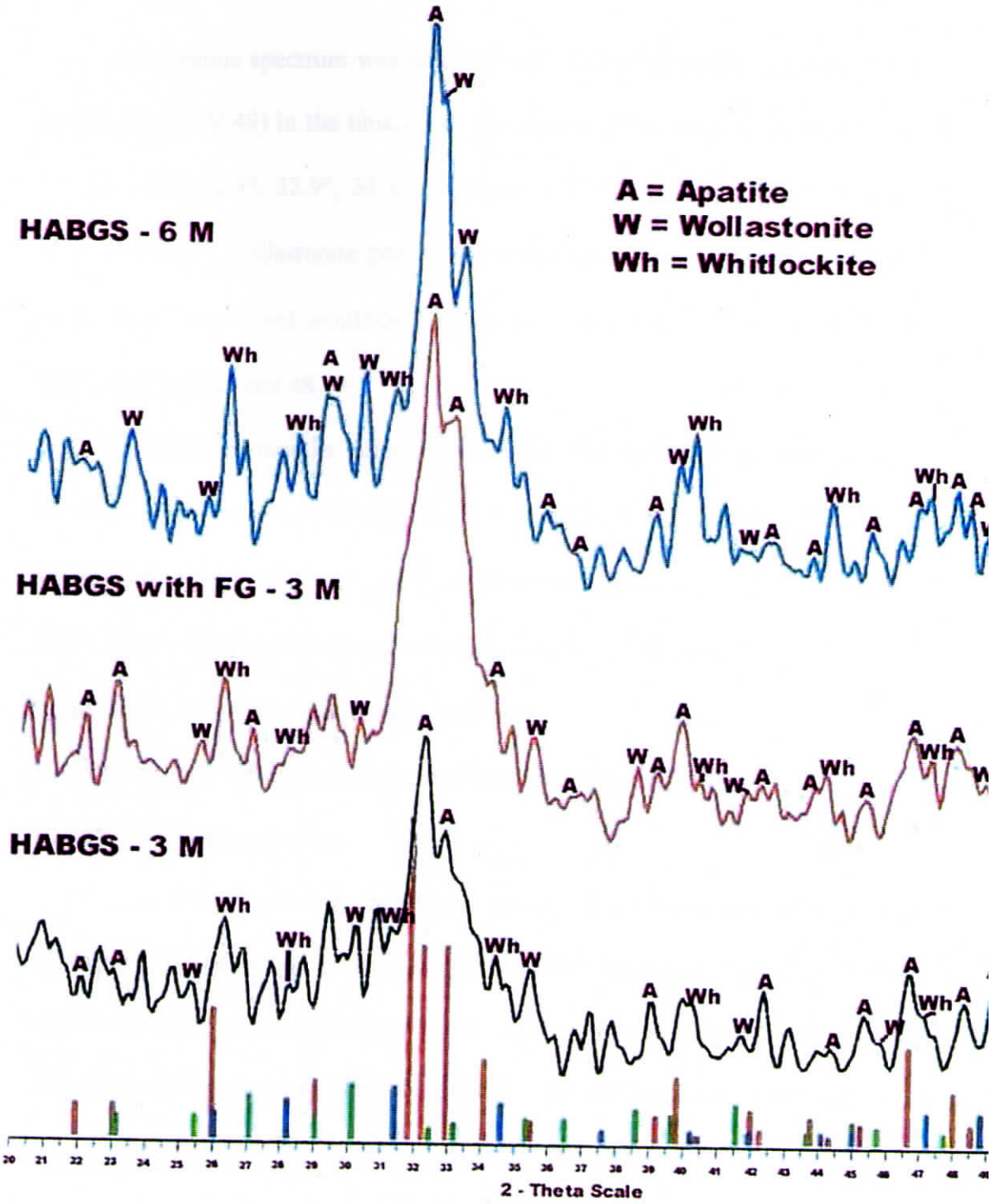

Figure -V-49

X-ray diffraction (XRD) spectra of HABGS granules after implantation in rabbit tibia bone after 3 & 6 months. The major peaks that are observed were apatite (A), wollastonite (W) and whitlockite (Wh) peaks of the material and bone. The brown bar - denotes apatite($Ca_{10}(PO_4)_6(OH)_2$);purple- Wollastonite [$CaO\ SiO_2$/ $CaO\ SiO_3$] & blue - Whitlockite (tricalcium phosphate [$Ca_3(PO)_4$]

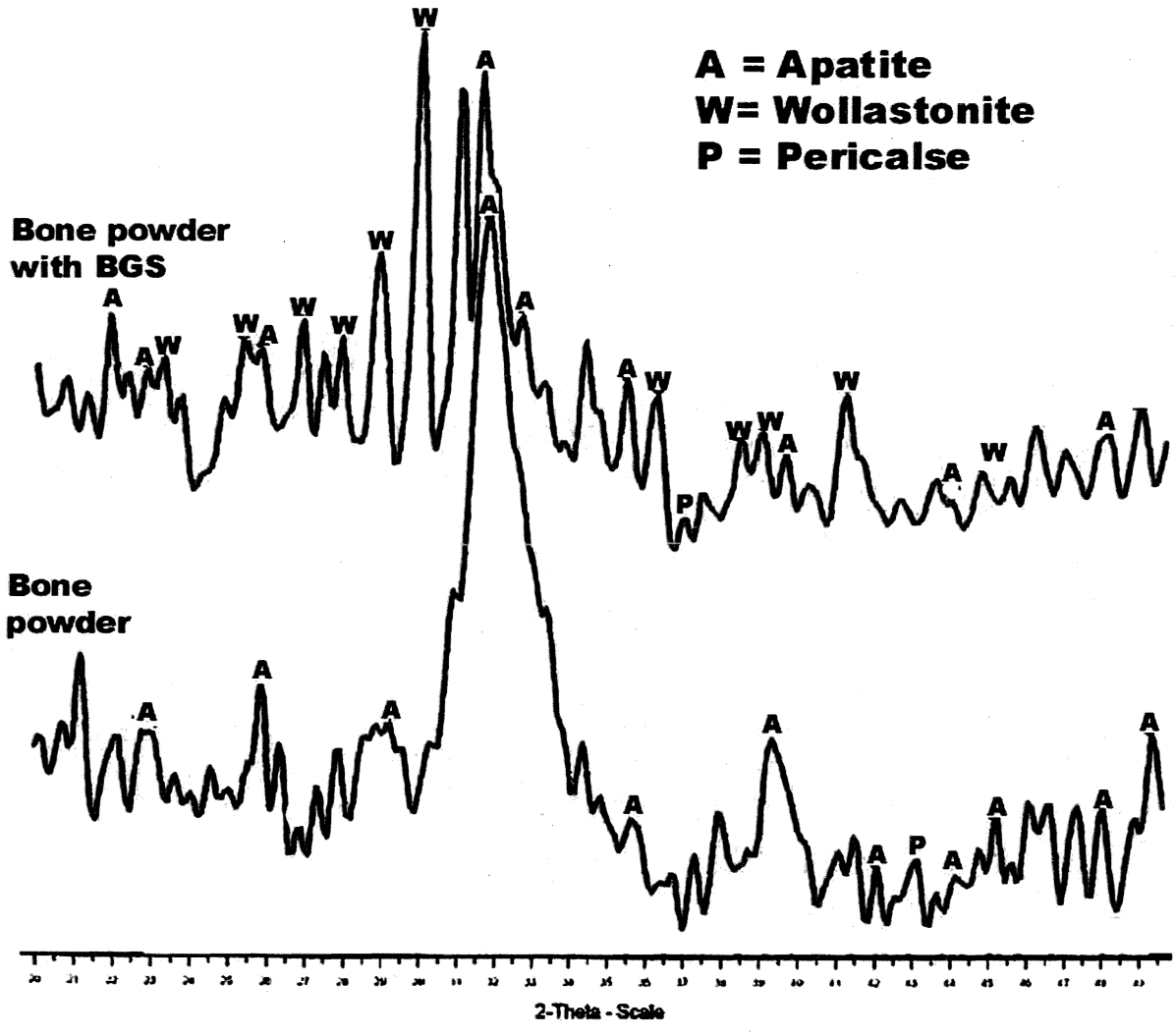

Figure -V-46

X-ray diffraction (XRD) spectra of raw bone powder and BGS with raw bone powder of rabbit tibia bone. The major peaks that are observed were the apatite (A) peaks of the material and bone, the wollastonite (W)peaks of the material and periclase (P) of bone.

Amorphous spectrum was obtained with FG coated HABGS granules after 3 months (Figure.V.49) in the tibia bone. The apatite peaks were observed at an angle 22°, 23°, 27°, 32.3°, 32.9°, 34.1°, 36.5°, 38°, 39.8°, 42°, 43.7°, 45.1°, 46.6°, 48°, 48.3° and 49.4°, wollastonite peaks were observed at an angle 25.5°, 30.1°, 35.4°, 38.6°, 39.6°, 41.6° and whitlockite peaks were observed at an angle 26.1°, 28.2°, 40.2°, 44.1°, 47.2° and 48.9°.

HABGS 6 months after implantation (Figure.V.49) showed amorphous spectrum. Apatite peaks were observed at an angle 22 °, 29°, 32.3°, 35.5°, 36.5°, 38°, 42.3°, 43.6°, 45.1°, 46.6°, 48°, 48.3°, wollastonite peaks were observed at angle 29°, 30.1°, 32.5°, 33.2° and 41.6 and whitlockite peaks at an angle 23.2°, 26.1°, 28.3°, 31.4°, 34.5°, 40.2°, 44.1°, 47.2° and 48.9°.

V.2.12 Fourier Transform Infrared Spectroscopy (FT-IR)

V.2.12.1 Hydroxyapatite

The FT-IR spectrum of HA implanted in the tibia bone after 3 months (Figure.V.50 A) revealed a sharp ^{-}OH peak at 3487 cm^{-1} and CH peaks at 2979 cm^{-1}, and amide peaks which could be albumin or fibronectin at 1652 cm^{-1} and 1556 cm^{-1}. The C-O: carbonate peaks was observed at 1455 and 1418 cm^{-1} and the 1348 cm^{-1} could be C-F group. The ν_3 PO_4 peaks were identified at 1119 cm^{-1}, 1059 cm^{-1} and 1033 cm^{-1}. The ν_4 PO_4 peaks were identified at 603 cm^{-1}, 560 cm^{-1} and 530 cm^{-1}. ν_2 carbonate peak was identified at 872 cm^{-1}.

The spectrum of HA coated with FG after 3 months (Figure.V.50 B) revealed blunt ^{-}OH peak at 3338 cm^{-1} and the C-H peaks at 2926 cm^{-1} and 2855 cm^{-1}. The amide peaks were observed at 1665 cm^{-1} and 1556 cm^{-1}. The ν_3 CO_3 peaks were observed at 1456 cm^{-1} and 1418 cm^{-1} and the ν_2 CO_3 group at 870 cm^{-1}. The ν_3 PO_4

group was identified at 1034 cm^{-1}, the ν_4 PO_4 groups at 603 cm^{-1}, and 562 cm^{-1} and the ν_2 PO_4 groups were identified at 466 cm^{-1}.

The spectrum of HA implanted in tibia bone after 6 months (Figure.V.50 C) revealed a sharp ^{-}OH peak at 3567 cm^{-1} and a blunt peak at 3480 cm^{-1}. C-H peaks were observed at 2965 cm^{-1}, 2927 cm^{-1} and 2855 cm^{-1}. Amide peaks were observed at 1759 cm^{-1}, 1652 cm^{-1} and 1557 cm^{-1}. The ν_3 CO_3 group was identified at 1457 cm^{-1} and 1418 cm^{-1} and the ν_2 CO_3 peaks at 871 cm^{-1}. The ν_3 PO_4 groups were observed at 1102 cm^{-1}, 1041 cm^{-1} and 959 cm^{-1} and ν_4 peaks at 602 and 564 cm^{-1}.

V.2.12.2 Bioactive Glass System (BGS)

The FT-IR spectrum of BGS implanted in tibia bone after 3 months (Figure.V.51 A) showed blunt ^{-}OH peak at 3433 cm^{-1} and no C-H peaks were observed. Sharp peaks of amide were observed at 1654 cm^{-1} and 1546 cm^{-1}. ν_3 CO_3 groups were identified at 1455 cm^{-1} and 1418 cm^{-1} and ν_2 CO_3 peaks at 871 cm^{-1}. ν_3 PO_4 peaks were observed at 1030 cm^{-1} and ν_4 PO_4 peaks at 604 cm^{-1} and 561 cm^{-1}.

The spectrum of FG coated BGS implanted in tibia bone after 3 months (Figure.V.51 B) showed blunt ^{-}OH peak at 3339 cm^{-1} and the peaks at 2926 cm^{-1} and 2854 cm^{-1} were assigned to C-H group. The amide peaks were observed at 1752 cm^{-1}, 1664 cm^{-1} and 1555 cm^{-1}. The ν_3 CO_3 peaks were observed at 1455 cm^{-1}, 1418 cm^{-1} and the ν_2 CO_3 peaks at 870 cm^{-1}. The ν_3 PO_4 peaks were identified at 1030 cm^{-1}, the ν_4 PO_4 peaks at 604 cm^{-1} and 561 cm^{-1} and the ν_2 PO_4 peaks at 469 cm^{-1}.

The spectrum of BGS implanted in tibia bone after 6 months (Figure.V.51 C) showed blunt ^{-}OH peak with high absorption at 3449 cm^{-1} and C-H peaks at 2972 cm^{-1}, 2927 cm^{-1} and 2857 cm^{-1}. Amide peaks were observed at 1651 cm^{-1} and 1557 cm^{-1}. The ν_3 CO_3 peaks were observed at 1457 cm^{-1}, 1418 cm^{-1} and the ν_2 CO_3

peaks at 870 cm^{-1}. The ν_3 PO_4 peak was observed at 1028 cm^{-1} and the ν_4 peaks at 603 cm^{-1} and 561 cm^{-1}. The ν_2 PO_4 peaks were also observed at 471 cm^{-1} and 416 cm^{-1}.

V.2.12.3 Triphasic Bioactive Calcium Phosphate Ceramic System (HABGS)

The FT-IR spectrum of HABGS implanted in tibia bone after 3 months (Figure.V.52 A) showed sharp ^{-}OH peak at 3482 cm^{-1} and a blunt peak at 3338 cm^{-1}. C-H peaks were observed at 2972 cm^{-1}, 2925 cm^{-1} and 2854 cm^{-1}. The peaks observed at 1652 cm^{-1} and 1556 cm^{-1} were assigned to amide groups. The ν_3 CO_3 peaks were observed at 1458 cm^{-1} and 1419 cm^{-1} and the ν_2 CO_3 peaks at 871 cm^{-1}. The PO_4 groups was observed in two regions the ν_3 1031 cm^{-1} and ν_4 603 cm^{-1}, 561 cm^{-1} and 532 cm^{-1}.

The spectrum of FG coated HABGS implanted in tibia bone after 3 months (Figure.V.52 B) showed blunt ^{-}OH peak at 3436 cm^{-1} and C-H group peaks were also observed at 2979 cm^{-1} and 2929 cm^{-1}. Amide peaks were observed at 1654 cm^{-1} and 1545 cm^{-1}. The ν_3 CO_3 groups were observed at 1455 cm^{-1} and 1419 cm^{-1} and the ν_2 CO_3 groups at 870 cm^{-1}. The ν_3 PO_4 groups were observed at 1026 cm^{-1} and ν_4 groups at 604 cm^{-1} and 560 cm^{-1}.

The spectrum of HABGS implanted in tibia bone after 6 months (Figure.V.52 C) revealed a blunt ^{-}OH peak at 3422 cm^{-1} and prominent C-H peaks at 2965 cm^{-1}, 2925 cm^{-1} and 2855 cm^{-1}. Amide peaks were observed at 1652 cm^{-1} and 1557 cm^{-1}. The CO_3 groups were observed at two positions ν_3 at 1457 cm^{-1} and 1418 cm^{-1} and the ν_2 peak at 871 cm^{-1}. The ν_3 PO_4 group was observed at 1030 cm^{-1}, the ν_4 groups at 603 cm^{-1} and 560 cm^{-1} and the ν_2 peaks at 471 cm^{-1} and 435 cm^{-1}.

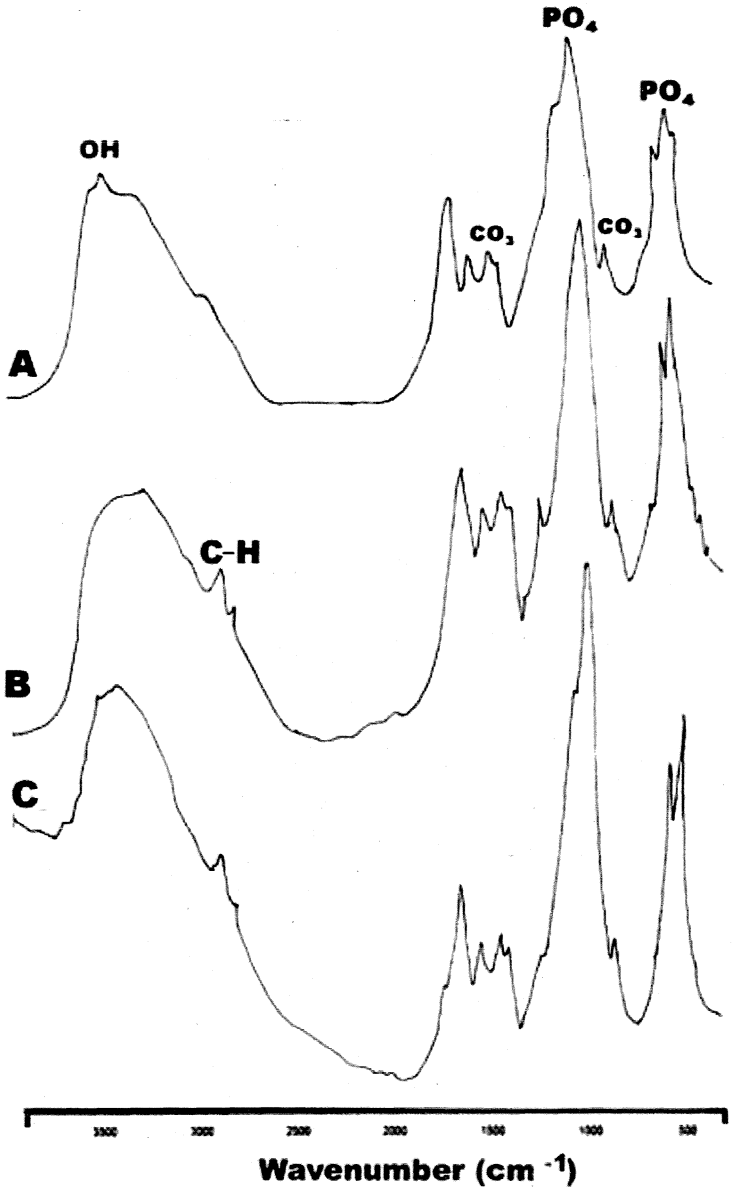

Figure -V-50

Fourier Transform Infrared spectra of HA implanted in rabbit tibia bone: A - HA after 3 months; B - HA coated with FG after 3 months & C - HA after 6 months. The characteristic peaks of hydroxyl (OH), C-H, carbonate (CO_3) and the phosphate (PO_4) groups were observed after implantation.

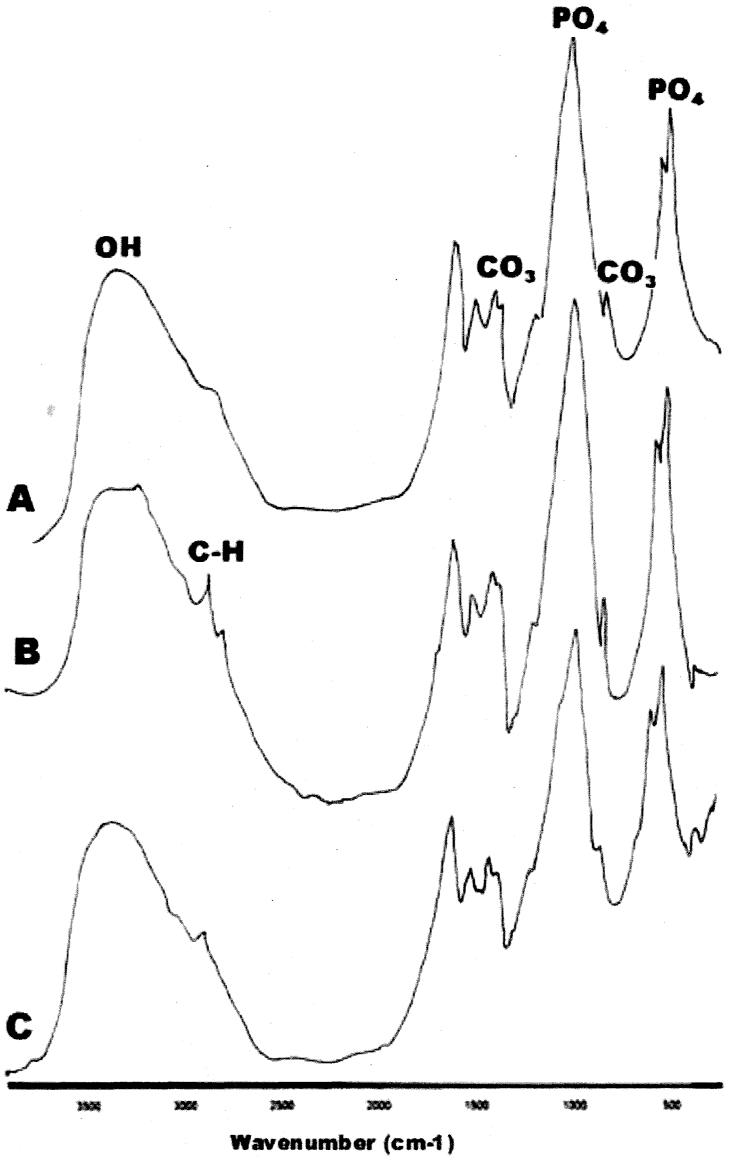

Figure -V-51

Fourier Transform Infrared spectra of BGS implanted in rabbit tibia bone: A - BGS after 3 months; B - BGS coated with FG after 3 months & C - BGS after 6 months. The characteristic peaksof hydroxyl (OH), C-H, carbonate (CO_3) and the phosphate (PO_4) groups were observed after implantation.

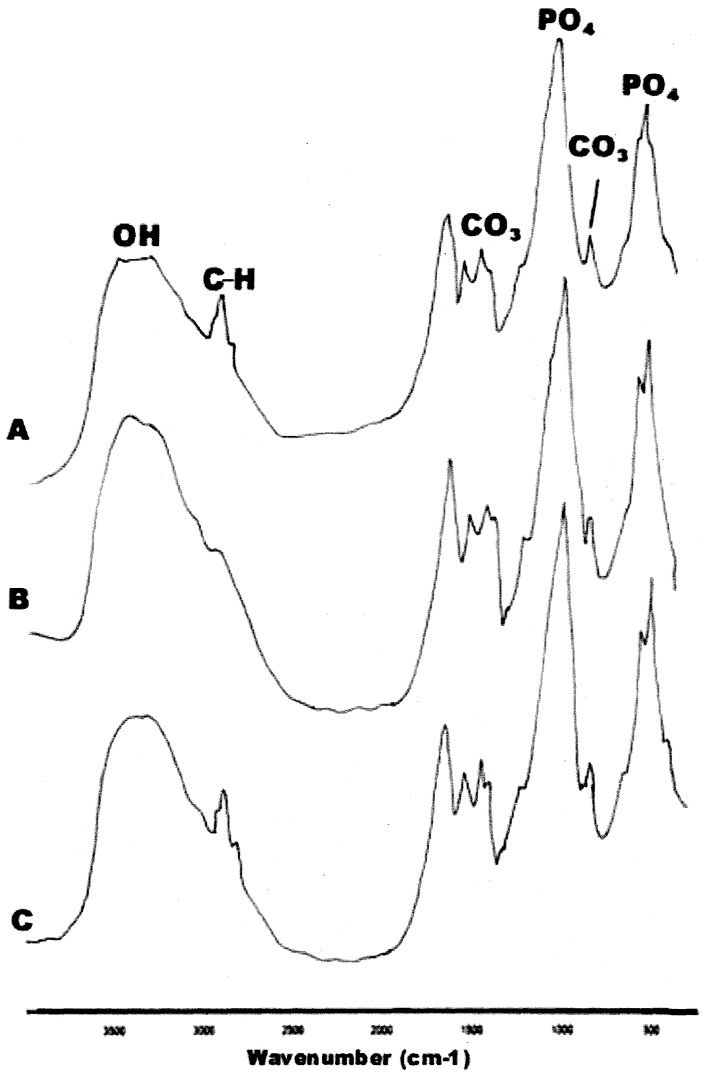

Figure -V-52

Fourier Transform Infrared spectra of HABGS implanted in rabbit tibia bone: A - HABGS after 3 months; B - HABGS coated with FG after 3 months & C - HABGS after 6 months. The characteristic peaksof hydroxyl (OH), C-H, carbonate (CO_3) & the phosphate (PO_4) groups were observed after implantation.

V.2.13 SEM-EDAX

HA after implantation did not show much change in the percentage of calcium (Ca) and phosphorus (P) after 3 and 6 months (Table.V.11). The calcium and phosphorous was 62.59 % and 36.50 % after 3 months and even after 6 months the calcium and phosphorous content at the bone implant interface was 63.48 % and 36.32 %. Magnesium (Mg) around the implant after 3 and 6 months showed 0.91 % and 0.21 % (Figure.V.53 B & C).

The percentage of Ca and P around BGS implants was 51.89 % and 33.49 % after 3 months and 55.01 % and 36.61 % after 6 months. The Mg content around the implant was 2.46 % after 3 months and after 6 months it increased to 3.18 %. Silica (Si) around the BGS implants was initially high at 12.16 % after 3 months but after 6 months it reduced to 5.49 % (Figure.V.54 B & C).

The percentage of Ca and P around the HABGS implants was 59.79 % and 39.10 % after 3 months and after 6 months 60.61 % and 37.75 % of Ca and P was observed around the implant. Mg was not detected in the 3 months sample around the implant, but after 6 months 1.18 % of Mg was detected at the implant-new bone interface. Si content was 1.43 % at 3 months and by 6 months only 0.45 % was detected (Figure.V.55 B & C).

Table V.11

Group	Control	Calcium		Phosphorous		Magnesium		Silica	
		3 M	6 M	3 M	6 M	3 M	6 M	3 M	6 M
HA	1.67	62.59	63.48	36.50	36.32	0.91	0.21	-	-
BGS		51.89	55.01	33.49	36.61	2.46	3.18	12.16	5.49
HABGS		59.79	60.61	39.10	37.75	-	1.18	1.43	0.45

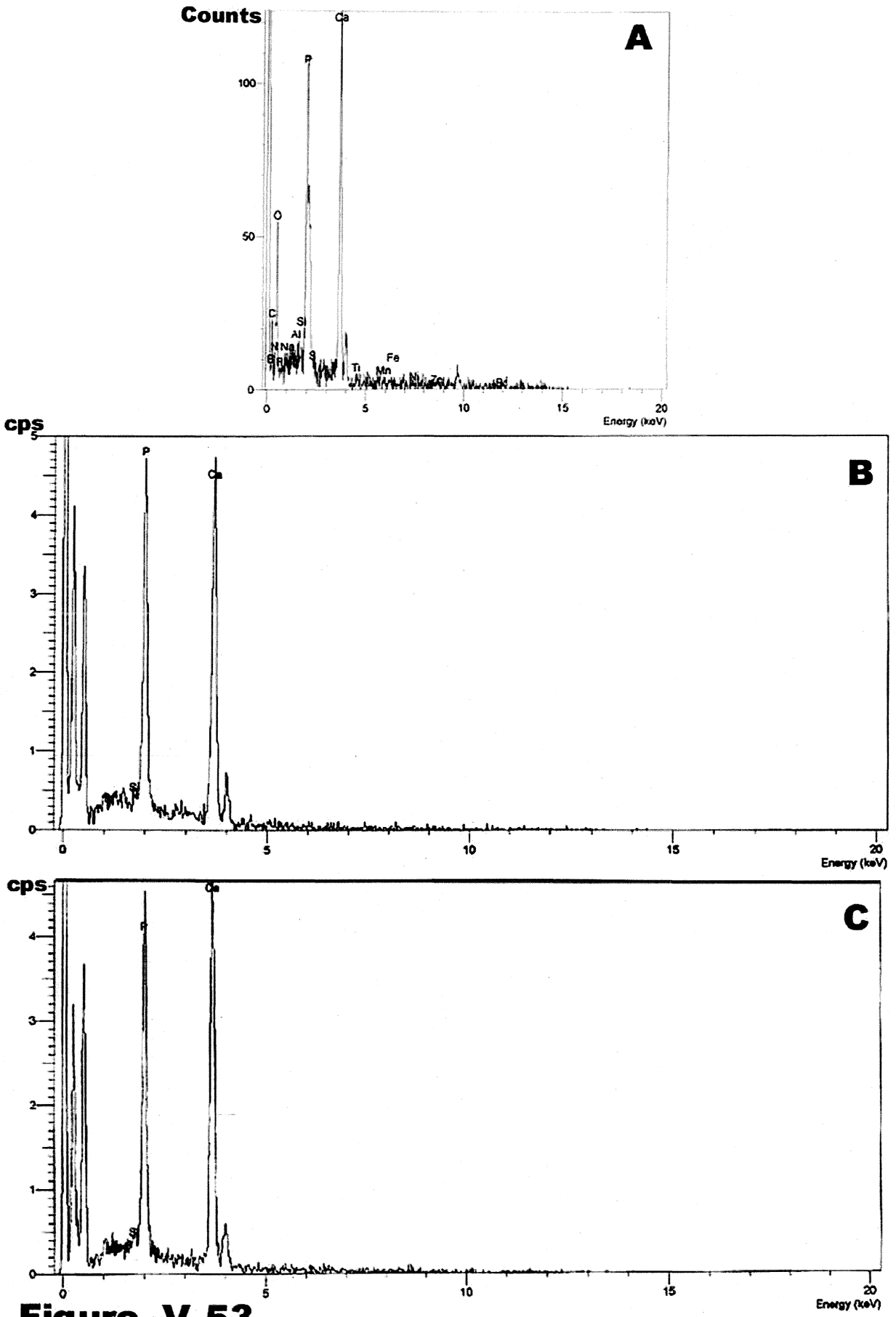

Figure -V-53

Energy Dispersive X-ray Analysis (EDAX) spectra of HA after implantation in rabbit tibia bone after 3 & 6 months : A - HA raw granules; B & C - HA after 3 and 6 months after implantation. The dispersion of calcium (Ca) and phosphorous (P) at the interface were observed.

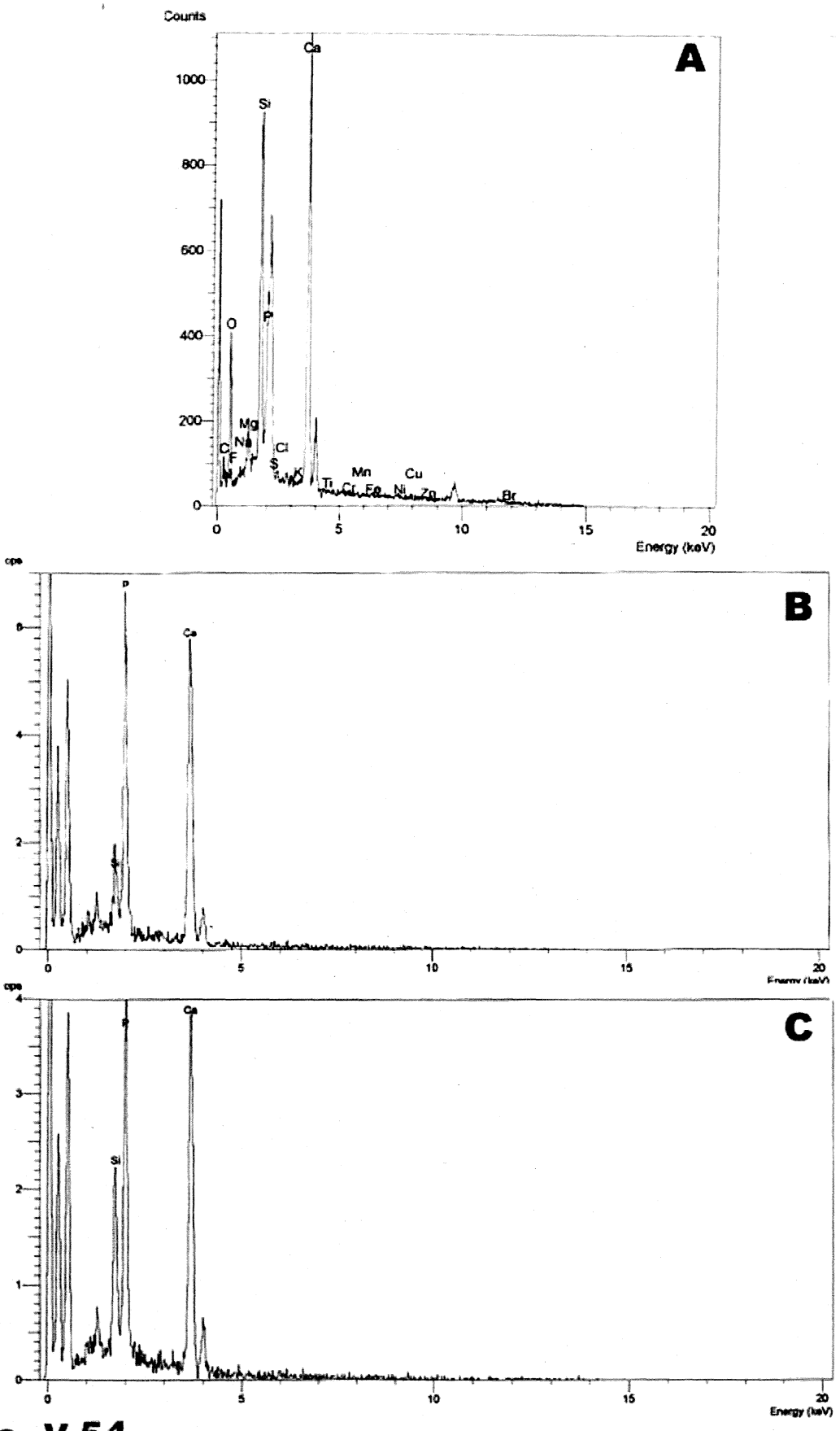

Figure - V-54

Energy Dispersive X-ray Analysis (EDAX) spectra of BGS after implantation in rabbit tibia bone after 3 & 6 months : A - BGS raw granules; B & C - BGS after 3 and 6 months after implantation. The dispersion of calcium (Ca) ,silica (Si) & phosphorous were observed at the interface of the implant and new bone.

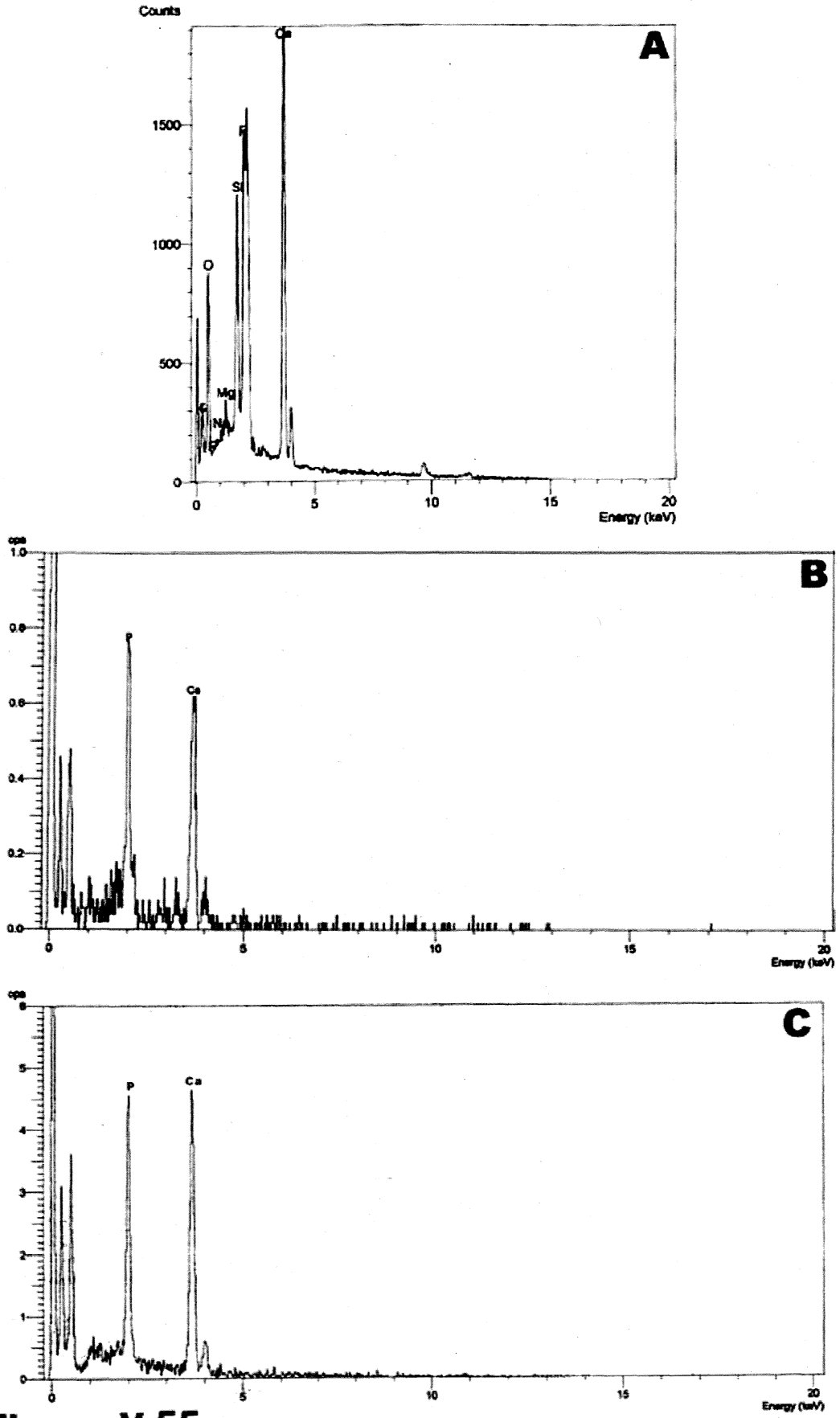

Figure -V-55

Energy Dispersive X-ray Analysis (EDAX) spectra of HABGS after implantation in rabbit tibia bone after 3 & 6 months : A - HABGS raw granules; B & C - HABGS after 3 & 6 months.
The dispersion of calcium (Ca) ,silica (Si) and phosphorous (P) were observed in the raw spectrum (A); B & C did not showed silica in the interface of the implant and the new bone after 3 and 6 months

V.2.13.1 Calcium phosphate ratio

The calcium phosphate (Ca/P) ratio was calculated to find out the distribution of the calcium and phosphate around an implant at different time (Table.V.12). The Ca/P ratio of HA after 3 and 6 months was 1.714 and 1.74. BGS showed Ca/P ratio of 1.549 and 1.51 after 3 and 6 months. HABGS implanted samples showed a Ca/P ratio of 1.529 and 1.605 after 3 and 6 months.

Table V.12

Group	Ca/P ratio	
	3 Months	6 Months
HA	1.714	1.74
BGS	1.549	1.51
HABGS	1.529	1.605

V.2.14 In Vivo Orthotopic Implantation: Discussion

Over the past three decades, various biomaterials have come into widespread use in clinical practice both for the repair of osseous defects and augmentation procedures. So the concomitant need for grafts, especially bioactive ceramics is given considerable attention (Passuti *et al* 1990; Le Geros 1988; Ricci *et al* 1992; de Groot *et al* 1988; Schepers *et al* 1993) to restore or replace lost, diseased or congenitally missing bone. The use of ceramics as implantation materials originated from research in the early 1970s, which lead to the introduction of a variety of bioceramics. Calcium phosphate ceramics have received attention because much effort has been directed to the development of bone implant materials because of their close chemical and crystal resemblance of these materials to the bone mineral. The exceptional biocompatibility is attributed to their being primarily composed of calcium and phosphorous ions, which are the most common constituents of vertebrate hard tissue systems (de Groot 1980, 1983; Jarcho 1981). Therefore, it is clearly understood that materials whose physicochemical characteristics similar to tissues and organs are highly desirable for bone regeneration. Furthermore, HA in the form of porous granules (Roth *et al* 1984) is of considerable interest as possible bone graft substitutes or as carriers of antibiotics (Wahlig *et al* 1986) or osteogenic substances (Urist *et al* 1984) or even for any other drugs.

Several animal models has been tried to test the material for osteocompatibility before clinical application. The art of selection of an animal model will decide on the output of the data one is expecting. The following aspects are crucial in deciding the selection of the animal model for bone implant experiments.

a. Bone architecture (in comparison to human bone)

b. Implantation site (Cortical or Cancellous)

c. Bone remodeling rate

d. Age and physiology of the animal

e. Short term or long term response of the implant

Fracture healing is investigated extensively in different mechanical conditions in rats, rabbits, dogs and sheep. Rat cortical bone is not Haversian and remodeling occurs primarily along the endosteal and periosteal surfaces (Kelley *et al.*, 1990). Hence its reaction to injury will, therefore, differ from that of human, or other Haversian bones. Manual external fractures are not reproducible.

Rabbit as an animal model for studying fracture healing has more advantage than rat models. Rabbits are also relatively easy to handle and maintain, could sustain long periods of sedation, they are known to maintain uniformity in their genetic characteristic and hence one would expect only a little change in anatomical and physiological changes (Markowitz, 1964). The cortical bone is Haversian and the stimulation of remodeling after injury is more similar to that of other larger mammals. Larger size of rabbit bones enables the use of several methods for the stabilization of fractures. Thus plates of various designs, medullary nails, or external fixators have been used to stabilize osteotomies of the femur and tibia (Greiff, 1978; Wang *et al.*, 1981).

Dogs have bone mechanics similar to human bone, but bone turnover rate is 2-3 times faster. Sheep permits study of materials at physiological loads approaching those of humans.

Broadly for convenience the implant site is divided into following categories to understand the nature of bone that has formed within the defect: a) Periosteum, b) Cortical bone, c) Endosteum, d) Periosteal-cortical region (or) sub-periosteum, e) cortical-endosteal (or) pre-endosteum and, f) host bone - new bone interface.

Radiographically the materials were seen well integrated with the host bone, irrespective of the type of the material at 6 months. But, the radioopacity of the implant site with HA, BGS and HABGS granules differed at 3 and 6 months, suggesting different bone formation rate and implant degradation. Quantitative image analysis of the X-ray image revealed that the initial cortical bone width (TW) was 6.6 mm for HA, BGS 6 mm and 5.5 mm for HABGS implanted in the mid diaphyseal region of the tibia bone. After 6 months the TW of the cortical bone for HA, BGS and HABGS came down to a uniform 6 mm width. Whereas, the implant width (IW) increased from 2.2 mm to 3.2 mm for HA, for BGS the IW decreased from 3 mm to 2.8 mm and for HABGS the IW decreased from 3.2 mm to 2.7mm after 6 months. This decrease in the IW is due to the bioactive nature of the material. HA dissolute slowly, whereas BGS and HABGS degrades with time and hence the change in the IW. The uniformity in the cortical bone TW suggests that bone remodeling is normal with respect to the three types of bioactive material and has not changed the normal architecture of the bone leading to fracture.

Contact microradiographic images of the cross-section of Polymethyl methacrylate embedded implant site showed bone formation rate was more pronounced in HABGS and BGS granules even though, there were few gaps after 3 months in the periosteal and endosteal regions of BGS and in mid cortical regions of HABGS, which may be due to active material degradation or resorption or mineralisation within the newly laid osteoid. HA, BGS and HABGS after 6 months showed better material-new bone-host bone bonding. No gaps were observed, which suggested that healing was normal without any adverse reaction after 6 months. FG coated HA, BGS and HABGS granules also showed good osseointegration radiographically (data not shown). Contact microradiography was not performed on the FG coated implant granules.

The absence of any inflammation or necrosis at the gross level of the implant site indicated that, the healing of the defect was normal without any adverse reaction by the material even after 3 and 6 months.

Osseointegration of the material with the host bone or the newly formed bone is a prerequisite for the implant success or failure. Morphologically, osseointegration is realized when there is direct contact of viable bone with the surface of the implant without an interposition of soft tissue at the light microscopical level (Boss, 1999). SEM of the uncoated and FG coated HA, BGS and HABGS ceramic granules showed osseointegration with the host bone suggesting the healing was uneventful.

The interfacial gaps between the bone and the implant should be less than 50 μm to reduce interfacial movements. SEM of the implanted granules showed gaps of 7-20 μm, which is within in the normal range (50 μm). Osseointegration brings about a long-lasting and mechanically stable fixation of an implant's textured surface to the bone. Allowing direct load transfer, osseointegration reduces stress shielding and its accompanying bone resorption. Implant subjected to interfacial movements of less than 30 μm is surrounded by thriving osseous tissue. Implant gaps larger than 150 μm lead to micromotion and prevented differentiation of mesenchymal cells into osteoblast cells, leading to fibrous encapsulation (Rubin and Lanyon, 1984).

The fluorescence labeling proved that HA, BGS and HABGS implanted specimens initiated bone formation by osteoconduction, where the material allows the bone to be formed on its surface. The fluorescence was observed from the host bone towards the implant granules and also observed within the cracks, periphery of the material, host bone - new bone interface and also in the Haversian canals after 3 months. The porosity of the material and the bioactive nature of the material definitely favored bone formation which is quite evident from the yellow

fluorescence observed within the pores of the HA granules and within the degrading gaps of the BGS and HABGS granules.

The fluorescence not only determined the initiation of bone formation, but also the pattern of bone mineralisation. The yellow fluorescence was observed in the periosteum, endosteum and mid cortical regions and also in the host bone - new bone interface, which suggested that bone formation is initiated from all the sides evenly with HA granules. With BGS granules the fluorescence was observed only in the mid cortical region and in the host bone new bone interface, but not in the periosteum or endosteum, this pattern of bone formation suggests that healing is in the longitudinal axis of the bone, i.e. from the host bone towards the defect and not from the periosteal or endosteal regions. HABGS implanted specimens showed bone mineralisation pattern similar to HA.

Fibrin glue coated HA material showed bone formation by osteoinduction which is quite evident from the tetracycline fluorescence seen around the implant granules that was administered after 1 month and alizarin complexone injected after 2 months showed red fluorescence away from the implant in the mid cortical region and also adjacent to the periosteum and endosteum, which clearly suggests that bone formation was by osteoinduction, i.e. from the implant towards the host bone.

BGS coated with FG showed bone formation similar to HA where the bone formation was from the implant towards the host bone suggesting osteoinduction. But, the process of mineralisation was too complex with BGS where the fluorescence pattern changed from section to section in the same defect. The yellow tetracycline fluorescence was observed in the endosteum, periosteum, mid cortical bone and the host bone new bone interface. The fluorescence is not observed in all the regions in one section. This could be due to the inductive property of the FG as well as by

osteoconduction process of the BGS granules happening at two different time periods.

HABGS coated with FG showed yellow fluorescence in all directions in the endosteum, periosteum, mid cortical region, host bone-new bone interface and also within the implants in a single section, suggesting both osteoinduction and osteoconduction process happening simultaneously. This could be due to the composite nature of the HABGS material that favored this bimodal bone formation pattern.

The polarized sections of the HA material after 3 and 6 months showed a definite pattern where the collagen was laid perpendicular to that of the host bone. Polarization was more pronounced at the interface of the host bone and the newly formed bone, suggesting the remodeling process to be more pronounced at the interface rather than around the defect after 6 months. Image analysis helped in identifying the different polarizing bone collagen fibers. The yellow coloured (newly laid bone), the blue coloured (mineralized mature bone) could be easily distinguished in Figure.V.62 (D-F). This distinction helped in understanding the distribution of mineralized collagen (newly laid and mature).

Polarization micrographs of new bone trabeculae revealed oblique alignment of the lamellae to the implant surface. Because collagen fibers have a parallel orientation within a lamella, it can be deduced that the collagen fibers were aligned obliquely, as well as parallel, to the implant surface. The result was similar to those of various bioactive materials that were mainly based on the direct observations in TEM (Du *et al.*, 1998).

Jarcho (1981) showed an interdigitation of collagen fibers with the surface of dense polycrystalline HA based on observations using ion beam thinning techniques.

Using a bone cell culture model, Sautier *et al.*, (1994) observed collagen fibrils arranged either parallel or perpendicular to the first-formed electron-dense layer on the surface of the bioactive glass-ceramic containing crystalline apatite and wollastonite. Muller-Mai *et al.*, (1995) demonstrated both parallel and oblique orientation of the mineralized collagen fibers in the bone to the surface of an organoapatite implant containing nanopeptide and nanoapatite

In woven bone tissue, such as callus formation, collagen fibrils show no orientation, the fibrils show no orientation, the fibrils are haphazardly intermingled, and the amount of ground substance encountering the fibrils appear more abundant than in lamellar bone tissue. In osteoid tissue, the degree of aggregation and arrangement of collagen fibrils increases in the vicinity of the calcifying matrix, i.e. close to the calcification front (Fornasier 1977, Bonucci 1984). In compact bone of human osteons, collagen fibrils have been shown to be arranged according to a twisted plywood architecture (Giraud-Guille, 1988). Extremely small amounts of other types of collagen (II, III, V, X) have been detected in bone matrix, but their presence is generally explained as a contamination or is due to a pathologic condition in the bone matrix.

No inflammatory reaction was observed at 3 and 6 months post-implantation, and the healing of the defect was normal with all the three bioactive ceramic granules at all time periods with and without fibrin glue. Ceramics implanted in orthotopic sites, showed good osteoconductive properties and facilitated bone formation without causing an inflammatory reaction. Investigations on the properties of different types of ceramics have shown that porous HA has an osteoconductive capacity greater than that of dense synthesized HA, probably because its pores have an average size which optimizes cell ingrowth and angiogenesis (White and Shors, 1986; Hollinger and

Chaudhari, 1992). When implanted in orthotopic sites, porous HA is vascularised (Grenga *et al.,* 1989) and its pores are rapidly occupied by fibrillar connective tissue, which is then rapidly replaced by bone tissue.

The HA, BGS and HABGS granules are 300 – 350 μm in size. The particle size also has definite role on the inflammatory reactions as well as in osteogenesis process. The biological behaviour of Ca-P can be largely influenced by physicochemical properties such as Stoichiometry (Nery *et al.,* 1992), Crystallinity (Bohne *et al.,* 1993), Solubility (Daculsi and LeGeros., 1996), Specific surface area (Prudhommeaux *et al.,* 1996), Porosity and granulometry. Granulometry, though apparently a quite complicated variable, has rarely been studied. Yet, it is logical to suppose that cellular reactions to implanted biomaterials are influenced by the shape and size of powder granules. Likewise, inflammatory responses have been assessed in terms of different bioceramic shapes (Lehtinen *et al.,* 1990). Grain size of the particle is crucial when small particles are implanted or induced by the grains release during the degradation of implanted blocks (Figure.V.56A).

The bone formation was by intramembranous ossification at all periods and no cartilage was observed with any of the three types of ceramics implanted in rabbit tibia bone. The defect was completely healed by 3 months in all the groups but the type of bone formed differed with the type of granules that was implanted (Figure.V.56B). Bone formation depends on the non-toxic surface that allows cell attachment and proliferation (Basle *et al.,* 1993). The sequence of events observed following implantation of biomaterials; connective tissue proliferation, formation of woven bone and later, deposition of lamellar bone, is similar to that typical of the early stages of embryonic bone formation or of bone fracture healing (Basle *et al.,* 1993)

In our earlier experiments at 2 weeks postimplantation of HA, bone formation was observed as a trabecular network around the implant. Osteoblast cells were seen lining the trabeculae bone and few fibroblast cells was observed within the defect. No inflammatory reaction was observed around the granules, which suggests that healing of the defect was normal, without any adverse reaction. The trabeculae bone was seen originating from the endosteum as well as from the interface of the host bone. Six weeks after post-implantation the trabeculae network has transformed into a woven bone and almost completely filled the entire defect, without any intervening fibrous tissue. No inflammatory reaction was observed and the material was intact.

Mature woven bone was seen around the implants after 3 months and after 6 months the woven bone is completely replaced by lamellar bones. HA after 3 months showed mature woven bone in the cortical-periosteal zone, whereas in the cortical-endosteal zone the mature bone is undergoing transformation into lamellar bone with well-developed Haversian canals. This was also observed with BGS granules after 3 months, but in HABGS the process of transformation of woven to lamellar was seen in the mid-cortical region. FG coated HA, BGS and HABGS granules showed a definite pattern of bone healing, but differed from the bone mineralization pattern of uncoated HA, BGS and HABGS granules. Hence, it is quite clear that the bone formation pattern differed based on the type of implant, implanted.

The implant bone mineralization mechanism was different for HA, BGS and HABGS granules which is evident from the gaps that were observed around the implant in the defect. Uncoated and FG coated HA showed few gaps of 10 to 15 μm only in the periosteal-cortical region after 3 months. But, by 6 months no gaps were

found in the periosteal-cortical region, instead few gaps of 10 μm were observed in endosteal zone. This gap suggests two possible pathways.

a. The bone remodeling is in progress in the endosteal region after 6 months with HA
b. Since, the gap is not found in any other area and only in the endosteal zone, it could be possibly due to the mechanical load on these granules.

BGS implanted in tibia bone showed few gaps in the cortical-endosteal zones but not in the periosteal-cortical region. But, HABGS showed gaps in the periosteal as well as the mid cortical region after 3 months. And by 6 months BGS did not show any gap around the implant and HABGS continued to show some gap of 15 μm in the cortical-periosteal zone. This data suggests that bone healing in BGS was better without any gaps after 6 months due to the high bioactive nature of this material.

Osteoblast cells were seen around the material in the early period of 2 weeks, 6 weeks and 12 weeks and after 24 weeks osteoblast cells were not clearly identified with all the three granules. Osteoclast cells were not observed even after 24 weeks with HA, BGS and HABGS granules. But occasional monocytes were observed around the granules. Osseointegration brings about a long-lasting and mechanically stable fixation of an implant's textured surface to the bone. Allowing direct load transfer, osseointegration reduces stress shielding and its accompanying bone resorption (Chae *et al.*, 1992), and hence the osteoclast activity is less around the implants.

All the three granules (HA, BGS and HABGS) were well osseointegrated with the newly formed bone after 6 months. The mechanism of osseointegration in the healing potential of the osseous tissues in the presence of an implant is highly complex and needs extensive understanding. The process of osseointegration may be a chemical, physical or biological bonding, which highlights the need for

improvisation of the material properties to conduct new bone around the defect as well as to improve the mineralizing bone to integrate with the implant firmly.

HA, TCP and BG are usually considered as ideal bioactive ceramic bone substitute. These are materials, which generally, bond to surrounding osseous tissue and enhance bone tissue formation. Since, direct bonding to bioactive glasses was first observed (Hench *et al.,* 1971) considerable progress has been made in understanding the basic mechanisms of the formation of bone-biomaterial bond and its effect on bone formation.

The examination of bonding zone revealed the consistent presence of an interfacial hydroxyapatite layer (Neo *et al.,* 1993). Larger the solubility rate of the ceramic, the more pronounced is the enhancement of the bone tissue growth (Ducheyne *et al.,* 1990). Among the bioactive ceramics dense HA has a limited reactivity in vitro (Ducheyne *et al.,* 1993). Thus, in *in vivo* experiments, a lesser effect on bone tissue formation was found (Schepers *et al.,* 1991).

Considering more reactive calcium-phosphate ceramic consisting of equal amounts of β-tricalcium phosphate and hydroxyapatite, a decrease in average crystal size and an increase in microporosity were observed after implantation in osseous defects in dogs for 6 months (Daculsi *et al.,* 1989). HA after implantation did not show any change in the pore size, whereas BGS showed material degradation starting from the center by 3 months and after 6 months the material remained as a shade in the bone. HABGS showed typical tissue response, where it promoted bone growth over the partially degraded surface.

Numerous works on bioactive ceramics, glasses, or glass-ceramics have indicated that *in vivo* formation of a Ca-P rich layer and surface bone-like apatite is the key step in bone bonding behavior of these materials (Tracy and Doremus, 1984;

Gross and Strunz, 1985 and Neo *et al.,* 1993). From the *in vitro* simulated studies and heterotopic implantation of HA, BGS and HABGS granules significant information was obtained with regard to the bioactive property of these materials. The materials favoured apatite formation in protein rich medium and protein free medium within 24 h *in vitro* and *in vivo* in the extraskeletal sites good soft tissue response was observed, without any thick fibrous encapsulation or inflammatory reaction.

The majority of bone cells that attain the implant surface will arrive through migration of precursors through the 3-D network created in the resolving blood clot following surgery. Ohgushi *et al.,*(1992; 1996) proved the stimulatory role of the biological apatite layer on osteoblastic differentiation and thus that the apatite formed on the surfaces of synthetic HA and A-W glass ceramic can enhance osteoblast apposition and / or attachment of stromal stem cells to activate osteoblastic differentiation. Thus, the speed of formation of CO_3^- apatite or biological apatite on the surfaces of bioactive materials *in vivo* (Hench 1994). Our results with BGS granules implanted in rabbit tibia bone also support this hypothesis (Figure.V.58).

Schepers *et al.* (1991) reported that 45S5 bioactive glass granules with a narrow size range were excavated by preferential resorption after implantation. With the silica gel removed, what remained was the calcium phosphate-rich layer formed *in vivo.* Within the excavated centers, osteoprogenitor cells differentiated to cells expressing the osteoblast phenotype. Since silicon is an essential element required for bone tissue formation (Carlile *et al.,* 1970; 1986 and Landis *et al.,* 1986) the fact that bone tissue forms in excavated granules allowed Lai et al. (1998) to propose that the differentiation of the osteoprogenitor cells might be related to exposure to the silica gel during the resorption process, as described by Hench (1998). BGS and HABGS implants bonded well with the newly formed bone. The silica component of the

material was very low with BGS after 3 and 6 months and completely absent in HABGS after 3 and 6 months as observed by EDAX. This silica from these materials did not cause any adverse reactions in the bone tissue, and did not deposit and caused any calcification in any of the organs like kidney, liver, thyroid glands and intestine (data not shown). Numerous studies indicated that cell-mediated resorption is an important process involved in the fate of implants materials (de bruijn *et al.,* 1994; Kwong, *et al.,* 1989; van der Meulen, 1994)

Bioactive materials with higher solubility than HA, such as β and α tricalcium phosphate structures, have demonstrated much faster osseointegration (Hollinger *et al.,* 1989). This observation is in correlation to our findings that, BGS and HABGS showed better bone ingrowth and implant bonding than HA.

Elliner *et al. (*1986) and Nery *et al.,* (1988) has demonstrated that composites with a biphasic structure, based on HA and β-tricalcium phosphate phase causes local Ca and P enrichment, which then reprecipitates with proteins from the biological fluid enhancing the formation of new bone (Le Geros and Daculsi, 1990). Larger the solubility rate of the ceramic, the more pronounced is the enhancement effect of bone tissue growth (Ducheyne*et al.,*1990). Among the bioactive ceramics, dense, stoichiometric hydroxyapatite has a limited reactivity in vitro (Ducheyene *et al.,* 1993). Thus, in *in vivo* experiments, a lesser effect on bone tissue formation was found (Schepers *et al.,* 1991).

Daculsi *et al.,* (1989) investigated the dissolution of biological and ceramic apatites and indicated that lattice defects and surfaces of the crystals were the starting points of the process. Therefore, the low crystallinity, carbonate substitution, and nanometer size of the minerals in the composite are central to the rapid turnover of the implant surface.

Among bioactive ceramics, glass ceramics containing apatite and wollastonite crystals have been found to have a high mechanical strength and showed newly formed apatite layer on their surfaces in the body environment (Kokubo *et al* 1990; Kitsugi *et al* 1987; Nakamura *et al* 1985) similar to the apatite layer of natural bone where carbonate can substitute for phosphate, resulting in carbonate containing HA (Fourman *et al* 1972).

HA material is porous (100 – 120 μm) and BGS and HABGS does not have macropores, but have pore size of ~ 30 μm. Bone ingrowth into HA was observed as early as 2 weeks post-implantation and by 3 months and 6 months mature woven bone was observed within the pores. BGS and HABGS did not show any bone within the pores, due to the degradation of the material the bone is seen growing within the material rather than into the pores.

The ingrowth of bone into porous materials is affected by the geometry and osteoconductivity of the substrate, as well as the duration of implantation. It is understood that an implant must have a sufficient pore size of 100-400 μm for the development of mineralized bone, along with interconnecting fenestrations between the larger pores to support the vascular tissue required for continued mineralized bone maturation.

Macroporosity is conducive to osteoconduction, but also has many effects on the mechanical behaviour of BCP ceramics (Passuti and Daculsi, 1989; de Groot, 1988). It is generally admitted that 80 – 100 μm is the minimal pore size for osteoconduction, although some results in the literature are contradictory. A pore size of 50 - 400 μm is recommended for metallic implant fixation to provide better bone ingrowth than with larger pores of 400 - 800 μm (Bobyn *et al.,* 1980). Some studies have reported notable bone ingrowth for pores smaller than 100 μm (Eggli *et al.,*

1988), but many authors consider that only pores larger than 100 - 150 μm facilitate ingrowth of mineralized bone (Uchida *et al.,* 1985; Daculsi, 1990).

The mechanical properties of BCP ceramics improve rapidly *in vivo* due to bone ingrowth in macropores and reprecipitation of biological apatites in micropores (Martin *et al.,* 1989; Trecant *et al.,* 1994; Korkusuz *et al.,* 1995). To provide a good compromise between satisfactory bone ingrowth and acceptable mechanical resistance, many animal and clinical studies recommended calcium phosphate ceramics with approximately 50 % Macroporosity (Uchida *et al.,* 1985; Eggli *et al.,* 1988). Macropore percentage has a greater influence than macropore diameter on the compressive strength of BCP ceramics (Bouler *et al.,* 1996).

Malard *et al.,* (1999) reported that particles of 10-20 μm diameter induced significantly greater bone ingrowth than higher granulometries. After 21 days, new bone formed with these particles had developed twice as fast as that with the 200 - 400 μm particles and three times as fast as that with 80 - 100 μm particles. Particles of 200 - 400 μm did not induce any inflammatory reaction, although they produced higher bone ingrowth than 80-100 μm particle size.

Image analysis of the percentage of bone formation in tibia bone was calculated based on the selective thresholding of the image, which helped in clearly demarcating the implant and bone and thereby helped in quantifying the exact percentage of new bone formed in an implanted site (Figure.V.62 A-C). HA showed 71.4 % of bone for 28.6 % of implant after 3 months and 67.9 % of bone for 32.1 % of implant after 6 months. The difference in the percentage of bone versus implant between the 3 and 6 months group is very less. FG coated HA showed 70.23 % of bone for 29.77 % of implant after 3 months. BGS showed 84.2 % of bone for 15.8 % of implant after 3 months and 80.5 % bone for 19.5 % implant after 6 months. FG

coated BGS showed 72 % of bone for 28% of implant. The decrease in the percentage of new bone after 6 months is not significant, since the shade of the implant is also quantified as implant area, even though it is replaced by bone. HABGS showed 72.1 % bone for 27.9 % implant after 3 months and 74.5 % bone for 25.5 % implant after 6 months. HABGS coated with FG showed 65.2 % new bone for 34.8 % of implant.). Ono *et al.*, (1990) reported 89% of A W-glass-ceramic surface were covered with new bone within 4 weeks of implantation into rat tibia). AW-GC and Bioglass also bond to bone through an apatite layer formed on their surface after implantation (Hench 1991b; Kitsugi *et al* 1987).

Vascularity of bone would favour early bone healing with any implant. Ham (1930) stated that interference of the blood supply during fracture repair resulted in cartilage deposits and non-union of fractures. The bone vasculature studies carried out by $BaSO_4$ method revealed fine microcapillaries around the implant (may be Volkmann's canals) suggesting neo-vascularization after implantation. This is further confirmed by the histological observation of the Haversian canal formation. Well developed Haversian canals were seen around the implants by 6 months with HA, BGS and HABGS granules. Image analysis of the rate of bone growth or osteoid deposition around the Haversian canal (fluorescence sections) revealed a very slow process of bone mineralization of 1μm/day, between two different Haversian canals of 30 μm distance.

Serum calcium, phosphorous, alkaline phosphatase, acid phosphatase, protein, creatinine, PTH and calcitonin showed normal activity after 3 and 6 months post-implantation with HA, BGS and HABGS. Maintenance of plasma ionized calcium concentration within a narrow range is the central theme in mineral homeostasis. The parathyroid gland serves as principal regulator of this process. The

absence of any abnormal increase in the PTH level in the serum is directly proportional to the normal calcium levels in the rabbit serum. And hence, the hormone calcitonin the major calcium ion regulator in the plasma did not increase. This is further confirmed by the histological observation of the implant site, where no osteoclast activity is seen around the implant bone-interface.

Bone mineralization rate was quantified by image analysis for uncoated HA which showed 3 μm/day and for FG coated HA the bone mineralization rate was 3.3 μm/day. Uncoated BGS showed 2.8 μm/day and FG coated BGS showed 6.6 μm/day of bone formation after 3 months. Uncoated HABGS showed 3 μm/day and FG coated HABGS showed 4.3 μm/day bone mineralization. Undoubtedly growth factor coated bioactive material increased the rate of bone mineralization, when compared to uncoated bioactive granules.

Osteocytes are mature osteoblast cells seen mineralized within the bone matrix. Image analysis for the size of the osteocytes was performed to understand the functional status of these osteocytes in the mineralized matrix, based on their size (Figure V.60 and Figure V.61). The statistical significance for the size of the osteocytes was made based on the comparison between the osteocytes seen within the newly formed bone and the osteocytes adjacent to the defect. Sham defect filled with FG and FG coated HA and HABGS showed significant increase in the size of the osteocytes. The increase in the size of the osteocytes is directly proportional to the activity of the cells in the mineralized matrix.

XRD of the HA, BGS and HABGS granules after implantation in the rabbit tibia bone revealed apatite peaks of bone and not the typical synthetic apatite HA peaks. The wollastonite ($CaO.SiO_3/CaO.SiO_2$) peaks and the whitlockite (β-tricalcium phosphate-$Ca_3.(PO)_2$) and few brushite peak (dicalcium phosphate dihydrate- $Ca\,HPO_4.2H_2O$) were observed after implantation and several other

phases were also observed along with these peaks. An extensive study has to be performed to characterize the different phase evolved with these bioactive ceramic implants.

Oxyhydroxyapatite [$Ca_{10}(PO_4)_6O$], α-TCP, β-TCP or β-whitlockite, TTCP and OCP have all been detected, post processing, in varying amounts via XRD, FT-IR and chemical analysis. These compounds are not apatites per se, since the crystal structure differs from that of actual apatite. Differences in the structure, chemistry, and composition of apatites arise from differences in material processing techniques, time, temperature and atmosphere. Understanding the processing, composition, structure, processing synergy for calcium phosphate ceramics helps us understand the in vivo function of these materials.

FT-IR spectra of HA, BGS and HABGS revealed carbonated apatite peaks. ν_3 and ν_4 peaks of the CO_3 were observed, which is typical of the bone apatite. The C-H that was observed in dissolution studies after the immersion of the bioactive granules was observed in bone samples also. The significance of this C-H peak is not clear. BGS and HABGS did not show any typical wollastonite peaks that were observed in the raw samples between 1118 cm^{-1} – 716 cm^{-1}. This possibly suggests that the silicate peaks after implantation has formed some complex with other functional groups. Stoichiometric hydroxyapatite is neither calcium nor hydroxyl-deficient, and nor contains hydrogen bonds. The bone mineral substance contains 3 to 4 percent carbonate ions instead of phosphate ions. The presence of carbonate induces misalignment in the bone mineral crystal, provoking an increase in its chemical reactivity. Bone mineral substance appears as needle-like and plate-like crystals 1.5 to 5 nm thick, 5 to 10 nm wide, and 50 to 100 nm long (Bonucci 1984, Glimcher 1984). Bone crystals show a highly specific surface and have reactive surfaces

(Posner 1987), allowing for numerous ionic substitutions (fluoride in particular). Bone mineral substance is a microcrystalline analogue of the mineral hydroxyapatite Ca_{10} $(PO_4)_6$ $(OH)_2$, with a calcium deficiency of about 5 to 10 percent. This deficiency is balanced by a combination of missing hydroxyl ions and hydrogen bonds between oxygens of orthophosphate (Posner 1985, 1987).

EDAX studies showed very low silica content around the implant (Figure.V.57) site in HABGS and BGS after 3 and 6 months.

The calcium phosphate (Ca/P) of the mineralized bone at the implant material interface was 1.714 and 1.74 for HA after 3 and 6 months. BGS showed Ca/P ratio of 1.549 and 1.51. HABGS showed 1.529 and 1.605 after 3 and 6 months. The Ca/P ratio for bone is 1.77 (Drissens, 1980) and the stoichiometric HA is having a Ca/P ratio of ~ 1.67. The Ca/P ratio is higher in HA and lower in BGS and HABGS. The significance of this may directly correlate to the mineralization of the bone with the implant. HA showed normal mineralization pattern, whereas BGS and HABGS has the nucleating agent silica (Si), which might have initiated complex with the inorganic ions and hence Ca/P ratio is low when compared to HA.

HYPOTHESIS

The bioactive nature of the ceramic and glass-ceramic granules (HA, BGS and HABGS) material is well understood after *in vitro* and *in vivo* studies and we propose an hypothesis for the initiation of bone mineralization process leading osseointegration with respect to the indigenously developed HA, BGS and HABGS granules (Figure.V.5.59).

Even though, the pH (**a**) of the microenvironment favours dissolution, it is the bioactive nature of the implant material that stabilizes the pH to be stable or unstable at the local site. If the material degrades quickly, it may bring high alkaline/acidic microenvironment and is toxic, (or) if the material is very slow in degrading (or) less bioactive (or) the neutralizing effect (pH) is not quick by the implant/local site, it could lead to a prolonged acidic pH (minutes to hours/days) and there by leading to inflammation.

In *in vitro* (**b**), the response of calcium phosphate ceramics on the pH chiefly depends on the chemical and physical property and also by the local effect of the medium and the cells on the material. The response of bioactive calcium phosphate ceramic implant in *in vitro* and *in vivo* (**c**) conditions directly depends on the pH of the local micro/macroenvironment. The mechanism a, b and c favours the pH increase and decrease, which results in the material to undergo slow dissolution or rapid dissolution in *in vitro* and *in vivo* conditions (**d**).

i) The dissolution can also have a positive and negative effect on the local pH.
ii) The pH change in turn dictates positive and negative biological signal that will decide on further response by the cells (*in vitro* / *in vivo*).

Dissolution will lead to release of the calcium and phosphate ions (**e**) in the local medium until it reaches the saturation level. Once it reaches the saturation level (*in vitro* and *in vivo*) it gets precipitated with the local medium (physiological medium) resulting in the redeposition on the material or on the surroundings of the implant.

i) If the material is highly bioactive the reprecipitation/deposition of the ions onto the material or surrounding the material will get delayed until it is getting supersaturated. Dissolution not only favours (**f**) releasing of the ions in the medium but also favours the protein adsorption on to the material surface, which is a simultaneous process (Strictly based on the bioactive nature of the material).

i) If the material is less bioactive it will lead to less or slow release of the calcium phosphate ions into the medium and thereby triggering quicker protein adsorption on to the material, leading to: preventing or slowing down the release of the calcium phosphate ions.

ii) If the protein adsorbed onto the material surface does not have enough precipitated calcium and phosphate ions, may lead to a slow biomineralization process both in *in vitro* or *in vivo*.

Precipitation (**g**) is achieved after saturation, and favours apatite formation on the material surface reacting with the local physiological medium.

i) If the local medium is not physiologically rich in ions or has a less bioactive medium it may lead to a delay in the apatite formation (Both *in vitro* and *in vivo*, taking into account the material is less bioactive).

ii) Apatite formation is triggered even if the local physiological medium is less rich in ions. Since the material is bioactive, and the ions released during dissolution will favour early apatite formation, and thereby favouring biomineralization.

The protein adsorption (**h**) on the material surface is followed immediately after dissolution and precipitation (in bioactive implant materials), thereby favouring/not favouring the cell attachment, proliferation, differentiation.

i) The even adsorption of the protein on the material might be due to the less bioactive surface of the implant material.

ii) Dissolution of the implant before precipitation facilitates the intergranular porosity to increase, thereby facilitating the protein adsorption much deeper into the intergranular spaces and on the surface of the material. The bioactive nature of the implant helps the cells to adhere to the surface firmly.

iii) Less bioactive and dense surface of implants will lead to thick protein adsorption, where the cells will adhere and may proliferate but will not favour differentiation, due to the less bioactive nature of the implant.

Osteoinduction **(j-1)** is the process where the implant stimulates/or the cells release growth factors that help in the proliferation and differentiation of committed and induced osteoprogenitor cells (pre-osteoblast-like cells) into osteoblast cells which will initiate biomineralization. Osteoconduction **(j-2)** is the result of bone growing from the defect site towards the implant (in close apposition to the implant) due to the bioactive /osteocompatibility property of the implant. Osteoinduction and Osteoconduction **(j-3)** are also directly related to the physical, chemical and biological property apart from where the material is (extraskeletal or in skeletal tissue). Osteoinduction and osteoconduction **(m)** can exist together in conditions where the material has both inducting and conducting properties:

i) **Physical property**: The porosity, the sintering temperature, the grain structure, and the crystalline or amorphous nature of the material decide the induction and conduction process.

ii) **Chemical property**: The calcium phosphate ratio, pH, chemically inert or bioactive nature of the material in physiological medium, may contribute to the conduction and induction process.

iii) **Biological property**: The cell response to the implant and the implant response on the cell decides the involvement of the type of cells, growth factor release, proliferation and differentiation of the cells, and in turn decides the pattern of healing [indirect-endochondral or direct bone formation -membranous].

Based on the information i) to iii) mentioned above, the material having all the three properties will definitely undergo osteoinduction and osteoconduction but the

percentage or the response of induction and conduction may vary based on time, material, defect size and site.

Osteoinduction/Osteoconduction process stimulates osteoblast cells to lay down collagen (**n**) and speeds up the biomineralization process. Osseointegration (**o**) is directly proportional to the speed at which the biomineralization process is triggered (if the biomineralization process is slow it may lead to unwanted tissue ingrowth) and the bioactive nature of the implant (that prevents the unwanted cells to group into a fibrous tissue and favour bone apposition).

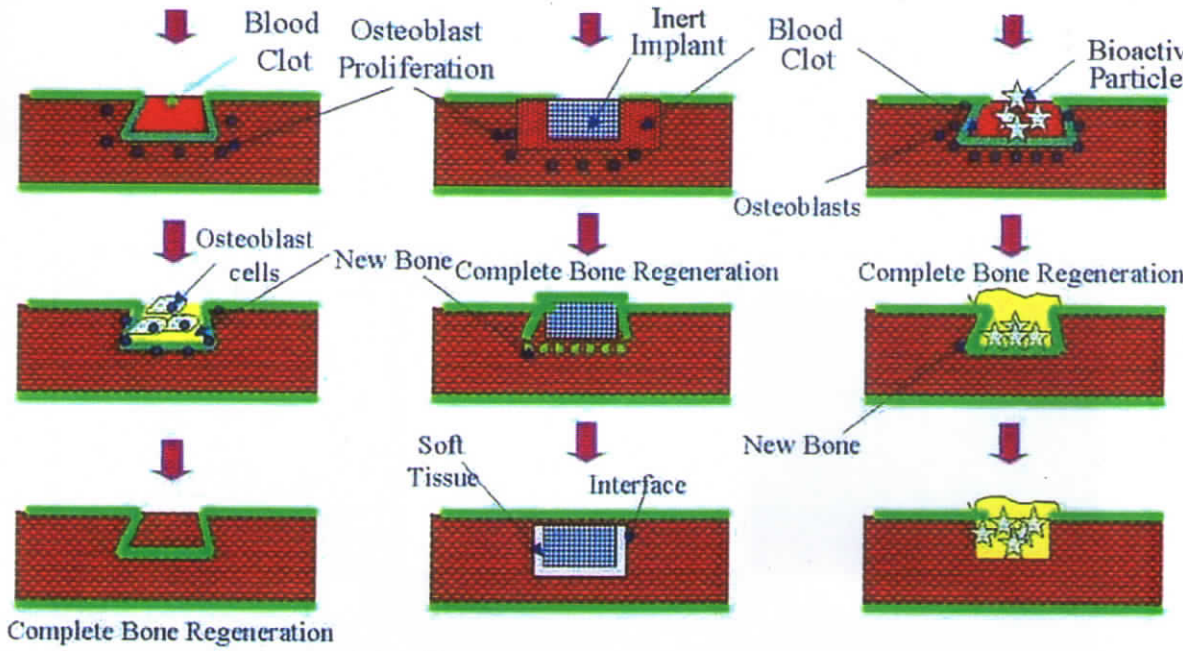

(Adopted from D.F. Williams, J Mat Sci 1987;22:3421-3445)

B

IMPLANTATION PROCEDURE AND THE HEALING PATTERN IN TIBIA BONE IMPLANTED WITH BIOACTIVE CERAMICS

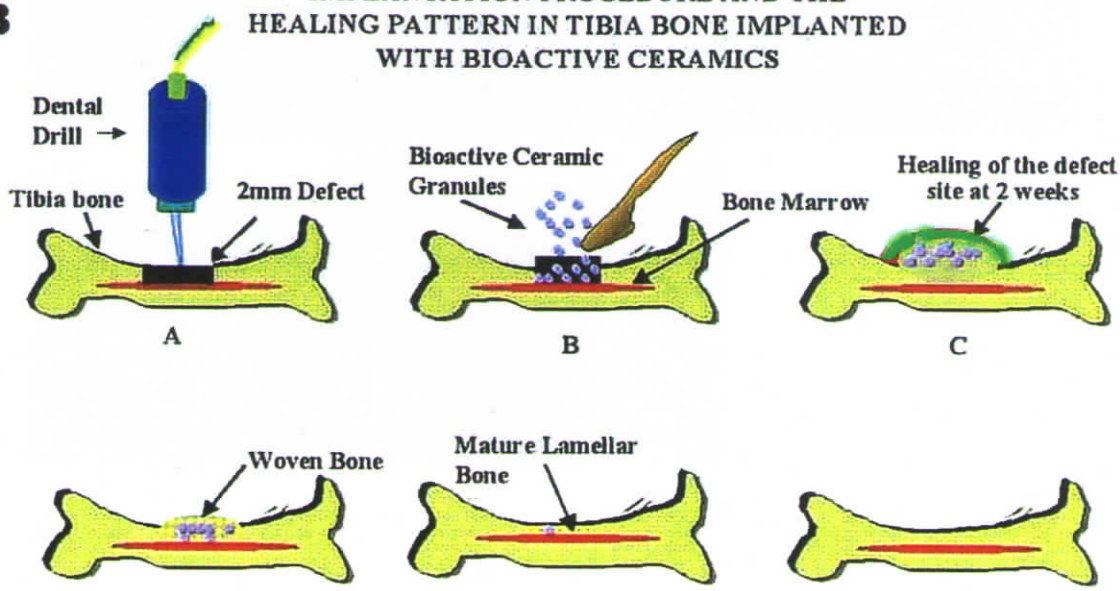

D
Healing of the defect- hard callus is replaced by 1 month

E
The defect has completely healed by 3 months with a few granules still persisting (HA, BGS & HABGS granules)

F
The implants are completely resorbed and replaced by host tissue at 6 months to 1 year (Except HA granule, BGS (80%) and HABGS granules (70%) are replaced

Figure - V-56

Schematic representation of the the healing of bone with impalnt: A - difference between the normal healing of a defect to that of the metalic implant and a bioactive implant; B - bone healing with respec to the bioactive ceramics sysnthesized in-house at SCTIMST.

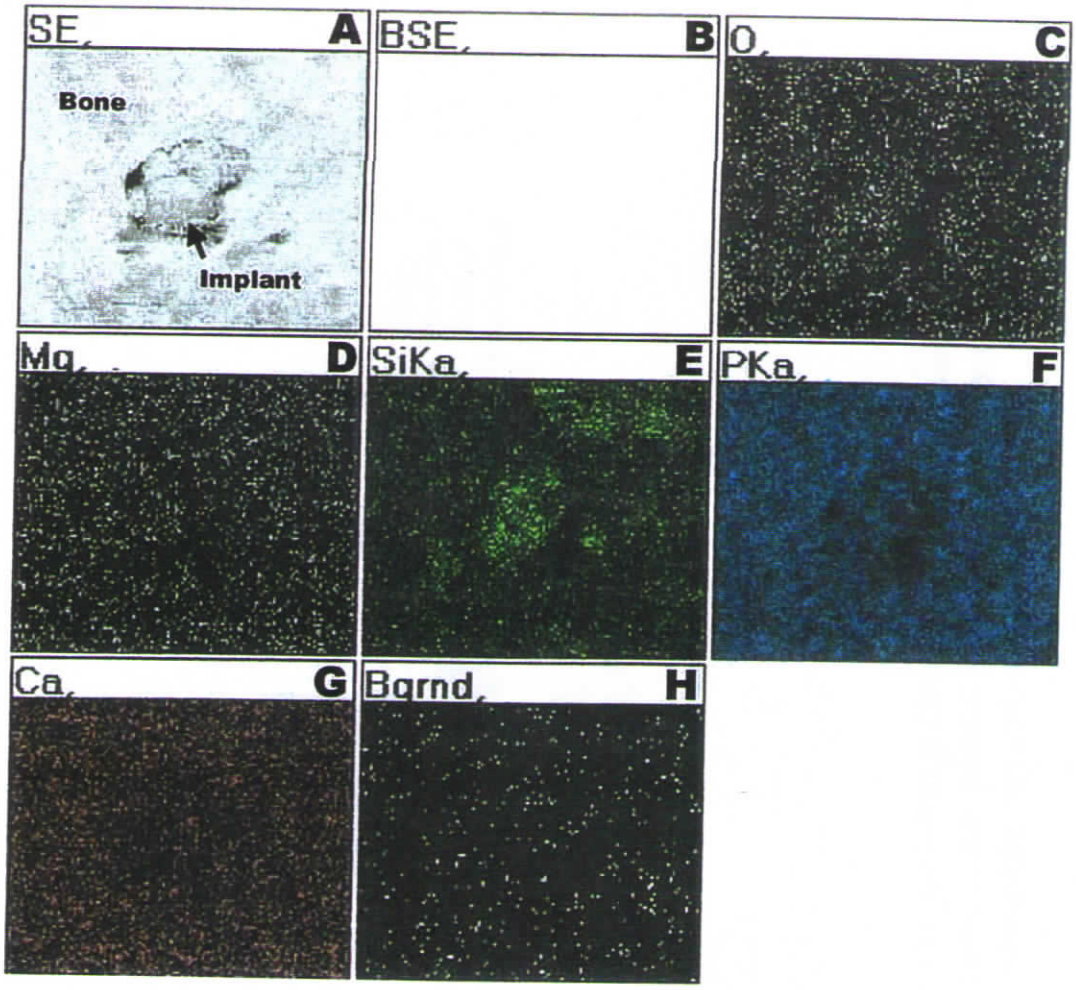

Figure -V-57

SEM-EDAX image of rabbit tibia bone implanted with BGS granules after 3 months showing the distribution of element around the implant bone interface. A - implant bone interface (arrow); B- blank; C - oxygen; D - magnesium; E - silica; F - phosphorous; G - calcium and H - background.

Figure -V-58

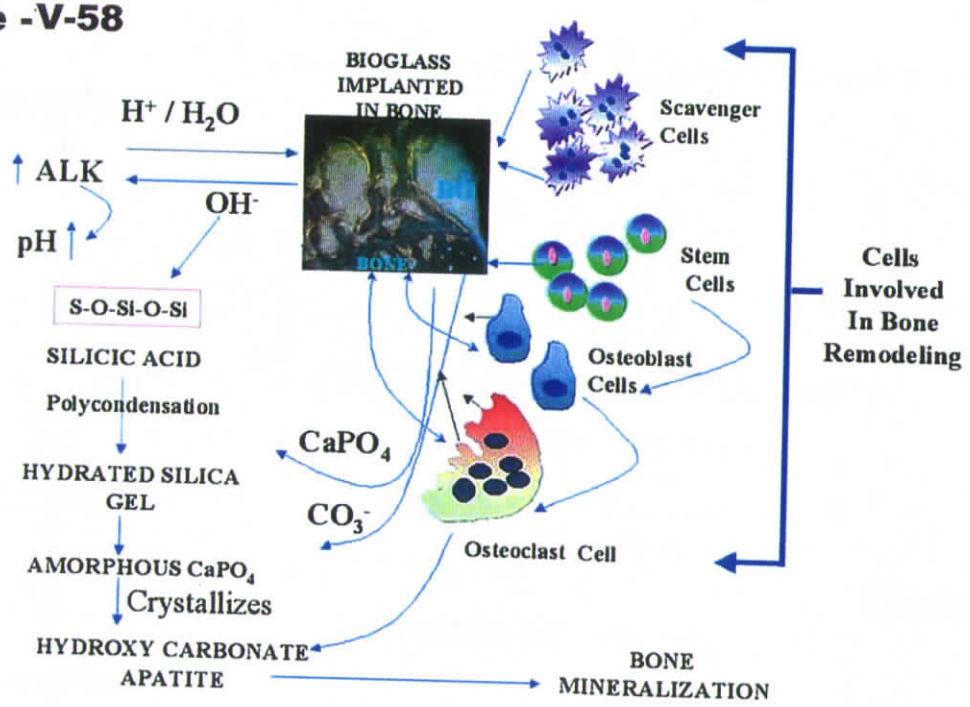

Schematic diagram showing the possible cascade of reactions that might take place *in vivo* with bioactive glass ceramic system - AW type

Figure -V-59

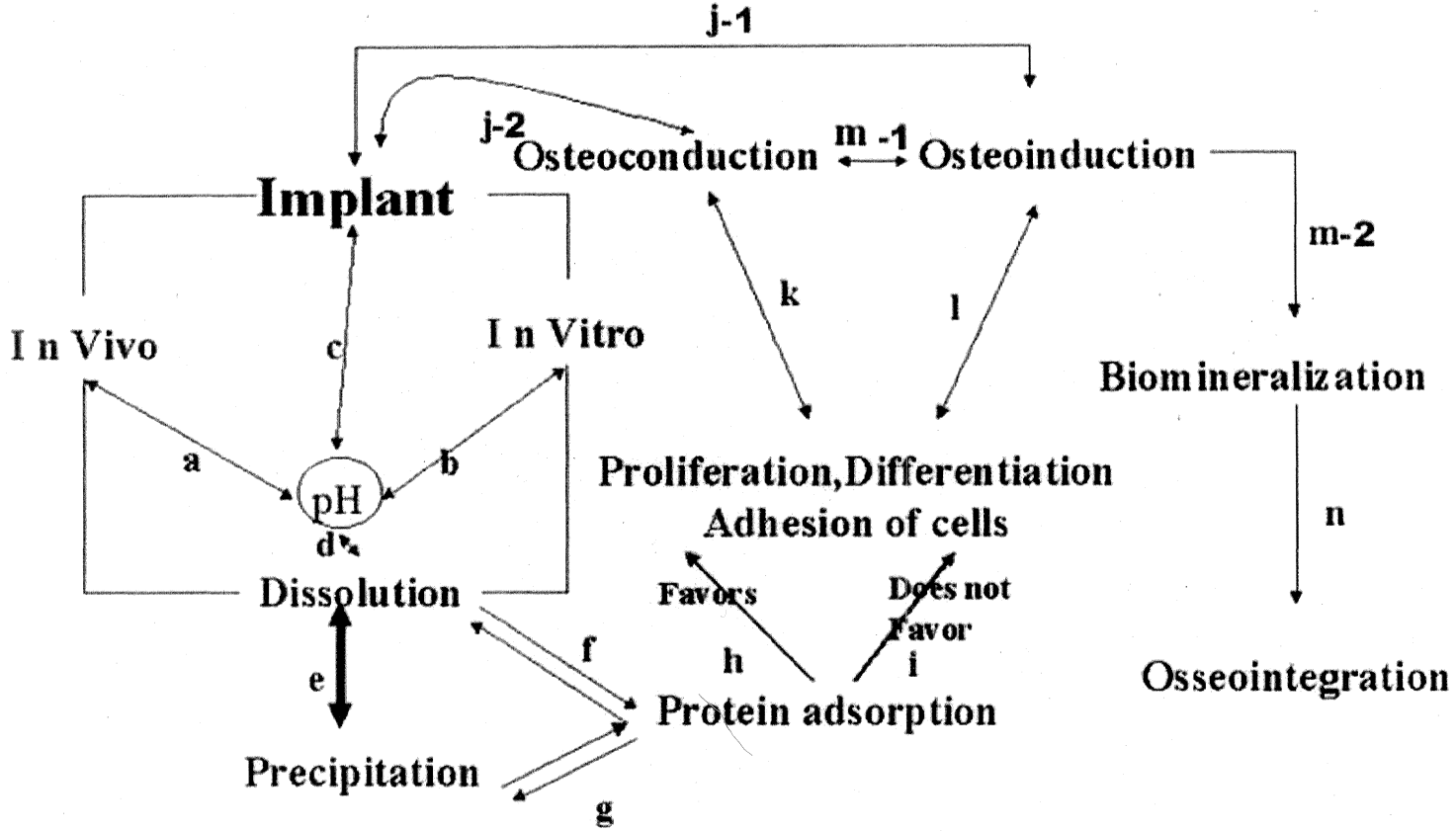

Mechanism of bioactive ceramic granules reacting to physiological actions *in vitro* and in *in vivo* : An understanding towards osseointegration

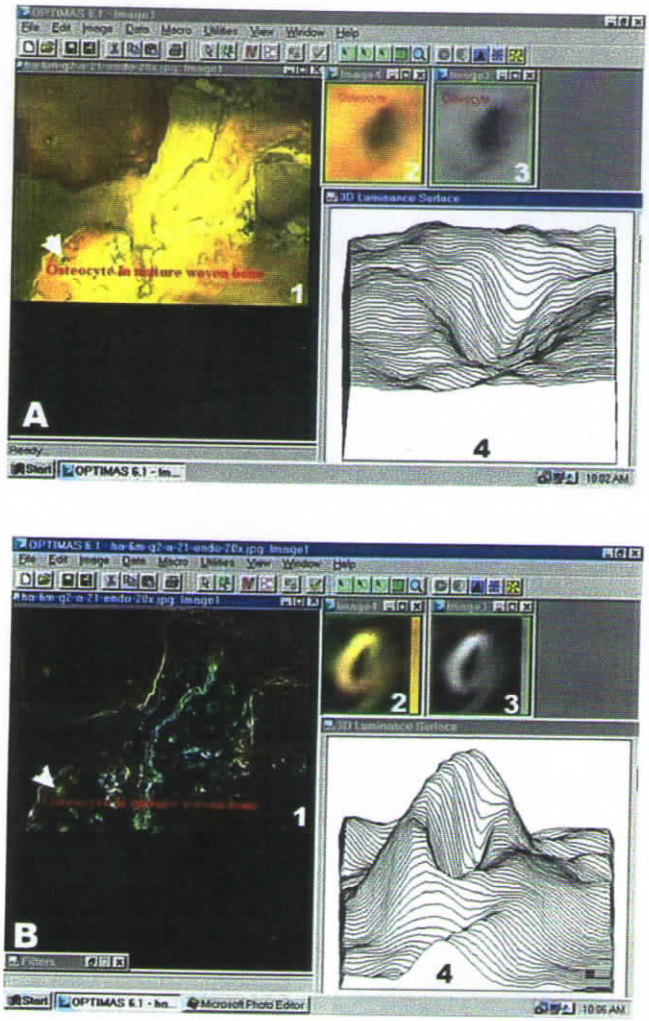

Figure -V-60

Photomicrographs of HA implanted sections showing Image of an osteocyte before (A) and after (B) applying filter in rabbit tibia bone after 6 months. Image 1of A and B is before and after aplying filter; 2 - individual osteocyte (arrow) under R G B mode, 3 - same osteocyte under 8-bit grey scale and 4 - osteocyte in 3-D luminance mode.

Note: osteocyte appearence changes before and after filter.

Figure-V-61

Photomicrographs of BGS implanted sections showing Image of an osteocyte before and after applying filter in rabbit tibia bone after 3 months. A-Image before and after applying filter; B & C -Osteocyte before and after applying filter.

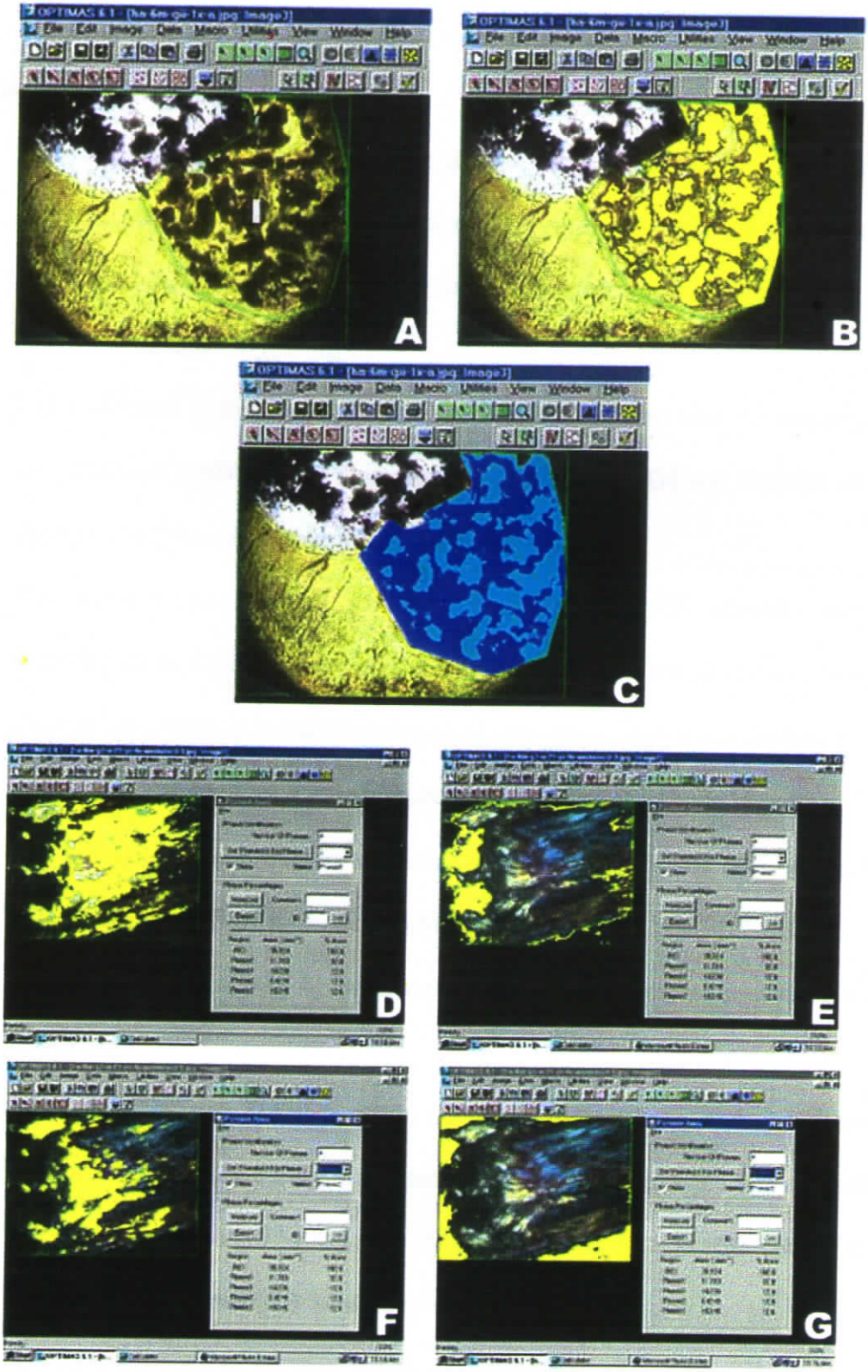

Figure -V-62

Photomicrographs showing the method employed for quantifying the percentage of new bone formed in a defect after implantation. A - bone with the implant (I); B - implant alone thresholded (yellow); C - bone alone thresholded (blue); D to G - image under polarized light: D - mineralized areas (yellow), E - newly mineralized bone (yellow), F - active mineralized bone (yellow) and G - surrounding areas, where polarization is absent.

V.2.15 Conclusion

1. Bone mineralization was by osteoconduction with uncoated HA, BGS and HABGS granules and showed osteoinduction with FG coated HA granules and a bimodal action of osteoinduction and osteoconduction with BGS and HABGS granules.
2. The new bone formed around the bone is well integrated with the uncoated HA, BGS and HABGS after 6 months. FG coated HA, BGS and HABGS also showed good osseointegration with the new bone.
3. The mineralization pattern for HA, BGS and HABGS granules were identified to be different based on the fluorescent uptake, and the type of bone formed, i.e. woven or lamellar bone around the implant after 3 and 6 months.
4. Porosity of HA granules (100- 120 μm) definitely favoured bone ingrowth.
5. X-ray radiograph and contact microradiograph of implant site showed good osseointegration of the material with the host bone.
6. The bone formation was by intramembraneous ossification without cartilage formation.
7. Silica in BGS and HABGS were non-toxic to the bone and the tissue architecture around the bone was intact. The percentage of bone formed with BGS granules was 80.5 % and with HABGS granules 74.5 % after 6 months. Whereas, HA showed 67.9 % of bone after 6 months.
8. A new mechanism of osteoinduction and osteoconduction process happening simultaneously in the osteogenesis process with BGS and HABGS granules was observed.

9. Biochemical evaluation of the serum calcium, phosphorous, protein, ALP, ACP, PTH and calcitonin did not show any adverse change after 3 and 6 months, suggesting that the bone healing was uneventful.
10. Bone mineralization rate was high for FG coated BGS granules (6.6 μm/day), FG coated HA showed 3.3 μm/day and HABGS coated with FG showed 4.3 μm/day. Whereas, uncoated HA, BGS and HABGS showed ~ 3μm/day new bone formation.
11. XRD, FT-IR and EDAX studies revealed good material tissue response. A new observation is made with respect to the Ca/P ratio of the bone around the implant. BGS and HABGS showed Ca/P ratio of 1.51 and 1.6 after 6 months, whereas, HA showed a very high Ca/P ratio 1.74 after 6 months. This change in the Ca/P ratio could be due to the nucleating agent, silica (Si) present in the BGS and HABGS.

Figure - VI-1

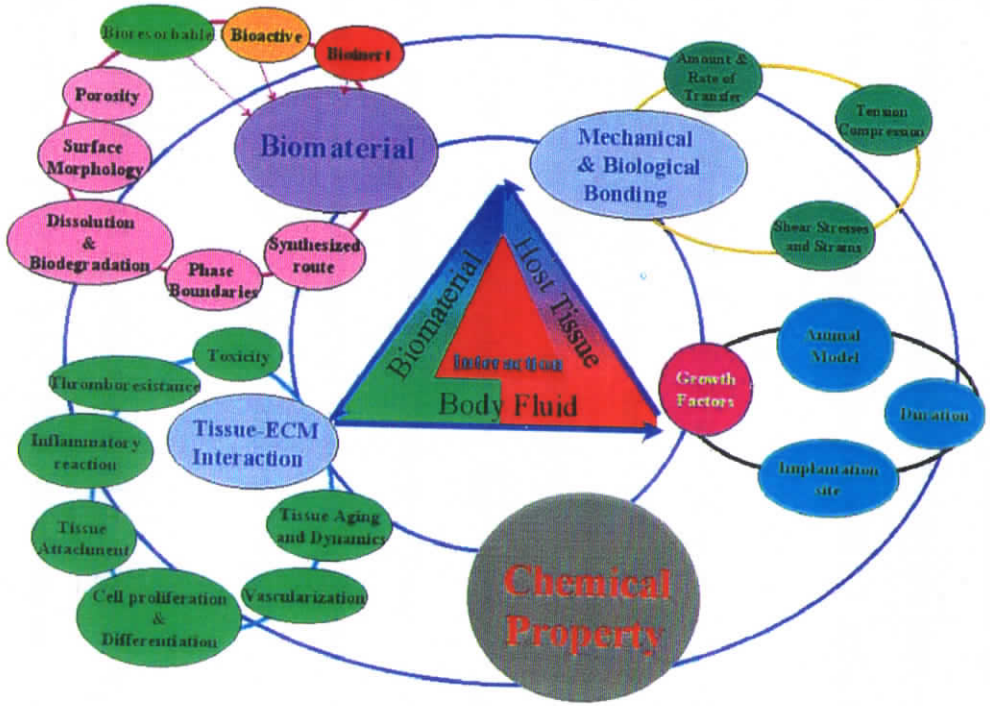

Schematic diagram of the possible major pathways involved in the sucess or failure of an implant

CHAPTER – VI

COMPARISON OF BIOACTIVE CERAMICS

VI. COMPARISON OF BIOACTIVE CERAMICS

Comparison of synthetically prepared bioactive ceramics with the commercially available ceramics.

The biomaterials research is a multidisciplinary field where different scientific disciplines work for a common goal. "*Developing an ideal material for an intended tissue is the dream of biomaterials researchers*". The materials developed for an intended application has to be developed based on the knowledge of the physiological environment, which will be in contact with the material/implant. Sufficient knowledge on biomaterials at the: tissue/cell/organelle/gene level has been studied to understand the interaction between the "*man made material and the God given body*".

Even though, 40 years or more of research has been done, only diminutive information on the material - tissue response has been understood. Since, the "*World of Biomaterials*" is large, the knowledge pool that is achieved in one field, for e.g. in cardiovascular implants, did not transform into other disciplines, like how the study of "Nuclear Physics" transformed into "Nuclear Medicine". This gap has to be minimized and the only option, which I think could be, is the "Triangular Interactions" of:

Industry ◄—► Research and Development Institutions ◄—► Academic Institutions.

Biomaterials are used in various medical disciplines, to name a few major areas such as orthopaedics, cardiology, ophthalmology and Neurology. Developing an ideal material, whose physicochemical properties are stable for a long–term performance is the need of the hour. Although several medical devices and implants were developed, they fail to give the appropriate desired response.

Several arguments over the failure in achieving stable biomaterials were made like:

a. Man cannot replace God's creation- A myth or a reality?

b. Lack of proper definition for what biomaterials are really-----

c. Short-term duration is O.K. Long-term duration, will be thought of later---

d. The material developed for a normal body can it be used in a diseased condition?

Likewise, so many queries follow, for which scientific explanations are required.

Our Institute's "Bioceramics" programme was aimed at developing better ceramic materials, which has close chemical property to that of natural bone, which might augment the healing process in a normal fractured bone.

Calcium phosphate ceramics are ceramic materials with varying calcium to phosphate ratios. HA as a biomaterial, stems from the perceived advantage of using a material similar to the mineral phase in bone and teeth for replacing these materials. Better tissue bonding is therefore expected.

Additional advantages of bioactive ceramics include low thermal and electrical conductivity, elastic properties similar to those of bone, controlled degradation rates through unique material properties and the possibility of ceramics as coatings on metals. These advantages would minimize the stress shielding confronted by implants, and favour better bone ingrowth into the implant. Since, stress shielding by the implant would lead to implant failure, using HA would minimize this problem, was reported by Chang *et al.,* (1996).

Generally HA blocks are used to fill wide osseous defects, while HA granules are preferred in other cases, especially if osseous parts of irregular shape must be filled or reconstructed.

An approximate qualitative evaluation of the HA implanted tibia bone showed 71.4 % of bone for 28.6 % of the implant after 3 months and after 6 month the bone tissue constituted about 67.9 % for 32.1% of the implant area. Holmes *et al.*, (1988) has reported that for a 4-month old specimen the bone tissue constituted about 30 % of the implant volume. From this observation it is clear that HA showed comparatively higher bone growth rate within 3 months.

Several investigators observed the reduction of bone ingrowth with increasing depth into the porous HA. Eggli *et al.*,(1988) reported that the percentage of bone at given depths declined considerably from the surface to the center of 3-mm diameter cylinders implanted into the cancellous bone of rabbits. Whereas, this indigenously prepared HA did not show any such reduction in bone growth in a 2 mm defect of rabbit tibia bone.

Martin *et al.*, (1993) demonstrated that bone ingrowth into Interpore 200 after 1 year reached a level of 74 % when placed in the cortical bone of the radius of dogs. In long-term implants the pore spaces were filled with Haversian type bone, which suggests that the vascularization of the pore space is complete and mature bone is present. The bone ingrowth into the pores of the indigenously synthesized HA was completed by 3 months (71.4 %).

In long-term implants, decreasing amounts of bone ingrowth were still observed as the depth into the implant increases, even though the porosity in the interior regions is equivalent to that at the surface. Within the pore space of the implants, the percent apposition against the HA was observed to be greater than the percent ingrowth into the available space for all lengths of implantation time (Ayers *et al.*, 1999). Earlier work showed that bone ingrowth into a porous implant is not optimized or predicted exclusively by the loading environment (Hollister, *et al.*,

1993). Patient age had very little affect on the amount or time for bone to grow into the available pore spaces (Ayers *et al.*, 1999). HA implants with 0.5 to 1 mm size granules and a pore size of 100 –200 μm was implanted (2 mm defect size: critical defect in rabbit) in tibia bone and after 1 year (data not shown in this thesis) the implant still persisted and showed bone ingrowth into the pores, without any gap at the implant new bone interface.

Even though, HA is classified under bioactive ceramic material, its bioactive property is very slow as observed from our dissolution experiments and histological findings. However, BGS (AW-type) and HABGS a composite developed in this Institute have high osteogenic property and degradability.

The concept of bioactivity was introduced with respect to bioactive glasses via the following hypothesis: "*The biocompatibility of an implant material is optimal if the material elicits the formation of normal tissues at its surface, and in addition, if it establishes a contiguous interface capable of supporting the loads that normally occur at the site of implantation*". Chemical reactions are limited to the surface (about 300 – 500 μm) of the glasses and bulk properties are not affected by surface reactivity. The implant surface releases Na^{+} ions and subsequently also Ca^{2+} and P^{5+} ions. The degree of activity (and physiologic response) is dependent on the chemical composition of the glass and may vary by over an order of magnitude.

Hench (1994) proposed that the soluble silicon activated stem cells producing TGF-β, which is reversibly adsorbed and desorbed in the hydrated silica calcium phosphate gel layers formed on the glass, which stimulates differentiation and subsequent growth of stem cells leading to rapid proliferation of bone in contact with bioactive glass.

Ceravital developed by Pfeil and Bromer (1973) is another glass, with different alkali oxide concentrations from Bioglass. The physiological responses of Bioglass and Ceravital are similar. It is hypothesized that the general biologic response to both glasses is the nucleation of hydroxyapatite crystals at the implant surface within an ordered collagen matrix, followed by the formation of mineralized bone.

Eg. a glass ceramic containing oxyapatite and fluorapatite [$Ca_{10}(PO_4)_6(O, F_2)$] and β-Wollastonite (SiO_2 –CaO) in MgO –CaO-SiO_2 glassy matrix (AW-system). If the physiological environment is correctly stimulated in terms of ion concentration, pH, and temperature, this layer consists of carbonate containing hydroxyapatite of small crystallites with a defective structure, and the composition and structural characteristics are similar to those of bone. A-W glass ceramic bonds to living bone, through a thin calcium and phosphorous rich layer that is formed at the surface of the glass ceramic.

BGS is an A-W type ceramic material, which is a highly reacting material to pH, temperature and ionic concentration. But, the striking feature is its inductive and degradability property. The material releases calcium and phosphorous very quickly upon reacting with the physiological solution and the apatite formation is detected as early as 6 h (data not shown). The bioactive nature of the material is confirmed by our heterotopic, where induction of bone was observed with fibrin glue within 15 days after implantation in mice quadriceps muscle. Whereas, Urist (1988) reported that ectopic bone formation in the mouse thigh with sealed BMP/NCP composite implants induced bone formation at Day 21. This is the first report to confirm the osteoinduction property of an indigenously synthesized ceramic granule with indigenously prepared fibrin glue (FG) as early as Day 15.

The mechanism of osteoinduction with this bioactive ceramic granules leading to neo-osteogenesis in the muscle is given in Figure (V-16). The osteoinduction property of these ceramic granules was also observed in bone. The rate of bone formation was comparatively higher than HA. BGS showed 84.2 % of bone and only 15.8 % of implant was remaining after 3 months. After 6 months 80.5 % of bone was observed and only 19.5 % of implant remained (the reasons for this value is explained in chapter V. orthotopic –discussion). After 6 months the material was completely replaced by lamellar bone without any trace of implant.

HABGS implants also showed osteoinduction with FG. After implantation in bone 72.1 % of new bone and 27.9 % of implant was quantified after 3 months. After six months 74.5 % of new bone and 24.5 % of implant was quantified. The implant showed a different osteogenic process where, the bone was seen within the cracks of the implant, which appeared as if bone was growing on the surface of the implant.

HABGS and BGS showed relatively two different mechanisms of osteogenesis. The possible cascades of action that leads to stimulation of mesenchymal stem cells and mineralization is shown in Figure (V-58) and the complete mechanism that leads to osteogenesis and osseointegration with the implant is given in Figure (V-59).

To conclude HA, BGS and HABGS are found to be ideal bioactive ceramic granules and their osteogenic property is very high. To choose an ideal material for an ideal tissue response one has to understand the interplay that normally takes place in an *in vitro* or *in vivo* system and this "Chakra" (circle) has to be kept in mind before developing and evaluating a material for an intended *in vivo* application (Figure VI.1).

CHAPTER – VII

SUMMARY

SUMMARY

The objective of this study was mainly focused on - to evaluate HA, BGS and HABGS ceramic granules synthesized in-house at BMT Wing, SCTIMST for its cytocompatibility and osteocompatibility and in turn, to suggest the mechanism of healing in bone with respect to the three different granules.

The *in vitro* dissolution experiments were carried out in different simulated physiological media with and without protein, to understand the bioactive property of HA, BGS and HABGS granules prior to the cell culture and *in vivo* studies. From these simulated studies, it was understood that protein rich medium did not delay the process of apatite formation on the materials irrespective of the amount of protein that adsorbed on the material.

The physicochemical property of the material definitely played a major role in the stimulation of the osteogenesis and osseointegration process.

The dissolution studies confirmed the bioactive property of the three materials with respect to the pH influence. The *in vitro* evaluation of the bioactive ceramic granules/discs showed hardly any toxicity and exhibited good cell attachment and spreading.

Heterotopic studies revealed that the uncoated HA, BGS and HABGS granules were non-toxic, and evoked less fibrous encapsulation around the material. FG coated granules showed good tissue response without any fibrous tissue encapsulation or inflammatory reaction. BGS and HABGS showed osteoinduction with FG but HA did not. The main observation was that induction of new bone was observed at 15^{th} day after implantation, which is far ahead of the earlier reported data of 21 days in the same animal model.

The orthotopic implantation studies proved the materials to be well tolerated with good osteointegration. The degradation of the material and the bone formation pattern was different for the three granules with and without FG.

CONCLUSION

These granules can be used for implantation based on the type of healing one requires. HA, BGS and HABGS not only acted as a scaffolding material but also enhanced the bone formation due to their close chemical properties to that of bone. The porosity of HA material favoured better bone anchorage and the less degrading ability of the material will favour a better scaffold for bone in conditions where the material is expected to remain to support bone formation at its own pace. BGS and HABGS material can be an ideal material where one expects a quick healing at the shortest span of time. The degradation of the material and the sustained release of the ions favoured early mineralization and with time the material will degrade completely to be replaced by new bone. However, the composite material would provide a better scaffold and augment bone formation and thereby prove to be a surgeon patient friendly implant.

FUTURE PROSPECTS

1. To evaluate the bone tissue response of HA, BGS and HABGS granules in a large bone defect
2. To study the healing mechanism of these ceramics in a diseased animal model and
3. To enhance healing of the defect by using growth factors or cells in combination with the materials.

BIBLIOGRAPHY

BIBLIOGRAPHY

Addadi L and Weiner S. Interactions between acidic proteins and crystals: strereochemical requirement in biomineralization Prc.Natl.Acad.Sci. 1985; 82: 4110-4114

Albee FH, and Morrison HF. Studies in bone growth: triple calcium phosphate as stimulus to osteogenesis, Ann. Surg., 1920,71:32-39

Anderegg. G. *et al.,* (1954) Helv. Chim Acta 35, 113

Anderson HC, Marker PC, and Fogh J. Formation of tumors containing bone after intramuscular injection of transformed human amnion cells (FL) into cortisone-treated mice. Americal Journal of Pathology, 1964;44:507

Anderson WAD. Pathology, 6th ed. Mosby, St. Louis. 1971.p.16

Anselme K, Sharrock P, Hardouin P and Dard M. In vitro growth of human adult bone-derived cells on hydroxyapatite plasma –sprayed coatings J Biomed Mater Res 1997;34:247-259

Aoki, H. Medical Applications of hydroxyapatite-Bone mineral, drug delivery system, cancer and HIV, IVH and CAPD, Dental implant,(1994) Takayama Press System Center Co., Inc. Japan

Arbes H, Bosch P, Lintner F, Salzer M. First clinical experience with heterologou cancellous bone grafting combined with the fibrin adhesive system (F.A.S) Arch Orthop Trauma Surg 1981; 98:183.

Asada K, Yoshida K, Shimazu A, Yunoki H, and Ishida N. Nippon Seikeigeka Gakkai Zasshi 1987, 61: 155-169

Ashton BA, Allen TD, Howlett CR, Eagleson CC, Hattori A and Owen M. Formation of bone and cartilage by marrow stromals cells in diffusion chambers in vivo. Clin Orthop 1980;151:294.

Ayers, R.A., Wolford, L.M., Bateman, T.A., Ferguson, V.L., and Simske, S.J. Quantification of bone ingrowth into porous block hydroxyapatite in humans. J Biomed Mater Res 1999, 47:54-59

Baginski, E.S. (1973) Clin Chme Acta, 46, 46

Bajpai,P.K., and Benghuzzi, H.A. JBMR.1988,22:1245-1266

Baron R, Neff L, Louvard D and Courtoy P J 1985 J. Cell Biol. 101 2210

Baschkirzew NJ, and Petrow NN. Beitrage zur freien knochenuberpflanzung. Deutsche Zeitschrift fur Chirurgie, 1912;113:490.

Basle, M.F., Rebel, A., Grizon, F., Daculsi, G., Passuti, N., Filmon, R. Cellular response to calcium phosphate ceramics implanted in rabbit bone. J Mat. Sci. Mat. Med. 1993; 4:273-280

Beck SL, Deguzman L, Wyne LP, Xu Y, Mc Fatridge LA, Gillett NA, Amento EP. TGF-β1 induces bone closure of skull defects. J. Bone Miner Res 1991;61:1257-1265

Beevers, C.A., and McIntyre, D.B. The atomic structure of fluorapatite and its relation to that of tooth and bone mineral, Miner Mag. 27 (1956) 254-259.

Ben-Nissan B, Cha, C, and Evans L. Crystallographic and spectroscopic characterisation and morphology of biogenic and synthetic apatites. 1980

Benum P, Lyng S, Alm T, and Johannsenn N. Porous ceramics as a bone substitute in the medial condyle of the tibia. An experimental study in sheep. Long-term observations. Acta Orthopaedica Scandinavia, 1977; 48, 150

Bhaskar SN, Brady JM, Getter L, Growen MP, and Driskell T. Biodegrdation of ceramic implants in bone, Oral Surg. 1971; 32:336.

Blaschke R J, Howlett A R, Desprez P Y, Peterson O W and Bissell M J 1994 Methods Enzymol. 245 535

Bobyn, J., Pillar, R., Cameron, H., Weatherly, G. The optimal pore size for the fixation of porous surfaced metal implants by the ingrowth of bone. Clin Orthop Rel Res 1980;150:263-270

Bohner M. Calcium orthophosphates in medicine: from ceramics to calcium phosphate cements. Injury. Int.J. Care Injured 31 (2000) S-D37-47

Bonfield TLE, Colton E, and Anderson JM. Fibroblast stimulation by monocytes cultured on protein adsorbed biomedical polymers. I. Biomer and polydimethyl siloxane. J Biomat Mater Res. 1991; 25:165-175

Bonses RW, and Tausskay HH. J. Biol Chem 1945;158:581

Bonucci, E. The structural basis of calcification In: Ultrastructure of the connective tissue matrix (Ed. Ruggeri A, Motta P M). Martinus Nijhoff Publishers, Boston 1984: 165-191

Bosch P, Braun F, Eschberger J, Kovac Q, Spangler HP. The action of highly concentrated fibrin on healing. Arch Orthop Unfallchir 1977; 89:25

Boskey A.L. and Posner Overview of cellular elements and macromolecules implicated in the initiation of mineralization, in The Chemistry And Biology Of Mineralized Tissues ed. W. Butler, Birmingham, Alabama,1984; pp. 325-343.

Boskey AL. Matrix proteins and mineralisation: An overview. Connect Tissue Res 1996; 35:357-363

Boss, J.H. Osseointegration Journal of Long-term effects of medical implants, 1999, 9 (1&2): 1-10

Boucek RJ. Factors affecting wound healing. Otolaryngol, Clin. N. Am.17(2),243,1984

Bouhne, E., Pouezat, J.A., Peru, L., Daculsi, G. Heating of calcium phosphate crystals: Morphological consequences and biological implications. Cells Mater 1993;3:377-382

Bouler, J.M., Trecant, M., Delecrin, J., Royer, J., Passuti, N., Daculsi, G. Macroporous biphasic calcium phosphate ceramics: Influence of five synthesis parameters on compressive strength. J Biomed Mater Res 1996;32:603-609

Boyne PJ, Strunz TJ, and Shaghat JP. Three year long term study of implants of hydroxyapatite in dog alveolar bone, sth ANN. Meet. Soc. Biomaterials (1982)

Brighton CT, Hunt RM. Early histological and ultrastructural changes in medullary fracture callus. J Bone Joint Surg 1991; 73 A: 832-847.

Brinker, C.J and Scherer, G.W. Sol-Gel Science (Academic Press, San Diego, CA, 1990).

Bromer H, Pfeil E and Kass HH. German Patent 2, 326, 100 (1973)

Brown WE, and Chow LC. A new calcium phosphate, water-setting cement, in ceramics research progress (American Ceramic Society, Westerville, Ohio, 1986) pp. 352-379.

BrownPW and Fulmer M. Kinetics of hydroxyapatite formation at low temperature J Am Soc 1991;74:934-940

Bruhn HD, Christophers E, Pohl J and Schoel G. Regulation der fibroblasten proliferation durch Fibrinogen/Fibrin, Fibronectin und Faktor XIII. In Schimpf K Eds. Fibrin,

Bucholz RW, Carlton A, and Holmes RE. Hydroxyapatite and tricalcium phosphate bone graft substitutes, Orthop. Clin. N. Amer. 1987; 18:323-334.

Carlisle EM. Silicon as an essential trace element in animal nutrition. Ciba Found Symp 1986;121:123-139.

Carlisle EM. Silicon: A possible factor in bone calcification. Science 1970; 167: 279-280.

Chae JC, Collier JP, Mayor MB, Surprenant VA, Dauphinais LA. Enhanced ingrowth of porous-coated Co Cr implants plasma-sprayed with tricalcium phosphate. J Biomed Mater Res 1992; 26:93-102.

Chang, Y.S., Oka, M., Takashi, N., Gu, H.. Bone remodeling around implanted ceramics J Biomed Mater Res 1995; 29:527-533

Chen C S, Mrksich M, Huang S, Whitesides G M and Ingber D E 1997 Science 276 1425

Christel P, Meunier A, Dorlot JM, Crolet JM, WitvoetJ, Sedel L, and Boutin P. Ann.N.Y.Acad.Sci.1988,523:234-256

Claes L, Burri C, Gerngross H, Mutschler W. Bone healing stimulated by plasma factor XIII. Osteotomy experiments in sheep. Acta Orthop Scand 1985; 56: 57.

Clark A.E., Hench, L.L., and Paschall, H.A. The influence of surface chemistry on implant interface histology: a theoretical basis for implant material selection. J. Biomed. Mater. Res., 10, 161, 1976.

Clarke, KJ, Graves SE, Wong AJC, Triffit, JT, Francis MSP, Czerruszka JT. Investigation into the formation of mechanical properties of a bioactive matrial based on collagen and calcium phosphate J Mat Sci Mat Med 1993; 4:107-110

Cohen J, and Harris WB. Three dimensional anatomy of Haversian systems. J Bone Jt Surg 1958;40A:419-434.

Coleman, D.L., Kind, R.N., and Andrade, J.D. The foreign body reaction: a chronic inflammatory response. J.Biomed. Mater. Res., 8, 199, 1974

Cook SD, Dalton JE, Tan EH, Whitecloud-III TS, Rueger DC. *In vivo* evaluation of recombinant human osteogenic protein (rhOP-1) implants as a bone graft substitute for spinal fusions. Spine 1994;19:1655-1663.

Daculsi G, LeGeros R Z and Mitre D 1989 Calcif. Tiss. Int. 45 95

Daculsi G, LeGeros RZ, Nery E, Lynch K, and Kerebel B. JBMR. 1989,23:883-894

Daculsi G. Biphasic clcium phosphate concept applied to artificial bone, implant coating and injectable bone substitute. Biomaterials 1998;19: 1473-1478.

Daculsi, G., Le Geros, R.Z., Heughebaert, M., Barieux, I. Formation of carbonate-apatite crystals after implantation of calcium phosphate ceramics. Calcif Tissue Int 1990;46:20-27

Daculsi, G., LeGeros, J.P Three dimensional defects in hydroxyapatite of biological interests. J Biomed Mater Res 1996;31:485-501

Daculsi, G., LeGeros, R.Z., and Mitre, D. Crystal dissolution of biological and ceramic apatites Calcif Tissue Int 1989, 45:95-103

Daculsi, G., LeGeros, R.Z., Nery, E., Lynch, K., Kerebel, B. Transformation of biphasic calcium phosphate ceramics in vivo: Ultrastructural and physicochemical characterization J Biomed Mater Res 1989;23:883-894

Daculsi, G., LeGeros,R.Z., Nery,E., Lynch,K., and Kerebel,B. JBMR. 1989,23:883-894

Daculsi, G., Passut, N., Martin, S., and Deudon, C. JBMR24 (1990) 379

Damien CJ, Ricci JL, Alexander H, Patat JL . Formation of a calcium phosphate rich layer on absorbable calcium carbonate bone graft substitutes. Calcif Tissue Int 1994; 55:151-158.

Davies J E 1990 *Handbook of bioactive ceramics* (eds) J Wilson-Hench (CRC Press: Boca Raton) 1 195

de Bruijn, J.D., Bovell, Y.P., Davies, J.E., van Blitterswijk, C.A. Osteoclastic resorption of calcium phosphates is potentiated in postosteogenic culture conditions. J Biomed Mater Res 1994, 28:105-112

de Groot K 1980 Biomaterials 1 47

de Groot K, Geesink R, Klein CPAT, Serekian P. Plasma sprayed coatings on HA. JBMR,1987;21:1375-81

De Groot K, Klein C.P.A.T, Wolke J.C.G, and de Bliek-Hogervost J.M.A. Chemistry of calcium phosphate bioceramics, in Handbook of Bioactive Ceramics. Vol.II, eds. T.

de Groot K, Tencer A, Waite P, Nichols J and Kay J 1988 in *Bioceramics: materials characteristics versus in vivo behaviour* (ed)s P Ducheyne and J Lemons New York Academic Sciences p. 272

de groot K. Ceramics of calcium phosphates: preparation and properties. In: de Groot K, editor. Bioceramics of calcium-phosphate. Boca Raton: CRC Press, 1983. p.99-114

de Groot, K. Effect of porosity and physico-chemical properties on the stability, resorption and strength of calcium phosphate ceramics. Ann NY Acad Sci 1988;253:227-233

de Meyer, E.A.P., Verbeeck R.M.H., Naesans, D.E.J. Crystal Growth, 1994, 135, 539-547.

del Cerro M, Cogen J, del Cerro C. Stevenel's blue, an excellent stain for optical microscopical study of plastic embedded tissues. Microscopica Acta 1980; 83: 117-121.

Denissen, H.W., and de Groot, K. J. Prosthet. Dent. 1979; 42: 55.

Dennis JE, Haynesworth SE, Young RG Caplan AI. Osteogenesis in marrow-derived mesenchymal cell porous ceramic composites transplanted subcutaneously: effect of fibronectin and laminin on cell retention and rate of osteogenic expression. Cell Transplantation, Vol. 1:1992. p 23-32.

Diaz-Flores L, Guiterrez R, Lopez-Alonso A, Gonzalez R, Varela H. Pericytes as a supplementary source of osteoblasts in periosteal osteogenesis. Clin Orthop Rel Res 1992; 275: 280-286.

Dinges HP, Redl H, Thurnher M, Schiesser A, Schlag G. Morphometric studies on wound healing after systemic administration of Adriamycin and local application of fibrin sealant. Pathol Res Pract 1986; 181: 746.

Doremus RH. Bioceramics (Review). J. Mat. Sci. Mat. Med. Vol.27, 1992, 285-297

Driessens FCM. Formation and solubility of calcium phosphates in relation to the phase composition of the material in calcified tissues. In Bioceramics of Calcium Phopshate, ed. K. de Groot (CRC Press, Boca Raton, Florida, 1983) p-1

Drissens FC.Z. Nautrforsch 1980,35c:357

Drobeck, H.P., Rothstein, S.S., Gmmaer, K.K., Sherer, A.D., and Slighter, R.G. Histologic observation of soft tissue responses to implanted, multifaceted particles and discs of hydroxyapatite J Maxillofac Surg 1984;42:143.

Du, C., Cui, F.Z., Feng, Q.L., Zhu, X.D., and de Groot, K. Tissue response to nano-hydroxyapatite/collagen composite implants in marrow cavity J biomed 1998

Ducheyene P, Beight J, Cuckler J, Evans B, Radin S. Effect of calcium-phosphate coating characteristics on early postoperative bone tissue ingrowth. Biomaterials 1990;11:531-40.

Ducheyne P, Radin S, King L. The effect of calcium phosphate ceramic composition and structure on in vitro behaviour. I. Dissolution. J. Biomat. Mat. Res. 1993, 27:25-34.

Ducheyne P, Van RW, Heughebaert JC, and Heughebaert M. Biomaterials 1986,7:97-103

Ducheyne, P., Beight, J., Cuckler, J.M., Evans, B., Radin, S. Effect of calcium-phosphate coating characteristics on early postoperative bone tissue ingrowth. Biomaterials 1990; 11:531-540

Ebrahimpour , perez and Nancollas induced crystal growth of calcium oxalate monohydrate at hydroxyapatite surfaces. The influence of human serum albumin, citrate and magnesium, Langmuir 1991;7:577-583

Eggli, P.S., Muller, W., Schenk, R.K. Porous hydroxyapatite and tricalcium phosphate cylinders with two different pore size ranges implanted in the Cancellous bone of rabbits. Clin Orthop Rel Res 1988;232:127-138

EI Feki, H, Rey C and Vignoles M. I.B.I.D. 49(1991) 269-274.

EI- Ghannam A, Ducheyne P and Shapiro I M 1995 *J. Biomed. Mater. Res.* 29 359

El-Ghannam A, Ducheyne P, Shapiro IM. Effect of serum protein adsorption on osteoblast adhesion to bioactive glass and hydroxyapatite. J. Orthop Res 1999;17:340-5

El-Ghannam A, Ducheyne P, Shapiro IM. Formation of surface reaction products on bioactive glass and their effects on the expression of the osteoblastic phenotype and the deposition of mineralized extracellular matrix. Biomaterials 1997; 18: 295-303.

Ellinger RF, Nery EB, Lynch KL. Int J Period Restor Dent 1986; 3: 223.

Elliot JC. Clin orthop rel res. 1974, 93, 313-345.

Epstein N. Smithsonian, December 1989:509.

Evans R W, Cheung H S and McCarty D J 1984 *Calcified Tissue International* 36 645

Fibrinogen und Fibrinkleber, Stuttgart: Schattauer; 1980. p 217-220.

Fisher LW, and Termine JD. Noncollagenous proteins influencing the local mechanisms of calcification," Clin. Orthop.Rel. res., 1985; 200:362-384

Fisher RA, and Yates E. Statistics table for biological, agricultural and medical research. 1948 oliver and Boyd, London.

Fornasier, V.L. Osteoid: an Ultrastructural study, Hum Pathol 1977; 8(3):243-254

Fourman P P, Levell R J and Morgan D B 1972 *Calcium metabolism and the Bone* F A Davies Co., (Philadelphia) p. 3

Friedenstein AJ. Hard tissue growth, repair, and remineralization. In: Ciba Foundation Symposium, Elsevier-Excepta Medica, Amsterdam, 1973;6:230.

Fujiu T Ogino M, Kariya M, and Ishimura T. "New explanation of the bonding behaviour of fluorine coating bioglass, J. Non- Crystal. Solids, 1983; 56: 417-422

Fukuchi N and Akao M. Effect of hydroxyapatite microcrystals on macrophage activity. Bio-Medical Materials and Engineering 1995; 5:219-231.

Giraud-Gille, M.M. Twisted plywood architecture of collagen fibrils in human compact bone osteons, Calcif Tisue Int 1988; 42(3): 167-180

Gitelam H.J. (1967), Anal Biochem. 18, 521,

Glimcher, M.J. Recent studies of the mineral phase in bone and its possible linkage to the organic matrix by protein bound phosphate bonds. Philos Trans R Soc Lond (Biol) 1984;304 (1121):479-508

Golden A. Pathology, Understanding Human Disease, Williams and Willkins, Baltimore, 1982, pp.3-41

Gregoire M, Orly I, Menanteau J The influence of calcium phosphate biomaterials on human bone cell activities. An in vitro approach. J Biomat Mater Res 1990;24:165-177.

Grenga, T.E., Zins, J.E., Bauer, T.W. The rate of vascularization of coralline hydroxyapatite Plast Reconstr Surg 1989, 84:245-249

Grieff J. Bone haling in rabbits after compression osteosynthesis: a comparative study between the radiological and histological findings. Injury, 1978; 10:257-267

Grieff, J Bone healing in rabbits after compression osteosynthesis: a comparative study between the radiological and histological findings. Injury 1978, 10:257-267.

Gross U, Brandes J, Strunz V, Bab I, and Sela J. The ultrastructure of the interface between a glass ceramic and bone, J. Biomed. Mater. Res., 1981; 15:291

Gross U, Raimund Kinne, Hermann-Josef Schmitz and Volker Strunz "The response of bone to surface-active glasses/glass-ceramics", In CRC Critical Reviews in Biocompatibility by Larry L. Hench, CRC press, Vol.4, Issue 2 (1988) pp. 155-180)

Gross U, Schmitz HJ, and Strunz V. Ann. N,Y. Acad.Sci. 1988, 523:211-226

Gross, U., and Strunz, V. The interface of various glasses and glass-ceramics with a bony implantation bed. J Biomed Mater Res 1985, 19:251-271

Grote,J.J., Van Blitterswijk, C.A., and Kuijpers,W. Ann. Otol Rhinol Laryngol Suppl. 1986, 123:1-5

Guillemin G, Patat JL, Fournier J, Chetail M. The use of coral as a bone graft substite. J Biomed Mater Res 1987; 21:557-567.

Gurr E. Biological staining methods. 8th eds. Buckinghamshire, England: Searle Diagnostic Gurr Products, 1973, p 111.

Hardy V. and Furedi H. Minofer, "Adsorption of human serum albumin on precipitated hydroxyapatite, J. Colloid Interface. Sci., 69, 460-468 (1979)

Hauschka PV, and Carr SA. "Calcium-dependent alpha-helical structure in osteocalcin. Biochemistry 1982;.21: 2538-2547

Hauschka PV, Mavrako, E, Iafrat, MD. Growth factors in bone matrix: isolation of multiple types by affinity chromatography on heparin-sepharose. J Biol Chem 1986;261:12665

Heimburger S, Wolf M, Cherry G, and Meyers MB. An evaluation of the effects of cartilage powder on wound healing. Archives of Surgery 1967;95:643.

Heimke G, Griss P, Jentschura G, and Werner E. Bioinert and bioactive ceramics in orthopaedic surgery, in Mechanical properties of biomaterials, Hastings, G.W. and Williams, D.F., Eds. John Wiley & Sons, New York, 1980,207

Hench L L 1991a *J. Am. Ceram. Soc.* 74 1487

Hench L L 1991b *The Bone-Biomaterial Interface* (ed) J E Davies (Univ. of Toronto Press) p.33

Hench L L 1994 *Bioactive ceramics: Theory and clinical applications in Bioceramics* (eds) O H Anderson and A Yli-Urpo (Buterworth-Heinemann Ltd. Oxford, England) p.3

Hench L L and Andersson O 1993 *Introduction to Bioceramics* (Advanced Series in Ceramics – vol 1) (eds) L L Hench and J Wilson (World Scientific Publishing Co Pvt Ltd: Singapore New Jersey) 3 p. 41

Hench L L and West J K 1996 *Life Chem. Rep.* 13 187

Hench L.L. and G.P. LaTorre, "Reaction kinetics of bioactive ceramics Part IV: Effect of glass and solution composition," in Bioceramics 5, eds. T. Yamamuro, T. Kokubo and T.

Hench L.L., and Ethridge, E.C. Biomaterials: An interfacial approach: Academic Press; New York (1982)

Hench LL Bioactive ceramics: Theory and clinical applications. IN: Andersson O, Yli-Urpo A, Happonen RP, editors. Bioceramics 7. Oxford, UK: Butterworth-Heinemann; 1994. p 3-14.

Hench LL J. Amer Ceram Soc. 1991;74(7):1487-1510

Hench LL, and Ethridge EC. Biomaterials, An Interfacial Approach, Academic Press, New York, 1982, 1

Hench LL, Splinter RJ, Allen WC, and Greenlee TK. JBMR Symposium. 1972,2:117-141.

Hench LL, Surface reaction kinetics and adsorption of biological moietis: A mechanistic approach to tissue attachment In: Davies JE, eds. The bone-biomaterial interface. Toronto, University of Toronto Press:1991. P 33-48.

Hench LL. Bioactive Ceramics in Bioceramics: Materials Characteristics Versus In Vivo Behaviour. P. Ducheyne and J.Lemons (eds.). Annals N.Y. Acad. Sci., Vol.523, 1988

Hench LL. Bioactive ceramics. In: Ducheyne P, Lemons JE, editors. Bioceramics: material characteristics versus in vivo behaviour. Newy York: The New York Academy of Sciences, 1988. P.54-71.

Hench LL. Bioactive ceramics: Theory and clinical applications In Anderson O, Yli-rpo A, Happonen R P, eds. Bioceramics Vol. 7 Oxford, UK: Butterworth-Heinemann 1994.p 3-14.

Hench LL. Bioactive glass : Present and future. In: LeGeros RZ, LeGEROS J, editors. Bioceramics 11. Singapore: World Scientific Publishing; 1998. p 31-36.

Hench LL. Bioceramics: from concept to clinic. J. Am Ceram Soc 1991;74(7):1487-510.

Hench LL., and Paschal, HA. Direct chemical bond of bioactive glass ceramic materials to bone and muscle, J Biomed Mater. Res 1981;15(6):805

Hench, L., Splinter, R., Greenlee, T., Allen, W. Bonding mechanisms at the interface of ceramic prosthetic materials. J Biomed Eng 1971;2:117-141

Hench, L.L., and Ethridge, E.C., Biomaterials:An Interfacial Approach, Academic Press, New York, 1982

Hench, L.L., and Paschall, H.A. Direct chemical bond of bioactive glass ceramic materials to bone and muscle, J Biomed Mater. Res 1981;15(6):805,.

Hench, L.L., Splinter,R.J., Allen, W.C., and Greenlee, T.K. JBMR Symposium. 1972,2:117-141.

Hench,L.L and West, J.K. The sol-gel process, Chem Rev. 90 (1990) 33-72.

Heughebaert, M., Le Geros, R.Z., Gineste, M., Guilhem, A. and Bonel, G., Physicochemical characterization of deposits associated with HA ceramics implanted in nonosseous sites, J. Biomed. Mater. Res. 1988, 22, 257-268

Holand W, Vogel W, Naumann K, and Gummel J. Machinable bioactive glass ceramic, in Glass Current Issues, NATO ASI series No.92, Wrigth, A.F and Dupuy, J., Eds. Martinus Nijhoff, Boston, 1985, 670

Hollinger JO, Schmitz JP, Mizgala JW, Hassler C. J. Biomed Mater Res 1989; 23:17.

Hollinger, J., and Chaudhari, A. Bone regeneration materials for the mandibular and craniofacial complex. Cell and Materials 1992, 2:143-151

Hollister, S.J., Kikuchi, N., Goldstein, S.A. Do bone ingrowth processes produce a globally optimized structure? J Biomech 1993, 26:391-407

Holmes RE, Mooney RW, Bucholz RW, and Tencer A.F. Clin. Orthop. Relat. Res., 188, 282-292

Holmes, R.E., and Hagler, H.K., Plast.Reconstr.Surg. 81 (1988) 662.

Holtzer H. Induction of chondrogenesis: a concept in quest of mechanisms. In: Epithelial-Mesenchymal Interactions. Fleischmajer, T. and Billingsham, w.E. Eds., Williams and

Homminga G, Bulstra S, Bouwmeester P, van Der Linden A. Perichondral grafting for cartilage lesions of the knee. J Bone Joint Surg 1990; 72 B: 1003-1007.

Hubbard, W. Physiological calcium phosphates as orthopaedic biomaterials, (Ph.D. thesis, Marquette University,1974).

Hulbert SF, Matthews JR, Klawitter JJ, Sauer BW, and Leonard RB. Biomed. Maters. Symp., 1974; 5: 85-97

Hyakuna K, Yamammuro T, Kotoura Y, Kakutani Y, Kitsugi T, Tagagi H, Oka M, and Kokubo T. Surface reactions of calcium phsophate ceramics to various solutions, J.Biomed.Mater.Res., 1990; 24:471-488

Hyakuna K, Yamamuro T, Kotoura Y and Oka M 1990 *J. Biomed. Mater. Res.* 24 471

Hyakuna K, Yamamuro T, Kotoura Y, Kakutani Y, Kitsugi T, Takagi H, Oka M and Kokubo T 1989 *J. Biomed. Mater. Res.* 23 1049

Ikenga, M., Ohura, K., Nakamura,T., Kotoura, Y., Yamamuro, T., Oka, M., Ebisawa, Y., and Kokubo,T. In bioceramics(W. Bonfield, G. W. Hastings, and K.E. Tanner, Eds.), Butterworth-Heineman, London, 1991, Vol.4, pp-99-103

Iler PK Coagulation of colloidal silica by calcium ions, mechanism, and effect of particle size. J. Colloid Interface Sci. 1975; 55:476-488.

Iler, R.K. The chemistry of silica (J. Wiley and Sons, Inc., New York, 1979).

Inoue T, Cox JE, Pillar RM and Melcher AH. Effect of the surface geometry of smooth and porous-coated titanium alloy on the orientation of the fibroblast in vitro J Biomed Mater Res 1987;21:107-126

Jarcho M., Salsbury RL, Thomas MB, and Doremus RH J. Mat. Sci. 14 (1979) 142

Jarcho, M. Calcium phosphate ceramics as hard tissue prosthesis, Clin Orthop.Relat. Res., 1981; 157: 259.

Jarcho,M. hydroxyapatite synthesis and characterization in dense polycrystalline forms, J. Mater. Sci. 11:2027-2035 (1976)

Johnson LC. Morphologic analysis: the kinetics of diease and general biology of bone. In: Bone Biodynamics, Frost HM ed. Little Brown, Boston, 1964.

Kasuga T, Nakajima K, Uno T, and Yoshida M. J.Am.Ceramic.Soc.1992,75:1103-1107

Kawamura M, Urist MR. Human fibrin is a physiologic delivery system for BMP Clin Orthop 1988; 235: 302-310.

Kay, J.F. Calcium phosphate coatings for dental implants, Dent. Clin. North. Amer. 36 (1992) 1-18

Kelley, P.J., Montgomery, R.J., and Broonk, J.T. Reaction of the circulatory system to injury and regeneration. Clin Orthop 1990, 254:257-288

Kelly PJ, Montgomery RJ, and Bronk JT. Reaction of the circulatory system to injury and regeneration. Clin Orthop 1990, 254: 275-288

Kind PRM, and King E J. Clin Path, 7, 322.

King EJ, and Jagatheesan KA. (1959) J. Clin Path. 12:85

Kitsugi T, Nakamura T, Yamamuro T, Kokubo T, Shibuya T and Takagi M 1987 *J. Biomed. Mater. Res.* 21 1255

Kitsugi T, Yamamuro T, Nakamura T, Kokubo T, Takagi M, Shibuya T, Takeuchi H, Ono M. Bonding behaviour between the bioactive ceramics in vivo. JBMR, 1997; 34:79-86.

Kitsugi, T. Yamamuro T, Nakamura T, Kokubo, T. The bonding of glass ceramics to bone. Int. Orthop. 1989; 13:199-206.

Klein CAPT, Driessen AA, de Groot K, and van den Hoof A."Biodegradation behaviour of various calcium phosphate materials in bone tissue. JBMR 1983;17:769-784.

Klein CP, de Blieck-Hogervorst J M, Wolke J G and de Groot K 1990 *Biomaterials* 11 509

Klein CPAT, de Groot K, and Namavar F. The interactions of calcium phosphate crystals and polymorphonuclear leucocytes monitored by luminol dependent chemiluminecence, Trans. 2nd World Cong. Biomaterials, 1987, 84

Klein, C., Patka, P. and den Hollander, W. Macroporous calcium phosphate bioceramics in dog femora: A histological study of interface and biodegradation. Biomaterials 10 (1989) 59-62.

Knighton D , Hunt T K, Thakral KK Goodson WH. III: Role of platelets and fibrin in the healing sequence. An *in vivo* study of angiogenesis and collagen syntheses. Ann Surg 1982; 196:379.

Kobayashi,S., Hara,H., Okudera,H.,Takemae,T.,and Sugita,K. Neurosurgery 1987,21:751-755.

Kokubo T, Biomaterials, 1991, 12, 155-163.

Kokubo T, Ito S, Sakka S , and Yamamuro T. J.Mat.Sci.1986,21:536

Kokubo T, Ito S, Shigematsu M, Sakka S, and Yamamuro T. Mechanical properties of a new type of apatite-containing glass-ceramic for prosthetic application, J.Mater.Sci., 1985; 20: 2001

Kokubo T, Kushitani H, Sakka S, Kitsugi T, and Yamamuro T. Effects of ions dissolved from bioactive glass-ceramic on surface apatite formation. J Mat. Sci.: Mat.Med. 4, 1, 1-4, 1993.

Kokubo T, Kushitani H, Sakka S, Kitsugi T, and Yamamuro T. JBMR.1990,24:721-734

Kokubo T, Kushitani H, Sakka S, Kitsugi T, Yamamuro T. Solutions able to reproduce in vivo surface-structure changes in bioactive glass-ceramic A-W J Biomed Mater Res 1990; 24:721-34

Kokubo, T., van Blitterswijk, C.A. editors. Bone-bonding biomaterials. Leiderdorp, The Netherlands: Reed Healthcare Communications, 1993. p 111-120

Korkusuz, F., Karamete, K., Irfanoglue, B., Yetkin, H., Hastings, G.W., Akkas, N. Do porous calcium hydroxyapatite ceramics cause porosis in bone? A bone densitometry and biomechanical study of cortical bones of rabbits. Biomaterials 1995;16:537-543

Koster K, Heide H, Konig R. Resorbable calcium phosphate ceramics under load, Langenbecks Arch. Chir. 1977; 343: 174.

Krizek TJ. The normal body defences against foreign implants. In Biomaterials in Reconstructive Surgery, Rubin, L.R. (ed.), C.V. Mobsy Co., St. Louis (1983), 9-16

Kwong, C.H., Burns, W.B., and Cheung, H.S. Solubilization of hydroxyapatite crystals by murine bone cells, macrophages and fibroblasts, Biomaterials, 1989, 10:579-584

Lai W, Ducheyne P, Garino J. Removal pathway of silicon released from bioactive glass granules in vivo. In: LeGeros RZ, LeGeros J, editors. Bioceramics 11. Singapore: World Scientific Publishing; 1998. p 383-386.

Landis WJ, Lee DD, Brenna JT, Chandra S, Morrison GH. Detection and localization of silicon and associated elements in vertebrate bone tissue by imaging ion microscopy. Calcif Tissue Int 1986; 38:52-59.

Lash J, Holtzer H, and Whitehouse MW. In vitro studies on chondrogenesis: the uptake of radioactive sulfate during cartilage induction. Deve Biol 1960; 2:76-89

Lash J, Holtzer S, and Holtzer H. An experimental analysis of the development of the spinal column. Aspects of cartilage induction. Exp. Cell Res 1957; 13:292-303

Le Geros R., and Le Geros JP. Dense hydroxyapatite In Advances series in ceramics - vol.1"An introduction to bioceramics" ed. Hench.L.L. and Wilson.J. World Scientific Publications, Singapore, 1993 pp.139-180.

Le Geros RZ (1990) Calcium phosphates in oral biology. In: Myers Ha (ed) Monogr Oral Sci 15:5-45

Le Geros RZ, Daculsi G, Orly I, Abergas T, Torres W Solution-mediated transformation of octacalcium phosphate (OCP) to apatite. Scan Microsc 1989; 3:129-138

Le Geros RZ, Lee DD, Quirolgico G, Shirra WP, Reich L (1983) *In vitro* formation of dicalcium phosphate dihydrate, $CaHPO_4.2H_2O$ (DCPD). Scan Elect Microsc 407-418

Le Geros Rz, Orley I, Gregopre M, Agergas T, Kzimroff J and Tarpley T. Physicochemical properties of calcium phospate biomaterials used as bone substitute. Trans. 13th Annual metteing of Society for Biomaterials, p-84

Le Geros RZ. Apatites in biological systems. Prog Crystal Growth Charact 1981:4:1-45.

Le Geros Source Paper: Characterisation of HA and carbonated apatite by photo acoustic FTIR spectroscopy, J.Mat.Sci.Mat.Med. vol.8, 1997, pp 1-4

Le Geros, R.Z. Nature 1965, 206, 403-404

Lee A, editors. Clinical Implant materials. Amsterdam: Elsevier, 1990. P.255-8.

LeGeros R Z and LeGeros J P 1993 *An Introduction to Bioceramics (Advanced Series in Ceramics* - Vol. 1) (ed)s L L Hench and J Wilson World Scientific Publishing Co. Pvt. Ltd. Singapore New Jersey 9 p. 139

LeGeros R Z 1988 Adv. Dent. Res. 2 164

LeGeros R Z, Daculsi G, Orly I and Gregoire M 1991 *The Bone -Biomaterial Interface* (ed) J E Davies University of Toronto Press p. 76

LeGeros RZ and Tung MS. Chemical stability of carbonate and fluoride containing apatites.. Caries. Res 1983; 419-429

LeGeros,R.Z. Calcium phosphates in oral biology and medicine, Monographs in oral sciences. Vol.15, ed. H.Meyers (S.Karger, Basel, 1991).

LeGeros,R.Z.Crystallographic studies of the carbonate substitution in the apatite structure (Ph.D. Thesis, Newy York University, 1967).

Lehtinen, R., Kuusilehto, A., Nikkanen, U.M. Bone response to hydroxyapatite particles of different shapes in rabbit tibia J Oral Maxillofac Surg 1990;48:1075-1078

Lelievre S A, Weaver V M, Nickerson J A, Larabell C A, Bhaumik A, Petersen O W, and Bissell M J 1998 Proc. Nat. Acad. Sci. USA 95 14711

Lerner R, Binur NS. Current status of surgical adhesives. J Surg Res 1990; 48: 165-181.

Li , Zhang. The electrochemistry of glass surface and its application to the bioactive glass in solution. J. Non-Cryst Solids 1990;119: 112-118

Li P, de Groot K. Better bioactive ceramics through sol-gel process. J.Sol-Gel. Sc Technol. 1994, 12; 155-163.

Li P, Ohtsuki C, Kokubo T, Nakanishi K, Soga N, de Groot K. The role of hydrated silica, titania, and alumina in inducing apatite on implants. JBMR 1994;28:7-14.

Li P, Ohtsuki C, Kokubo T, Nakasihi K, Soga N, Kawamura T, Yamamuro T. Apatite formation induced by silica gel in a SBF. J.Am Ceram Soc. 1992; 75:2094-2097.

Lind M, Schumacker B, Soballe K, Keller J, Bunger C. Transforming growth factor-β enhances fracture healing in rabbit tibiae. Acta Orthop Scand 1993; 64:553-556

Ludwigson,D.C. Today's prosthetic metals. J.Metals16:1-25;1964.

Mahy PR, Urist MR. Experimental heterotopic bone formation induced by bone morphogenetic protein and recombinant human interleukin-1B. Clin Orthop Rel Res 1988;237:236

Malard, O., Bouler, J.M., Guicheux, J., Heyman, D., Pilet, P., Coquard, C., Daculsi, G. Influence of biphasic calcium phosphte granulometry on bone ingrowth, ceramic resorption, and inflammatory rections: Preliminary in vitro and in vivo study J Biomed Mater Res 1999;46:103-111

Markowitz, J. Experimental surgery, Baltimore, The Williams and Wilkins Company, 5th ed. 1964

Maroudas N G 1975 *J. Theor. Biol.* 49 417

Marrini E, Valdinucci F, Silvestrini G, Moretti S, Carlesimo M, Poggio C, Bonnuci E. Morphological investigations on bone formation in hydroxyapatite-fibrin implants in human maxillary and mandibular bone. Cells and Maters 1994; 4:3.

Martin RI and Brown PW, Formation of hydroxyapatite in serum . J.Mat.Sci.Mat.Med. 1993; 5, 96-102

Martin, R.B., Chapman, M.W., Holmes, R.E., Sartoris, D.J., Shors, E.C., Gordon, J.E., Heitter DO, Sharkey NA, Zissimos AG. Effects of bone ingrowth on the strength and non-invasive assessment of a coralline hydroxyapatite material. Biomaterials 1989;10:481-488

Marvin H, Meyer, Michael H. A fibrin adhesive sealant for the repair of osteochondral fracture fragments. Clin Orthop Rel Res 1984; 182: 258-263.

Matlaga B F and Salthouse T N 1983 *J. Biomed. Mater. Res.* 17 185

Matsuda T, and Davies JE. Biomaterials 1987, 8:275-284.

Matsuda T, Yamauchi K and Ito G 1987 *J.Biomed. Mater. Res.* 21 4992

Mayne PD. Plasma enzymes in diagnosis. In clinical chemistry in diagnosis and treatment. ELBS 1994 chapter 15: 299-313.

Mazdiyansi KS. In better ceramics through chemistry, Elsevier Science, Alburquerue, 1984.

Meunier A, Rey C, Bardin T. Variation in the inflammatory properties of basic calcium phosphate crystals according to crystal type. Arthritis Rehum 1996;39:1319-1326

Meyer,J.L., and Eanes,E.D. Calcif Tissue Res.1978,25:59

Miller SC, Bowman BM, Smith JM and Jee WSS. Characterizationof endosteal bone-lining cells from fatty marrow bone sites in adult beagles Anat Rec 1980;198:163

Minami,M., Yamazaki,J., Kato,S., and Ishii, S. J. Arthroplasty 1988,3:157-166

Misiek DJ, Kent JN, and Carr RF. Soft tissue responses to hydroxyapatite particles of different shapes, J.Oral Maxillofac. Surg 1984; 42:150-160

Morrison GM, Johnson HL, and Hazard JB. Promotion of fracture repair. J Bone and Joint surg 1937;19:425

Movat HZ. The inflammatory reaction, Elsevier, Amsterdam,1985

Muller-Mai, C.M., Stupp, S.I., Voigt, C., and Gross, U. Nanoapatite and organoapatite implants in bone: Histology and ultrastructure of the interface J Biomed Mater Res 1995, 29:9-18

Mulliken JB, Kaban LB, Glowacki J. Induced osteogenesis- the biological principle and clinical applications. J Surg Res 1984; 37: 487.

Murashov VV, Leszcynski J. Adsorption of the phosphate groups on silica hydroxyls: an ab initio study. J.Phys.Chem. A. 1999; 103:1228-1238.

Nageotte J. Osteogenese dans les greffes d' os mort. Comptes Rendus hebdomadaires des Seances de l' academie des sciences, 1920;171:280

Nakamura T, Yamamuro T, Higashi S, Kokubo T and Ito S J. Biomed. Mater. Res. 1985;19: 685

Nakamura T, Yamamuro T, Higashi S, Kokubo T, and Ito S, JBMR, 19, 685-698 (1985)

Nakamura T, Yamamuro T, Higeshi S, Kokubo T, and Ito S. A new glass ceramic for bone replacement, J. Biomed. Mater. Res., 1985; 19: 685

Nakamura T. Bioceramics in Orthopaedic Surgery, In Bioceramics Vol.9 Proceedings of the 9th International Symposium on ceramics in Medicine. Otsu, Japan, Nov.1996. ed.

Nakamura,T., Yamamuro, T., Higashi, S., Kokubo, T., and Ito, S., JBMR, 19, 685-698 (1985)

Nancollas GH, In biological mineralizations, GH Nancollas Ed. Dahlem Konferenzen, Springer-Verlag, 1982 a pp 79-99

Nelson DGA, and Featherstone JDB. *ibid.* 34, 1982, S69-81.

Neo, M., Nakamura, T., Ohtsuki, C., Kokubo, T., and Yamamuro, T. Apatite formation on three kinds of bioactive material at an early stage *in vivo*: A comparative study by transmission electron microscopy, J Biomed Mater Res 1993, 27:999-1006

Neo, M., Nakamura, T., Yamamuro, T., Ohtsuki, C., Kokubo, T. Transmission microscopic study of apatite formation on bioactive ceramics in vivo. In: Ducheyne, P.,

Nerry EB, Pflughoeft LKL, and Rooney GE. Functional loading of bioceramic augmented alveolar ridge: A pilot study, J. Prosthet. Dent. 43 (3). (1989) 338.

Nery EB, LeGeros RZ, Lynch KL, Kalbleisch J. J Dent Res 1988; 67: 178

Nery, E.B., LeGeros, R.Z., Lynch, K.L., Lee, K. Tissue response to biphasic calcium phosphate ceramic with different rations of HA/beta TCP in periodontal osseous defects. J Periodontal 1992;63:729-735

Neupert G and Vogel W. Growth of fibroblasts and epithelioid cells on a new machinable bioactive glass ceramic in comparison with non-reactive materials. Exp Pathol 1984; 26:113-116

Niwa S, Sawai K, Takahasi S, Tagai H, Ono M, Fukuca Y (1980) Experimental studies on the implantation of hydroxyapatite in the medullary canal of rabbits. Biomaterials 1:65-71.

Noda M and Camilliere JJ. *In vivo* stimulation of bone formation by transforming growth factor-β. Endocrinology 1989;124:2991

Nogami H and Urist MR. A substratum of bone matrix for differentiation of mesenchymal cells into chondro-osseous tissues in vitro. Exp. Cell Res 1970; 63:404.

Ohgushi H, Dohi Y, Yoshikawa T, Tamai S, Tabata S, Okunaga K, Shibuya T. Osteogenic differentiation of cultured marrow stromal stem cells on bioactive glass ceramics. J Biomed Mater Res 1996; 32: 341-348.

Ohgushi H, Okumura M, Yoshikawa M, Inoue K, Senpuku K, Tamai S. Bone formation process in porous calcium carbonate and hydroxyapatite. J Biomed Mater Res 1992; 26: 885-896.

Ohtsuki C,.Kokubo T, and Yamamuro T. Mechanism of apatite formation on CaO-SiO_2-P_2O_5 glasses in a simulated body fluid.J.Non-Crystal.Solids 143 (1992) 84-92.

Ohura K, Kankamura T, Yamamuro T, Kokubo T, Ebisawa Y, Kotoura Y, and Oka M, "Bone bonding ability of P_2O_5-free CaO-SiO_2

Okazaki M., Moriwaki, Y., Aoba, T., Doi Y., Takahashi J. Caries Res. 1981, 477-483

Ono K, Shikata J, Shimizu K, Yamamuro T. Bone-fibrin mixture in spinal surgery. Clin Orthop Rel Res 1992;275: 133-139.

Ono K, Yamamuro T and Nakamura T 1990 *Biomaterials* 11 265

Ono K, Yamamuro T, Nakamura T, and Kokubo T. A-W GC-Fibrin mixture as a new bone graft substitute. ORS 35th Annual Meeting, Las Vegas, Nevada, 1989.

Operative Medicine Vol. 7 Berlin: Springer-Verlag. 1986: p 189-197.

Orell S. Studien uber knochenimplantaion und knochenneubildung, implantation von ospurum. Acta Chirurgica Scandinavica, 1934;74:Supplementum 31

Orly I, Gregoire M, Menanteau J and Dard M 1989 J. Biomed. Mater. Res. 23 1433

Orthopaedic Research Society, February15-18, 1993, San Francisco, p. 478.

Ostle B In: Statistics in research. 1996, Oxford and IBH Publications, New Delhi.

Osyczka AL, Turyna B, Dubin A and Laczka M. Comparison of biocompatibility of gel-derived bioactive ceramics in macrophage culture conditions. Biomaterials 1997; 18:1243-1250.

Owen M. Bone and Mineral Research, Vol.3 Elsevier Science Publishers, Amsterdam, 1985, 1-25

Palacios CJ, Monia E. The mixture of fibrin sealant and a porous ceramic as osteoconductor: an experimental study. Schlag G, Redl, H, eds. Fibrin Sealant in

Passuti N, Daculsi G and Martin S 1990 in *Clinical Implant Materials* (ed)s

Passuti N, Daculsi G, Martin S. Macroporous calcium phosphate ceramics for long bone surgery in human and dogs-clinical and histological studies. In: Heimke G, Soltesz U, Boca Raton, FL: CRC Press, 1990, pp. 245-253
Passuti, N., and Daculsi, G. Ceramiques en phosphates de calcium chirurgie orthopedique. Presse Med 1989;18:28-31
Pazzaglia UE, Gabbi C, Locardi B, Di NA, Zatt G, and Cherubino P. JBMR. 1989,23:1289-1297

Peacock EE. Inflammation and the cellular response to injury. In Peacock EE. Eds. Wound Repair. Philadelphia: W B Saunders; 1984. p 1-14.

Peelen, J.G.J., Rejda, B.V., and de Groot, K. Ceramurgia Int. 4 (1978) 71.

Pereira MM, Clark AE, Hench LL. Effect of texture on the rate of hydroxyapatite

Perkins S and Fleischman RA. Hematopoietic microenvironment. Origin, lineage, and transplantability of the stromal cells in long-tem bone marrow cultures from chimeric mice. J Clin Invest 1988;81:1072.

Pettis GY, Kaban LB, and Glowacki J. Tissue response to composite ceramic hydroxyapatite/demineralised bone implants J. Oral Maxillofac. Surg. 1990; 48:1068-1074.

Piecuch J.F. Extraskeletal implantation of a porous hydroxyapatite ceramic, J. Dent.Res., 1982; 61:1458-1460

Pietrowski G, del Valle R, and Miller BD. The mechanical strength of the bone-ceramic bond, U.S. Army Med Res Dev Command Rep 1971; 2:15

Posner, A.S. Bone mineral and the mineralisation process. In: Bone and mineral research (Ed. Peck W A). Elsevier Science Publishers, Amsterdam 1987; 5:65-116

Posner, A.S. The mineral of bone. Clin Orthop 1985; 200:87-99

Prudhommeaux, G., Schiltz, C., Lote, F., Hina, A., Champy, R., Bucki, B., Ortiz, B.E.,

Radin S, Ducheyne P, Falaize S, Hammond A. Transformation of bioactive glass granules into Ca-P shells in vitro. J. Biomed Mater Res 1999.

Radin S, Ducheyne P, Rothaman B, Conti A. The effect of in vitro modeling conditions on the surface reactions on bioactive glass. J. Biomed Mater Res 1997; 37:363-75

Radin S, Ducheyne P. The effect of bioactive ceramic composition and structure on in vitro behaviour: III Porous versus dense ceramics. J. Biomed Mater Res 1994;28:1303-9

Radin S, Ducheyne P. The effect of serum proteins on solution induced surface transformations of bioactive ceramics. J. Biomed Mater. Res. 1996; 30: 273-80

Radin SR, Ducheyne P. The effect of calcium phosphate ceramic composition and structure on in vitro behaviour.II. Precipitation. J. Biomed. Mater. Res 1993;27:35-45

Radin, S., Ducheyne, P., Rothman, B., and Conti, A. The effect of *in vitro* modeling conditions on the surface reactions on bioactive glass. J. Biomed Mater Res 1997;37:363-375

Rahn BA, Gerber HA, Simpson F, Straumann, F and Perren SM. Cultured cells contacting implant materials of different surface treatment. Biomaterials 1980, Winter GD, Gibbons DF and Plent H Jr. (eds.), John Wiley, New York, 1982, pp.39-44.

Rath NC, Reddi AH. Collagenous bone matrix is a local mitogen. Nature 1979; 278: 855

Ratnoff OD, Menzie CJ. A new method for the determination of fibrinogen in small samples of plasma. Lab Clin Med 1951; 37: 316 – 320.

Ravaglioli, A., and Lee, A.J.C. Eds. Elsevier, Amsterdam, 1987, 223.

Reddi AH, Huggins CB. Influence of geometry of transplanted tooth and bone on transformation of fibroblasts. Proc Soc Exp Biol Med 1973; 143: 634-637.

Rehman and Bonfield Journal of Mat Science and Materials in Medicine, 8 (1997) 1-4

Rhinelander and Baragry Microradiography in bone healing. I undisplaced closed fracture. J Bone Joint Surg 1962; 44A:1273

Rhinelander Circulation of bone In: the biochemistru and physiology of bone, Vol.2. Bourne, G.H. (Ed). Academic Press. New York. 1972; pp 1-77

Ricci J L, Blumenthal N C, Spivak J M and Alexander H 1992 J. Oral and Maxillofacial Surg. 50 969

Ripamonti U, van den Heever B, van Wyk J. Expression of the osteogenic phenotype in porous hydroxyapatite implanted extraskeletally in baboons. Matrix 1993; 13: 491-502.

Ripamonti U. Inductive bone matrix and porous hydroxyapatite composites in rodents and nonhuman primates. In CRC Handbook of bioactive ceramics, volume 2. Calcium phosphate and hydroxyapatite ceramics, ed. By t. Yamamuro, L.L. Hench, and J. Wilson,

Ripamonti U. Osteoinduction in porous hydroxyapatite implanted in heterotopic sites of different animal models. Biomaterials 1996; 17:31-35

Ripamonti U. The morphogenesis of bone in replicas of porous hydroxyapatite obtained from the conversion of calcium carbonate exoskeletons of coral, J. Bone Jt. Surg. [Am.], 1991; 73A:692-703

Rizkalla AS, Jones DW, Hall GC, and Sutow E. J.Br.Ceram.Trans. J. 1992,91:41-44.

Roth H, Muller W and Spiessl B 1984 Monatsschr. Zahnmed. 94 222

Rubin, C.T., and Lanyon, L.E. Regulation of bone formation by applied dynamic loads, J. Bone Joint Surg. 1984, 66A:397-402

Salthouse, T.N., and Matlaga, B.F. Effects of implant surface on cellular activity and evaluation of histocompatibility, in Evaluation of Biomaterials, Winter, G.D., Leray, J.L., and de Groot, J. Ed., John Wiley & Sons, New York, 1980, 295.

Sautier, J.M., Kokubo, T., Ohtsuki, J.R., Nefussi, H., Boulekbache, M., Oboeuf, S., Loty, C., and Forest, N. Bioactive glass-ceramic containing crystalline apatite and wollastonite initiates biomineralization in bone cell culture, Calcif Tissue Int 1994, 55:458-466

Schakenraad JM, Busscher, H.J., Wildevuur, C.R.H., and Arends, J. The influence of substratum free energy on growth and spreading of human fibroblasts in the presence and absence of serum proteins. J Biomed Mater Res 1986;20:773

Schepers E et al. Bioactive glass particulate material as a filler for bone lesions. J Oral Rehab 1991;18:439-452.

Schepers E, De CM, and Ducheyne P. J.Oral Rehabil. 1988,15:473-487

Schepers E, Declercq M, Ducheyne P, Kempeneers R. Bioactive glass particulate material as a filler for bone lesions. J. Oral Rehab 1991;18:439-52

Schepers E.J.G., Declercq, M., Sucheyne, P., Kempeneers, R. Bioactive glass particulate material as a filler for bone lesions. J Oral Rehab 1991;18:439-452

Schepers EJG, Ducheyne P, Barbier L, Schepers S. Bioactive glass particles of narrow size range: a new material for the repair of bone defects. Implant Dent 1993; 2:151-6.

Schilling JA. Wound healing. Surg. Clin. N. Am., 56(4), 859, 1976

Schlag G, Redl H. Fibrin sealant in orthopaedic surgery. Clin Orthop Rel Res 1988; 227: 269 – 285.

Schwarz N, Redl H, Zeng L, Schlag G, Dinges HP, Eschberger J. Early osteoinduction in Rats is not altered by Fibrin Sealant. Clin Orthop Rel Res 1993; 293:353-359.

Shands AR. Studies in bone formation: The effect of the local presence of calcium salts on osteogenesis, J. Bone Jt. Surg., 1937, 19: 1065-1076.

Shors EC, Holmes RE, and Kraut R. Bone formation and implant degradation of coralline porous ceramics placed in bone and ectopic sites, Trans 39th Annual Meeting of the

Sierra D H S. Fibrin sealant adhesive systems: a review of their chemistry, material properties and clinical application. J Biomater Applic 1993; 7: 309-352.

Sierra D H S. Fibrin sealant adhesive systems: a review of their chemistry, material properties and clinical application. J Biomater Applic 1993; 7: 309-352.

Silver FH, Wang MC, Pins GD. Preparation of fibrin glue: A study of chemical and physical methods. J. Applied Biomat 1995; 6: 175-183.

Smith DC, and William, D.F. (eds.) Biocompatibility of dental materials, Vo.4, CRC press, Boca Raton, FL, 1982.

Snow, K.R., Muzina,D.J., and Bajpai, P.K. Biomed.Sci.Instrum.1989,25:203-211

Stewart WJ. Experimental bone regeneration: Using lime salts and autogenous grafts as sources of available calcium, Surgery, Gynecology, and Obstetrics, 1934, 59:867-871.

Strub JR, Gaberthuel TW. Trikalziumphopshat und desen biologisch abbaubare keranik in der parodontale knochen chirurgie, Eine Literaturubersicht, Schweiz. Monatsschr. Zahnheilkd 88 (1978) 798.

Tabuchi C, Simmons DJ, Fausto A, Binderman I, and Avioli LV. Effect of dihydrotachysterol on bone induction in ovariectomised rats. Bone Miner 1989;5:359-370

Taylor S R and Gibbons D F 1983 *J. Biomed. Mater. Res.* 17 205

Termine JD. In biological mineralisation, I.Sipkin, Ed., John Wiley and Sons, New York, 1973: pp.397-411

Thomas KA, Kay JF, Cook CD, and Jarcho M. The effect of surface microstructure and hydroxyapatite coating on the mechanical strength and histologic profiles of titanium implant materials. JBMR. 1987;21:1395.

Thompson JS, and Urist MR. Opposing actions of calcitonin and cortisone upon osteogenesis in heterotopic site. Clin Orthop 1973;90:201-208

Thompson W D, Campbell R, Evans T. Fibrin degradation and angiogenesis: Quantitative analysis of the angiogenic response in the chick chorioallantoic membrane. J Pathol 1985; 145:27.13.

Tracy, B.M. and Droremus, R.H. Direct electron microscopy studies of the bone-hydroxyapatite interface J Biomed Mater Res 1984, 18:719-726

Trecant, M., Delecrin, J., Royer, J., Daculsi, G. Mechanical changes in macroporous calcium phosphate ceramics after implantation in bone Clin Mater 1994;15:233-240

Uchida, A., Nade, S., McCartney, E., Ching, W. Bone ingrowth into three different porous ceramics implanted into the tibia of rats and rabbits. J Orthop Res 1985;3:65-77

Urist M R, Lietze A and Dawson E 1984 Clin. Orthop. 187 277

Urist MR and Mc Clean FC. Calcification and ossification 1. Calcificationin the callus in healing fractures in normal rats. J Bone Joint Surg 1941;25:375-426

Urist MR, De Lange RJ, Finuman GAM. Bone cells differentiation and growth factors. Science 1983; 220: 680.

Vallet-Regi M, Arcos D, Perez-Pariente J. Evolution of porosity during *in vitro* hydroxycarbonate apatite growth in sol-gel glasses. JBMR, 51, 23-28, 2000.

Van Blitterswijk CA, Koerten HK, and Grote J.J. Biological performance of whitlockite, in Advances in biomaterials, Vol.6, eds. P. Christel, A. Meunier and A.J.c. Lee (1986), p.27

van Blitterswijk, C.A., Grote, J.J., Kuijpers, W., Daems, W.Th., and de Groot, K. Macropore tissue ingrowth: a quantitative and qualitative study on hydroxyapatite ceramic, Biomaterials, 7. 137, 1986.

van der Meulen, J., and Koerten, H.K. Inflammatory response and degradation of three types of calcium phosphate ceramic in a non-osseous environment J Biomed Mater Res 1994, 28:1455-1463

Van Raemdonck W., Ducheyne P, De Meester P. Calcium phopshate ceramics: In: Ducheyne P, Hastings GW, editors. Metal and ceramic biomaterial. Vol.II. Strength and surface. Boca Raton: CRC Press, 1983. p.99-114.

Vargervik, K. Critical sites for new bone formation. In Bone Grafts and Bone Substitutes, ed. By M.Habal and A. Reddi, Philadelphia, PA: W.B. Saunders, 1992,pp.112-120.

Varma H K and Sivakumar R 1996 Preparation and characterisation of free flowing hydroxyapatite powders. Proceedings of 2nd International Symposium on Inorganic phosphate materials Nagoya Japan

Verrier S, Bareille R, Rovira A, Dard M and Amedee J. Human osteoprogenitor responses to orthopaedic implant: mechanism of cell attachment and cell adhesion. J Mat Sci Mat Med 1996;7:46-51.

Vogel A I 1980 *Text Book of Quantitative Inorganic Analysis* 5th edition ELBS London

Vrouwenvelder W C A , C G Groot and K de Groot 1992 *Biomaterials* 13, 382

Vrouwenvelder W C A, Groot C G and de Groot K 1994 *Biomaterials* 15 97

Wagner "Tierexperimentelle Untersuchungen zur Knochen Regeneration Genormter Defekte nach der implantation einer Trikalziumphosphat keramik, Disch. Zahnarztl. Z. 36 (1981)82.

Wahlig H and Dingeldein E 1986 in *Proceedings of the Sixth European Conference on Biomaterilas*, Bologna Italy p. 196

Walters MA, Leung YC, Blumenthal NC, Le Geros RZ, and Konsker KA. "A Raman and infrared spectroscopic in vestigation of biological hydroxyapatite," J. Inorgan.Biochem., 39, 193-200 (1990)

Wang, G.J., Dunstan, J.C., Reger, S.I., Hubbard, S., Dillich, J., and Stamp, W.G. Experimental femoral fracture immobilized by rigid and flexible rods (a rabbit model). Clin Orthop 1981, 154:286-290

Weiner, Arad and Traun 1991

Wells HG. Calcification and ossification, Arch. Internal Medicine, 1911; 7:721-753

White, E., and Shors, E.C. Biomaterial aspects of interpore-200 porous hydroxyapatite.

Williams D.F. (Ed.). Biocompatibility of clinical implant materials, Vol. 1, CRC Press, Boca Raton, FL, 1981.

Williams D.F. A model for biocompatibility and its evaluation, J. Biomed. Eng. 11:185-191 (1989)

Williams, D.F., Eds. John Wiley & Sons, New York, 1980,207

Willkins, Baltimore, 1968;152-164

Wilson J, and Merwin GE. Biomaterials for facial bone augmentation: comparative studies, J. Biomed Mater Res 1988;22(A2):159.

Wilson J, and Merwin GE. Biomaterials for facial bone augmentation: comparative studies, J. Biomed Mater Res 1988;22(A2):159.

Wilson J, and Nolletti, D. Bonding of soft tissues to bioglass. In. Handbook of bioceramics, Vol.I

Wilson J, Low S, Fetner A, and Hench LL. Bioactive materials for periodontal applications, In: Biomaterials in Clinical Applications, Pissoferrato, A., Marchetti, P.G.,

Wilson J, Schoen FJ, Pigott GH, and Hench LL. Toxicology and biocompatibility of bioglasses J Biomed Mater Res 1981; 15(6),805

Wilson J., Clark, A.E., Walker,R.D., and Ramer, M. In Bioceramic (W. Bonfield, G. W. Hastings, and K.E. Tanner, Eds.), Butterworth-Heineman, London, 1991, Vol.4, pp-99-103

Wilson, J., and Merwin, G.E. Biomaterials for facial bone augmentation: comparative studies, J. Biomed Mater Res 1988;22(A2):159.

Wilson, J., and Merwin, G.E. Biomaterials for facial bone augmentation: comparative studies, J. Biomed Mater Res 1988;22(A2):159.

Wilson, J., and Nolletti, D. Bonding of soft tissues to bioglass. In. Handbook of bioceramics, Vol.I

Wilson, J., Low, S., Fetner, A., and Hench, L.L. Bioactive materials for periodontal applications, In: Biomaterials in Clinical Applications, Pissoferrato, A., Marchetti, P.G., Ravaglioli, A., and Lee, A.J.C. Eds. Elsevier, Amsterdam, 1987, 223.

Wilson, J., Schoen, F.J., Pigott, G.H., and Hench, L.L. Toxicology and biocompatibility of bioglasses J Biomed Mater Res 1981; 15(6),805

Wornom IL, Buchman SR. Bone and cartilage tissue. In: Cohen IK, Digelmann RF. Lindbald WJ. Eds. Wound healing, Biochemical and Clinical Aspects. Philadelphia, PA. W.B. Saunders: 1992. p356-383.

Wornom IL, Buchman SR. Bone and cartilage tissue. In: Cohen IK, Digelmann RF. Lindbald WJ. Eds. Wound healing, Biochemical and Clinical Aspects. Philadelphia, PA. W.B. Saunders: 1992. p356-383.

Yamamuro, L.L. Hench and J. Wilson (CRC Press, Boca Raton, Florida, 1990) pp. 3-16.

Yamasaki H, Sakai H. Osteogenic response to porous hydroxyapatite ceramics under the skin of dogs. Biomaterials 1992; 13: 308-312.

Yamasaki H. Heterotopic bone formation around porous hydroxyapatite ceramics in the subcutis of dogs. Jpn J Oral Biol 1990; 32:190-192.

Yamasaki, H. Heterotopic bone formation around porous hydroxyapatite ceramics in the subcutis of dogs, Jpn. J. Oral Biol. 1990, 32, 190-192

Yang Z, Yuan H, Tong W, Zou P, Chen W, and Zhang X. Osteogenesis in extraskeletally implanted porous calcium phosphate ceramics: variability among different kinds of animals. Biomaterials 1996;17:2131-2137

Yang Z., Yuan H, Tong W, Zou P, Chen W, Zhang X. Osteogenesis in extraskeletally implanted porous ceramics: variability among different kinds of animals. Biomaterials 1996;17:2131-2137

Yang ZJ, Yuan H, Tong W, Zou P, Chen W, Zhang X. Osteogenesis in extraskeletally implanted porous calcium phosphate ceramics: variability among different kinds of animals. Biomaterials 1996;17: 2131-2137.

Yoshikawa H, Hashimoto J, Masuhara K, Takaoka K, and Ono K. Inhibition by tumor necrosis factor of induction of ectopic bone formation by osteosarcoma-derived bone-inducing substance Bone 1989;9:391-396

Young RA. ibid. Suppl. 53 (1974) 193-203.

ANNEXURE - I

LIST OF PAPER PUBLICATIONS

S. Abiraman, H. K. Varma, P.R. Umashankar, Annie John

Fibrin Glue as an Osteoinductive Protein in a Mouse Model

Biomaterials (2002) - Accepted

Annie John, **S. Abiraman**, H. K. Varma, T. V. Kumari and P. R. Umashankar

Bone growth response with porous hydroxyapatite granules in a critical sized lapine tibial-defect model

(2002)– Bulletin of Materials Science, vol. 25. No. 2, pp 141 – 154.

S. Abiraman, H.K Varma, T. V. Kumari, and P.R. Umashankar, Annie John,

Preliminary in vitro and in vivo characterizations of a sol-gel derived bioactive glass-ceramic system

(**Communicated to Bulletin of Materials Science Journal**)

S. Abiraman, Annie John, P.R. Umashankar, R.Rajesh and R. Sivakumar

In vivo response of hydroxyapatite and bioglass implanted in rabbit tibia-defect model

(Published in Biomedical Materials and Devices–New Frontiers Ed.)
Dr. M. Jayabalan

Transactions of the Tenth National Conference of the Society for Biomaterials and Artificial Organs (India) November 11-12, 1998.